CCMS-88-11

VIRGINIA TECH

CENTER FOR COMPOSITE MATERIALS AND STRUCTURES

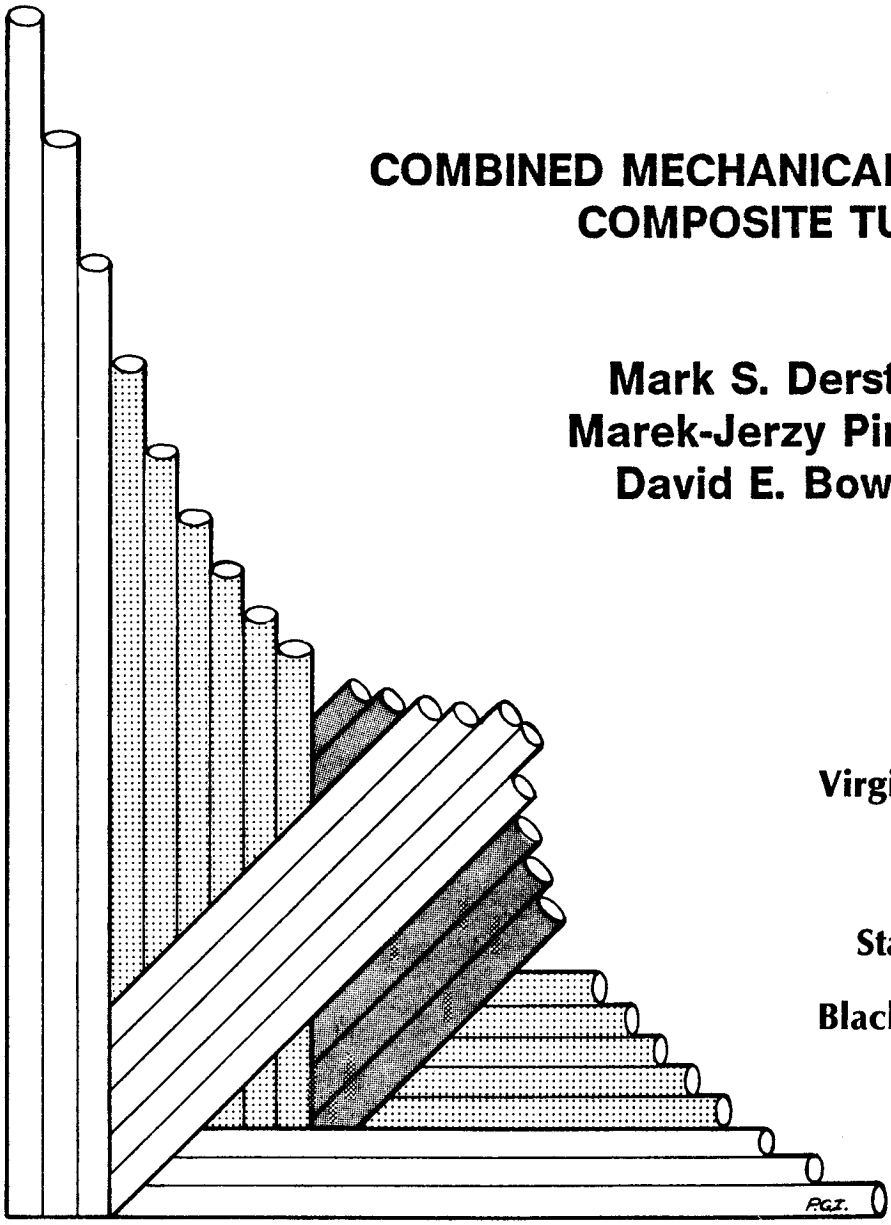

COMBINED MECHANICAL LOADING OF COMPOSITE TUBES

Mark S. Derstine
Marek-Jerzy Pindera
David E. Bowles

Virginia Polytechnic Institute and State University

Blacksburg, Virginia 24061

June 1988

College of Engineering
Virginia Polytechnic Institute and State University
Blacksburg, Virginia 24061

June 1988

CCMS-88-11
VPI-E-88-18

Combined Mechanical Loading of Composite Tubes

Mark S. Derstine
Marek-Jerzy Pindera
David E. Bowles

Department of Engineering Science and Mechanics

Abstract

An analytical/experimental investigation was performed to study the effect of material nonlinearities on the response of composite tubes subjected to combined axial and torsional loading. The effect of residual stresses on subsequent mechanical response was included in the investigation. Experiments were performed on P75/934 graphite/epoxy tubes with a stacking sequence of $[15/0/\pm 10/0/-15]_s$ using pure torsion and combined axial/torsional loading. In the presence of residual stresses, the analytical model predicted a reduction in the initial shear modulus. Experimentally, coupling between axial loading and shear strain was observed in laminated tubes under combined loading. This phenomenon was predicted by the nonlinear analytical model. The experimentally observed linear limit of the global shear response was found to correspond to the analytically predicted first ply failure. Further, the failure of the tubes was found to be path dependent above a critical load level.

Acknowledgement

This research was performed under the sponsorship of the NASA - Virginia Tech Composites Program and funded by NASA Grant NAG-1-343. This support is gratefully acknowledged. The authors would also like to express their appreciation of Tamara Knott and Deidre Hirschfeld for their technical assistance in the experimental work performed during this investigation.

Table of Contents

List of Illustrations

List of Tables

1.0 Introduction

The use of composite materials in tubular structures has become popular in recent years. Tubes made from graphite/epoxy have been used in the INTELSAT 6 Communication Satellite, and they are also under consideration by NASA for use in the truss structure of the space station[1]. In addition to spacecraft applications, composite tubes are also being considered for automobile drive shafts and for robotic arms. For applications such as these where high stiffness and dimensional stability are critical, a thorough understanding of the response of the composite tubes subjected to combined thermomechanical loading is imperative.

Polymer-based materials, such as the graphite/epoxy used in these tubes, frequently exhibit nonlinear constitutive behavior of the reversible or irreversible kind, depending on the direction of loading. This nonlinearity can have a significant effect on the distribution of stresses and strains within a tube. For this reason, an analytical tool employing a sufficiently general nonlinear constitutive theory is desired for predicting the response of composite tubes subjected to combined mechanical loading. This kind of tool will allow for a more accurate prediction of the state of stress, strain, and deformation in a composite tube.

Load path dependence is a phenomenon which occurs in nonlinear materials with dissipative response characteristics. This is defined by the state of stress and strain at a given state of loading being different for each different path taken to reach that state of load-

ing. An investigation of this phenomenon at the global level will be possible with an appropriate nonlinear analytical model at the ply level.

1.1 Literature Review

Much work has been done in recent years to develop analytical models that predict the response of anisotropic cylinders. Many different approaches such as shell theory, finite element analysis, and exact and variational approaches to elasticity theory have been utilized. Different variations of shell theory have been used to investigate the response of composite cylinders to torsion, tension (or compression), bending or a combination of these[2-8]. These analyses have yielded generally good predictions for thin walled cylinders ($r_o/t > 10$) where through-the-thickness strains can be neglected.

Rizzo and Vicario[9] used finite element analysis to predict the response of laminated tubes consisting of generally anisotropic layers with all coupling terms included. Unlike the shell theories described previously, this analysis included the effects of gripping the tube. The authors investigated the effects of varying the thickness-to-diameter and length-to-diameter ratios for different orientations of unidirectional tubes. In addition, they investigated the effect of different gripping arrangements on the subsequent mechanical response.

More recently, elasticity solutions for the composite tube problem have been developed. Cohen and Hyer[10] developed three axisymmetric elasticity solutions to determine residual stresses in cross-ply tubes: plane stress, plane strain, and generalized plane strain. They found that the generalized plane strain solution provided the best predictions of the three. The results from the elasticity solutions were compared with results from classical lamination theory, and it was found that there are limitations to approximating the response in a tube with a flat plate solution.

Hyer, Cooper, and Cohen[11] subsequently developed a solution to predict the response due to uniform temperature change based on the principle of complimentary virtual work. The results from this solution were compared with the elasticity solution developed previously[10] and agreed quite well. This work was restricted to cross-ply tubes.

The elasticity solution for cross-ply tubes was extended by Hyer and Cooper[12] to investigate the problem of a cross-ply composite tube subjected to a circumferential temperature gradient. Finally, the axisymmetric elasticity solution was extended by Rousseau, Hyer, and Tompkins[13] to predict the response of arbitrary laminated tubes subjected to mechanical loads as well as uniform temperature changes.

All of the analytical tools described above have employed a linear constitutive theory. Orgill and Wilson[14] have developed an analytical model to approximate the response of tubes using a nonlinear analysis. A strength of materials approach was used for analyzing tubes consisting of a single orthotropic layer. Both geometric and material nonlinearities were considered. The geometric nonlinearities were handled using an incremental procedure. At each load increment, the finite changes in the tube geometry (wall thickness, inside diameter, outside diameter, etc.) were computed and adjustments made to the cylinder dimensions. The material nonlinearities that were considered arose from finite changes in the orientation of the fibers in the layers due to deformations in the tube. The nonlinear constitutive behavior was determined from experimental methods and approximated by $\sigma_{11} = E_o\varepsilon_{11} + B\varepsilon_{11}^3 + C\varepsilon_{11}^5$ with similar expressions for σ_{22} and τ_{12}. This type of approximation assumes that there is no interaction between the stress components and that the stress-strain response is elastic.

Loading path dependence on the response of composite materials has not been so thoroughly investigated. Loading path dependence as it relates to the stress state at failure of composite tubes has been investigated by Choo[15]. This research was limited to hoop wound (90°) tubes. An extensive experimental program was carried out in which tubes were tested in combinations of compression and torsion or compression and internal pressure. It was found that in the fiber fracture mode, the state of failure stress was load path independent.

In the matrix fracture mode the state of failure stress was found to be load path independent in some cases.

1.2 Objectives

The objective of the present investigation is to characterize the response of composite tubes under combined mechanical loading. Towards this end, and analytical/experimental program will be undertaken. The analytical program entails the development of a model capable of predicting the response of composite tubes subjected to combined thermomechanical loading. The analytical model will be developed in a general fashion to include different types of mechanical loading such as axial force, torque and internal and external pressures. Thermal effects will also be included to account for residual stresses induced by the fabrication process. An elasticity approach based on the solution obtained by Rousseau, et al.,[13] will be used. The present model modifies this solution with the incorporation of a nonlinear constitutive theory. In addition, an efficient algorithm based on the structural matrix approach was incorporated for solving the resulting equations. This algorithm is particularly useful for laminated tubes with a large number of layers.

The predictions of the model will be correlated with the results of an experimental program. The experimental program will specifically investigate the response of composite tubes subjected to combined axial and torsional loading. The tubes used in this investigation are two inch nominal diameter tubes with a wall thickness of approximately 0.060 inches. They are fabricated using P75/934 graphite epoxy tape with a stacking sequence of $[15/0/\pm 10/0-15]_s$. This configuration is one under consideration by NASA for use in the truss structure of the Space Station.

2.0 Analytical Model

2.1 Introduction

Rousseau, et al.,[13] developed an exact planar elasticity solution using a linear constitutive theory to study thermally induced stresses and deformations in composite tubes. In the present investigation, the effects of material nonlinearities will be studied. Towards this end, a general nonlinear constitutive model will be incorporated into the solution obtained by Rousseau, et al., to permit the usage of any nonlinear constitutive theory that is desired. Once the nonlinear solution is complete, a suitable nonlinear model will be incorporated.

Due to the nonlinear effects, a modification to the numerical solution technique is desired to improve the computational efficiency of the analytical model. For this purpose, the Local/Global Stiffness Matrix formulation will be incorporated. Although thermal effects and the effects of internal and external pressures will not be included in the experimental portion of this work, the analytical formulation will include the presence of these types of loading for more generality. The material properties will be assumed to be temperature independent.

Figure 1 shows the coordinate system and nomenclature used for a laminated tube. The inside and outside radii of the tube are denoted by r_0 and r_N respectively, where N is the total

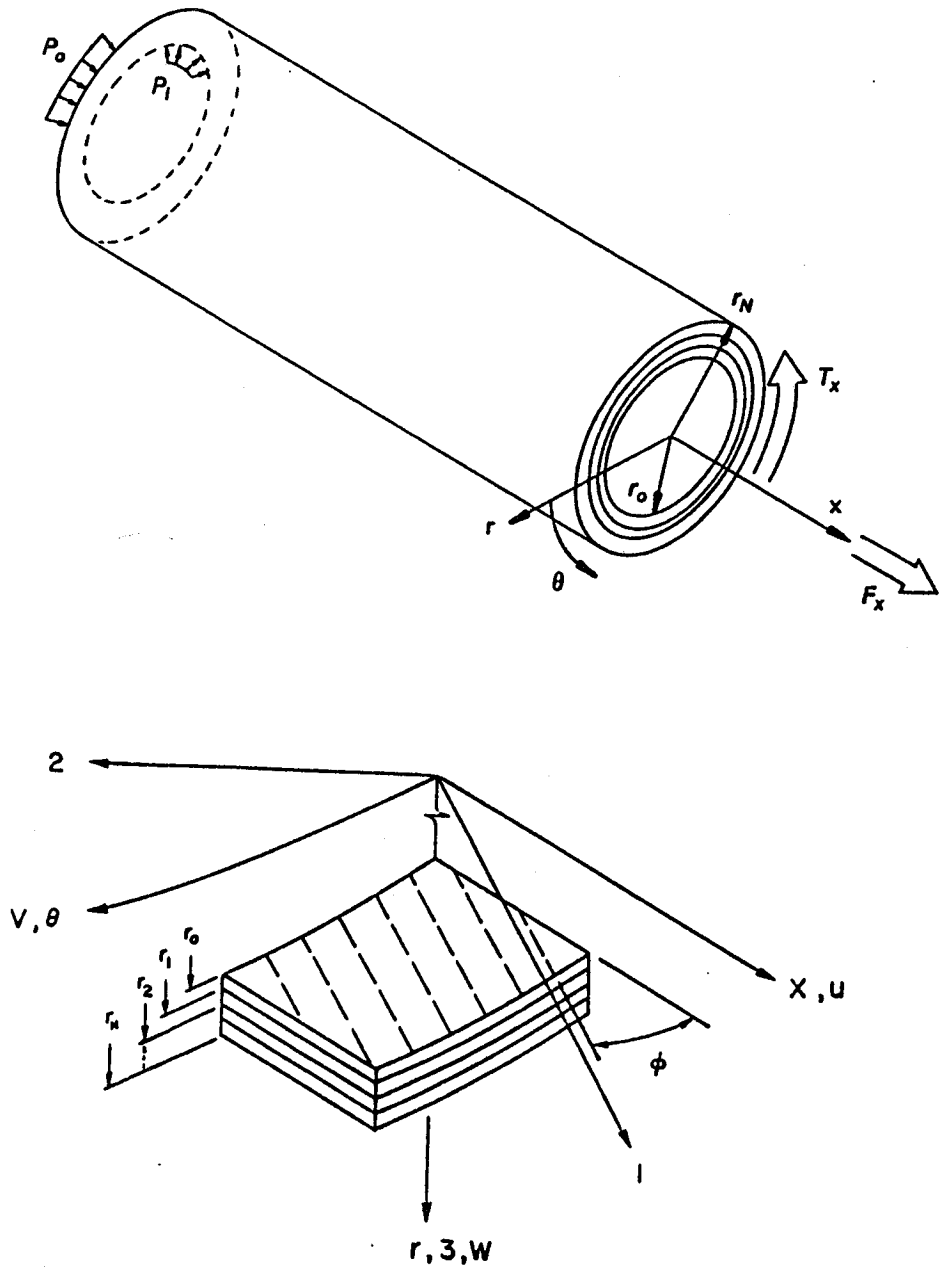

Figure 1. Coordinate System

number of layers in the tube. The radii of the interfaces between layers are denoted as r_1, r_2, etc. The governing equations to be derived will be developed in cylindrical coordinates; x represents the axial coordinate, θ represents the circumferential coordinate, and r represents the radial coordinate. The displacements in the x, θ, and r directions will be represented by u, v, and w respectively. The ply orientation angle is ϕ, and the principal material coordinates are oriented such that the 1-axis corresponds to the fiber direction, the 2-axis is normal to the fiber but in the lamina surface, and the 3-direction is normal to the lamina surface. The internal and external pressures are denoted by P_i and P_o respectively, and the applied axial and torsional loads are denoted as F_x and T_x respectively.

2.2 *Formulation*

2.2.1 Field Equations

In the equations that follow, the contracted notation for the stresses and strains in the principal material coordinates will be used, i.e.

$$\begin{bmatrix} \sigma_1 \\ \sigma_2 \\ \sigma_3 \\ \sigma_4 \\ \sigma_5 \\ \sigma_6 \end{bmatrix} = \begin{bmatrix} \sigma_{11} \\ \sigma_{22} \\ \sigma_{33} \\ \tau_{23} \\ \tau_{13} \\ \tau_{12} \end{bmatrix} \quad \text{and} \quad \begin{bmatrix} \varepsilon_1 \\ \varepsilon_2 \\ \varepsilon_3 \\ \varepsilon_4 \\ \varepsilon_5 \\ \varepsilon_6 \end{bmatrix} = \begin{bmatrix} \varepsilon_{11} \\ \varepsilon_{22} \\ \varepsilon_{33} \\ \gamma_{23} \\ \gamma_{13} \\ \gamma_{12} \end{bmatrix}$$

For the purposes of this derivation, the field equations will be considered for a single layer and then combined to form a solution for a complete laminated tube. The equations to

be used are the Equilibrium Equations, Compatibility Equations, Strain-Displacement Equations, and Constitutive Equations. The Equilibrium Equations in cylindrical coordinates are

$$\frac{\partial \sigma_r}{\partial r} + \frac{1}{r}(\sigma_r - \sigma_\theta) + \frac{1}{r}\frac{\partial \tau_{r\theta}}{\partial \theta} + \frac{\partial \tau_{xr}}{\partial x} + R_r = 0 \qquad [2.1a]$$

$$\frac{\partial \tau_{\theta r}}{\partial r} + \frac{1}{r}\frac{\partial \sigma_\theta}{\partial \theta} + \frac{\partial \tau_{x\theta}}{\partial x} + \frac{2}{r}\tau_{\theta r} + R_\theta = 0 \qquad [2.1b]$$

$$\frac{\partial \tau_{xr}}{\partial r} + \frac{1}{r}\frac{\partial \tau_{x\theta}}{\partial \theta} + \frac{\partial \sigma_x}{\partial x} + \frac{1}{r}\tau_{xr} + R_x = 0 \qquad [2.1c]$$

where R_x, R_θ, and R_r are the respective body forces. The Strain-Displacement Equations are

$$\varepsilon_x = \frac{\partial u}{\partial x} \qquad [2.2a]$$

$$\varepsilon_\theta = \frac{1}{r}\left(\frac{\partial v}{\partial \theta} + w\right) \qquad [2.2b]$$

$$\varepsilon_r = \frac{\partial w}{\partial r} \qquad [2.2c]$$

$$\gamma_{\theta r} = \frac{1}{r}\left(\frac{\partial w}{\partial \theta} - v + r\frac{\partial v}{\partial r}\right) \qquad [2.2d]$$

$$\gamma_{xr} = \frac{\partial u}{\partial r} + \frac{\partial w}{\partial x} \qquad [2.2e]$$

$$\gamma_{x\theta} = \frac{\partial v}{\partial x} + \frac{1}{r}\frac{\partial u}{\partial \theta} \qquad [2.2f]$$

The general form of the Compatibility Equations in cylindrical coordinates are

$$\frac{\partial^2 \varepsilon_r}{\partial x^2} + \frac{\partial^2 \varepsilon_x}{\partial^2 r^2} - \frac{\partial^2 \gamma_{xr}}{\partial x \partial r} = 0 \qquad [2.3a]$$

$$\frac{\partial^2 \varepsilon_\theta}{\partial x^2} - \frac{1}{r}\frac{\partial^2 \gamma_{x\theta}}{\partial x \partial \theta} + \frac{1}{r^2}\frac{\partial^2 \varepsilon_x}{\partial \theta^2} + \frac{1}{r}\frac{\partial \varepsilon_x}{\partial r} - \frac{1}{r}\frac{\partial \gamma_{xr}}{\partial x} = 0 \qquad [2.3b]$$

$$\frac{\partial^2 \varepsilon_r}{\partial \theta^2} - r\frac{\partial \varepsilon_r}{\partial r} - \frac{\partial^2 (r\gamma_{x\theta})}{\partial \theta \partial r} + \frac{\partial}{\partial r}\left(r^2 \frac{\partial \varepsilon_\theta}{\partial r}\right) = 0 \qquad [2.3c]$$

$$\frac{\partial^2 \gamma_{\theta r}}{\partial x^2} - r\frac{\partial^2}{\partial x \partial r}\left(\frac{1}{r}\gamma_{x\theta}\right) - \frac{1}{r}\frac{\partial^2 \gamma_{xr}}{\partial x \partial \theta} + 2\frac{\partial^2}{\partial \theta \partial r}\left(\frac{1}{r}\varepsilon_x\right) = 0 \qquad [2.3d]$$

$$\frac{2}{r}\frac{\partial^2 \varepsilon_r}{\partial x \partial \theta} - \frac{\partial^2}{\partial \theta \partial r}\left(\frac{1}{r}\gamma_{xr}\right) + \frac{\partial}{\partial r}\left[\frac{1}{r}\frac{\partial}{\partial r}(r\gamma_{x\theta})\right] - \frac{1}{r^2}\frac{\partial^2}{\partial x \partial r}\left(r^2 \gamma_{x\theta}\right) = 0 \qquad [2.3e]$$

$$\frac{\partial^2 \gamma_{xr}}{\partial \theta^2} - 2r\frac{\partial \varepsilon_r}{\partial x} - \frac{\partial^2}{\partial \theta \partial r}(r\gamma_{x\theta}) + 2r\frac{\partial^2}{\partial x \partial r}(r\varepsilon_\theta) - \frac{\partial^2}{\partial x \partial \theta}(r\gamma_{\theta r}) = 0 \qquad [2.3f]$$

The constitutive equations in the principal material coordinates are:

$$\begin{bmatrix} \sigma_1 \\ \sigma_2 \\ \sigma_3 \\ \sigma_4 \\ \sigma_5 \\ \sigma_6 \end{bmatrix} = \begin{bmatrix} C_{11} & C_{12} & C_{13} & 0 & 0 & 0 \\ C_{12} & C_{22} & C_{23} & 0 & 0 & 0 \\ C_{13} & C_{23} & C_{33} & 0 & 0 & 0 \\ 0 & 0 & 0 & C_{44} & 0 & 0 \\ 0 & 0 & 0 & 0 & C_{55} & 0 \\ 0 & 0 & 0 & 0 & 0 & C_{66} \end{bmatrix} \begin{bmatrix} \varepsilon_1 - \varepsilon_1^T - \varepsilon_1^{NL} \\ \varepsilon_2 - \varepsilon_2^T - \varepsilon_2^{NL} \\ \varepsilon_3 - \varepsilon_3^T - \varepsilon_3^{NL} \\ \varepsilon_4 - \varepsilon_4^{NL} \\ \varepsilon_5 - \varepsilon_5^{NL} \\ \varepsilon_6 - \varepsilon_6^{NL} \end{bmatrix} \qquad [2.4a]$$

or the inverse

$$\begin{bmatrix} \varepsilon_1 - \varepsilon_1^T - \varepsilon_1^{NL} \\ \varepsilon_2 - \varepsilon_2^T - \varepsilon_2^{NL} \\ \varepsilon_3 - \varepsilon_3^T - \varepsilon_3^{NL} \\ \varepsilon_4 - \varepsilon_4^{NL} \\ \varepsilon_5 - \varepsilon_5^{NL} \\ \varepsilon_6 - \varepsilon_6^{NL} \end{bmatrix} = \begin{bmatrix} A_{11} & A_{12} & A_{13} & 0 & 0 & 0 \\ A_{12} & A_{22} & A_{23} & 0 & 0 & 0 \\ A_{13} & A_{23} & A_{33} & 0 & 0 & 0 \\ 0 & 0 & 0 & A_{44} & 0 & 0 \\ 0 & 0 & 0 & 0 & A_{55} & 0 \\ 0 & 0 & 0 & 0 & 0 & A_{66} \end{bmatrix} \begin{bmatrix} \sigma_1 \\ \sigma_2 \\ \sigma_3 \\ \sigma_4 \\ \sigma_5 \\ \sigma_6 \end{bmatrix} \qquad [2.4b]$$

where C_{ij} are the initial stiffnesses of the lamina, A_{ij} are the initial compliances, ε_i^T are the strains induced by a change in temperature, and the ε_i^{NL} are the nonlinear strains. This equation can be transformed to the global cylindrical coordinates of the tube. The result is as follows:

$$\begin{bmatrix} \sigma_x \\ \sigma_\theta \\ \sigma_r \\ \tau_{\theta r} \\ \tau_{xr} \\ \tau_{x\theta} \end{bmatrix} = \begin{bmatrix} \overline{C}_{11} & \overline{C}_{12} & \overline{C}_{13} & 0 & 0 & \overline{C}_{16} \\ \overline{C}_{12} & \overline{C}_{22} & \overline{C}_{23} & 0 & 0 & \overline{C}_{26} \\ \overline{C}_{13} & \overline{C}_{23} & \overline{C}_{33} & 0 & 0 & \overline{C}_{36} \\ 0 & 0 & 0 & \overline{C}_{44} & \overline{C}_{45} & 0 \\ 0 & 0 & 0 & \overline{C}_{45} & \overline{C}_{55} & 0 \\ \overline{C}_{16} & \overline{C}_{26} & \overline{C}_{36} & 0 & 0 & \overline{C}_{66} \end{bmatrix} \begin{bmatrix} \varepsilon_x - \varepsilon_x^T - \varepsilon_x^{NL} \\ \varepsilon_\theta - \varepsilon_\theta^T - \varepsilon_\theta^{NL} \\ \varepsilon_r - \varepsilon_r^T - \varepsilon_r^{NL} \\ \gamma_{\theta r} - \gamma_{\theta r}^{NL} \\ \gamma_{xr} - \gamma_{xr}^{NL} \\ \gamma_{x\theta} - \gamma_{x\theta}^T - \gamma_{x\theta}^{NL} \end{bmatrix} \qquad [2.5a]$$

where $\overline{C}_{ij}$ are the transformed initial stiffnesses of the lamina. This equation can be inverted to give strains in terms of stresses.

$$\begin{bmatrix} \varepsilon_x - \varepsilon_x^T - \varepsilon_x^{NL} \\ \varepsilon_\theta - \varepsilon_\theta^T - \varepsilon_\theta^{NL} \\ \varepsilon_r - \varepsilon_r^T - \varepsilon_r^{NL} \\ \gamma_{\theta r} - \gamma_{\theta r}^{NL} \\ \gamma_{xr} - \gamma_{xr}^{NL} \\ \gamma_{x\theta} - \gamma_{x\theta}^T - \gamma_{x\theta}^{NL} \end{bmatrix} = \begin{bmatrix} \overline{A}_{11} & \overline{A}_{12} & \overline{A}_{13} & 0 & 0 & \overline{A}_{16} \\ \overline{A}_{12} & \overline{A}_{22} & \overline{A}_{23} & 0 & 0 & \overline{A}_{26} \\ \overline{A}_{13} & \overline{A}_{23} & \overline{A}_{33} & 0 & 0 & \overline{A}_{36} \\ 0 & 0 & 0 & \overline{A}_{44} & \overline{A}_{45} & 0 \\ 0 & 0 & 0 & \overline{A}_{45} & \overline{A}_{55} & 0 \\ \overline{A}_{16} & \overline{A}_{26} & \overline{A}_{36} & 0 & 0 & \overline{A}_{66} \end{bmatrix} \begin{bmatrix} \sigma_x \\ \sigma_\theta \\ \sigma_r \\ \tau_{\theta r} \\ \tau_{xr} \\ \tau_{x\theta} \end{bmatrix} \qquad [2.5b]$$

where $\bar{A}_{ij}$ are the transformed initial compliances of the lamina. For the moment, the nonlinear forms of the constitutive equations will be left in a general form with no specific nonlinear model used. This will be incorporated later in this chapter.

2.2.2 Boundary and Continuity Conditions

The field equations will be used to determine a general form of the governing equations for the displacements in the tube. To obtain a specific solution, the boundary conditions will be applied to the governing equations. On the outside surface of the tube ($r = r_N$), the tractions will be specified as follows:

$$\sigma_r(x, \theta, r_N) = -P_o \qquad [2.6a]$$

$$\tau_{\theta r}(x, \theta, r_N) = 0 \qquad [2.6b]$$

$$\tau_{xr}(x, \theta, r_N) = 0 \qquad [2.6c]$$

Similarly, the tractions on the inside surface ($r = r_o$) will be specified as

$$\sigma_r(x, \theta, r_o) = -P_i \qquad [2.7a]$$

$$\tau_{\theta r}(x, \theta, r_o) = 0 \qquad [2.7b]$$

$$\tau_{xr}(x, \theta, r_o) = 0 \qquad [2.7c]$$

For an arbitrary N layered tube, continuity of tractions and displacements at the interfaces of the layers must be fulfilled. The continuity of tractions can be expressed as

$$\sigma_r^{(k)}(x, \theta, r_k) = \sigma_r^{(k+1)}(x, \theta, r_k) \quad k = 1,2,...,N-1 \qquad [2.8a]$$

$$\tau_{\theta r}^{(k)}(x, \theta, r_k) = \tau_{\theta r}^{(k+1)}(x, \theta, r_k) \quad k = 1,2,...,N-1 \qquad [2.8b]$$

$$\tau_{xr}^{(k)}(x, \theta, r_k) = \tau_{xr}^{(k+1)}(x, \theta, r_k) \quad k = 1,2,...,N-1 \qquad [2.8c]$$

and the continuity of displacements are given by

$$u^{(k)}(x, \theta, r_k) = u^{(k+1)}(x, \theta, r_k) \quad k = 1,2,...,N-1 \qquad [2.9a]$$

$$v^{(k)}(x, \theta, r_k) = v^{(k+1)}(x, \theta, r_k) \quad k = 1,2,...,N-1 \qquad [2.9b]$$

$$w^{(k)}(x, \theta, r_k) = w^{(k+1)}(x, \theta, r_k) \quad k = 1,2,...,N-1 \qquad [2.9c]$$

where k represents the k^{th} layer in the tube and ranges from 1 to N-1. Finally, the total axial force, F_x, will be introduced to the tube as

$$F_x = \int_0^{2\pi} \int_{r_o}^{r_N} \sigma_r(x, \theta, r) r dr d\theta \qquad [2.10]$$

and the applied torque, T_x is

$$T_x = \int_0^{2\pi} \int_{r_o}^{r_N} \tau_{x\theta}(x, \theta, r) r^2 dr d\theta. \qquad [2.11]$$

These two equations will be referred to as the "integral force and torque equations."

2.2.3 Assumptions

The applied internal and external pressures are independent of θ and the temperature will be assumed to be spatially uniform. This leads to an axisymmetric problem, i.e. the stresses, strains, and displacements are independent of θ. For the portion of the tube that is

sufficiently far from the point of application of the axial force, F_x, and the torque, T_x, the stresses and strains will also be independent of the axial coordinate. These assumptions can be expressed as

$$\frac{\partial X}{\partial \theta} = 0 \qquad [2.12a]$$

$$\frac{\partial Y}{\partial x} = 0 \qquad [2.12b]$$

where

X = stress, strain, or displacement

Y = stress, or strain

2.3 *Solution*

2.3.1 Solution for Governing Equation

The governing equations will be derived for an individual layer. Application of boundary and continuity conditions will yield a system of equations for the radial displacements at the interfaces of the individual layers. Determination of the interfacial radial displacements in terms of the applied boundary conditions is sufficient for determination of the response of the tube in terms of global and local parameters.

Incorporating the assumptions of axisymmetry and the uniformity of the stresses and strains in the axial direction (which ensures that the radial displacement is a function of r only), the displacements take the form

$$u = u(x,r) \qquad [2.13a]$$

$$v = v(x,r) \qquad [2.13b]$$

$$w = w(r). \qquad [2.13c]$$

Using these assumptions, the field equations can be simplified as follows:

Strain-Displacement Equations:

$$\varepsilon_x = \frac{\partial u}{\partial x} \qquad [2.14a]$$

$$\varepsilon_\theta = \frac{w}{r} \qquad [2.14b]$$

$$\varepsilon_r = \frac{\partial w}{\partial r} \qquad [2.14c]$$

$$\gamma_{\theta r} = \frac{\partial v}{\partial r} - \frac{v}{r} \qquad [2.14d]$$

$$\gamma_{xr} = \frac{\partial u}{\partial r} \qquad [2.14e]$$

$$\gamma_{x\theta} = \frac{\partial v}{\partial x} \qquad [2.14f]$$

Compatibility Equations:

$$\frac{\partial^2 \varepsilon_x}{\partial r^2} = 0 \qquad [2.15a]$$

$$\frac{1}{r}\frac{\partial \varepsilon_x}{\partial r} = 0 \qquad [2.15b]$$

$$\frac{\partial}{\partial r}\left[\frac{1}{r}\frac{\partial}{\partial r}(r\gamma_{x\theta})\right]=0 \qquad [2.15c]$$

where the three remaining compatibility equations are satisfied identically.

Equilibrium Equations:

$$\frac{\partial\sigma_r}{\partial r}+\frac{1}{r}(\sigma_r-\sigma_\theta)=0 \qquad [2.16a]$$

$$\frac{\partial\tau_{\theta r}}{\partial r}+\frac{2}{r}\tau_{\theta r}=0 \qquad [2.16b]$$

$$\frac{\partial\tau_{xr}}{\partial r}+\frac{1}{r}\tau_{xr}=0 \qquad [2.16c]$$

where the body forces have been neglected.

These twelve equations ([2.14], [2.15], and [2.16]) will now be used to derive the general expressions for the displacements of a given lamina. Equation [2.15a], in conjunction with Equation [2.12b], can be integrated to solve for the axial strain, ε_x, directly.

$$\varepsilon_x(r)=Ar+B$$

where A and B are constants. Equation [2.15b], however, requires that A=0. Renaming B as ε_o, we find that the axial strain within the lamina is a constant.

$$\varepsilon_x(r)=\varepsilon_o \qquad [2.17]$$

Using equations [2.14a] and [2.17], the axial displacement u(x,r) can be solved for.

$$\varepsilon_x=\frac{\partial u}{\partial x}=\varepsilon_o$$

$$u(x,r)=\varepsilon_o x+f(r) \qquad [2.18]$$

Equation [2.15c] can be integrated to obtain

$$\gamma_{x\theta}(r) = Cr + \frac{D}{r} \qquad [2.19]$$

as the in-plane lamina shear strain. From equations [2.14f] and [2.19], the tangential displacement v(x,r) can be obtained.

$$\gamma_{x\theta} = \frac{\partial v}{\partial x} = Cr + \frac{D}{r}$$

$$v(x,r) = \left(Cr + \frac{D}{r}\right)x + g(r) \qquad [2.20]$$

Equations [2.16b] and [2.16c] can be solved for $\tau_{\theta r}$ and τ_{xr} respectively. This yields

$$\tau_{xr} = \frac{E}{r} \qquad [2.21]$$

$$\tau_{\theta r} = \frac{F}{r^2} \qquad [2.22]$$

Inserting equation [2.18] into [2.14e], we find that

$$\gamma_{xr} = \frac{df(r)}{dr}$$

From the constitutive relations

$$\gamma_{xr} = \bar{A}_{45}\tau_{\theta r} + \bar{A}_{55}\tau_{xr} + \gamma_{xr}^{NL}$$

substituting equations [2.21] and [2.22] and integrating, we find

$$f(r) = -\frac{\bar{A}_{45}F}{r} + \bar{A}_{55}E \ln r + F_1 + \int \gamma_{xr}^{NL} dr \qquad [2.23]$$

where F_1 is the rigid body translation.

Equation [2.20] can be inserted into equation [2.14d] to obtain

$$\gamma_{\theta r} = \frac{dg(r)}{dr} - \frac{g(r)}{r} - \frac{2D}{r^2}x$$

But, since the strains are functions of r only, D=0, therefore,

$$\gamma_{\theta r} = \frac{dg(r)}{dr} - \frac{g(r)}{r} \qquad [2.24]$$

Using the constitutive relations

$$\gamma_{\theta r} = \bar{A}_{44}\tau_{\theta r} + \bar{A}_{45}\tau_{xr} + \gamma_{\theta r}^{NL} \qquad [2.25]$$

Equating [2.24] and [2.25], and solving for g(r), we obtain

$$g(r) = -\frac{\bar{A}_{44}F}{2r} - \bar{A}_{45}E + G_1 r + r\int \frac{\gamma_{\theta r}^{NL}}{r}dr \qquad [2.26]$$

where G_1 is the rigid body rotation about the x-axis. Substituting these expressions into the expressions for the displacements, u and v, the resulting expressions for the displacements are

$$u(x,r) = \varepsilon_o x - \frac{\bar{A}_{45}F}{r} + \bar{A}_{55}E \ln r + \int \gamma_{xr}^{NL}dr + F_1 \qquad [2.27]$$

$$v(x,r) = \gamma_o r x - \frac{\bar{A}_{44}F}{2r} - \bar{A}_{45}E + r\int \frac{\gamma_{\theta r}^{NL}}{r}dr + G_1 r \qquad [2.28]$$

where the constant C has been renamed γ_o. The physical meaning of γ_o is the angle of rotation of the tube per unit length. Transforming γ_{xx}^{NL} and $\gamma_{\theta r}^{NL}$ to the principle material coordinates and neglecting rigid body motion gives

$$u(x,r) = \varepsilon_o x - \frac{\bar{A}_{45}F}{r} + \bar{A}_{55}E \ln r + \int (-n\varepsilon_4^{NL} + m\varepsilon_5^{NL})dr \qquad [2.29]$$

$$v(x,r) = \gamma_o xr - \frac{\bar{A}_{44}F}{2r} - \bar{A}_{45}E + r\int \frac{(m\varepsilon_4^{NL} + n\varepsilon_5^{NL})}{r}\,dr \qquad [2.30]$$

where

$$m = \cos\phi$$

$$n = \sin\phi$$

Consider the remaining equilibrium equation, [2.16a], and the constitutive equations for σ_r and σ_θ, namely

$$\sigma_\theta = \bar{C}_{21}(\varepsilon_x - \varepsilon_x^{NL} - \varepsilon_x^T) + \bar{C}_{22}(\varepsilon_\theta - \varepsilon_\theta^{NL} - \varepsilon_x^T) + \bar{C}_{23}(\varepsilon_r - \varepsilon_r^{NL} - \varepsilon_r^T) + \bar{C}_{26}(\gamma_{x\theta} - \gamma_{x\theta}^{NL} - \gamma_{x\theta}^T)$$

$$\sigma_r = \bar{C}_{31}(\varepsilon_x - \varepsilon_x^{NL} - \varepsilon_x^T) + \bar{C}_{32}(\varepsilon_\theta - \varepsilon_\theta^{NL} - \varepsilon_x^T) + \bar{C}_{33}(\varepsilon_r - \varepsilon_r^{NL} - \varepsilon_r^T) + \bar{C}_{36}(\gamma_{x\theta} - \gamma_{x\theta}^{NL} - \gamma_{x\theta}^T)$$

Replacing the total strains, ε_x, ε_θ, ε_r, and $\gamma_{x\theta}$, with their respective strain displacement expressions, and transforming the thermal and nonlinear strains into the principal material coordinates we obtain

$$\sigma_\theta = \bar{C}_{12}\frac{\partial u}{\partial x} + \bar{C}_{22}\frac{w}{r} + \bar{C}_{23}\frac{dw}{dr} + \bar{C}_{26}\frac{\partial v}{\partial x} - \left[n^2C_{11}\left(\varepsilon_1^{NL} + \varepsilon_1^T\right) + m^2C_{12}\left(\varepsilon_1^{NL} + \varepsilon_1^T\right) + 2mnC_{66}\varepsilon_{66}^{NL}\right] \qquad [2.31]$$

$$\sigma_r = \bar{C}_{13}\frac{\partial u}{\partial x} + \bar{C}_{23}\frac{w}{r} + \bar{C}_{33}\frac{dw}{dr} + \bar{C}_{36}\frac{\partial v}{\partial x} - C_{i3}(\varepsilon_i^{NL} + \varepsilon_i^T) \qquad [2.32]$$

where the repeated subscript, i, denotes a summation over the range i=1,2,3. At this point, it must be noted that two separate cases must be considered. These are the transversely isotropic lamina, where $\bar{C}_{12} = \bar{C}_{13}$, $\bar{C}_{22} = \bar{C}_{33}$, and $\bar{C}_{44} = 2(\bar{C}_{22} - \bar{C}_{23})$, and the monoclinic lamina. When the constitutive relations are substituted into the equilibrium equation we find, for transversely isotropic layers:

$$r^2\frac{d^2w}{dr_2} + r\frac{dw}{dr} - w = \frac{C_{i3}}{\bar{C}_{22}}\frac{d\varepsilon_i^{NL}}{dr} + \frac{1}{r}\left[\left(\frac{C_{i3}}{\bar{C}_{22}} - n^2\frac{C_{i1}}{\bar{C}_{22}} - m^2\frac{C_{i2}}{\bar{C}_{22}}\right)\left(\varepsilon_i^{NL} + \varepsilon_i^T\right) - 2mn\frac{C_{66}}{\bar{C}_{22}}\varepsilon_6^{NL}\right] \qquad [2.33a]$$

and for monoclinic layers

$$r^2\frac{d^2w}{dr^2} + r\frac{dw}{dr} - \frac{\bar{C}_{22}}{\bar{C}_{33}}w = K_1\varepsilon_o r + K_2\gamma_o r^2 + r^2\frac{C_{i3}}{\bar{C}_{33}}\frac{d\varepsilon_i^{NL}}{dr} - r\left[\frac{(n^2C_{i1} + m^2C_{i2} - C_{i3})(\varepsilon_i^{NL} + \varepsilon_i^T) + 2mnC_{66}\varepsilon_6^{NL}}{\bar{C}_{33}}\right] \qquad [2.33b]$$

where

$$K_1 = \frac{\bar{C}_{12} - \bar{C}_{13}}{\bar{C}_{33}}$$

$$K_2 = \frac{\bar{C}_{26} - 2\bar{C}_{36}}{\bar{C}_{33}}$$

Because the distribution of nonlinear strains through the thickness of the lamina is not known a priori, we will assume that they can be approximated by a fifth order polynomial, i.e.

$$\varepsilon_i^{NL} = a_i + b_i r + c_i r^2 + d_i r^3 + e_i r^4 + f_i r^5$$

For the moment we will assume that the constants a_i, b_i, c_i, d_i, e_i, and f_i are known constants. The reason for this assumption will become apparent later. With this assumption we can solve the differential equations for the radial displacement in terms of these constants a_i, b_i, c_i, d_i, e_i, and f_i . For transversely isotropic layers

$$r^2 \frac{d^2w}{dr^2} + r \frac{dw}{dr} - w = Q_1 r + Q_2 r^2 + Q_3 r^3 + Q_4 r^4 + Q_5 r^5 + Q_6 r^6 \qquad [2.34a]$$

where

$$Q_1 = \frac{F_i}{\bar{C}_{22}} (a_i + \varepsilon_i^T) - 2mn \frac{C_{66}}{\bar{C}_{22}} a_6$$

$$Q_2 = -2mn \frac{C_{66}}{\bar{C}_{22}} b_6 + \left(\frac{F_i}{\bar{C}_{22}} + \frac{C_{i3}}{\bar{C}_{22}} \right) b_i$$

$$Q_3 = \left(\frac{2C_{i3} + F_i}{\bar{C}_{22}} \right) c_i - 2mn \frac{C_{66}}{\bar{C}_{22}} c_6$$

$$Q_4 = \left(\frac{3C_{i3} + F_i}{\bar{C}_{22}} \right) d_i - 2mn \frac{C_{66}}{\bar{C}_{22}} d_6$$

$$Q_5 = \left(\frac{4C_{i3} + F_i}{\bar{C}_{22}} \right) e_i - 2mn \frac{C_{66}}{\bar{C}_{22}} d_6$$

$$Q_6 = \left(\frac{5C_{i3} + F_i}{\bar{C}_{22}} \right) f_i - 2mn \frac{C_{66}}{\bar{C}_{22}} d_6$$

$$F_i = C_{i3} - n^2 C_{i1} - m^2 C_{i2}$$

For the monoclinic layers, the differential equation becomes

$$r^2 \frac{d^2w}{dr^2} + r \frac{dw}{dr} - \frac{\bar{C}_{22}}{\bar{C}_{33}} w = T_1 r + T_2 r^2 + T_3 r^3 + T_4 r^4 + T_5 r^5 + T_6 r^6 \qquad [2.34b]$$

where

$$T_1 = K_1\varepsilon_o + \frac{F_i(\varepsilon_i^T + a_i)}{\bar{\bar{C}}_{33}} - 2mn\frac{C_{66}}{\bar{\bar{C}}_{33}}a_6$$

$$T_2 = K_2\gamma_o + \frac{(C_{i3} + F_i)}{\bar{\bar{C}}_{33}}b_i - 2mn\frac{C_{66}}{\bar{\bar{C}}_{33}}b_6$$

$$T_3 = \frac{(2C_{i3} + F_i)}{\bar{\bar{C}}_{33}}c_i - 2mn\frac{C_{66}}{\bar{\bar{C}}_{33}}c_6$$

$$T_4 = \frac{(3C_{i3} + F_i)}{\bar{\bar{C}}_{33}}d_i - 2mn\frac{C_{66}}{\bar{\bar{C}}_{33}}d_6$$

$$T_5 = \frac{(4C_{i3} + F_i)}{\bar{\bar{C}}_{33}}e_i - 2mn\frac{C_{66}}{\bar{\bar{C}}_{33}}e_6$$

$$T_6 = \frac{(5C_{i3} + F_i)}{\bar{\bar{C}}_{33}}e_i - 2mn\frac{C_{66}}{\bar{\bar{C}}_{33}}e_6$$

These equations can now be easily solved. The result for transversely isotropic layers is

$$w(r) = A_1 r + \frac{A_2}{r} + P_1 r \ln r + P_2 r^2 + P_3 r^3 + P_4 r^4 + P_5 r^5 + P_6 r^6 \qquad [2.35a]$$

where A_1 and A_2 are arbitrary constants and

$$P_1 = \frac{1}{2\bar{\bar{C}}_{22}}\left[F_i(a_i + \varepsilon_i^T) - 2mnC_{66}a_6\right]$$

$$P_2 = \frac{1}{3\bar{\bar{C}}_{22}}\left[(F_i + D_{i3})b_i - 2mnC_{66}b_6\right]$$

$$P_3 = \frac{1}{8\bar{\bar{C}}_{22}}\left[(F_i + 2C_{i3})c_i - 2mnC_{66}c_6\right]$$

$$P_4 = \frac{1}{15\overline{C}_{22}}[(F_i + 3C_{i3})d_i - 2mnC_{66}d_6]$$

$$P_5 = \frac{1}{24\overline{C}_{22}}[(F_i + 4C_{i3})e_i - 2mnC_{66}e_6]$$

$$P_6 = \frac{1}{35\overline{C}_{22}}[(F_i + 5C_{i3})f_i - 2mnC_{66}f_6]$$

For monoclinic layers, the result is

$$w(r) = A_1 r^{\lambda} + A_2 r^{-\lambda} + G_1 r + G_2 r^2 + G_3 r^3 + G_4 r^4 + G_5 r^5 + G_6 r^6 \qquad [2.35b]$$

where

$$\lambda = \sqrt{\frac{\overline{C}_{22}}{\overline{C}_{33}}}$$

$$G_1 = \frac{(\overline{C}_{12} - \overline{C}_{13})\varepsilon_o + F_i(\varepsilon_i^T + a_i) - 2mnC_{66}a_6}{\overline{C}_{33} - \overline{C}_{22}}$$

$$G_2 = \frac{(\overline{C}_{26} - 2\overline{C}_{36})\gamma_o + (C_{i3} + F_i)b_i - 2mnC_{66}b_6}{4\overline{C}_{33} - \overline{C}_{22}}$$

$$G_3 = \frac{(F_i + 2C_{i3})c_i - 2mnC_{66}c_6}{9\overline{C}_{33} - \overline{C}_{22}}$$

$$G_4 = \frac{(F_i + 3C_{i3})d_i - 2mnC_{66}d_6}{16\overline{C}_{33} - \overline{C}_{22}}$$

$$G_5 = \frac{(F_i + 4C_{i3})d_i - 2mnC_{66}e_6}{9\overline{C}_{33} - \overline{C}_{22}}$$

$$G_6 = \frac{(F_i + 5C_{i3})f_i - 2mnC_{66}f_6}{16\overline{C}_{33} - \overline{C}_{22}}$$

Equations [2.29], [2.30], [2.35a], and [2.35b] are the general solutions for the displacements of cylindrical lamina. The solution to a multilayered cylinder can now be found using the solution for the single lamina.

2.3.2 Application of Boundary Conditions

To fully solve a general N layered tube, the unknown constants in the solutions for the displacements must be solved. This gives 6 unknowns for each layer, E, F, ε_o, γ_o, A_1, and A_2. Therefore there are a total of 6N unknowns. These must be determined from the boundary and continuity conditions. Restating these conditions:

$$\sigma_r^{(1)}(r_o) = -P_i \qquad \sigma_r^{(N)}(r_N) = -P_o \qquad [2.36a,b]$$

$$\tau_{\theta r}^{(1)}(r_o) = 0 \qquad \tau_{\theta r}^{(N)}(r_N) = 0 \qquad [2.37a,b]$$

$$\tau_{xr}^{(1)}(r_o) = 0 \qquad \tau_{xr}^{(N)}(r_N) = 0 \qquad [2.38a,b]$$

$$\sigma_r^{(k)}(r_k) = \sigma_r^{(k+1)}(r_k) \qquad k = 1,2,...,N-1 \qquad [2.39]$$

$$\tau_{\theta r}^{(k)}(r_k) = \tau_{\theta r}^{(k+1)}(r_k) \qquad k = 1,2,...,N-1 \qquad [2.40]$$

$$\tau_{xr}^{(k)}(r_k) = \tau_{xr}^{(k+1)}(r_k) \qquad k = 1,2,...,N-1 \qquad [2.41]$$

$$u^{(k)}(r_k) = u^{(k+1)}(r_k) \qquad k = 1,2,...,N-1 \qquad [2.42]$$

$$v^{(k)}(r_k) = v^{(k+1)}(r_k) \qquad k = 1,2,..., N-1 \qquad [2.43]$$

$$w^{(k)}(r_k) = w^{(k+1)}(r_k) \qquad k = 1,2,...,N-1 \qquad [2.44]$$

Applying the shear stress-free boundary conditions, [2.37a,b] and [2.38a,b], we find that

$$E^{(1)} = E^{(N)} = 0$$

$$F^{(1)} = F^{(N)} = 0$$

from Equations [2.21] and [2.22]. Then from the continuity of shear tractions at the interfaces, [2.40] and [2.41], we find

$$E^{(k)} = F^{(k)} = 0 \quad k = 2,3,...,N-1$$

Therefore the $\tau_{\theta r}$ and τ_{xr} shear stresses, and, hence, σ_4 and σ_5, are zero through the thickness of the tube. The equations for the u and v displacements for the k^{th} layer reduce to

$$u^{(k)}(x,r) = \varepsilon_o^{(k)}x + \int (-n^{(k)}\varepsilon_4^{NL} + m^{(k)}\varepsilon_5^{NL})dr \qquad [2.45]$$

$$v^{(k)}(x,r) = \gamma_o^{(k)}rx + r\int \frac{(m^{(k)}\varepsilon_4^{NL} + n^{(k)}\varepsilon_5^{NL})}{r}dr \qquad [2.46]$$

In a later section, it will shown that ε_4^{NL} and ε_5^{NL} are zero throughout the tube due to the fact that σ_4 and σ_5 are zero. Therefore

$$u^{(k)}(x,r) = \varepsilon_o^{(k)}x \qquad [2.47]$$

$$v^{(k)}(x,r) = \gamma_o^{(k)}rx \qquad [2.48]$$

Applying the continuity of displacements at the interfaces of the layers to the u and v components

$$\varepsilon_o^{(k)}x = \varepsilon_o^{(k+1)}x$$

$$\gamma_o^{(k)} r_k x = \gamma_o^{(k+1)} r_k x$$

Therefore the values of ε_o and γ_o are identical in every layer. This means that the axial strain and the rotation per unit length are constant through the thickness of the tube, so

$$\varepsilon_o^{(k)} = \varepsilon_o$$

$$\gamma_o^{(k)} = \gamma_o$$

Then

$$u^{(k)}(x,r) = \varepsilon_o x \qquad [2.49]$$

$$v^{(k)}(x,r) = \gamma_o r x \qquad [2.50]$$

The remaining unknown constants are $A_1^{(k)}$, $A_2^{(k)}$, ε_o, and γ_o, or $2N+2$ constants. The remaining boundary conditions to be satisfied are equations [2.36a,b], [2.39], and [2.44]. These give 2N equations so two additional conditions are required. These are the integral force and torque equations

$$F_x = \int_0^{2\pi} \int_{r_o}^{r_N} \sigma_x(r) r dr d\theta$$

$$T_x = \int_0^{2\pi} \int_{r_o}^{r_N} \tau_{x\theta}(r) r^2 dr d\theta$$

or, written in terms of the stresses in the individual layers

$$F_x = 2\pi \sum_{k=1}^{N} \int_{r_{k-1}}^{r_k} \sigma_r^{(k)}(r) r dr \qquad [2.51]$$

$$T_x = 2\pi \sum_{k=1}^{N} \int_{r_{k-1}}^{r_k} \tau_{x\theta}^{(k)}(r) r^2 dr \qquad [2.52]$$

There are now a sufficient number of boundary conditions for a solution to be found.

2.3.3 Local / Global Stiffness Matrix Formulation

Rather than solving the 2N+2 equations by substituting the expression for the stresses and displacements into equations [2.36a,b], [2.39], [2.44], [2.51], and [2.52] and solving the resulting equations for $A_1^{(k)}$, $A_2^{(k)}$, ε_o, and γ_o, we will manipulate these equations with the objective of reducing the actual number of equations to be solved[16]. For simplicity define

$$w_k^+ = w^{(k)}(r_k) \quad w_k^- = w^{(k)}(r_{k-1})$$

$$\sigma_r^{(k)+} = \sigma_r^{(k)}(r_k) \quad \sigma_r^{(k)-} = \sigma_r^{(k)}(r_{k-1}).$$

Writing the expression for w_k^+ and w_k^- for transversely isotropic layers

$$w_k^+ = A_1^k r_k + \frac{A_2^k}{r_k} + P_1^k r_k \ln r_k + P_2^k r_k^2 + P_3^k r_k^3 + P_4^k r_k^6 + P_5^k r_k^5 + P_6^k r_k^6 \qquad [2.53a]$$

$$w_k^- = A_1^k r_{k-1} + \frac{A_2^k}{r_{k-1}} + P_1^k r_{k-1} \ln r_{k-1} + P_2^k r_{k-1}^2 + P_3^k r_{k-1}^3 + P_r^k r_{k-1}^4 + P_5^k r_{k-1}^5 + P_6^k r_{k-1}^6 \qquad [2.54a]$$

and for monoclinic layers

$$w_k^+ = A_1^k r_k^{\lambda_k} + \frac{A_2^k}{r_k^{\lambda_k}} + G_1^k r_k + G_2^k r_k^2 + G_3^k r_k^3 + G_4^k r_k^4 + G_5^k r_k r^5 + G_6^k r_k^6 \qquad [2.53b]$$

$$w_k^- = A_1^k r_{k-1}^{\lambda_k} + \frac{A_2^k}{r_{k-1}^{\lambda_k}} + G_1^k r_{k-1} + G_2^k r_{k-1}^2 + G_3^k r_{k-1}^3 + G_4^k r_{k-1}^4 + G_5^k r_{k-1}^5 + G_6^k r_{k-1}^6 \qquad [2.54b]$$

Solving these equations for A_1^k and A_2^k, we find

$$A_1^k = \frac{\frac{R_k^+}{r_{k-1}} - \frac{R_k^-}{r_k}}{\det_k}$$

$$A_2^k = \frac{r_k R_k^- - R_k^+ r_{k-1}}{\det_k}$$

where

$$\det_k = \frac{r_k}{r_{k-1}} - \frac{r_{k-1}}{r_k}$$

$$R_k^+ = w_k^+ - P_1^k r_k \ln r_k - P_2^k r_k^2 - P_3^k r_k^3 - P_4^k r_k^4 - P_5^k r_k^5 - P_6^k r_k^6$$

$$R_k^- = w_k^- - P_1^k r_{k-1} \ln r_{k-1} - P_2^k r_{k-1}^2 - P_3^k r_{k-1}^3 - P_4^k r_{k-1}^4 - P_5^k r_{k-1}^5 - P_6^k r_{k-1}^6$$

for transversely isotropic layers and

$$A_1^k = \frac{R_k^+ r_{k-1}^{-\lambda_k} - R_k^- r_k^{-\lambda_k}}{\det_k}$$

$$A_2^k = \frac{r_k^{\lambda_k} R_k^- - R_k^+ r_{k-1}^{\lambda_k}}{\det_k}$$

where

$$\det_k = \frac{r_k^{\lambda_k}}{r_{k-1}^{\lambda_k}} - \frac{r_{k-1}^{\lambda_k}}{r_k^{\lambda_k}}$$

$$R_k^+ = w_k^+ - G_1^k r_k - G_2^k r_k^2 - G_3^k r_k^3 - G_4^k r_k^4 - G_5^k r_k^5 - G_6^k r_k^6$$

$$R_k^- = w_k^- - G_1^k r_{k-1} - G_2^k r_{k-1}^2 - G_3^k r_{k-1}^3 - G_4^k r_{k-1}^4 - G_5^k r_{k-1}^5 - G_6^k r_{k-1}^6$$

for monoclinic layers. Expressing the normal radial stress in terms of the displacements using equations [2.14], [2.32], [2.49], and [2.50], we obtain

$$\sigma_r^k(r) = \bar{C}_{13}^k \varepsilon_o + \bar{C}_{23}^k \frac{w_k(r)}{r} + \bar{C}_{33}^k \frac{dw_k(r)}{dr} + \bar{C}_{36}^k \gamma_o r - (H_{13}^k \varepsilon_1^{NL} + H_{23}^k \varepsilon_2^{NL} + H_{63}^k \varepsilon_6^{NL} + \bar{C}_{33}^k \varepsilon_3^{NL}) \quad [2.55]$$

where

$$H_{1i} = \bar{C}_{1i} m^2 + \bar{C}_{2i} n^2 + 2mn\bar{C}_{6i}$$

$$H_{2i} = \bar{C}_{1i} n^2 + \bar{C}_{2i} m^2 - 2mn\bar{C}_{6i}$$

$$H_{6i} = mn(\bar{C}_{2i} - \bar{C}_{1i}) + (m^2 - n^2)\bar{C}_{6i}$$

If the expressions for A_1^k and A_2^k are substituted into the expressions for the radial displacement, w, which in turn is substituted into [2.55], we obtain an expression for the radial stress in the k^{th} layer in terms the radial displacements at the inner and outer radii of the layer. From this expression, we can easily write expressions for the interfacial tractions for each layer in terms of w_k^-, w_k^+, ε^o, and γ_o. In matrix form, these are

$$\begin{bmatrix} -\sigma_r^{k-} \\ \sigma_r^{k+} \end{bmatrix} = \begin{bmatrix} K_{11}^k & K_{12}^k & K_{13}^k & K_{14}^k \\ K_{21}^k & K_{22}^k & K_{23}^k & K_{24}^k \end{bmatrix} \begin{bmatrix} w_k^- \\ w_k^+ \\ \varepsilon_o \\ \gamma_o \end{bmatrix} - \begin{bmatrix} F_{NL}^{k-} + F_T^{k-} \\ F_{NL}^{k+} + F_T^{k+} \end{bmatrix} \quad [2.56]$$

where F_{NL}^{-} and F_{NL}^{+} contain all of the terms that contain the nonlinear constants a_i, b_i, c_i, d_i, e_i, and f_i, and F_T^{-} and F_T^{+} contain all of the terms that contain ε_i^T. K_{ij}^k is called the local stiffness matrix for a given layer, k. The expressions for these terms are given in Appendix A.

2.3.4 Assembly of Global Stiffness Matrix

The local stiffness matrices can be assembled into a global stiffness matrix by writing the traction equations at the inside surface, the interfaces between each layer, and the outside surface. For the inside surface

$$-\sigma_r^{1-} = P_i = K_{11}^1 w_o + K_{12}^1 w_1 + K_{13}^1 \varepsilon_o + K_{14}^1 \gamma_o - F_{NL}^{1-} - F_T^{1-}$$

For the k^{th} interface

$$\sigma_r^{k+} = K_{21}^k w_{k-1} + K_{22}^k w_k + K_{23}^k \varepsilon_o + K_{24}^k \gamma_o - F_{NL}^{k+} - F_T^{k+}$$

$$-\sigma_r^{(k+1)-} = K_{11}^{k+1} w_k + K_{12}^{k+1} w_{k+1} + K_{13}^{k+1} \varepsilon_o + K_{14}^{k+1} \gamma_o - F_{NL}^{(k+1)-} - F_T^{(k+1)-}$$

For the outside surface

$$\sigma_4^{N+} = -P_o = K_{21}^N w_{N-1} + K_{22}^N w_N + K_{23}^N \varepsilon_o + K_{24}^N \gamma_o - F_{NL}^{N+} - F_T^{N+}$$

The three resulting forms of the traction equations are:

for the inside surface

$$K_{11}^1 w_o + K_{12}^1 w_1 + K_{13}^1 \varepsilon_o + K_{14}^1 \gamma_o = P_i + F_T^{1-} + F_{NL}^{1-} \qquad [2.57]$$

for the k^{th} interface

$$K_{21}^{k}w_{k-1} + (K_{22}^{k} + K_{11}^{k+1})w_k + K_{12}^{k+1}w_{k+1} + (K_{23}^{k} + K_{13}^{k+1})\varepsilon_o + (K_{24}^{k} + K_{14}^{k+1})\gamma_o = (F_T^{k+} + F_T^{(k+1)-}) + (F_{NL}^{k+} + F_{NL}^{(k+1)-}) \quad [2.58]$$

and for the outside surface

$$K_{21}^{N}w_{N-1} + K_{22}^{N}w_N + K_{23}^{N}\varepsilon_o + K_{24}^{N}\gamma_o = -P_o + F_T^{N+} + F_{NL}^{N+} \quad [2.59]$$

where

$$w_k = w_k^+ = w_{k+1}^-$$

$$\sigma_r^{k+} - \sigma_r^{(k+1)-} = 0$$

In addition to these equations the integral force and torque equations must be included. In general, each of these equations will have coefficients of all of the interfacial displacements, w_k (k=0,1,...,N), ε_o, and γ_o as well as pseudo force terms due to the nonlinearities and a "force" due to a change in temperature. The integral force equation will be of the form

$$\sum_{k=0}^{N}\Phi_k w_k + \Phi_{N+1}\varepsilon_o + \Phi_{N+2}\gamma_o = F_x + F_{NL}^F + F_T^F \quad [2.60]$$

and the integral torque equation will be

$$\sum_{k=0}^{N}\Psi_k w_k + \Psi_{N+1}\varepsilon_o + \Psi_{N+2}\gamma_o = T_x + F_{NL}^T + F_T^T. \quad [2.61]$$

For example, consider an arbitrary 3 layer tube. Assembly of the global stiffness matrix yields:

$$\begin{bmatrix} K_{11}^1 & K_{12}^1 & 0 & 0 & K_{13}^1 & K_{14}^1 \\ K_{21}^1 & (K_{22}^1 + K_{11}^2) & K_{12}^2 & 0 & (K_{23}^1 + K_{13}^2) & (K_{24}^1 + K_{14}^2) \\ 0 & K_{21}^2 & (K_{22}^2 + K_{11}^3) & K_{12}^3 & (K_{23}^2 + K_{13}^3) & (K_{24}^2 + K_{14}^3) \\ 0 & 0 & K_{21}^3 & K_{22}^3 & K_{23}^3 & K_{24}^3 \\ \Phi_0 & \Phi_1 & \Phi_2 & \Phi_3 & \Phi_{N+1} & \Phi_{N+2} \\ \Psi_0 & \Psi_1 & \Psi_2 & \Psi_3 & \Psi_{N+1} & \Psi_{N+2} \end{bmatrix} \begin{bmatrix} w_o \\ w_1 \\ w_2 \\ w_3 \\ \varepsilon_o \\ \gamma_o \end{bmatrix} =$$

$$\begin{bmatrix} P_I \\ 0 \\ 0 \\ -P_o \\ F_x \\ T_x \end{bmatrix} + \begin{bmatrix} F_T^{1-} \\ F_T^{1+} + F_T^{2-} \\ F_T^{2+} + F_T^{3-} \\ F_T^{3+} \\ F_T^F \\ F_T^T \end{bmatrix} + \begin{bmatrix} F_{NL}^{1-} \\ F_{NL}^{1+} + F_{NL}^{2-} \\ F_{NL}^{2+} + F_{NL}^{3-} \\ F_{NL}^{3+} \\ F_{NL}^F \\ F_{NL}^T \end{bmatrix} \qquad [2.62]$$

or in short-hand notation

$$[M]\{W\} = \{\bar{F} + \bar{F}_{NL} + \bar{F}_T\} \qquad [2.63]$$

where

$[M]$ = global stiffness matrix

$\{W\} = \{w_o \; w_1 \; w_2 \ldots w_N \; \varepsilon_o \; \gamma_o\}^T$

$\{\bar{F}\} = \{P_I \, 0 \ldots 0 \; -P_o \, F_x \, T_x\}^T$

$\{\bar{F}_{NL}\}$ = global nonlinear force vector

$\{\bar{F}_T\}$ = global force vector due to temperature changes

This system of equations consists of N+3 equations that must be solved for the radial displacements at the interfaces, w_k, the axial strain, ε_o, and the rotation per unit length, γ_o . For a large number of layers, the local/global stiffness matrix scheme offers a nearly 50% reduction in the number of equations to be solved.

2.4 *Endochronic Theory*

The Endochronic Theory is a nonlinear constitutive model based on irreversible thermodynamics. It uses the concept of internal variables and is centered around a deformation scale (or intrinsic time scale) which is a material property. The deformation scale can either be dependent or independent of time. For this investigation, it will be assumed that the deformation scale is independent of time. This theory was developed by Valanis[17] [18] to describe such phenomena as cross-hardening in tension due to torsion and formation of hysteresis loops during loading and unloading cycles in isotropic materials. This theory was later extended to include anisotropic materials by Pindera and Herakovich[19]. A set of constitutive relations to model the in-plane behavior of transversely isotropic materials was obtained as a special case from the three dimensional formulation in order to correlate the theory with experimental data. The three dimensional relations developed by Pindera and Herakovich were subsequently incorporated into a three dimensional finite element model by Mathison, et al.,[20] to examine the behavior of compression-loaded laminates with a hole.

The equations used by Mathison, et al., are (without change):

$$\varepsilon_1 = A_{1j}\sigma_j \pm B_{11}|\sigma_1|^{n_1} \qquad [2.64a]$$

$$\varepsilon_2 = A_{2j}\sigma_j + \int_0^z B_{22}^{\circ}(z - z')^{n_2} \frac{\partial \sigma_2}{\partial z'} dz' \qquad [2.64b]$$

$$\varepsilon_3 = A_{3j}\sigma_j + \int_0^z B_{22}^{\circ}(z - z')^{n_2} \frac{\partial \sigma_3}{\partial z'} dz' \qquad [2.64c]$$

$$\varepsilon_4 = A_{4j}\sigma_j + \frac{1}{2}\int_0^z B_{22}^{\circ}(z - z')^{n_2} \frac{\partial \sigma_4}{\partial z'} dz' \qquad [2.64d]$$

$$\varepsilon_5 = A_{5j}\sigma_j + \int_0^z B_{66}^{\circ}(z - z')^{n_6} \frac{\partial \sigma_5}{\partial z'} dz' \qquad [2.64e]$$

$$\varepsilon_6 = A_{6j}\sigma_j + \int_0^z B_{66}^{\circ}(z - z')^{n_6} \frac{\partial \sigma_6}{\partial z'} dz' \qquad [2.64f]$$

where B_{11}, B_{22}°, B_{66}°, n_1, n_2, and n_6 are nonlinear material constants, A_{ij} are initial compliances of the material, z' is the variable of integration and

$$dz = \sqrt{S_{ij} d\sigma_i d\sigma_j}$$

and S_{ij} is a fourth order positive definite tensor whose components are material properties. B_{22}° and B_{66}° are constants pertaining to the dissipative type nonlinear response. B_{11} , on the other hand, describes the reversible nonlinear behavior in the fiber direction.

Recalling from the previous section, it was found that $\tau_{xr} = \tau_{\theta r} = 0$ throughout the thickness of the tube. Transforming these stresses to the principal material coordinates system, it can be shown that $\sigma_4 = 0$ and $\sigma_5 = 0$ throughout the thickness of the tube also. Extracting the nonlinear portion of the strain from equations [2.64d] and [2.64e]

$$\varepsilon_4^{NL} = \frac{1}{2}\int_0^z B_{22}^o (z - z')^{n_2} \frac{\partial \sigma_4}{\partial z'}\, dz'$$

$$\varepsilon_5^{NL} = \int_0^z B_{66}^o (z - z')^{n_6} \frac{\partial \sigma_5}{\partial z'}\, dz'$$

Since $\sigma_4 = \sigma_5 = 0$,

$$\frac{\partial \sigma_4}{\partial z'} = \frac{\partial \sigma_5}{\partial z'} = 0$$

therefore

$$\varepsilon_4^{NL} = \varepsilon_5^{NL} = 0$$

which is the result that was used in the previous section. Also, because $\sigma_4 = \sigma_5 = 0$, the elastic portion of the strains in Equations [2.64d] and [2.64e] are zero, therefore, the total strains, ε_4 and ε_5 are zero. Restating the endochronic constitutive equations

$$\varepsilon_1 = A_{1j}\sigma_j \pm B_{11}|\sigma_1|^{n_1} \qquad [2.65a]$$

$$\varepsilon_2 = A_{2j}\sigma_j + \int_0^z B_{22}^o (z - z')^{n_2} \frac{\partial \sigma_2}{\partial z'}\, dz' \qquad [2.65b]$$

$$\varepsilon_3 = A_{3j}\sigma_j + \int_0^z B_{22}^o (z - z')^{n_2} \frac{\partial \sigma_3}{\partial z'} dz' \qquad [2.65c]$$

$$\varepsilon_4 = 0 \qquad [2.65d]$$

$$\varepsilon_5 = 0 \qquad [2.65e]$$

$$\varepsilon_6 = A_{6j}\sigma_j + \int_0^z B_{66}^o (z - z')^{n_6} \frac{\partial \sigma_6}{\partial z'} dz' \qquad [2.65f]$$

Because the deformation scale, z, is a function of the loading history, which is, in general, complex, equations [2.65a-f] cannot be integrated exactly. Therefore, for these equations to be used in an numerical model, they must be integrated incrementally. The incremental form of the expression for ε_6 was derived by Mathison,et al.,[20] as follows:

$$\varepsilon_6^N = -\frac{\partial G_o}{\partial \sigma_6} + \frac{B_{66}^o}{(n_6 + 1)} \sum_{k=1}^{N} S6_k \left[(z_n - z_{k-1})^{n_6+1} - (z_n - z_k)^{n_6+1} \right] \qquad [2.66]$$

where

$$-\frac{\partial G_o}{\partial \sigma_6} = A_{6j}\sigma_j$$

$$S6_k = \left.\frac{\partial \sigma_6}{\partial z}\right|_k \simeq \frac{\Delta \sigma_6}{\Delta z_k} \qquad k = 1,2, \ldots ,N$$

$$z_N = \sum_{k=1}^{N} \Delta z_k$$

$$\Delta z_k = \sqrt{S_{ij}\Delta\sigma_i^k\Delta\sigma_j^k} \qquad (\text{k not summed})$$

$$N \equiv \text{number of increments}$$

The incremental forms for ε_2 and ε_3 are similar to equation [2.66].

2.5 *Failure*

For a complete investigation of the effect of combined thermomechanical loading on the global response of composite tubes, the prediction of failure within the tube using an existing failure criteria is desired. Three failure theories were evaluated for incorporation into the analytical model: Maximum Stress Theory, Tsai-Hill Theory, and Tsai-Wu Theory. Because consideration for interaction between the different stress components and for the difference in magnitudes of ultimate stresses in tension and compression are desired, the Tsai-Wu Theory was selected for use in the analytical model.

According to Tsai and Wu[21], failure will occur when

$$F_i\sigma_i + F_{ij}\sigma_i\sigma_j = 1 \quad i,j = 1,2,3,\ldots,6$$

where contracted notation has been used. F_i and F_{ij} are second and fourth order tensors respectively that are functions of the ultimate strengths of the material:

$$F_1 = \frac{1}{X_T} + \frac{1}{X_C}$$

$$F_2 = F_3 = \frac{1}{Y_T} + \frac{1}{Y_C}$$

$$F_4 = F_5 = F_6 = 0$$

$$F_{11} = -\frac{1}{X_T X_C}$$

$$F_{22} = F_{33} = -\frac{1}{Y_T Y_C}$$

$$F_{66} = \frac{1}{S^2}$$

$$F_{44} = F_{55} = 0$$

where X_T and X_C are the tensile and compressive strengths in the fiber direction, Y_T and Y_C are the tensile and compressive strengths in the transverse direction, and S is the in-plane shear strength. For the purpose of this investigation, the coupling terms, F_{12}, F_{13}, and F_{23}, will be neglected. This failure theory employs the stresses at a given point in the tube to predict failure, therefore, the prediction of failure using this theory in the analysis of tubes will only yield individual ply failures rather that the total failure of the tube.

2.6 *Numerical Procedure*

2.6.1 Approximation of $\varepsilon_i^{NL}(r)$

As stated in an earlier section, the nonlinear strains, $\varepsilon_i^{NL}(r)$, are approximated by a fifth order polynomial,

$$\varepsilon_i^{NL}(r) = a_i + b_i r + c_i r^2 + d_i r^3 + e_i r^4 + f_i r^5$$

in each layer. The unknown coefficients will be evaluated using the Least Squares Method (see Appendix B). This method requires that strains at six points within each layer must be known. Therefore each layer must be divided up into five or more sublayers of the same fiber orientation. This facilitates the calculation of $\varepsilon_i^{NL}(r)$ at each of the interfaces of the sublayers and, hence, permits the calculations of the unknown coefficients of the polynomial.

2.6.2 Iterative Technique

Many techniques for solving a system of nonlinear equations are currently in use including incremental procedures, iterative procedures, and step-iterative or mixed procedures[20]. For the solution of this problem, a step-iterative scheme was chosen. This scheme is simply a combination of an incremental procedure and a functional iterative procedure.

The functional iterative technique starts with an initial estimate for the displacements, {W}, and performs the following iteration procedure:

$$[M]\{W^{(r)}\} = \{F\} + \{F^T\} + \{F^{NL}(\{W^{(r-1)}\})\}$$

where r represents the iteration number. The iteration is continued until the solution of two successive iterations satisfies the convergence criteria.

The incremental procedure breaks the total load applied into finite increments. For each load increment, the functional iteration technique is performed to arrive at a solution for each load increment.

The global stiffness matrix, [M], contains only linear terms. Therefore it need only be decomposed once for the entire loading cycle. All of the nonlinear terms are contained in the pseudo force vector $\{F_{NL}\}$, therefore only the right-hand side of the equation must be changed from one iteration to the next.

A technique called scaled partial pivoting is used to solve the system of equations at each iteration. This technique is suitable for the case where the same stiffness matrix is used with

many force vectors as is the case in this situation. This procedure utilizes Gaussian elimination in which rows are interchanged and scaled in order to pivot from a position that will cause the least numerical roundoff errors. The elimination procedure is performed once on the global stiffness matrix, [M]. The row interchanges are stored, and at each iteration, they can be performed on the force vector. A solution for the displacements is then obtained from a back substitution procedure. This technique offers a significant savings in computing time over inversion of the stiffness matrix and subsequent multiplication with the force vector at each iteration[22].

The procedure that is followed in the step-iterative scheme is the constant stress formulation. For this formulation, the iterations are performed at essentially a constant stress level and the corresponding strains and displacements are determined for each load step. The iterative procedure followed for the constant stress formulation is as follows:

1. The system of equations is solved for w, ε_o, and γ_o.

2. Convergence of solution is checked.

3. The global strains, ε_x, ε_θ, ε_r, and $\gamma_{x\theta}$ are calculated from the radial displacements, ε_o and γ_o using equations [2.14a], [2.14b], [2.14c], and [2.14f].

4. The global strains are transformed into the principal material coordinates, and the stress in the principal material coordinates are determined from the constitutive equations, Equation [2.4a], using the nonlinear strains, $\varepsilon_i^{NL}(r)$, from the previous iteration.

5. The stress increments are determined from the difference of the current value of stress and the converged value from the previous iteration.

6. The nonlinear strains are calculated from the stress increments.

7. The nonlinear strains in each layer are approximated by fifth order polynomial.

8. The pseudo force vector, $\{F_{NL}\}$, is calculated from the nonlinear strains

This sequence is repeated until convergence of the solution is attained. A flow chart for the computer program is shown in Figure 2

2.7 *Program Verification*

In addition to performing the nonlinear tube analysis, the program developed is also capable of linear analysis. To verify the results obtained using the local/global stiffness formulation, the results obtained from the linear portion of the program developed for this study were compared with results obtained from the computer program developed by Rousseau, et al[13].

An arbitrary unsymmetric, unbalanced laminate with a stacking sequence of $[10/45/-30/60/0/-15/5/-75/90/50/-60/30/0/-25/82]_T$ was selected. The material used for this analysis was AS4/3502 graphite/epoxy (using the material properties given by Mathison, et al.,[20]). A general loading including all types of loading was chosen. The applied loads are:

$$F_x = 10000 \text{ lb.}$$
$$T_x = 1500 \text{ in-lb.}$$
$$P_i = 225 \text{ psi}$$
$$P_o = 100 \text{ psi}$$
$$\Delta T = -100°F$$

A comparison of the distribution of stresses through the thickness is shown in Figure 3 through Figure 6. There are no differences in the results from the two models.

To verify the nonlinear portion of the program, a pure shear state can be used as a test case

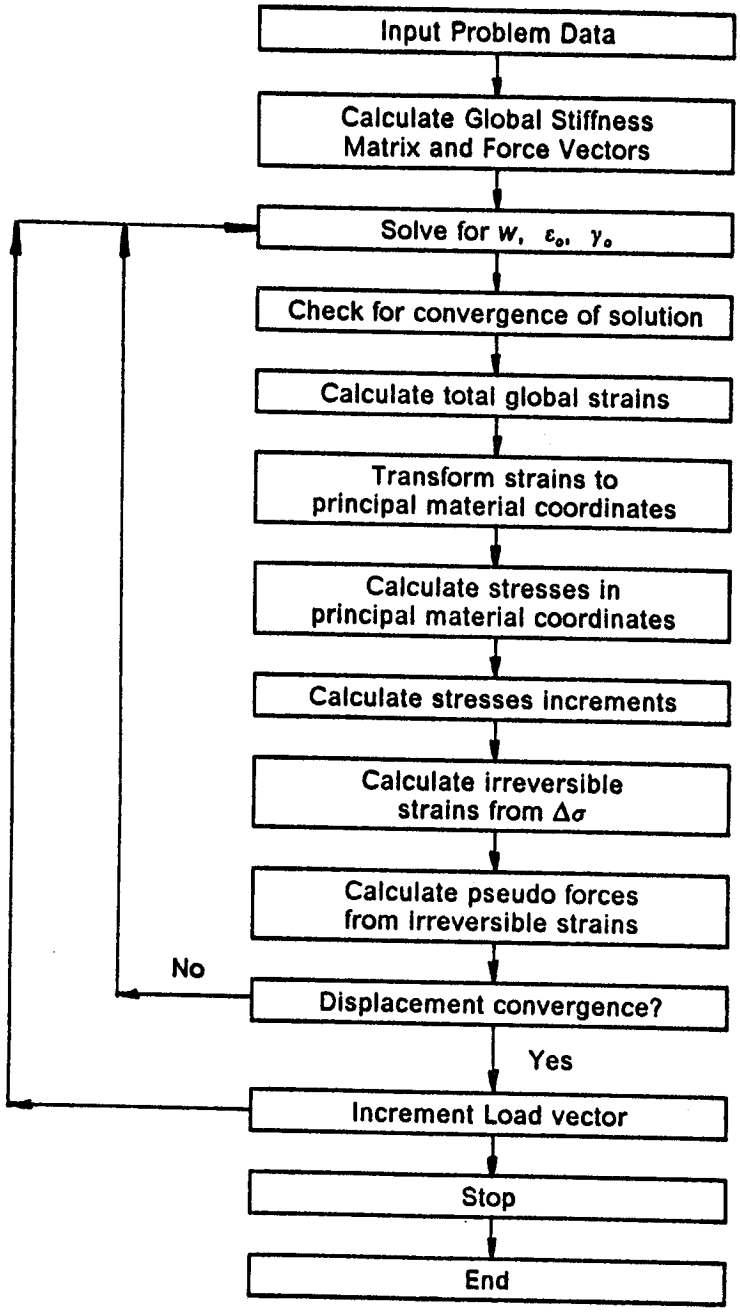

Figure 2. Flow chart for Computer Program

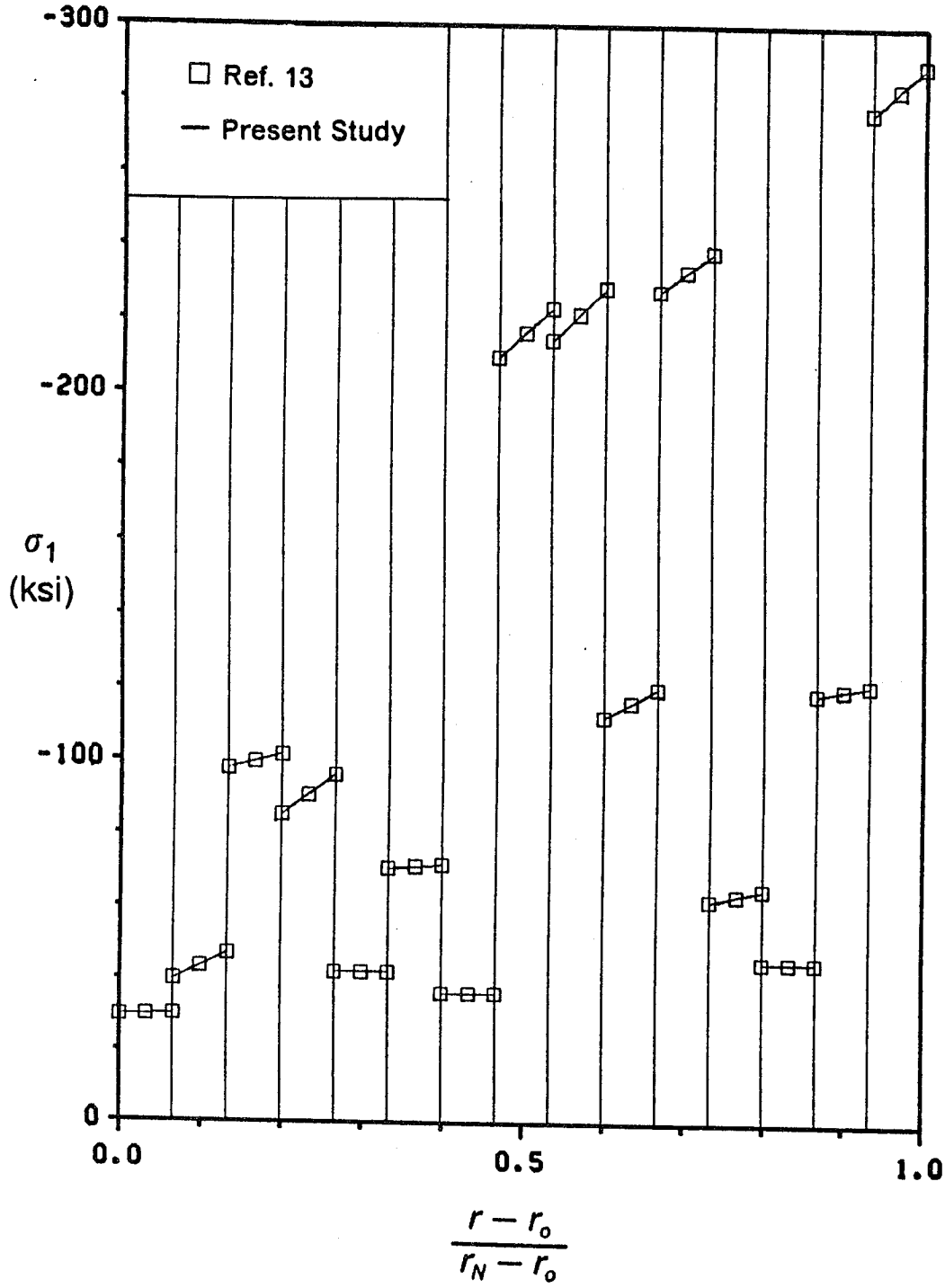

Figure 3. Verification of σ_1

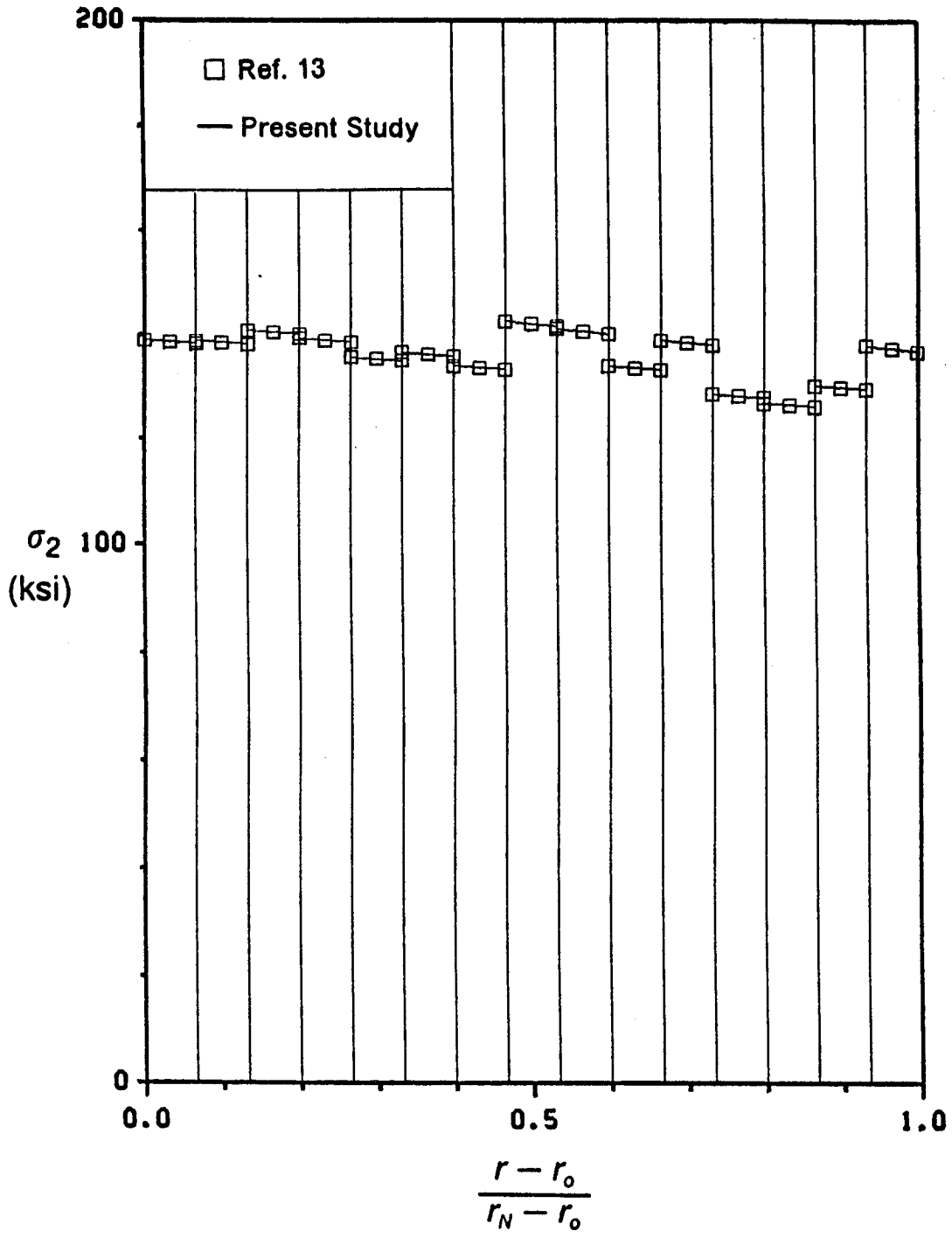

Figure 4. Verification of σ_2

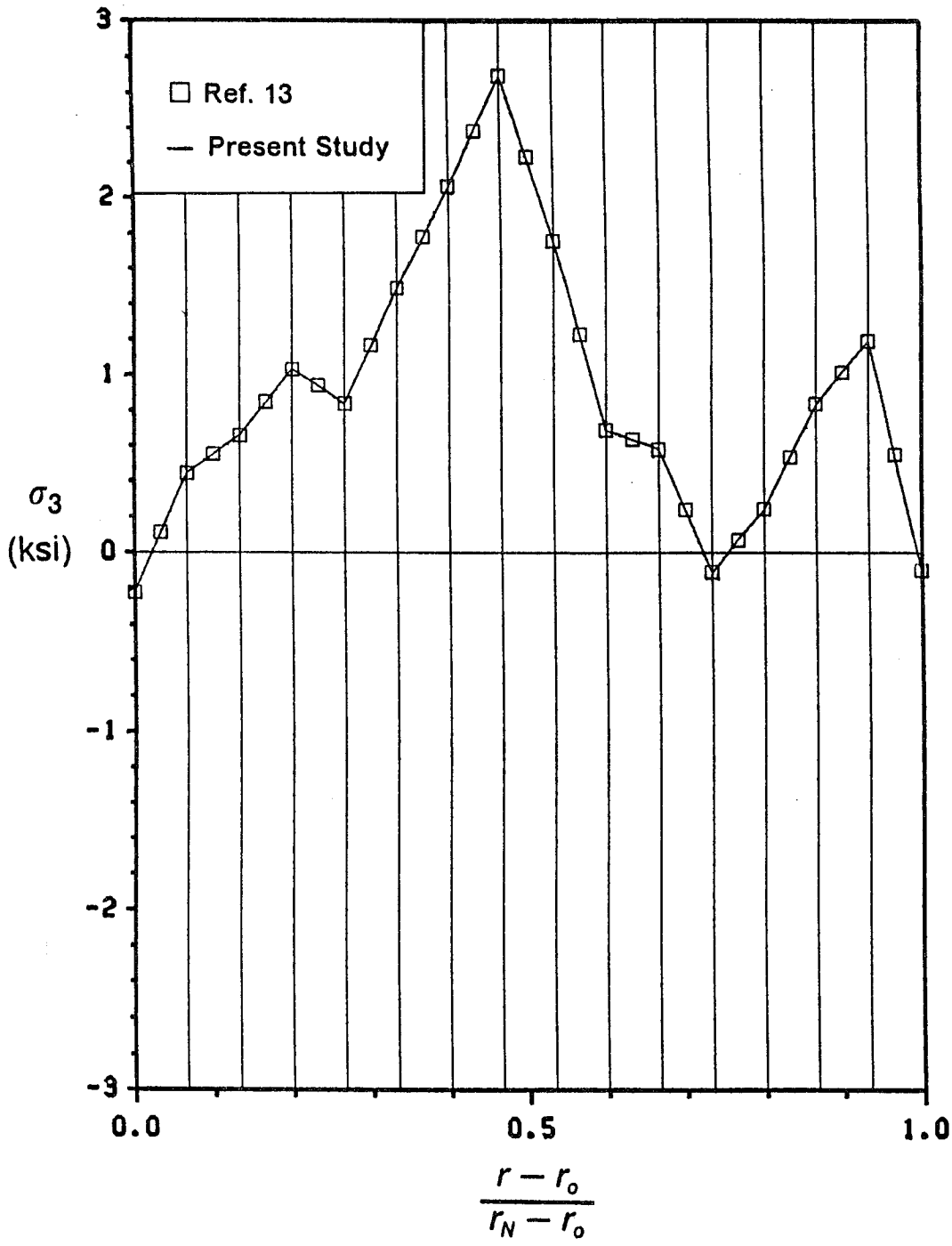

Figure 5. Verification of σ_3

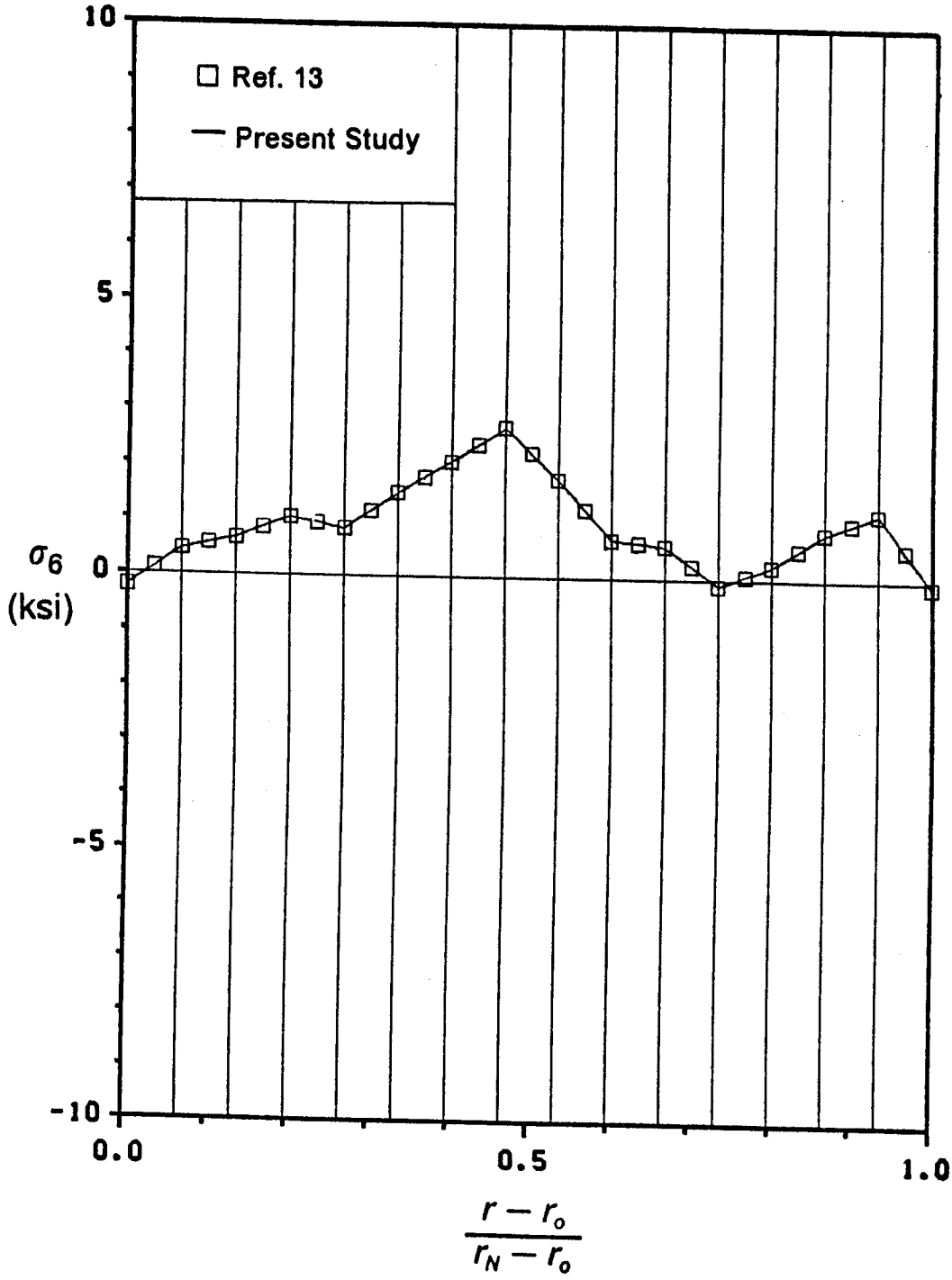

Figure 6. Verification of σ_6

$$\sigma_6 \neq 0$$
$$\sigma_i = 0, \quad i = 1,2,3,4,5.$$

For the pure shear state, Equation [2.64f] can be integrated exactly

$$\varepsilon_6 = A_{6j}\sigma_j + \int_0^z B_{66}(z - z')^{n_6} \frac{\partial \sigma_6}{\partial z'} dz'$$

where

$$\begin{aligned} dz &= \sqrt{S_{ij} d\sigma_i d\sigma_j} \\ &= \sqrt{S_{66}}\, d\sigma_6 \end{aligned} \qquad [2.67]$$

therefore

$$\begin{aligned} \frac{\partial \sigma_6}{\partial z} &= \frac{d\sigma_6}{dz} \\ &= \frac{1}{\sqrt{S_{66}}} \end{aligned}$$

Substituting for $\frac{\partial \sigma_6}{\partial z}$ in Equation [2.64f]

$$\varepsilon_6 = A_{6j}\sigma_j + \int_0^z \frac{B_{66}^o (z - z')^{n_6}}{\sqrt{S_{66}}} dz'$$

$$\varepsilon_6 = A_{6j}\sigma_j + \frac{B_{66}^o z^{n_6+1}}{\sqrt{S_{66}}\,(n_6 + 1)} \qquad [2.68]$$

Integrating Equation [2.67], we have $z = \sqrt{S_{66}}\,\sigma_6$. Substituting for z into Equation [2.68]

$$\varepsilon_6 = A_{6j}\sigma_j + \frac{B^o_{66}(S_{66})^{\frac{n_6}{2}}}{(n_6+1)}\sigma_6^{n_6+1}. \qquad [2.69]$$

The shear strains can now be determined for any shear stress.

A state of pure shear can be attained in a tube by applying pure torsion to a tube in which all of the layers are aligned with the fibers in the axial direction (0°). Comparing the analysis of a 0° tube in pure torsion with results from Equation [2.69], the analytical model can be verified for the nonlinear analysis of tubes. These results are shown in Figure 7.

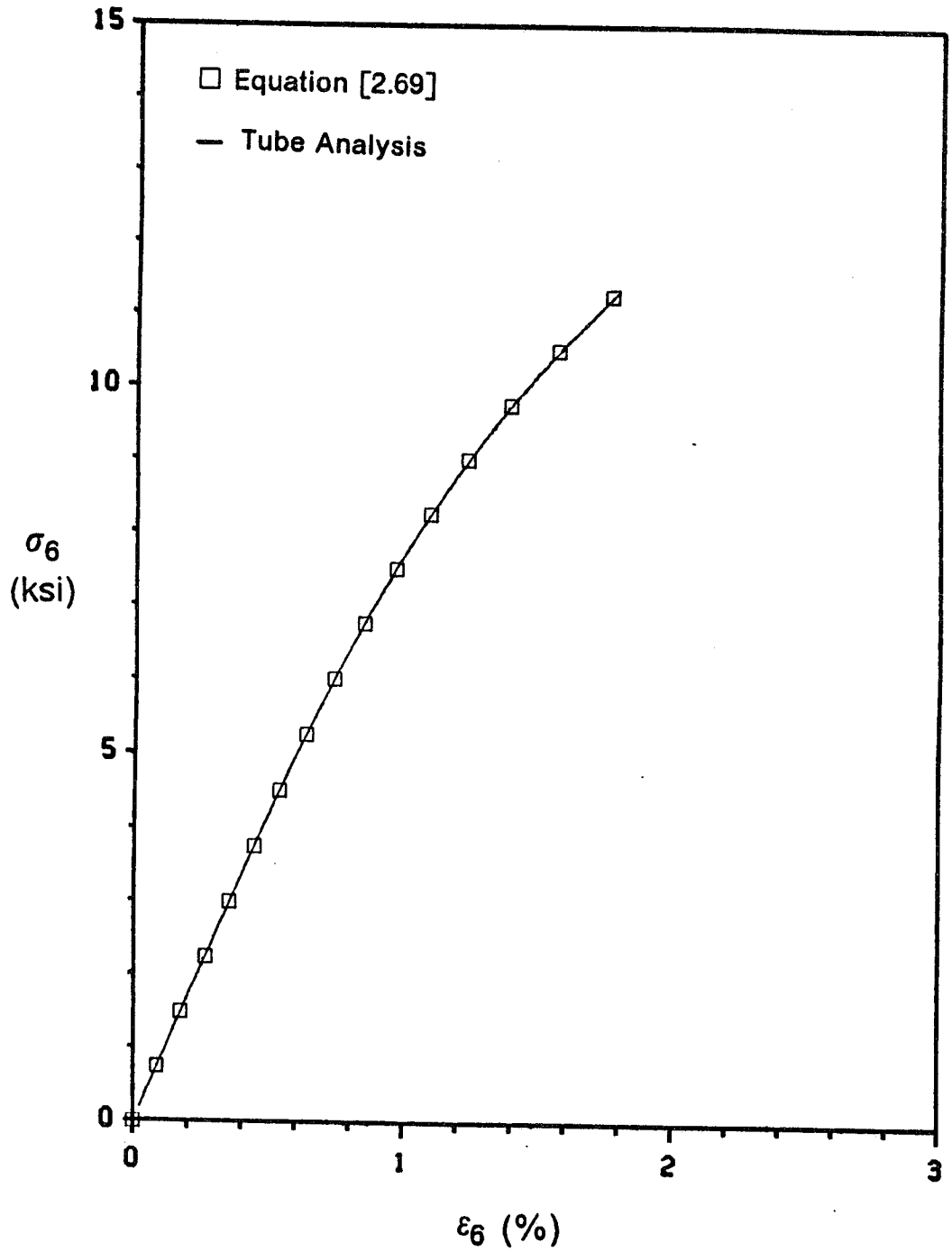

Figure 7. Nonlinear Program Verification

3.0 Experimental Procedure

3.1 Introduction

The experimental program consists of a series of flat coupon tests followed by biaxial tests on composite tubes. The flat coupon tests are comprised of a set of off-axis tension and compression tests and Iosipescu shear tests on coupons cut from a flat, 12 ply unidirectional panel made from P75/934 graphite/epoxy. The results of these tests will be used to generate material parameters that will subsequently be used in the analytical model to predict the response of the composite tubes. The laminated tubes will then be tested in combined axial and torsional loading, and the results will be compared with predictions of the model. The extent of the test program on the laminated tubes was limited because fewer tubes were available than initially planned for. A test fixture was also developed for the application of combined loading. The description of the design of the test fixture will be included in this chapter.

3.2 *Test Plan*

3.2.1 Material Characterization

The test matrix for the tests performed on the flat coupons is shown in Table 1. The material used in this study will be assumed to be transversely isotropic so there are five elastic properties to be determined: E_{11}, E_{22}, ν_{12}, ν_{23}, and G_{12}. The off-axis tension tests were performed to determine the in-plane material properties in tension and shear. Fiber orientations of 0° and 90° were used to determine the axial and transverse Young's moduli as well as the Poisson's ratio, ν_{12}. Fiber orientations of 10° and 45° were used to determine the axial shear modulus, G_{12}. The 45° orientation provides the most accurate prediction of the shear modulus while the 10° orientation gives a measure of the effect of the interaction of the σ_1 and σ_2 stress components on the shear response of the material. These tests were also used to determine the ultimate strengths of the material in tension.

The off-axis compression tests were performed to characterize the in-plane material response in compression. Three fiber orientations were tested: 0°, 45°, and 90°. The ultimate strengths in compression were also determined.

The Iosipescu tests were performed to characterize the in-plane shear response of the material under nearly pure shear conditions. The results from these tests will be compared with the 10° and 45° off-axis tests. Fiber orientations of 0° and 90° were used for the Iosipescu tests.

To supplement the tests performed on the flat coupons, tests were performed on unidirectional tubes. The test matrix for these tubes is shown in Table 2. Tubes with fiber orientations of 0°, 45°, and 90° were tested as a comparison for the flat panel tests.

Table 1. Flat Coupon Test Matrix

Test Type	Fiber Orientation	Number of Specimens
Tension	0° 10° 45° 90°	3 3 3 3
Compression	0° 45° 90°	3 3 3
Iosipescu	0° 90°	3 6

Table 2. Unidirectional Tube Test Matrix.

Tube No.	Type of Loading
0-01 0-02 0-03	Tension * Torsion
45-01 45-02 45-03	Torsion * Tension
90-01 90-02 90-03	** Torsion, Tension *** Torsion, Compression ***

* Received in damaged condition

** Failed in test fixture prior to testing

*** Two tests accomplished by performing first test well below failure load then performing second test.

3.2.2 Laminated Tube Tests

The laminated tube tests were performed on seven tubes with stacking sequences of $[15/0/\pm 10/0/-15]_s$. Four of the seven tubes had been thermally cycled between -150°F and +150°F for 3000 cycles prior to testing while three had not. The response to pure axial loading (tension or compression) was found to be linear to failure in preliminary tests performed on laminated tubes. The pure torsion response, on the other hand, was nonlinear. Because the nonlinear effects are of primary interest, the emphasis on the tests on the laminated tubes will be in pure torsion and torsion dominated biaxial loading. The seven tubes were tested using four different loading types:

Type I Loading Monotonic negative torsion to failure

Type II Loading Cyclic positive to negative torsion. The magnitude of torque is increased with each successive cycle.

Type III Loading Combined Loading - tension/positive torsion. The tension and torque are increased proportionally to a specified magnitude then unloaded proportionally. Pure torsion is applied to the same magnitude then pure tension is applied. Finally the tube in unloaded proportionally. The ratio of torque to tension is 1.73:1. This procedure is repeated with increasing magnitudes of loads.

Type IV Loading Combined Loading - compression/negative torsion. The same loading sequence as Type III is used except it is loaded in compression and negative torsion rather that tension and positive torsion. This procedure is also repeated with increasing magnitudes of loads.

Figure 8 shows the loading sequences used for each type. The test matrix for the laminated tubes is shown in Table 3. Table 4 through Table 6 show the magnitudes of the loads applied for Types II, III and IV. The designation for the tubes will be in the form LMXYY where

- LM defines the stacking sequence as $[15/0/\pm 10/0/-15]_s$
- X = C represents a thermally cycled tube
- X = B represents a baseline tube (no thermal cycling)
- YY is a sequential numbering of the tubes

3.3 *Material*

The material system chosen for this study consists of a P75 graphite fiber made by Amoco preimpregnated in a matrix of Fiberite 934 epoxy. The P75 fiber is a high modulus fiber, and the 934 epoxy is a standard epoxy used in many aerospace applications. Prior to this study, only some preliminary material properties for the linear region were available so the material system was characterized for the in-plane material properties in both the linear and nonlinear regions before conducting the biaxial tests on the laminated tubes.

3.3.1 Panel Configuration

For the purpose of characterizing the material, flat panels were fabricated using a 12 ply unidirectional layup of the P75/934 graphite/epoxy. The 12 ply configuration was chosen to

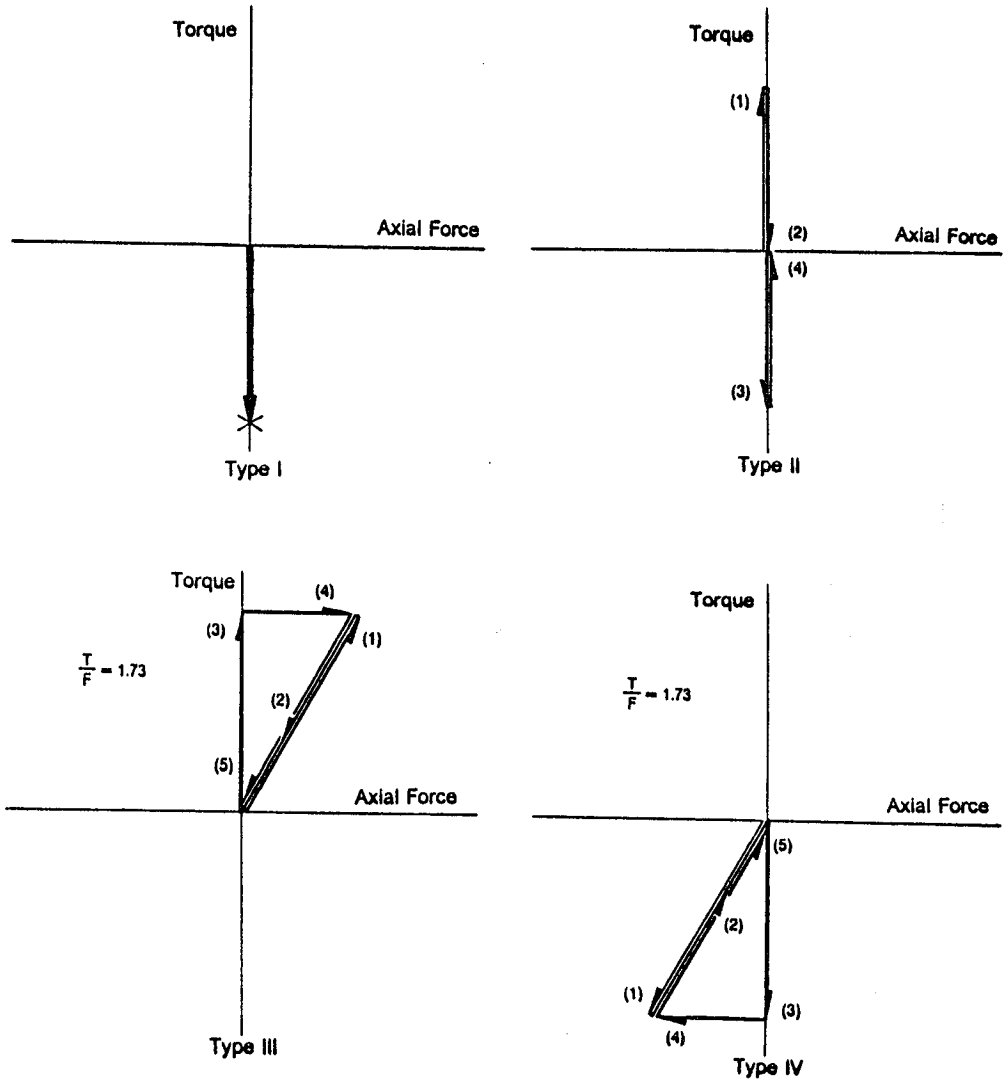

Figure 8. Load Sequences

Table 3. Laminated Tube Test Matrix

Tube	Condition	Load Type
LMB01	Baseline	IV
LMB02	Baseline	II
LMB04	Baseline	II
LMC05	Thermally Cycled	II
LMC06	Thermally Cycled	III
LMC07	Thermally Cycled	IV
LMC08	Thermally Cycled	I

Table 4. Load Magnitudes - Type II Loading

Tube	Cycle #	Torque (in-lb)
LMB02	1 2 3 4	1500 2500 3500 4500
LMB04	1 2	2500 3500
LMC05	1 2 3	1500 2500 3500

Table 5. Load Magnitudes - Type III Loading

Tube	Cycle #	Axial (lb)	Torque (in-lb)
LMC06	1	640	1160
	2	815	1410
	3	965	1660
	4	1105	1910
	5	1250	2160
	6	1400	2410
	7	1535	2660
	8	1680	2910
	9	1825	3160
	10	1970	3410
	11	2113	3660
	12	2402	4160
	13	2546	4410

Table 6. Load Magnitudes - Type IV Loading

Tube	Cycle #	Axial (lb)	Torque (in-lb)
LMB01	1	-640	-1160
	2	-815	-1410
	3	-965	-1660
	4	-1105	-1910
	5	-1250	-2160
	6	-1400	-2410
	7	-1535	-2660
LMC07	1	-640	-1160
	2	-815	-1410
	3	-965	-1660
	4	-1105	-1910
	5	-1250	-2160
	6	-1400	-2410
	7	-1535	-2660
	8	-1680	-2910

match the thickness of the tubes. The average thickness for the panels was measured to be 0.065".

Micrographs of the panel's cross section were taken to measure the volume fraction of the panels as well as to examine the distribution of the fibers in the matrix. A micrograph is shown in Figure 9. The fibers are evenly distributed through the thickness, and the ply boundaries are not distinguishable except for a few locations. The volume fraction of the panels were determined from the micrographs using an optical technique[23]. This technique yielded 65% for the fiber volume fraction.

3.3.2 Tube Configuration

The tubes used in this study are those that have been proposed by NASA for the truss structure of the Space Station. These tubes have been constructed from P75/934 graphite/epoxy with a stacking sequence of $[15/0/\pm 10/0/-15]_s$. The nominal inside diameter of the tubes is two inches with a twelve ply construction giving a wall thickness of approximately 0.060". For the purposes of this test program the tubes have been cut to a length of ten inches. In addition to the $[15/0/\pm 10/0/-15]_s$ configuration, which will hereafter be referred to as the "laminated tubes", unidirectional tubes were also constructed in fiber orientations of 0°, 45°, and 90° as mentioned earlier.

The tubes that were employed in this experimental program were obtained from two sources: Boeing Aerospace and Morton Thiokol. The tubes constructed by Boeing were primarily used for preliminary testing to evaluate the newly developed test fixture to be discussed in Section 3.4.3.4, while the tubes made by Morton Thiokol were used to obtain the results presented in Section 4.3. The manufacturing techniques employed by the two suppliers were somewhat different. The tubes made by Boeing Aerospace were fabricated using a unidirectional tape layup on a male mandrel. In addition, a two mil layer of aluminum was co-cured onto the inner surface of the tube. Morton Thiokol, on the other hand, fabricated the

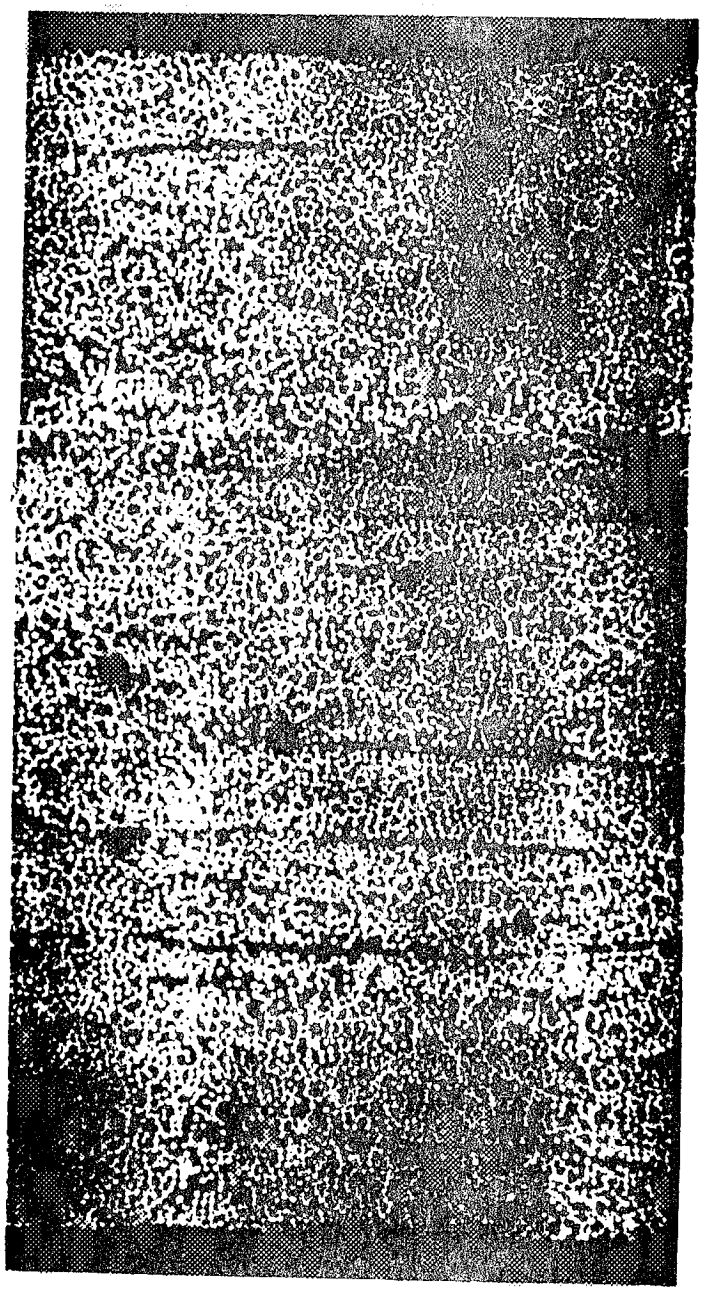

Figure 9. Micrograph of Panel

tubes using a female mandrel in which a tape layup was cured. These differences in manufacturing techniques led to differences in the dimensional repeatability of the tubes. The Boeing tubes possessed consistent inside diameters from one tube to the next due to the use of an internal male mandrel. The Morton Thiokol tubes had very consistent outside diameter owing to the female mandrel used. Because the outside diameter on the Boeing tubes and the inside diameter on the Morton Thiokol tubes were not controlled by a tool surface, the variation in the dimensions of the respective diameters varied considerably in some cases.

In addition to the laminated tubes, Morton Thiokol manufactured the unidirectional tubes. These tubes were made with a 12 ply layup using the same manufacturing technique and tooling as was used to produce laminated tubes with roughly the same dimensions.

Micrographs of the cross sections of the 0° and laminated tubes were taken. These appear in Figure 10 and Figure 11. The fiber volume fraction of the 0° tubes is significantly lower than that of the flat panels; the fibers are visibly much less dense than in the panel. In addition, the ply boundaries are much more pronounced. The fiber volume fraction for the 0° tubes was calculated to be 50% using the optical technique. The micrographs of the laminated tube show many of the same characteristics as the 0° tubes: pronounced ply boundaries and lower fiber volume fraction. It should also be noted that the plies toward the center of the laminate are compacted much less than the plies at the inner and outer surfaces. The overall fiber volume fraction was determined to be 51%. However, if the fiber volume fraction is determined within the layer only - not including the resin-rich regions at the interfaces - the volume fraction increases to 57%. The resin-rich regions at the ply interfaces, if considered as a separate ply, were determined to be approximately seven percent of the overall thickness of the laminate. With this knowledge, the "layers" of resin can be incorporated into the analytical model as separate layers.

The fiber volume fractions of the unidirectional tubes and the flat panel were also determined using the matrix digestion method according to the ASTM D-3171 test method. The volume fractions for the 0°, 45°, and 90° tubes were determined to be 53%, 52%, and 54.1% respectively[24], and the fiber volume fraction of the panel was found to be 54.3%. The result

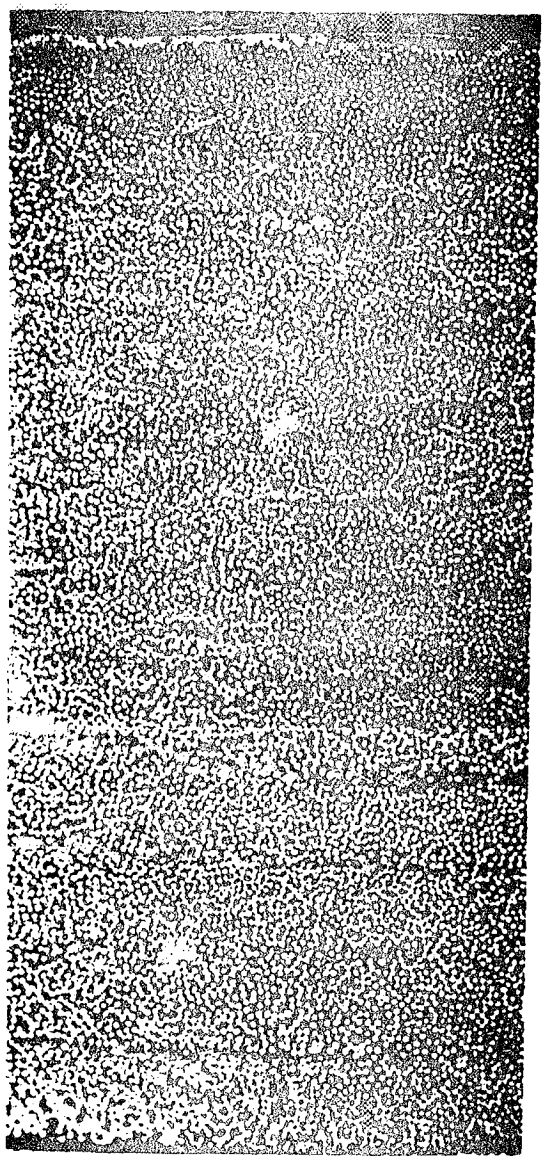

Figure 10. Micrograph of 0° Tube

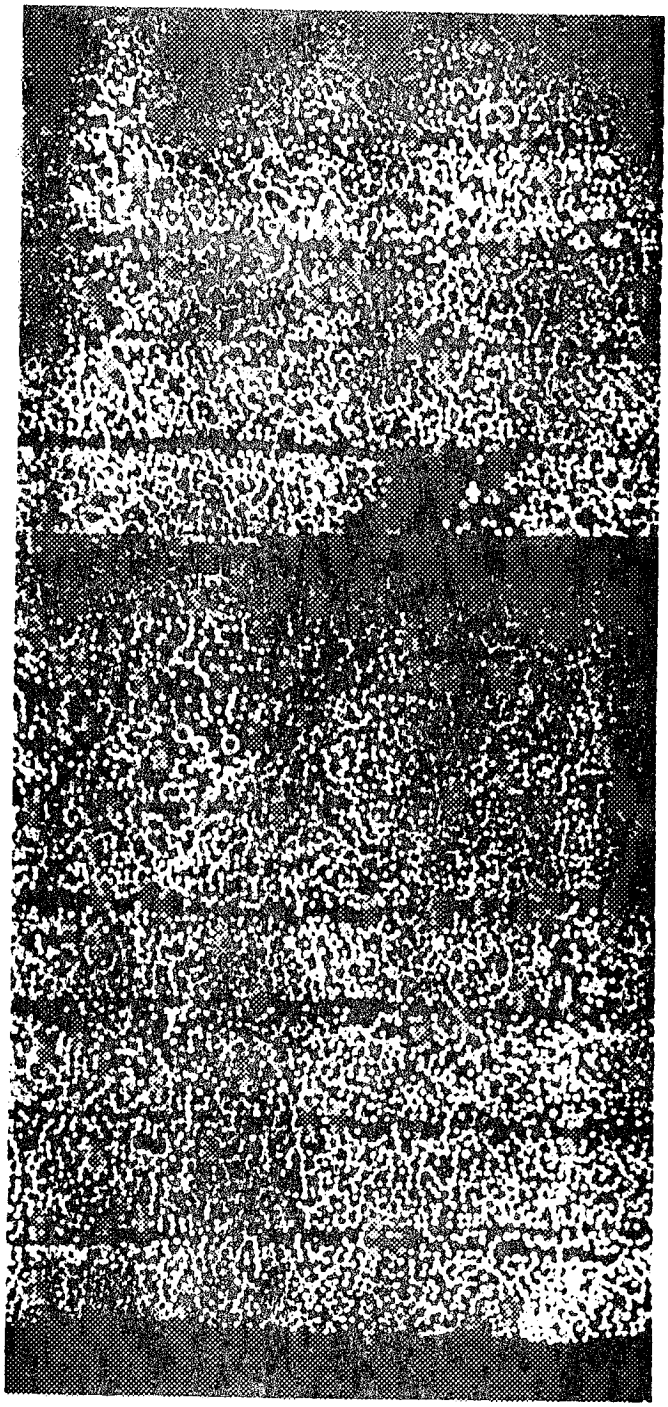

Figure 11. Micrograph of Laminated Tube

for the 0° tube compares favorably with the result using the optical technique. The result for the panel, however, was significantly lower than was determined using the optical technique. According to the results using the matrix digestion technique, the fiber volume fractions of the 0° tube and the panel are nearly the same, but a comparison the micrographs of the cross sections indicates that the fiber density in the panel is much higher than the 0° tube. Therefore the fiber volume fraction of 65% determined using the optical technique will be the value used in future analysis.

3.4 Test Method

3.4.1 Specimen Preparation

Prior to testing, all specimens were ultrasonically inspected to check for large voids or flaws. The flat panels were inspected prior to cutting the test coupons so that voids or flaws in the panels could be avoided. No detectable flaws were found in any of the panels. The tubes were inspected to determine their relative condition prior to testing since flaws could not be avoided due to the limited number of tubes available. The laminated tubes showed signs of possible voids and delaminations. A typical C-scan of a laminated tube is shown in Figure 12. The light areas signify an area of a possible delamination or void while the dark areas denote an area of good bonding. The micrographs presented in the previous section do not, however, show signs of delaminations. Following the C-scanning procedure the specimens were placed in a vacuum chamber to remove the moisture absorbed during the C-scanning procedure.

The off-axis tension coupons were cut on a diamond impregnated saw to nominal dimensions of ½" x 12" with fiber orientations of 0°, 10°, 45°, and 90°. Allowing for two inches

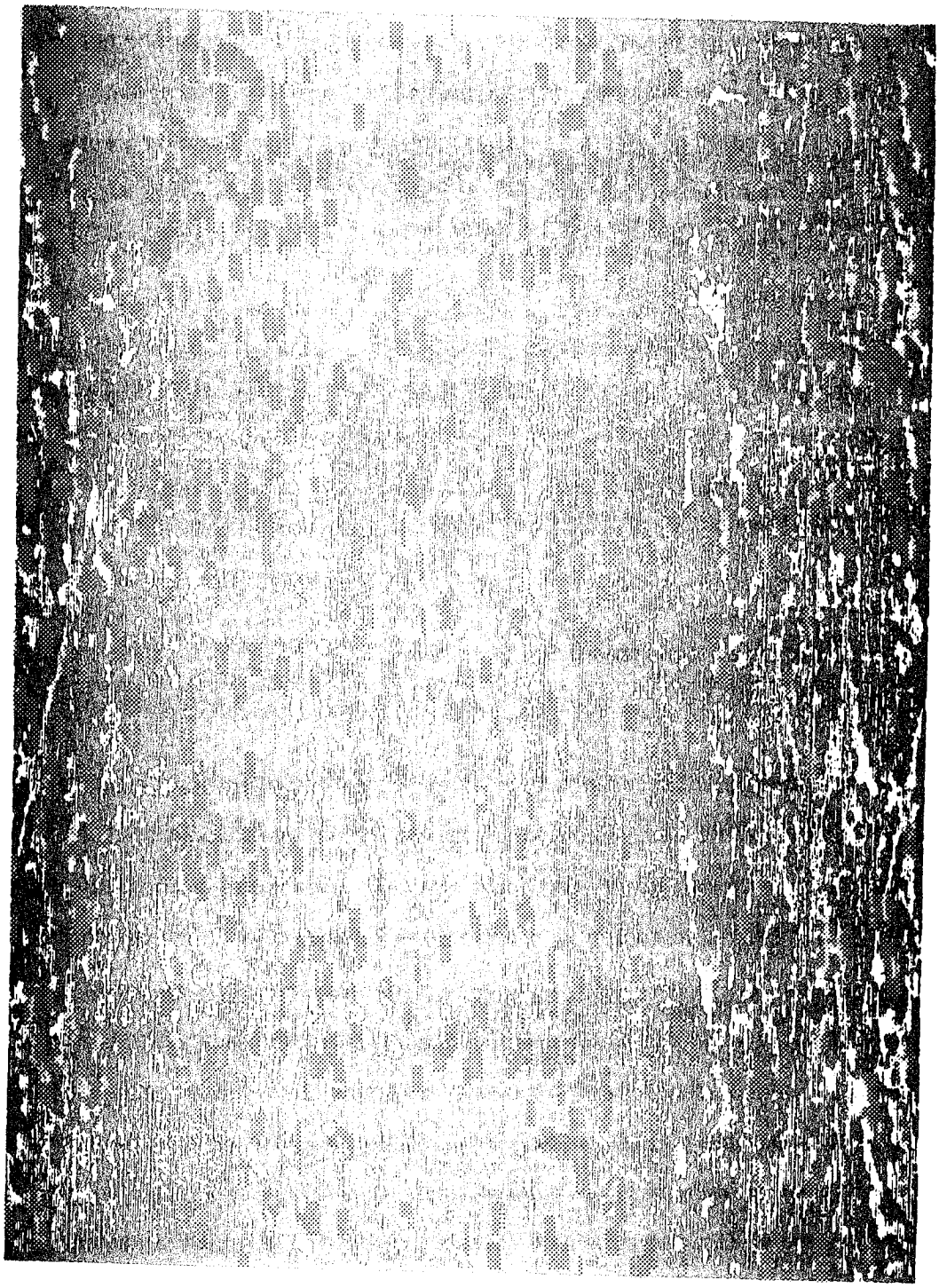

Figure 12. Typical C-scan of a laminated test

for grips at either end of the specimen, an aspect ratio of 16 was realized. At the center of each specimen a WK-00-120WR-350 Micro-Measurements stacked rosette was mounted with a WK-06-125AD-350 uniaxial strain gage mounted back-to-back to allow for bending correction. Three specimens of each fiber orientation were prepared. The off-axis compression specimens were cut to nominal dimensions of 1" x 1½", and the edges were ground for smoothness and parallelism. A FRA-2-11 2mm Texas Measurements stacked rosette was mounted at the center of each specimen, and a FLA-2-11 2mm uniaxial strain gage was mounted back-to-back. The Iosipescu specimens were cut and ground to the dimensions shown in Figure 13. A FRA-2-11 2mm stacked rosette was mounted at the center of the test section of each specimen.

3.4.2 Test Equipment

Two testing machines were used for the experimental work in this investigation. For the off-axis tension and compression tests and the Iosipescu tests, a screw driven displacement controlled UTS Machine was utilized. The tube tests were performed on an Instron biaxial, servo-hydraulic testing machine. This machine was capable of performing tests in either displacement or load control; load control was used for the tube tests in this investigation.

Computer controlled data acquisition systems were used with both the UTS and the Instron test machines. MATPAC2, a software package developed by Hidde, Beuth and Herakovich[25] was used in conjunction with the UTS machine. This system, in addition to acquiring the reading from the strain gages and load cell at three to four times per second, controlled the machine strain rate for the test. Following the test, MATPAC2 could correct for strain gage misalignment, initial curvature and bending, transverse sensitivity and actual fiber orientation. This software package was utilized on an IBM-XT Personal Computer interfaced with a Data Translation DT2805/5716 A/D - D/A board and a Vishay 2100 signal conditioner/amplifier.

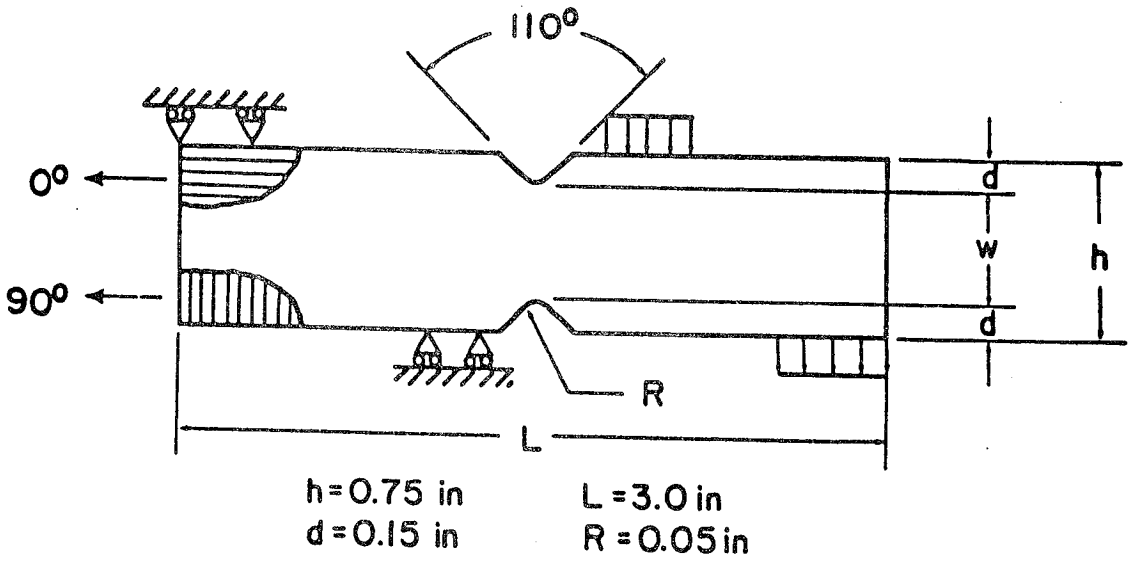

Figure 13. Iosipescu Specimen Geometry

Data from the tests performed on the Instron test machine was acquired on a variation of the MATPAC2 software system entitled MATPACO. This system is similar to MATPAC2 except that the Instron test machine was controlled independently of MATPACO. MATPACO was installed on an IBM-AT Personal Computer that was interfaced with an Orion Data Acquisition System signal conditioner. This system acquired data at a rate of two sweeps per second.

3.4.3 Test Fixtures

3.4.3.1 Off-Axis Tension

The test fixture employed for the off-axis tension tests was a rotating end grip type fixture. This fixtures reduces the effect of the end constraint that is caused by preventing rotation in the grips of the fixture. For a detailed description of the test fixture and the test methods see Pindera and Herakovich[28].

3.4.3.2 Off-Axis Compression

The fixture used for the compression tests employs an end loaded coupon supported by four circular pins to prevent out-of-plane displacements of the unloaded edges. A more detailed description of the fixture is given by Gürdal and Starbuck[27] and Pindera, et al.[28]

3.4.3.3 *Iosipescu*

The test fixture used for the Iosipescu tests is a modified version of the original model developed by Walrath and Adams[29].

3.4.3.4 *Tube Test Fixture*

In order for composite tubes to be loaded in combined tension (or compression) and torsion, a suitable fixture for introducing the loads was designed. The problem of gripping composite tubes has previously been examined by Highton and Soden[30] and Toombes, Swanson, Cairnes[31], and Guess and Haizlip[32]. Highton and Soden, working with a filament wound glass/epoxy tube, applied a tapered reinforcement consisting of additional layers of glass/epoxy and cast resin. A tapered collar was assembled around the reinforced end and bolted to flange at the end of the tube. Due to the taper, a radial stress was applied to the tube when bolted to the flange. This grip was designed for a specimen loaded in axial tension or compression and subjected to internal pressure.

Toombes, Swanson, and Cairnes[31] designed a grip similar to that of Highton and Soden for a tubular specimen to be loaded in axial compression and torsion. This design leaves no means for loading in axial tension.

Guess and Haizlip [32] designed two different end grip configurations. The first consisted of a two part grip that is adhesively bonded to the inner and outer surfaces of the tube. Because the adhesive did not provide sufficient maximum load a second design was considered. The second design consisted of an internal plug and an external split collar. A glass/epoxy fabric is overwrapped on the outside of the composite tube and cured onto the specimen. Threads are then machined onto the overwrap to mate with matching threads on the collar. The internal plug prevents collapse of the tube when the collar is clamped on the tube. This

design provides easy assembly and disassembly of the grips on the tube, but it requires that a glass/epoxy overwrap be applied to the tube and threads machined into the overwrap.

With these designs in mind, some goals for a fixture design were established. First, the tubes should not require any major modifications (such as was described by Highton and Soden and Guess and Haizlip). Second, the tubes should be easy to change between tests so that many tubes can be tested in a short period of time. Third, the fixture should not damage the tube during removal from the fixture so that more than one test can be performed on the same tube. Finally, the fixture must be capable of introducing axial tension or compression in combination with torsion. From these goals, a set of basic design requirements was determined.

The primary basis for the design of the fixture was that gripping the tube would be accomplished using friction alone. In order to minimize the amount of pressure necessary to exert on the tube to grip it in the fixture, the load should be introduced on both the inner and outer surfaces of the tube and the amount of gripping surface should be sufficiently large. The fixture must allow for variations in the inner and outer diameters of the tube.

The gripping fixture designed for this experimental program with the above criteria in mind mechanically grips the specimen by applying external pressure. The fixture consists of three basic components: the plug, the collar, and the base. All parts are made from carbon steel. The base consists of a circular plate and a protruding rod which can be gripped by the Instron hydraulic grips. The plug is bolted to the plate portion of the base using three 5/16" bolts and is then inserted into the end of the specimen. It is made in several different diameters so that a snug fit with the composite tube can be realized with the selection of the proper size plug. The collar, which consists of four identical parts, is then assembled around the specimen. It is also bolted to the base. Because both the collar and the plug are bolted to the base, the applied load is introduced to the specimen at both the inner and outer surfaces. This permits the gripping pressure to be reduced from what would be required if the load were introduced through only one surface. A schematic of the fixture is shown in Figure 14.

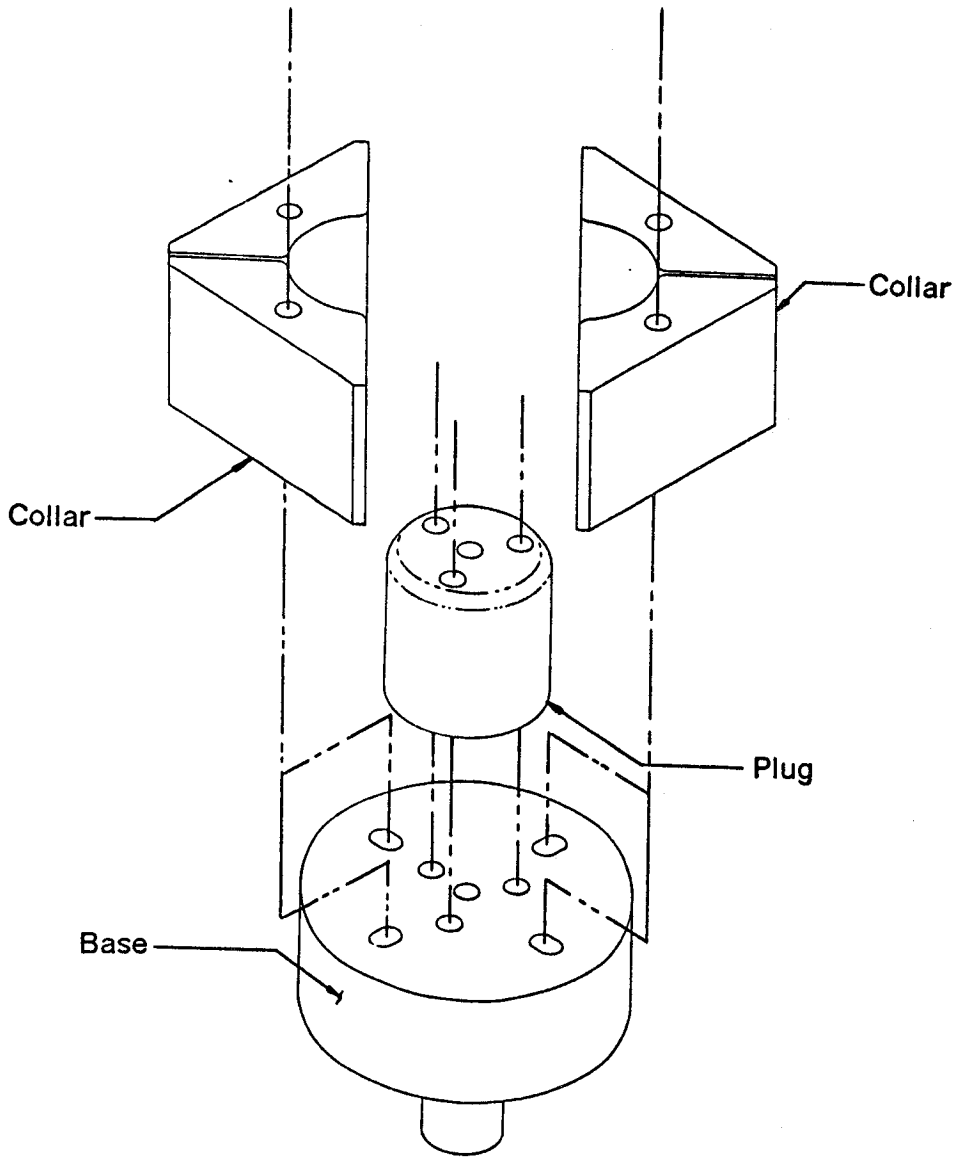

Figure 14. Tube Test Fixture Schematic

The procedure of mounting the grip onto the specimen can be performed while the base at each end of the specimen is gripped in the Instron's hydraulic grips. This allows for automatic alignment of the tube with the axis of the testing machine and provides a stable platform in which the bolts in the fixture can be easily torqued without applying any load to the tube.

A preliminary analysis was performed to determine the validity of the design outlined above. The length of contact between the tube and the collar and the plug was chosen to be 1.75 inches. This corresponds to a contact area of 11.46 square inches on the inner and outer surfaces. Using the load capacity of the Instron testing machine (20,000 lb tension/compression and 10,000 in-lb torsion) as the maximum design load, the maximum shear stress required at the interface of the grip and the tube was determined to be 982 psi. A conservative value for the coefficient of static friction was assumed for the steel grip/composite tube interface to be $\mu = 0.20$. From this, the magnitude of the radial stress generated by the grip required to deliver the necessary shear stress was determined to be 4912 psi.

Using the linear elastic portion of the analytical model developed in Chapter 2, the stresses induced into the tube by the grips alone were calculated. A worst case value of 9000 psi for the gripping pressure was used. In addition to calculating the stresses due to the pressure exerted by the grips, calculations were made to determine the stresses when the plug inserted in the tube does not fit perfectly, i.e. there is a gap between the tube and the plug. It was found that for all but the case of a unidirectional 90° tube, the gripping pressure required to close a gap of 0.010" between the tube and the plug was small compared to that necessary to grip the specimen under the design loads. The 90° specimens, however, require grip pressures in excess of 40 ksi in order to close the gap due to the high stiffness in the circumferential direction. Therefore it is imperative the plugs match the inside diameter of the tubes perfectly (or as near perfect as possible) for the 90° tubes. Aside from the 90° unidirectional case, the stresses due to the gripping pressure were calculated to be well below the ultimate strengths of the material to be used (P75/934 graphite/epoxy). Because the main thrust of this work was not to develop an analytical tool for predicting the complex stress

states induced by this grip fixture, a more rigorous analytical method for this purpose was not pursued. The results of the performed analysis were determined to be sufficiently promising to further pursue this design.

Once preliminary tests on the tubes manufactured by Boeing were initiated, it was noted that the tubes either slipped out of the grips or fractured in or near the grips. In order to alleviate this, the surfaces of the plug and the collar that come into contact with the composite tubes were grit blasted to provide a rougher surface. This permitted gripping at lower levels of pressures exerted by the collar on the tube. The fracturing of the tubes in or near the grips was due to stress concentrations induced by the grips. An attempt was made to alleviate this by using a torque wrench to tighten the grips onto the tube in a uniform pattern such that the collar is tightened evenly around the circumference of the tube.

Several preliminary experiments were performed on the tubes fabricated by Boeing for the evaluation of the test fixture. Heavily instrumented tubes were tested in pure axial tension and pure torsion. For both axial and torsional loading, a six inch test section was found to be sufficient to minimize the end effects in order to obtain a uniform state of deformation midway between the grips. In pure tension, a maximum axial stress of 30 ksi was achieved with failure occurring in the fixture. This is 60% of the load for which first ply failure is predicted. Under pure torsion, failure of the tube occurred at an applied torque of over twice the predicted torque for first ply failure. These results indicate that this test fixture is suitable for use in determining the response and failure of tubes under torsional loading, but the testing of tubes under pure tension is limited to loads well below predicted failure.

4.0 Experimental Results

4.1 Material Characterization

The presentation of the experimental results will begin with a description of the initial elastic properties of the material followed by a discussion of the nonlinear properties. Because the results of the characterization tests yielded consistent results, only representative test results will be presented in this chapter. A complete set of results is given in Appendix C. The data shown represents actual test data; no smoothing of the results has been performed.

4.1.1 Tensile Properties

Figure 15 shows the axial response of the four orientations of tensile coupons, and the Poisson's response for these tests is shown in Figure 16. The elastic properties and failure stresses obtained from these tests are summarized in Table 7.

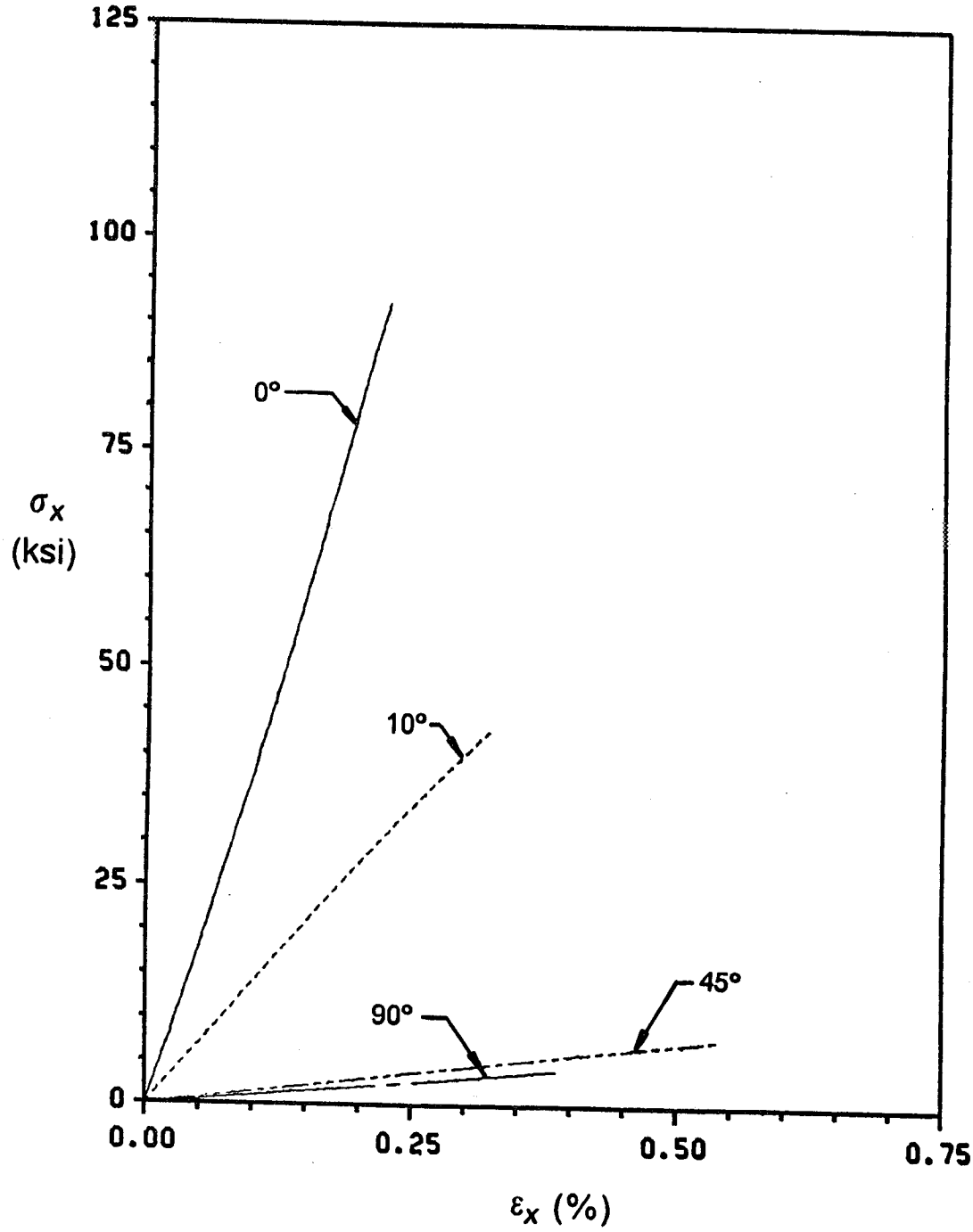

Figure 15. Axial Response of Tension Tests

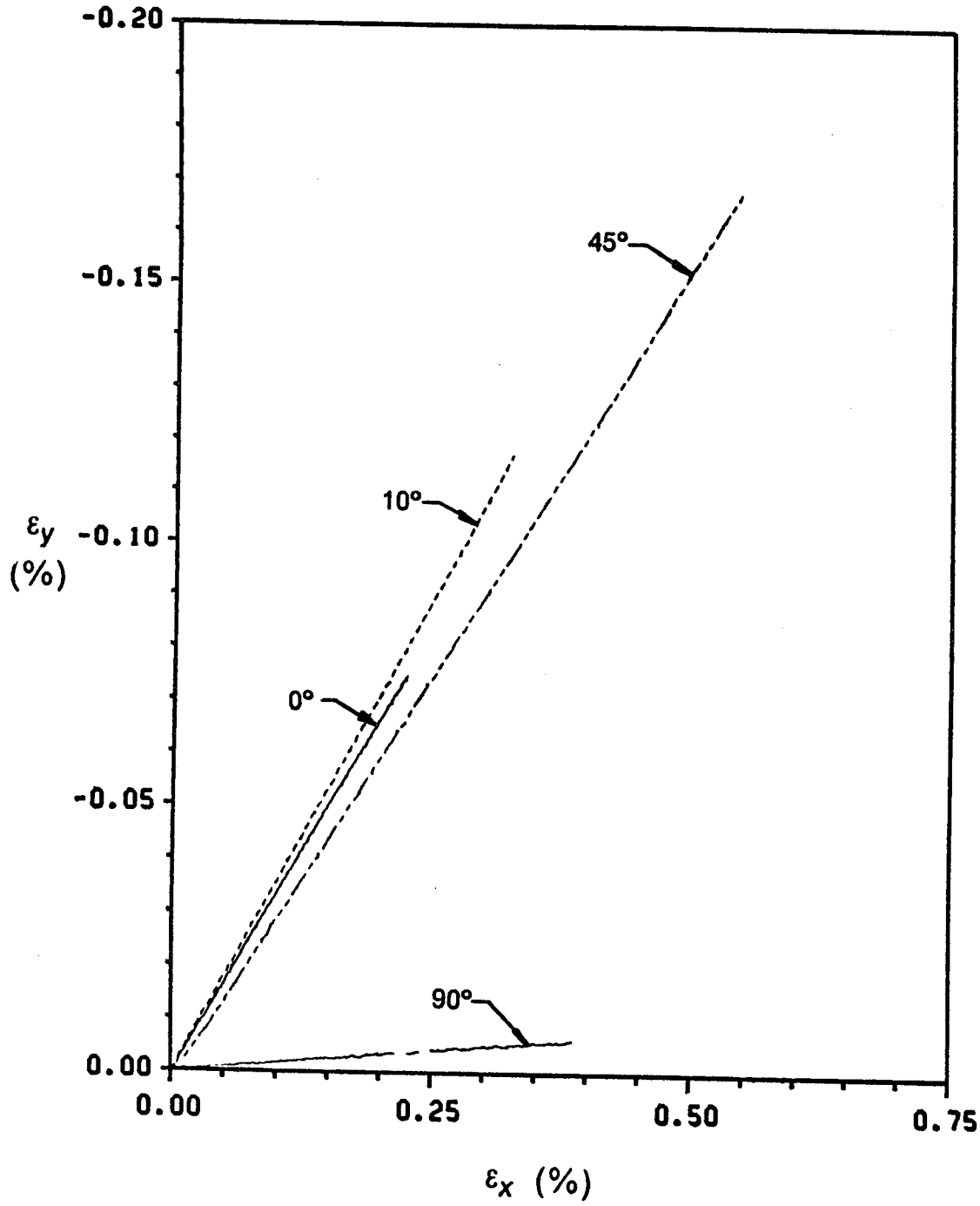

Figure 16. Poisson's Response of Tension Tests

Table 7. Summary of Average Tensile Properties

Type	Specimen	E_x (Msi)	ν_{xy}	G_{12}*(Msi)	σ_x^{ULT}(ksi)	ε_x^{ULT}(%)
Panel	1-00-01	35.25	0.340	-.-	92.96	0.225
	1-00-02	35.25	0.314	-.-	103.69	0.255
	1-00-03	35.25	0.340	-.-	100.35	0.256
	Average 0°	35.25	0.331	-.-	98.76	0.245
	1-10-01	12.61	0.450	0.625	42.31	0.345
	1-10-02	13.80	0.357	0.625	43.10	0.325
	1-10-03	13.80	0.366	0.625	32.73	0.246
	Average 10°	13.40	0.391	0.625	39.38	0.305
	3-45-01	1.47	0.309	0.555	7.75	0.544
	3-45-02	1.47	0.331	0.535	5.91	0.397
	3-45-04	1.53	0.295	0.584	7.30	0.482
	Average 45°	1.49	0.312	0.558	6.99	0.474
	3-90-01	1.04	0.016	-.-	4.05	0.388
	3-90-02	1.04	0.016	-.-	3.76	0.364
	3-90-03	1.04	0.016	-.-	3.57	0.346
	Average 90°	1.04	0.016	-.-	3.80	0.366
Tube	0-01	36.38	-.-	-.-	†	†
	0-03	46.67	-.-	-.-	†	†
	90-02	1.10	-.-‡	-.-	†	†
	90-03	1.17	-.-‡	-.-	†	†

* Apparent

† Tube not failed

‡ Data too noisy for accurate measurement

Figure 17 and Figure 18 show a comparison of experimental results for Young's modulus and Poisson's ratio with predictions of transformation theory, equations [4.1] and [4.2].

$$\frac{1}{E_{xx}(\phi)} = \frac{1}{E_{11}}\cos^4\phi + \left(\frac{1}{G_{12}} - \frac{2\nu_{12}}{E_{11}}\right)\sin^2\phi\cos^2\phi + \frac{1}{E_{22}}\sin^4\phi \qquad [4.1]$$

$$\nu_{xy}(\phi) = E_{xx}(\phi)\left[\frac{\nu_{12}}{E_{11}}\left(\sin^4\phi + \cos^4\phi\right) - \left(\frac{1}{E_{11}} + \frac{1}{E_{22}} - \frac{1}{G_{12}}\right)\sin^2\phi\cos^2\phi\right] \qquad [4.2]$$

The stress state in a multilayered tube is, in general, three-dimensional, therefore, an out-of-plane Poisson's ratio, ν_{23}, is required for subsequent experimental/analytical correlation to be presented in Chapter 5. Because only in-plane properties can be determined from the off-axis tests, a value for ν_{23} could not be determined experimentally. A value of 0.49 for ν_{23} was assumed based on Datta et al[33].

4.1.2 Compressive Properties

Figure 19 shows the results for the axial response of the compression tests performed on the three fiber orientations. The results for the Poisson's response from the compression tests are shown in Figure 20. A summary of the results for the material properties obtained from the compression tests is given in Table 8. Figure 21 and Figure 22 show a comparison of these results with transformation theory (Equations [4.1] and [4.2]).

To insure that the specimens were failing in compression rather than buckling, the 0° arm of the rosette was plotted with the uniaxial gage that was mounted on the opposite face of the specimen. Each specimen exhibited similar behavior so only a representative curve will be presented. The front and back response of a 0° compression specimen is shown in Figure 23. A sudden drop in the load prior to where the two curves separate indicates that an initial compressive failure occurs before buckling initiates. Therefore the failure stresses

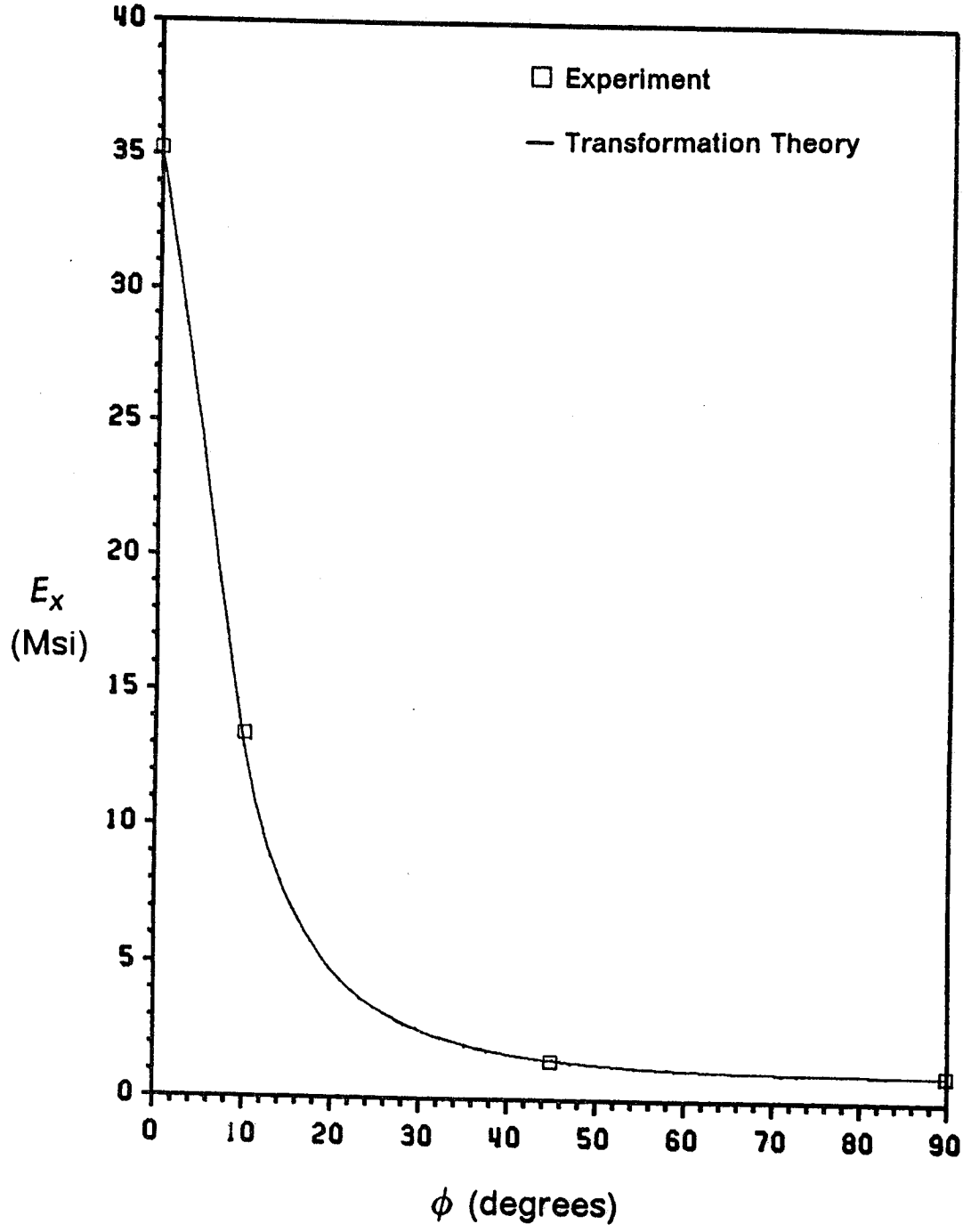

Figure 17. Comparison of Tensile Young's Modulus with Transformation Theory

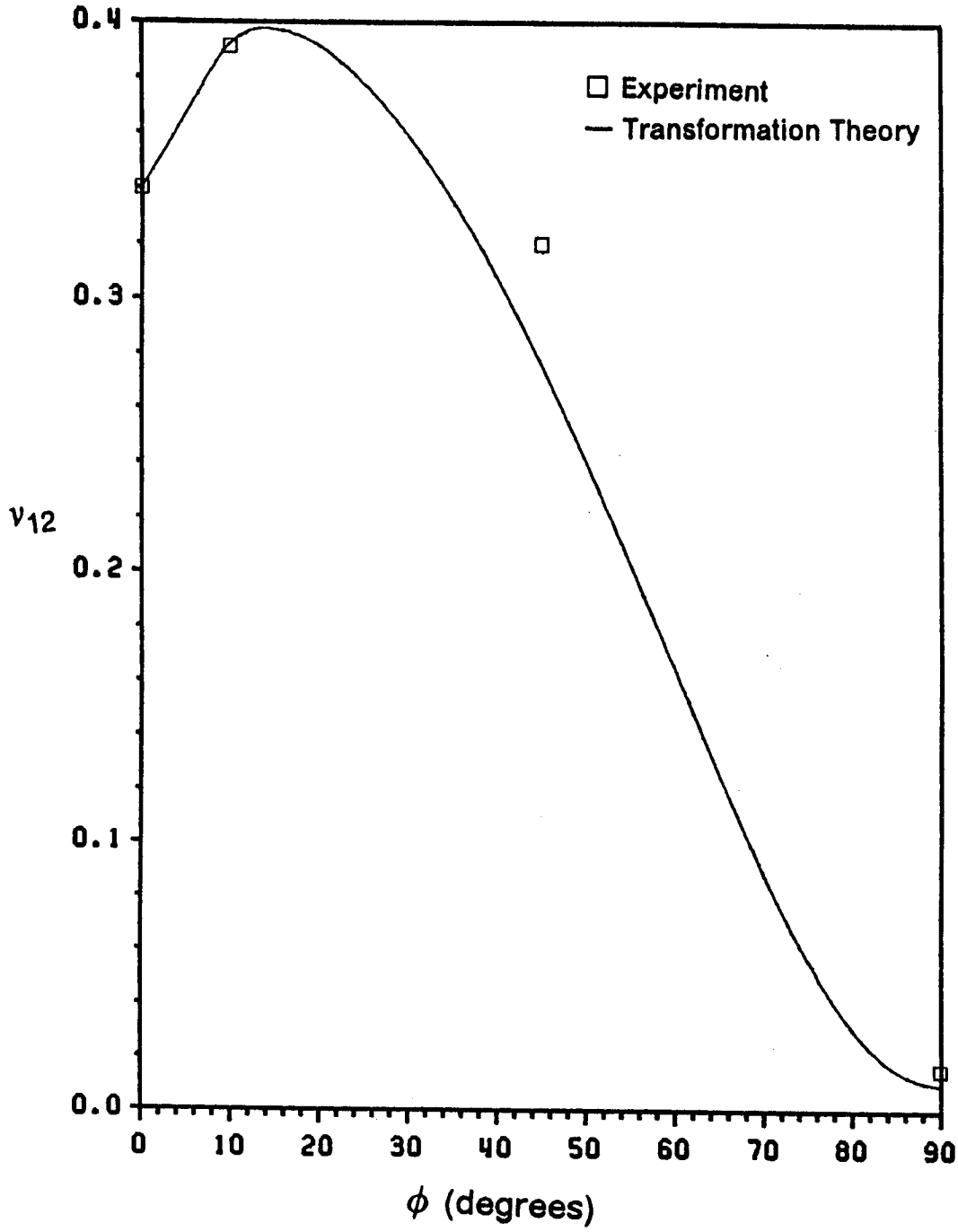

Figure 18. Comparison of Tensile Poisson's Ratio with Transformation Theory

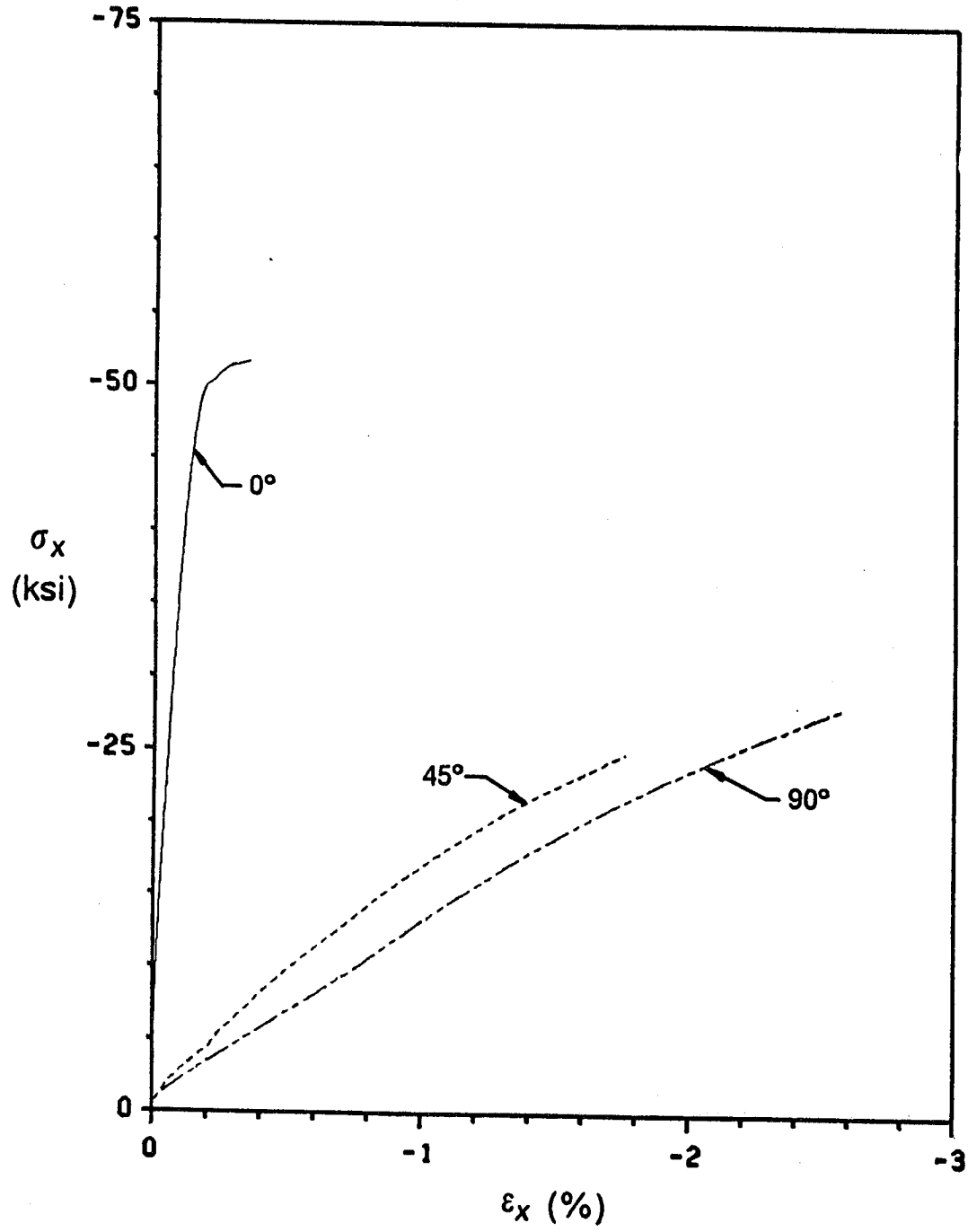

Figure 19. Axial Response in Compression Tests

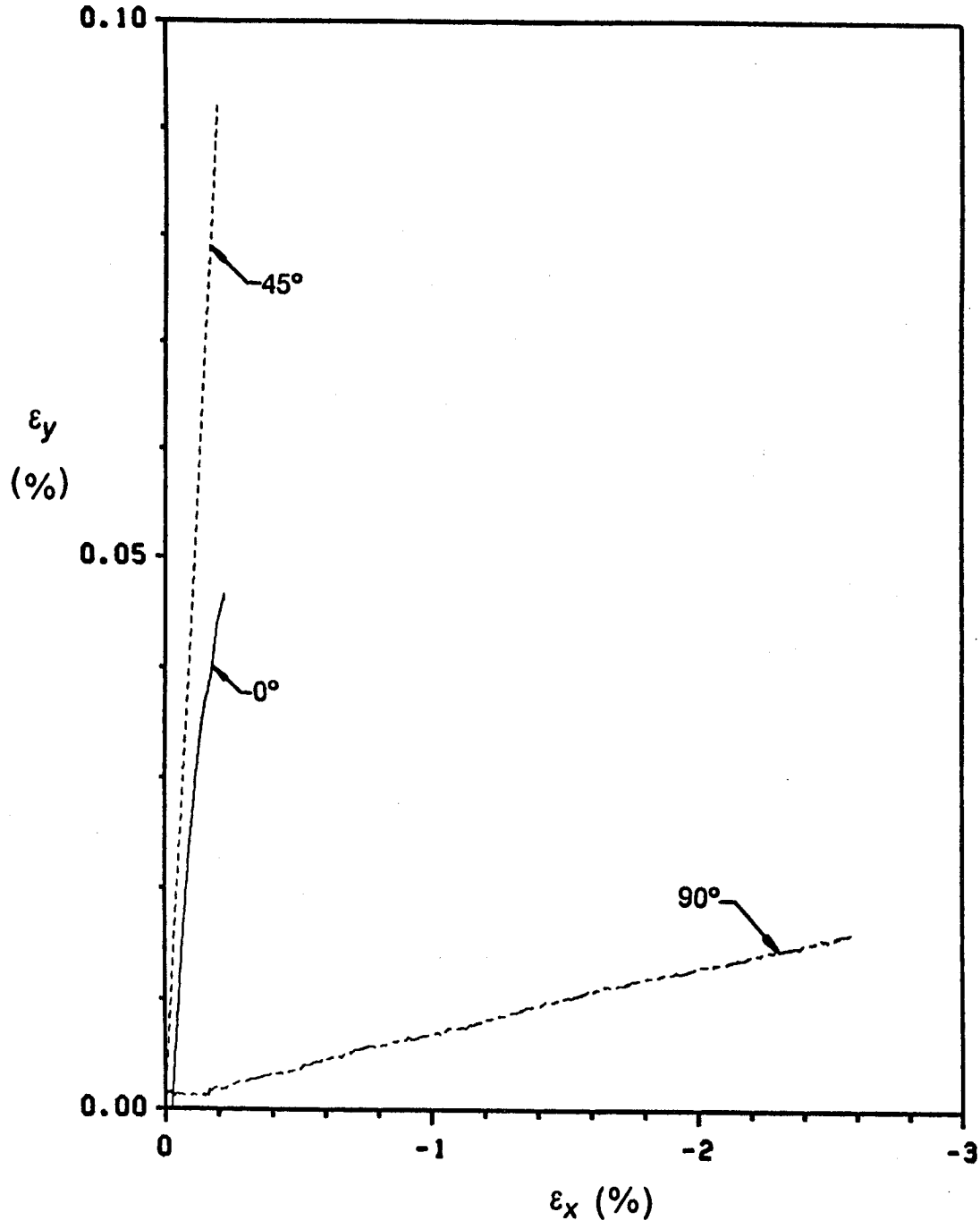

Figure 20. Poisson's Response in Compression Tests

Table 8. Summary of Average Compressive Properties

Type	Specimen	E_x (Msi)	ν_{xy}	G_{12}*(Msi)	σ_x^{ULT}(ksi)	ε_x^{ULT}(%)
Panel	C-00-01	34.48	0.314	-.-	-37.27	-0.115
	C-00-02	36.30	0.373	-.-	-49.00	-0.165
	C-00-03	36.82	0.363	-.-	-47.20	-0.160
	Average 0°	35.87	0.363	-.-	-44.49	-0.147
	C-45-01	1.49	0.447	0.483	-12.50	-0.664
	C-45-02	1.70	0.445	0.600	-18.84	-1.350
	C-45-04	1.70	0.573	0.486	-24.84	-1.760
	Average 45°	1.63	0.498	0.523	18.73	1.258
	C-90-01	1.20	0.0064	-.-	-28.09	-2.584
	C-90-02	1.20	0.0072	-.-	-27.50	-2.411
	C-90-03	1.20	0.0100	-.-	-27.50	-2.295
	Average 90°	1.20	0.0079	-.-	-27.70	-2.43
Tube	0-03	45.57	-.-	-.-	†	†
	90-03	1.06	-.-‡	-.-	†	†

* Apparent

† Tube not failed

‡ Data too noisy for accurate measurement

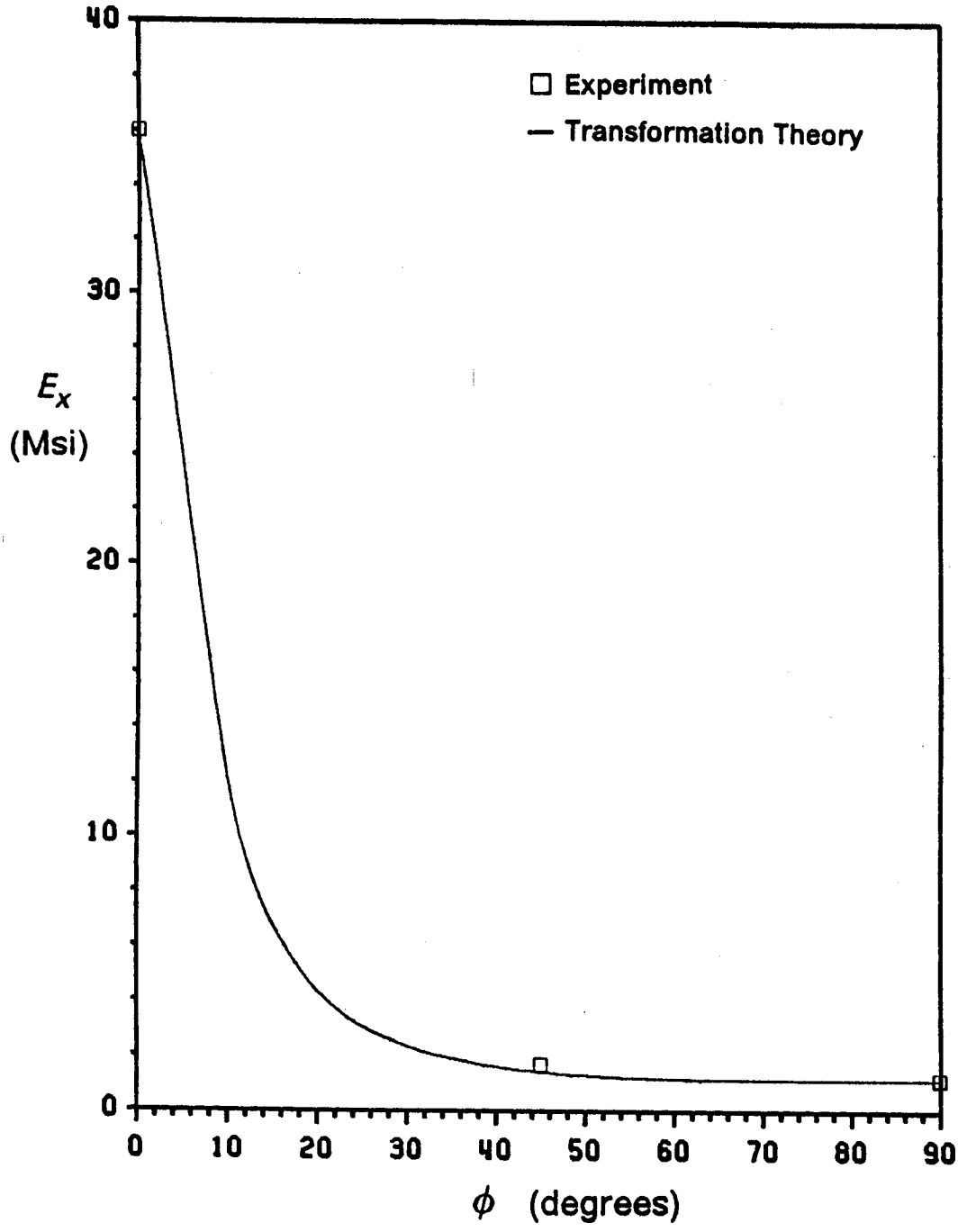

Figure 21. Comparison of Compressive Young's Modulus with Transformation Theory

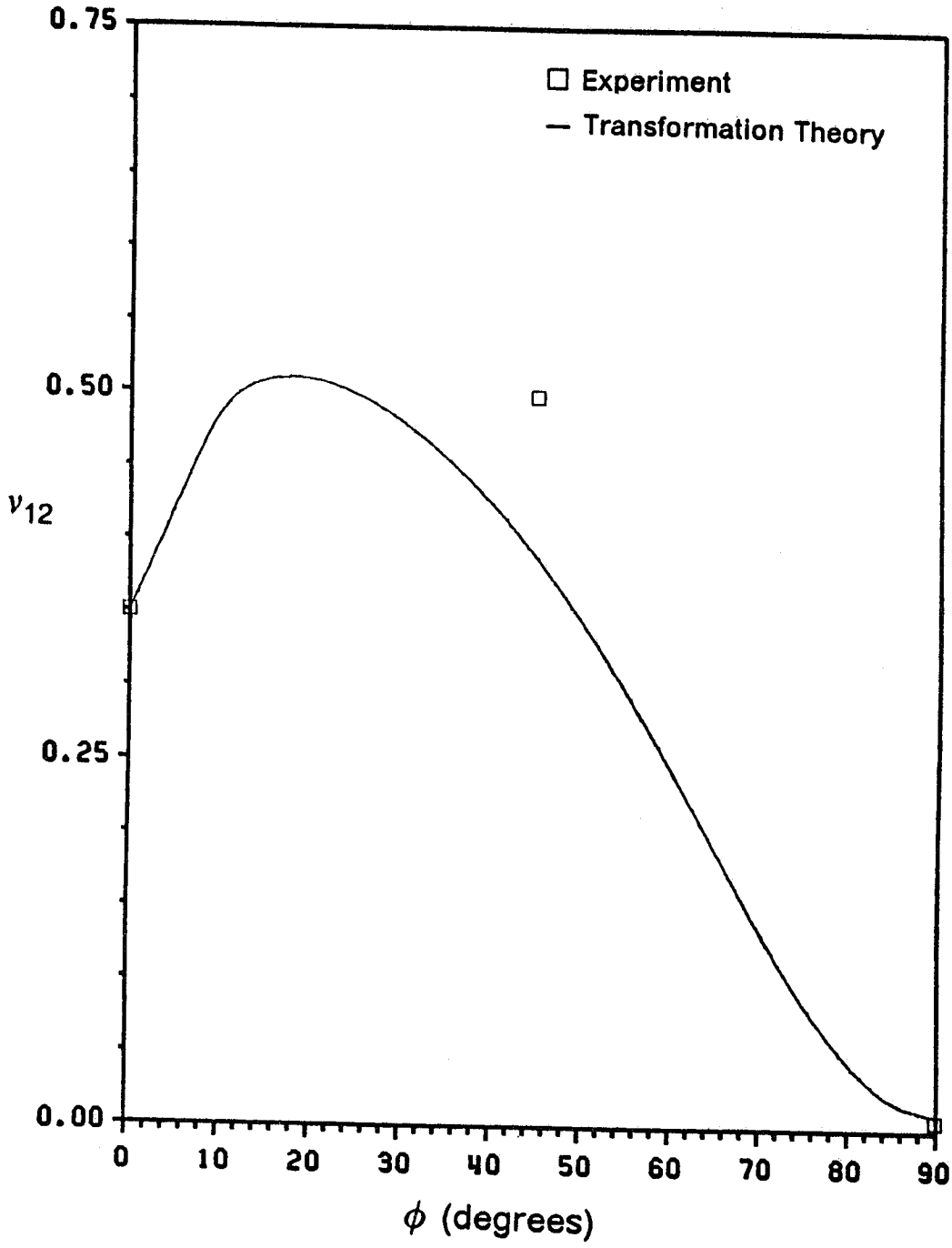

Figure 22. Comparison of Compressive Poisson's Ratio with Transformation Theory

observed in these tests are indeed representative of a compressive failure rather than a buckling failure.

4.1.3 Shear Properties

The shear modulus can be determined from 10° and 45° off-axis tension, 45° off-axis compression or the 0° and 90° Iosipescu tests. As described by Pindera et al.[34], the values of the initial shear moduli from the different tests must be corrected. The off-axis tension specimens are subjected to an end constraint effect because the ends of the specimens are rigidly clamped. The effect of the end constraint can be corrected by employing the Pagano-Halpin model as described by Pindera and Herakovich[26].

The Iosipescu specimens, although subjected to a nearly pure state of shear stress, have stress distributions across the test section that are not uniform. Because of this nonuniformity, the apparent values of G_{12} calculated using the average applied shear stress will not be the true shear modulus. By carrying out a finite element analysis to determine the actual distribution of shear stress across the test section, a more accurate value for G_{12} can be obtained by applying correction factors to the apparent data as pointed out by Pindera et al[34]. The results of these tests are shown in Table 9. Figure 24 shows results of the 10° and 45° off-axis and 0° and 90° Iosipescu tests before correction factors are applied. With the correction factors incorporated, good agreement between these tests can be seen in Figure 25.

4.1.4 Nonlinear Properties

The constant B_{11} and the endochronic constants, B^{o}_{22}, B^{o}_{66}, n_1, n_2, n_6, and , S_{ij} , are determined by assuming that for uniaxial states of stress, the nonlinear portion of the strain, ε_i^{NL} , can be approximated by a power law[19 20]

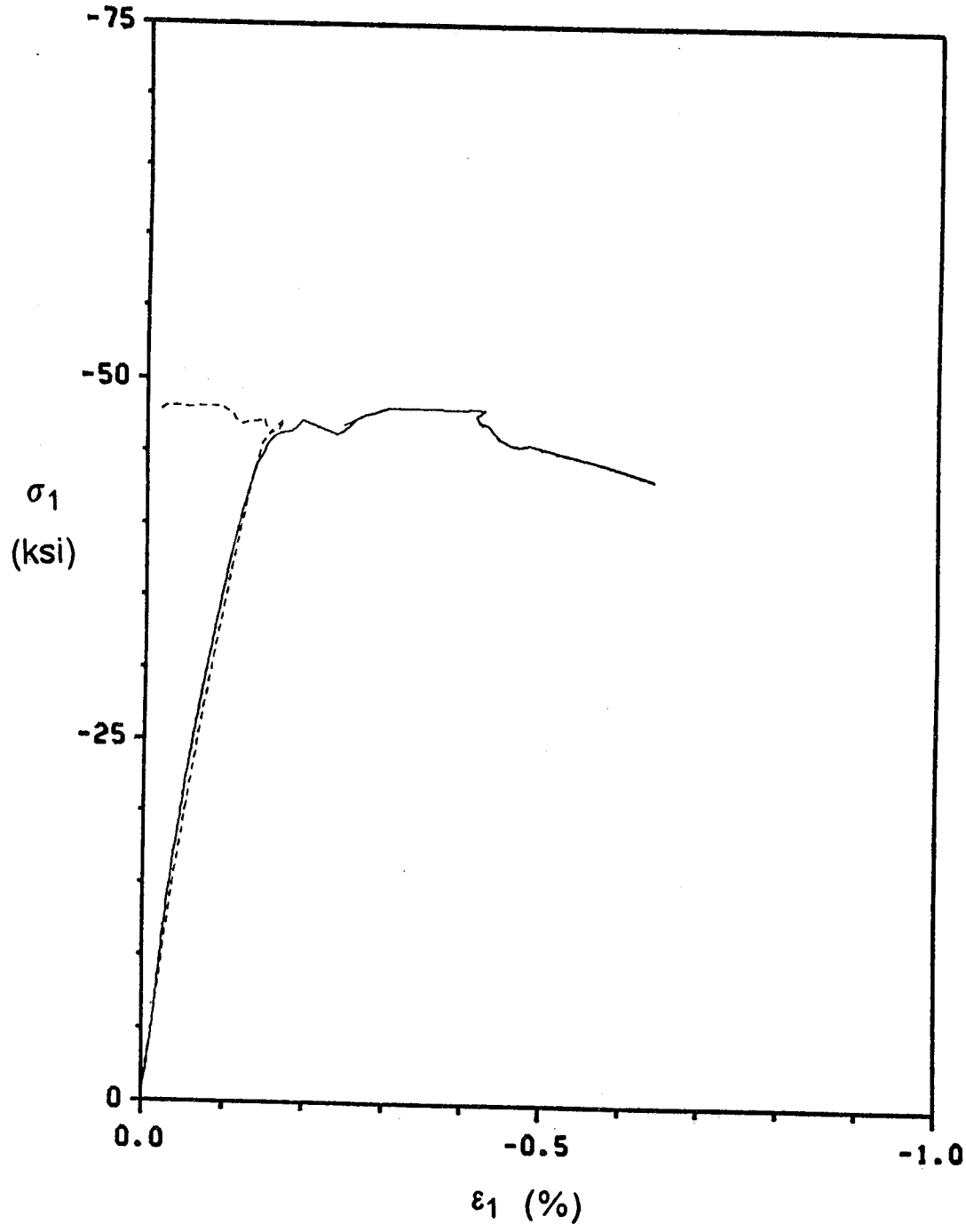

Figure 23. Comparison of Front and Back Strain Gages for Compression Test

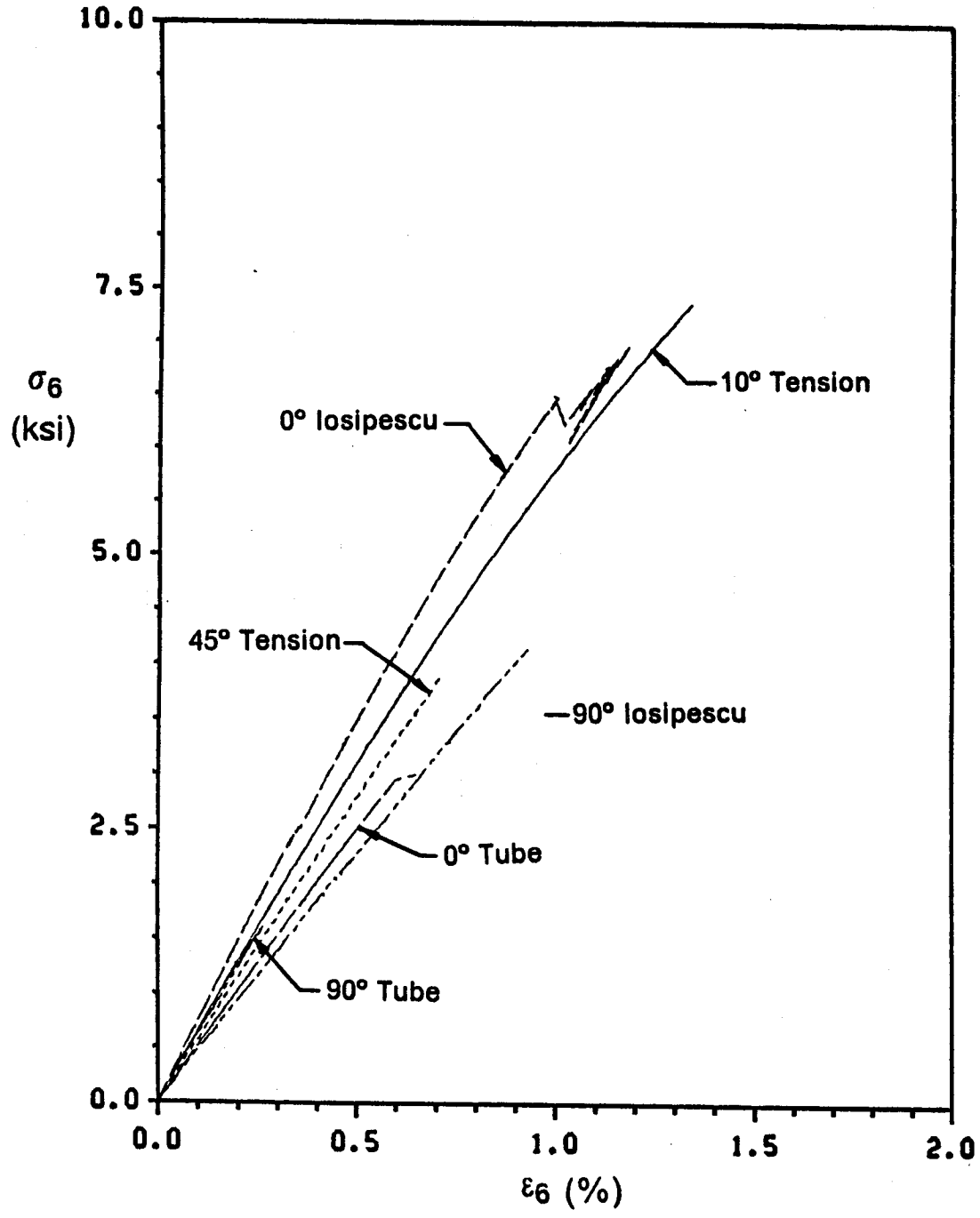

Figure 24. Shear Response Before Shear Correction Factors

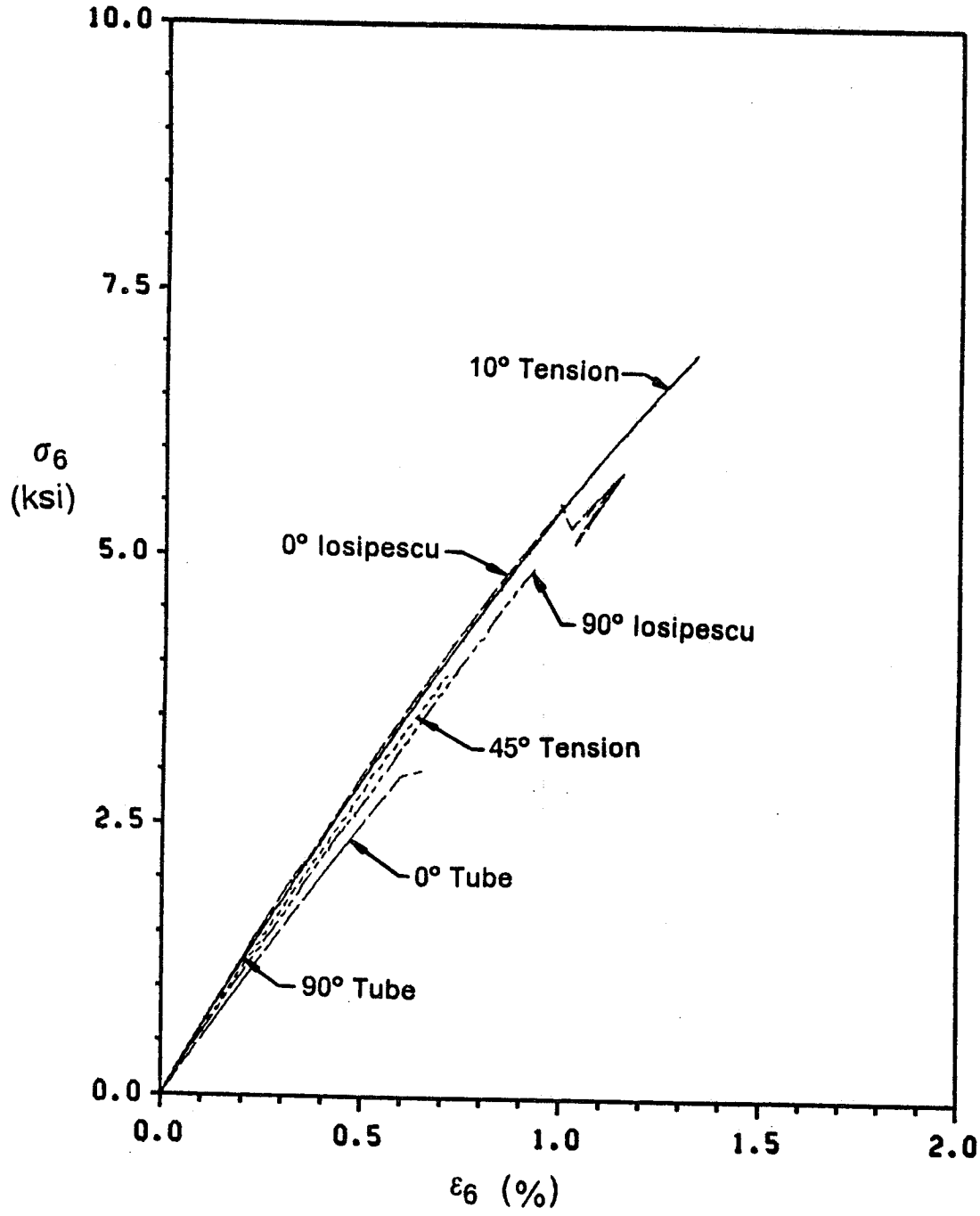

Figure 25. Shear Response After Shear Correction Factors

Table 9. Initial Shear Properties

Test	G_{12} * (Msi)	Correction	G_{12}(Msi)
10° Tension	0.625	0.940†	0.587
45° Tension	0.558	1.002†	0.559
45° Compression	0.523	--	0.523
0° Iosipescu	0.710	0.847*	0.601
90° Iosipescu	0.469	1.180*	0.553
0° Tube	0.553	--	0.553
90° Tube	0.605	--	0.605

† Pindera and Herakovich[28]

* Pindera et al[34]

$$\varepsilon_i^{NL} = C_i \sigma_i^{k_i}. \quad (i = 1,2,...,6 \quad i \text{ not summed}) \qquad [4.3]$$

This implies that the plot of $\ln \varepsilon_i^{NL}$ versus $\ln \sigma_i$ can be approximated by a straight line. Taking the natural logarithm of both sides of Equation [4.3] yields

$$\begin{aligned} \ln \varepsilon_i^{NL} &= \ln\left(C_i \sigma_i^{k_i}\right) \\ &= \ln C_i + \ln \sigma_i^{k_i} \quad (\text{i not summed}) \\ \ln \varepsilon_i^{NL} &= \ln C_i + k_i \ln \sigma_i \end{aligned} \qquad [4.4]$$

In the Cartesian coordinate system, Equation [4.4] can be represented as

$$y = mx + b$$

where

$$y = \ln \varepsilon_i^{NL}$$

$$x = \ln \sigma_i$$

$$m = k_i = \text{ slope}$$

$$b = \ln C_i = \text{ y-intercept}$$

Figure 26 shows the fiber direction response in tension and compression. The P75/934 graphite/epoxy exhibits a stiffening response in tension while the response softens in compression. The stiffening behavior in tension is bilinear with an initial modulus of 35.25 Msi as shown in Table 7, and the final modulus is 43.70 Msi which is a 24% increase in stiffness. To more accurately model this material, both the stiffening and softening effects will be incorporated.

The response of the 90° uniaxial tests are shown in Figure 27. In tension, the σ_2 versus ε_2 curve is linear to failure. In compression, the curve is linear for a significant portion of the response. For these reasons, the transverse response will be assumed to be

linear, therefore, the nonlinear endochronic constants associated with the transverse direction (B^{o}_{22}, n_2, S_{22}) will be set to zero.

Figure 25 shows the corrected curves for the shear response from the off-axis tension and compression and the Iosipescu tests. While the 0° and 90° Iosipescu test specimens are in a nearly pure state of shear, the 45° and 10° off-axis tensile specimens are not. Although there exist other significant components of stress along material principal directions in especially the 10° off-axis test, the degree of nonlinearity of each of the curves is nearly the same. This observation leads to the conclusion that the nonlinearity in the shear component of stress is uncoupled from the other components of stress. In other words, the presence of σ_1, σ_2, and σ_3 does not contribute to the nonlinear response in shear at the material level.

From the lamina tests discussed previously in this chapter, and, assuming the material is transversely isotropic, we conclude that the only nonlinear components of stress are σ_1 and σ_6 which are uncoupled. Because the nonlinear portion of the strain in the fiber direction is independent of the deformation scale, z, and the uncoupled nature of the nonlinearities, the only nonzero component of the S_{ij} matrix is the S_{66} component. With B^{o}_{22} and n_2 already determined to be zero, the only parameters required are B_{11}, B^{o}_{66}, n_1, n_6, and S_{66}. However, since the nonlinear response in the fiber direction stiffens in tension and softens in compression, two sets of B_{11} and n_1 will be necessary, i.e., for $\sigma_1 > 0$

$$\varepsilon_1^{NL} = B_{11}^{T} \sigma_1^{n_1^T}$$

and for $\sigma_1 < 0$

$$\varepsilon_1^{NL} = - B_{11}^{C} |\sigma_1|^{n_1^C}.$$

The nonlinear strain in the fiber direction is very well approximated by that of the power law, Equation [4.3] where $C_1 = B^{T}_{11}$(or B^{C}_{11}) and $k_1 = n^{T}_{1}$(or n^{C}_{1}) can be determined directly from a plot of ln ε_1^{NL} versus ln σ_1. $n^{T}_{1}(n^{C}_{1})$ is the slope and ln B^{T}_{11}(ln B^{C}_{11}) is the y intercept.

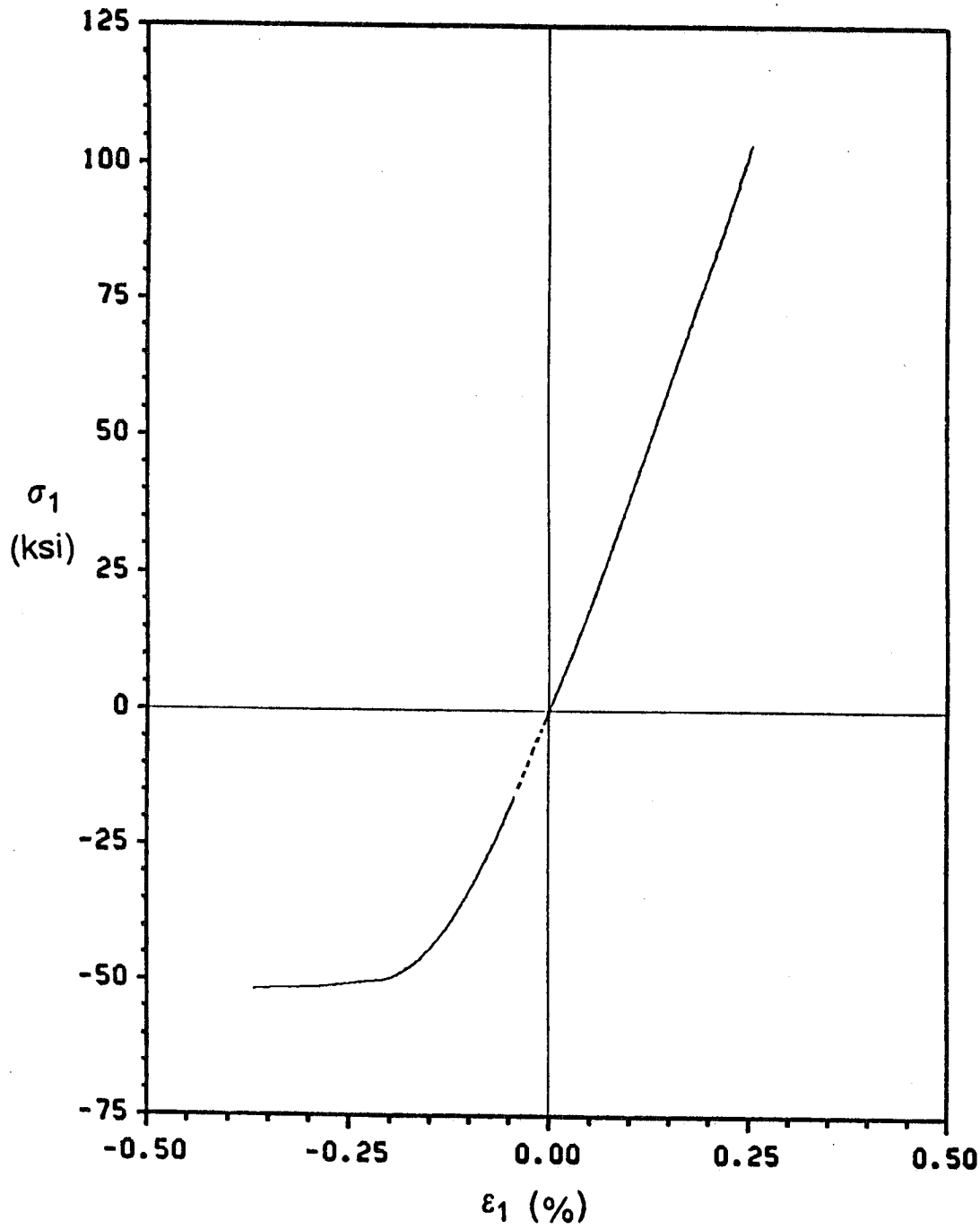

Figure 26. 0° Response

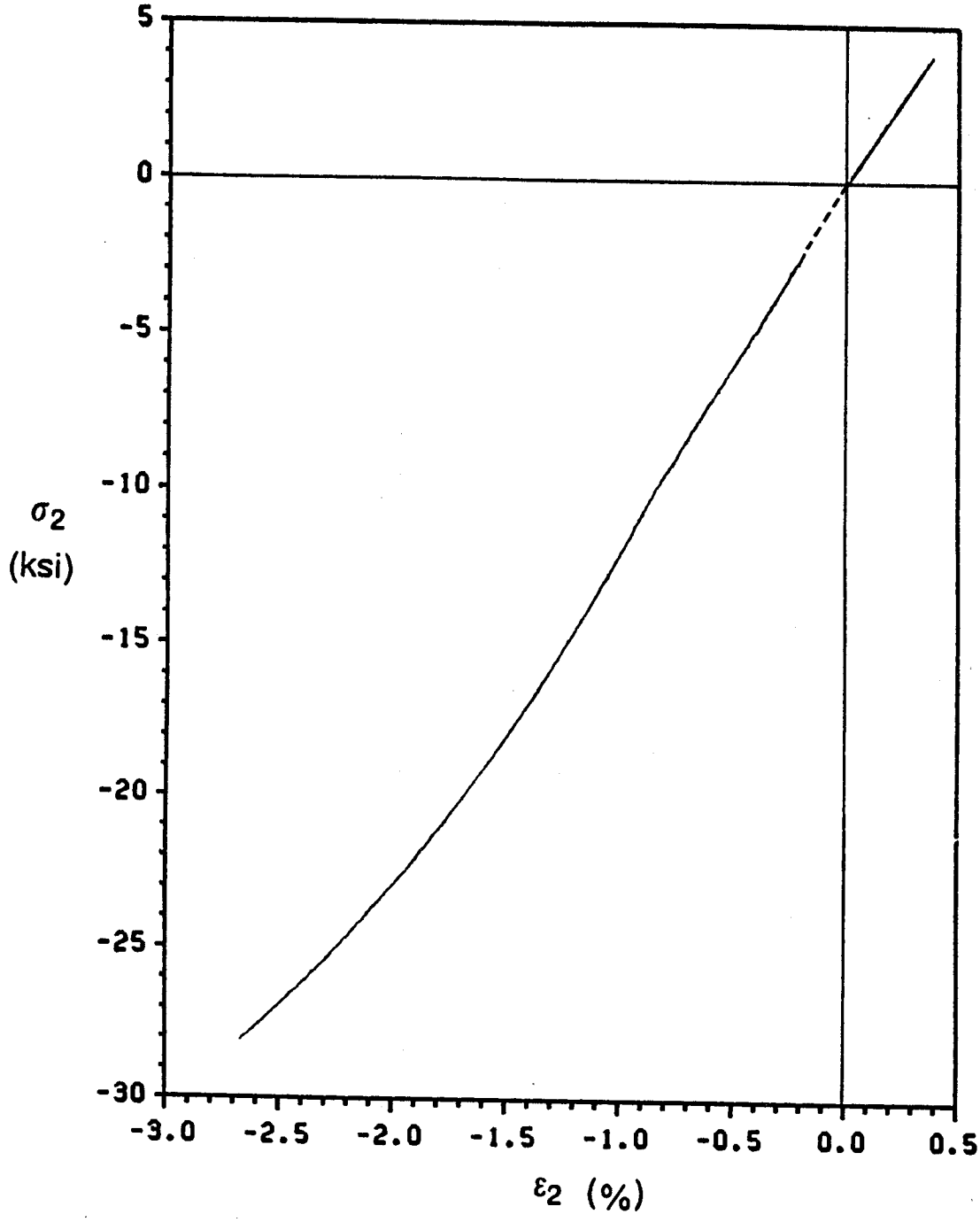

Figure 27. 90° Response

The values of n_6, B^o_{66}, and S_{66} can be determined from the graph of ln ε_6^{NL} versus ln σ_6 for the case of pure shear. For this stress state, the form of the nonlinear strains, ε_6^{NL} is given in Equation [2.69]

$$\varepsilon_6^{NL} = \frac{B^o_{66}(S_{66})^{\frac{n_6}{2}}}{n_6+1}\sigma_6^{n_6+1} \qquad [4.5]$$

Using Equation [4.3], Equation [4.5] can be represented by the power law approximation

$$\varepsilon_6^{NL} = C_6\sigma_6^{k_6}$$

where

$$C_6 = \frac{B^o_{66}(S_{66})^{\frac{n_6}{2}}}{n_6+1}$$

$$k_6 = n_6 + 1$$

The value of n_6 can be determined directly from the slope of the ln ε_6^{NL} versus ln σ_6 curve.

Because both B^o_{66} and S_{66} must be determined from a pure shear test, they cannot be independent quantities. Since B^o_{66} is simply a multiplicative constant, it will arbitrarily be set equal to 1. With B^o_{66} known, S_{66} can be determined from the y-intercept of the ln ε_6^{NL} versus ln σ_6 curve.

4.2 Summary of Material Properties

With the determination of the endochronic parameters, the P75/934 graphite/epoxy has been completely characterized in both the linear and nonlinear regions. A summary of the material properties to be used in the analytical model is shown in Table 10. The coefficients

of thermal expansion presented in Table 10 were determined by Bowles[24] for P75/934 with a fiber volume fraction of 50%.

The response and failure of the 0° specimens were significantly different in tension and compression. The 0° coupons exhibited a stiffening response in tension while the behavior in compression softened. In addition, the ultimate strength in compression, X_C, was less than 50% of the tensile ultimate strength, X_T. The initial moduli of the tension and compression tests differed by only 2% so a common value of 35.25 Msi will be used for both tension and compression.

The 90° specimens also exhibited a large difference in the failure properties in tension and compression; the ultimate strength in compression was over seven times the tensile ultimate strength. The initial response for both tension and compression was found to be linear. Although the initial Young's modulus in tension and compression differed by 10%, a common value of 1.04 Msi will be used for simplicity in the analytical model.

Under complex loading paths, unloading of the stresses can occur due to the sequence of loading. For an accurate analytical prediction of this kind of behavior, an appropriate scheme for modeling the unloading of the stresses is required. The two components of stress which exhibit nonlinear constitutive behavior for P75/934 are the shear component and the component in the fiber direction which were found to be uncoupled. Because the unloading response was not part of the material characterization performed in the experimental investigation, assumptions will be made as to the nature of the two nonlinear components of stress.

Because the nonlinear portion of the strain in the fiber direction was assumed to be independent of the deformation scale, z, the response is reversible. The reversible behavior of graphite composites in the fiber direction was verified by Pindera and Herakovich[35] using cyclic tests.

The nonlinearities in the shear component are dissipative in nature. For dissipative response, the stresses will be assumed to unload linearly while maintaining a constant nonlinear strain.

Table 10. Summary of Material Properties

Elastic Properties

$E_{11} = 35.25$ Msi
$E_{22} = 1.04$ Msi
$\nu_{12} = 0.331$
$\nu_{23} = 0.49$
$G_{12} = 0.570$ Msi

Failure Properties

$X_T = 98.8$ ksi
$X_C = -44.5$ ksi
$Y_T = 3.8$ ksi
$Y_C = -27.7$ ksi
$S = 5.85$ ksi

Thermal Properties

$\alpha_1 = -0.584 \times 10^{-6}/°F$

$\alpha_2 = 19.18 \times 10^{-6}/°F$

Endochronic Parameters

$B_{11}^T = 0.7840292 \times 10^{-12}$
$B_{11}^C = 0.2541205 \times 10^{-12}$
$B_{66}^o = 1.00$
$S_{66} = 0.1221467 \times 10^{-13}$

$n_1^T = 1.736261$
$n_1^C = 2.056897$
$n_s = 2.859718$

4.3 Laminated Tube Tests

As was mentioned in the previous chapter, the laminated tubes were tested in pure torsion and in torsion dominated biaxial loading. For the purposes of this investigation, only the global shear response of the tubes will be presented. For both the analytical predictions shown in the next chapter and the experimental results, the shear response will be presented in graphs of $\bar{\tau}_{x\theta}$ vs. $\gamma_{x\theta}$ where $\bar{\tau}_{x\theta}$ is the average applied shear stress

$$\bar{\tau}_{x\theta} = \frac{T_x r_N}{J}$$

and J is the polar moment of intertia of the tube cross section. The shear strain, $\gamma_{x\theta}$, is the strain on the surface of the tube either measured with a strain gage for the experimental results or calculated using the analytical model.

In the description of the experimental results that follows, the magnitude of the applied shear stress where the response begins to exhibit nonlinear behavior will be referred to as the "linear limit". This point is frequently called the proportional limit in the literature and textbooks.

4.3.1 Type I Loading

The response of tube LMC08 to pure monotonic negative torsion to failure is shown in Figure 28. The shear modulus of the tube in this test was $G_{x\theta} = 1.32$ Msi. The stress at which the response deviated from linear response was -6.0 ksi. Failure occurred at -8.88 ksi although cracking was audible at approximately 8 ksi.

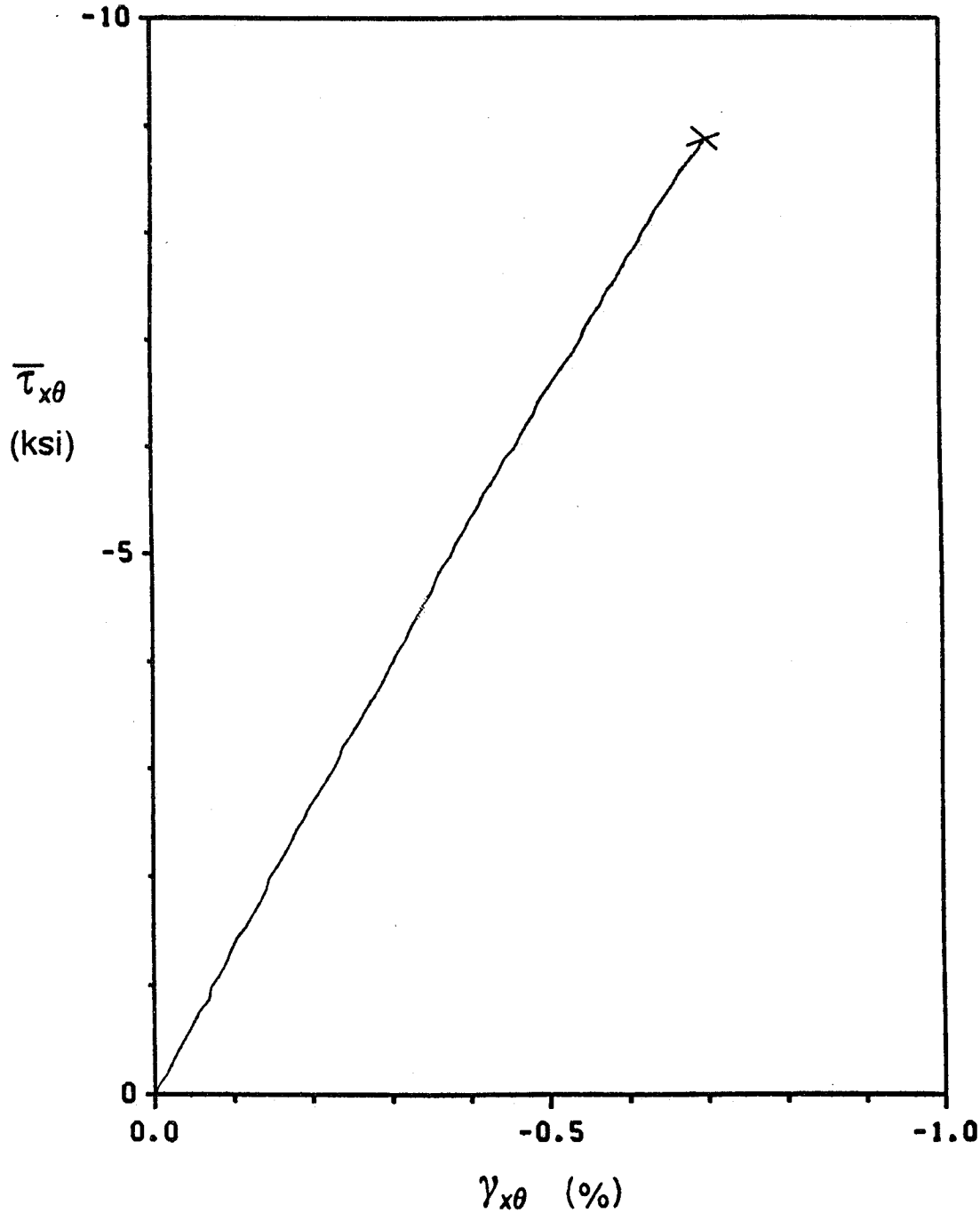

Figure 28. Shear Response of Tube LMC08 - Type I Loading

4.3.2 Type II Loading

The shear responses for the cyclic torsion tests of tubes LMB02, LMB04, and LMC05 are shown in Figure 29 through Figure 31 respectively. Each figure contains all loading cycles for a given tube with each successive loading cycle offset from the previous one by 0.10% strain.

4.3.2.1 Tube LMB02

The results of the cyclic torsion test on tube LMB02 are shown in Figure 29. The shear modulus, $G_{x\theta}$, is 1.42 Msi. The linear limit for this tube, as shown in the second and subsequent cycles, is 4.0 ksi.

On the final loading cycle, audible cracking in the tube was detected at an applied shear stress of approximately 9.5 ksi in positive torsion. On the subsequent load up in negative torsion, total failure of the tube occurred at a stress of 5.3 ksi which is approximately 60% of the stress attained in negative torsion in the previous load cycle. The unloading response in the final loading cycle exhibits noticeable hysteresis which may be a result of the cracking observed in the loading in positive torsion.

4.3.2.2 Tube LMB04

Figure 30 shows the shear response for tube LMB04. For both loading cycles, the shear modulus for the tube, $G_{x\theta}$, is 1.24 Msi. The linear limit, as observed in the first loading cycle, was 4.5 ksi in both positive and negative torsion. Failure occurred at the peak of the second cycle at an applied shear stress of 8.15 ksi.

In the first loading cycle, the unloading from positive torsion occurred elastically. However, in negative torsion, the response exhibited a hysteresis in the unloading. This type of

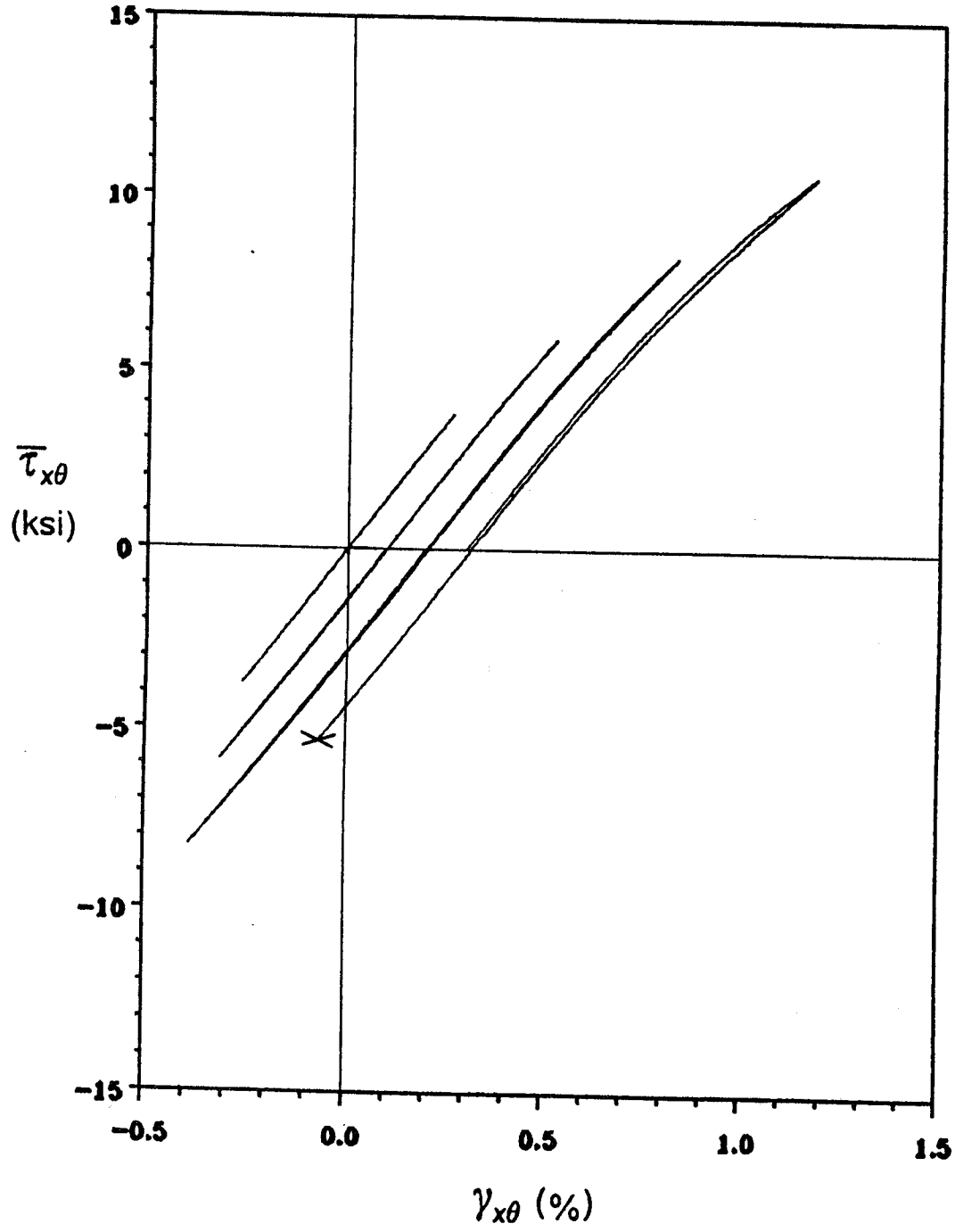

Figure 29. Shear Response of Tube LMB02 - Type II Loading

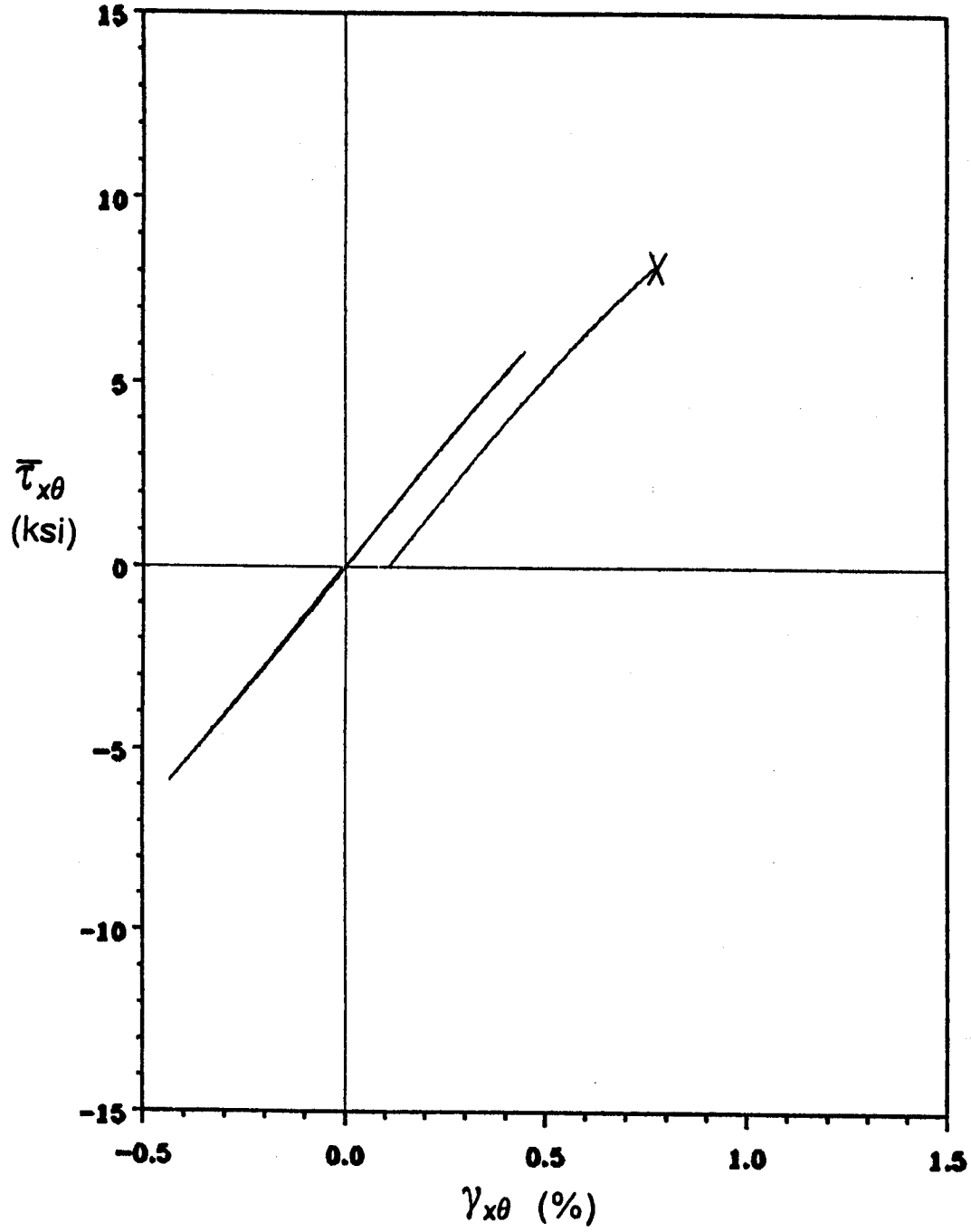

Figure 30. Shear Response of Tube LMB04 - Type II Loading

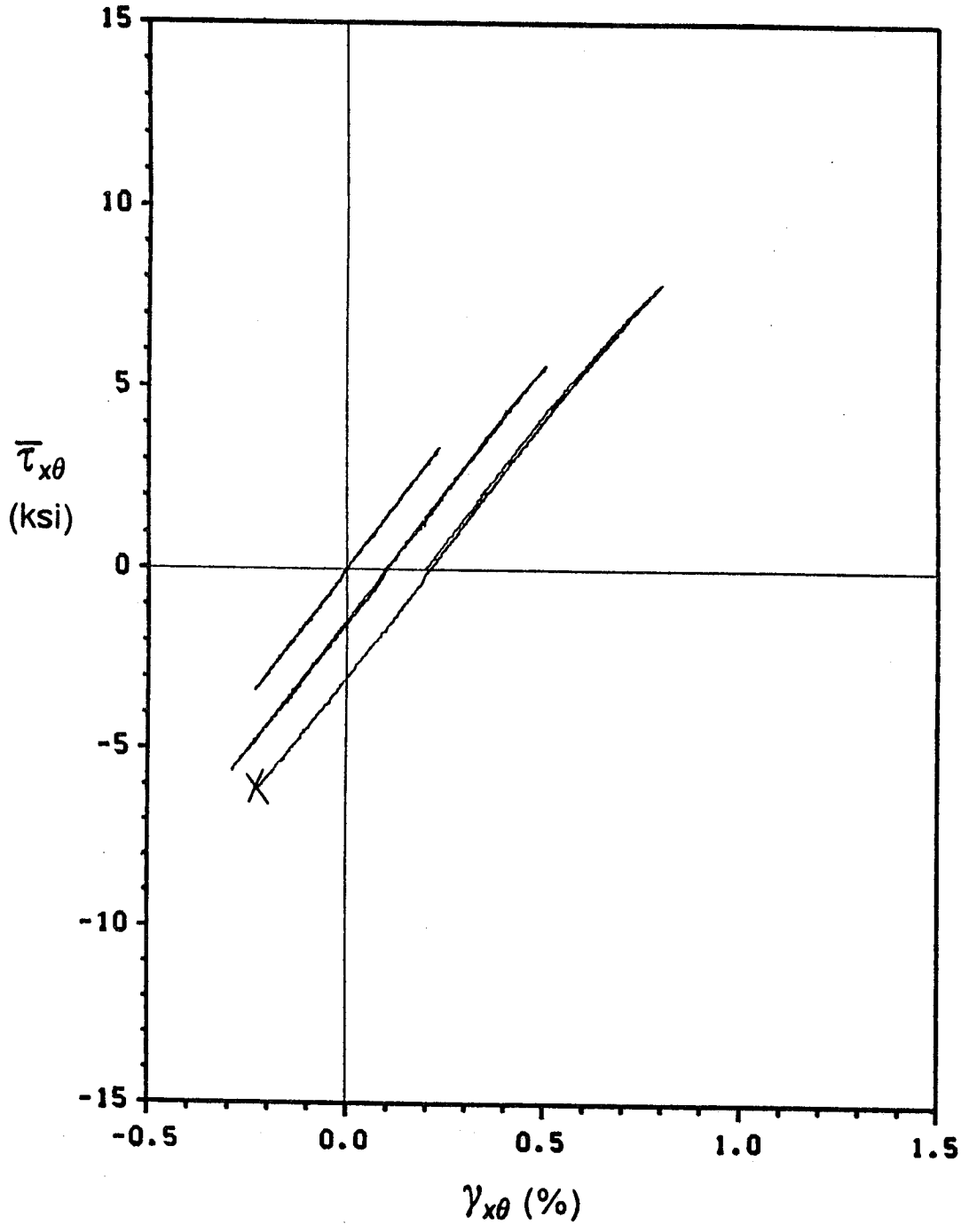

Figure 31. Shear Response of Tube LMC05 - Type II Loading

response could be due to either the onset of damage or a dissipative permanent strain in the material. On the subsequent loading in positive torsion, failure of the tube occurred at the peak of the loading cycle.

4.3.2.3 Tube LMC05

The shear response for Type II loading on tube LMC05 is shown in Figure 31. The initial shear modulus for this tube was the same for positive and negative torsion in these tests: $G_{x\theta} = 1.43$ Msi. The response of this tube is linear up to an applied shear stress of 4.8 ksi at which point the response began to soften. Failure occurred in this tube in a similar manner to the failure in tube LMB02; damage initiated in the positive torsion load up followed by failure in negative torsion at an applied stress of -6.11 ksi which is less than had been achieved in positive torsion. This test did exceed the stress applied in negative torsion in the previous load cycle.

4.3.3 Type III Loading

Tube LMC06 was tested using Type III loading; thirteen load cycles were successfully completed before failure occurred in the fourteenth cycle. The initial shear modulus of 1.27 Msi, as well as the curvature of the response was the same for each increment of load, therefore only the two final load cycles from each test will be presented to show the response through the entire loading cycle and the characteristics of failure. The linear limit for both combined proportional loading and pure torsion was 3.5 ksi.

Figure 32 shows the shear response for the thirteenth and fourteenth load cycles. The response due to combined proportional loading and unloading, as well as due to pure torsion and pure tension are indicated on the figure. The initial shear response for both the combined

proportional loading and the pure torsion are the same. The response due to pure torsion softens more than the combined proportional loading. Tension applied in addition to the torsion stiffens the response. Following the application of tension, the applied loads on the tube are the same as had been applied in proportional loading. The shear strain from the two loading paths, however, differs by 0.01%. This difference in shear strain indicates that the response may be exhibiting path dependent behavior.

The response of the final load cycle follows the same path in combined proportional loading until failure occurred at an applied shear stress of 9.5 ksi in combined proportional loading.

4.3.4 Type IV Loading

4.3.4.1 Tube LMB01

Tube LMB01 was tested in combined compression and negative torsion using the Type IV loading. Six load cycles were completed successfully before failure occurred in the seventh cycle. The shear response from the sixth and seventh load cycles is shown in Figure 33. The response for the seventh step is offset by 0.10% strain. The initial shear modulus for these tests was 1.37 Msi, and the linear limit for both pure torsion and combined proportional loading was -3.4 ksi.

The response due to combined proportional loading and unloading are indicated in Figure 33 as are the responses due to pure torsion and pure compression. The addition of compression to the negative torsion tends to soften the response by a small amount. This is in contrast to Type III loading where the pure torsion response was softer than for the combined proportional loading.

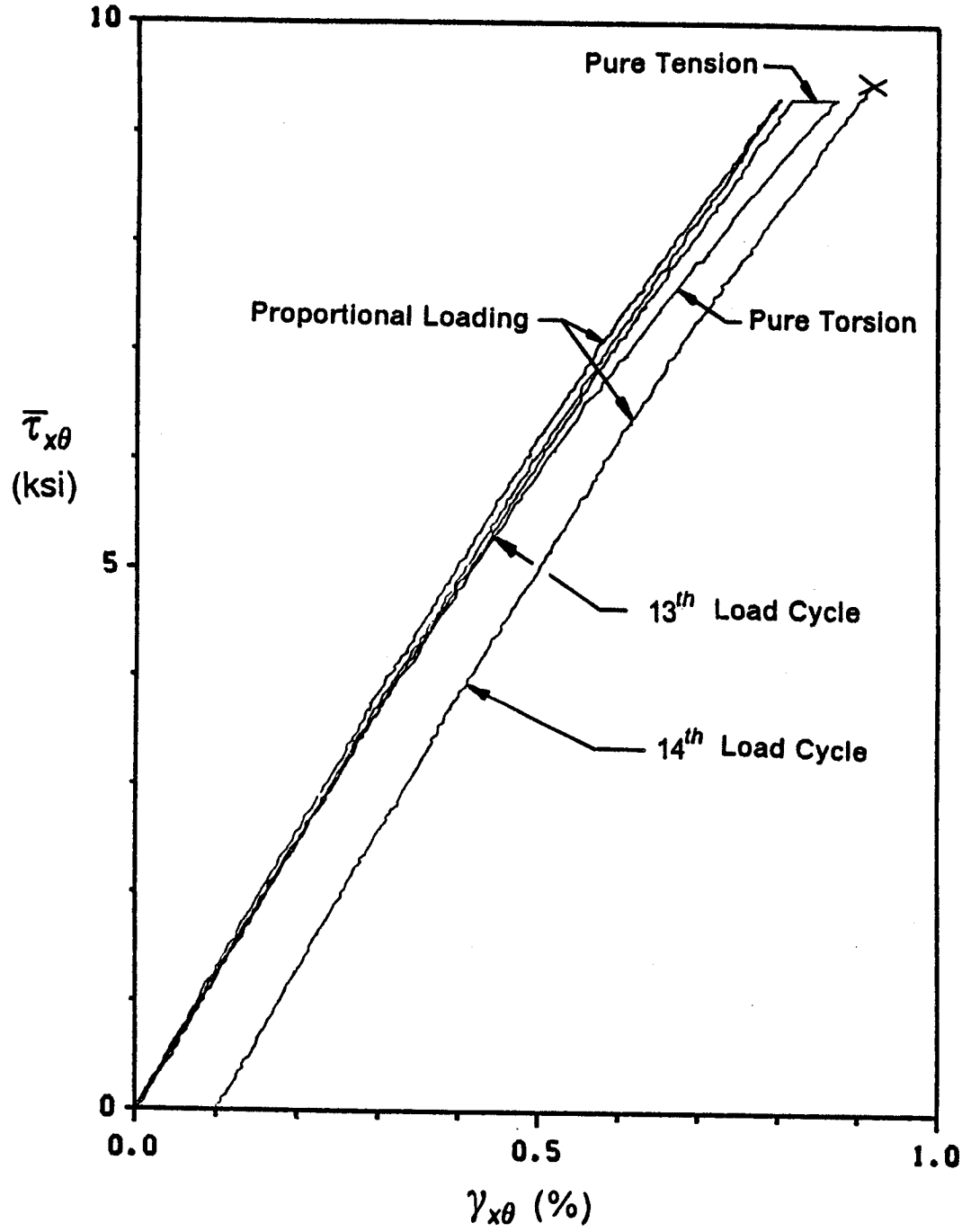

Figure 32. Shear Response of Tube LMC06 - Type III Loading

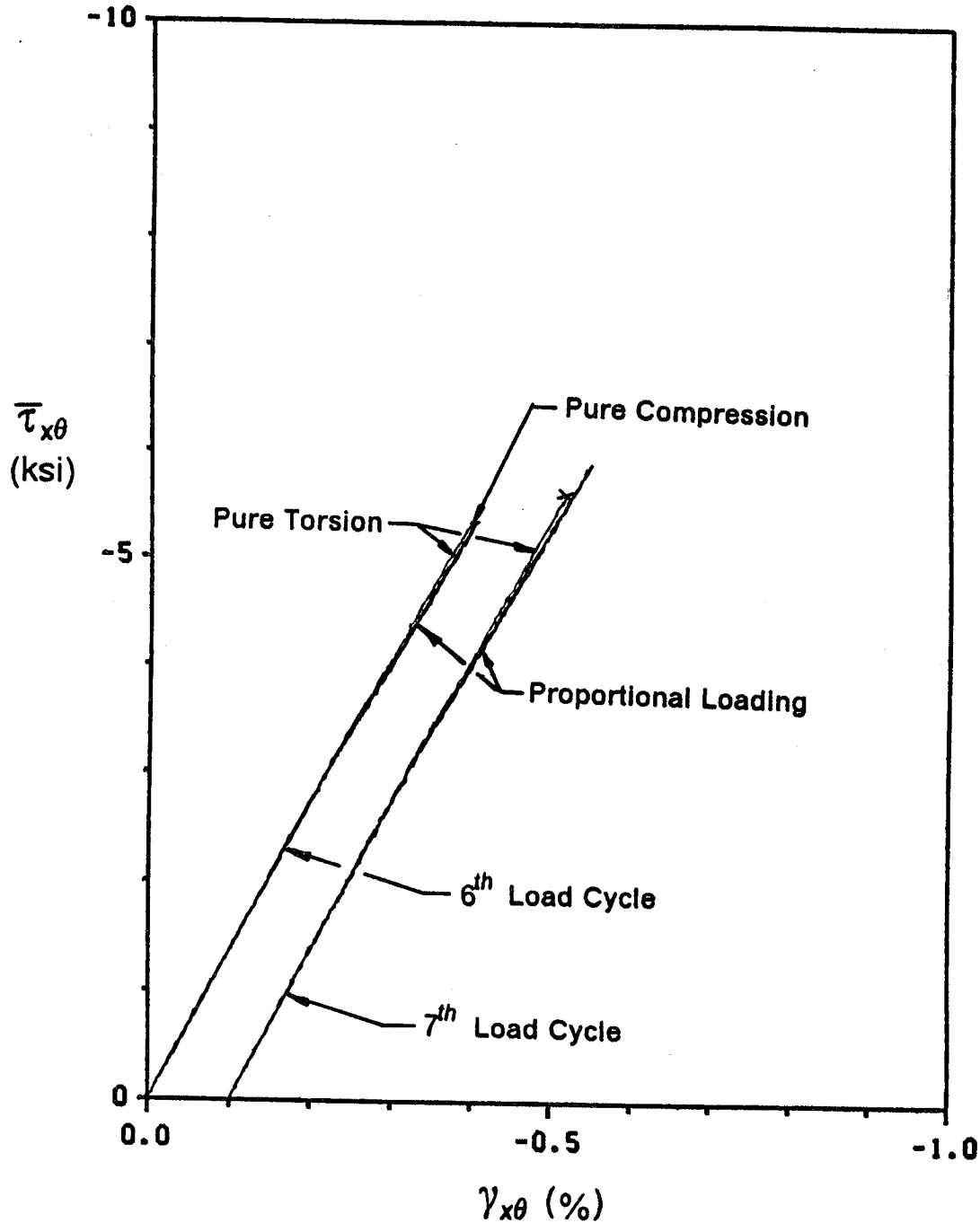

Figure 33. Shear Response of Tube LMB01 - Type IV Loading

For the final cycle the maximum loads were reached when loading proportionally in torque and compression. However, when loading in pure torsion, the tube failed at -5.6 ksi prior to reaching the torque that had been attained previously in combined proportional loading. The failure of the tube, in this case, is dependent on the loading path.

4.3.4.2 Tube LMC07

Tube LMC07 was tested using the same procedures and load cycles as tube LMB01. Despite the thermal cycling performed on this tube, seven successful load cycles were performed with failure not occurring until the eighth cycle. Figure 34 shows the results from the final two load cycles. The initial shear modulus for these tests was 1.30 Msi, and the linear limit for both pure torsion and combined proportional loading was 4.2 ksi.

The tendency for the pure torsion shear response to be stiffer than the combined loading as was detected in Tube LMB01 is not evident in this tube. The failure characteristic in this tube is the same as in LMB01: failure occurs when loading in pure torsion at -6.47 ksi following the combined proportional loading and unloading where the torsion load had reached a higher level.

4.3.5 Summary

Tests of four different load types were performed on the laminated tubes. A summary of the results for these seven tests is shown in Table 11.

For each of the seven tests performed on the laminated tubes, the initial shear modulus fell in the range between 1.42 Msi and 1.27 Msi. The experimentally observed variance in the modulus does not appear to be the result of any factor such as the effect of axial loading or

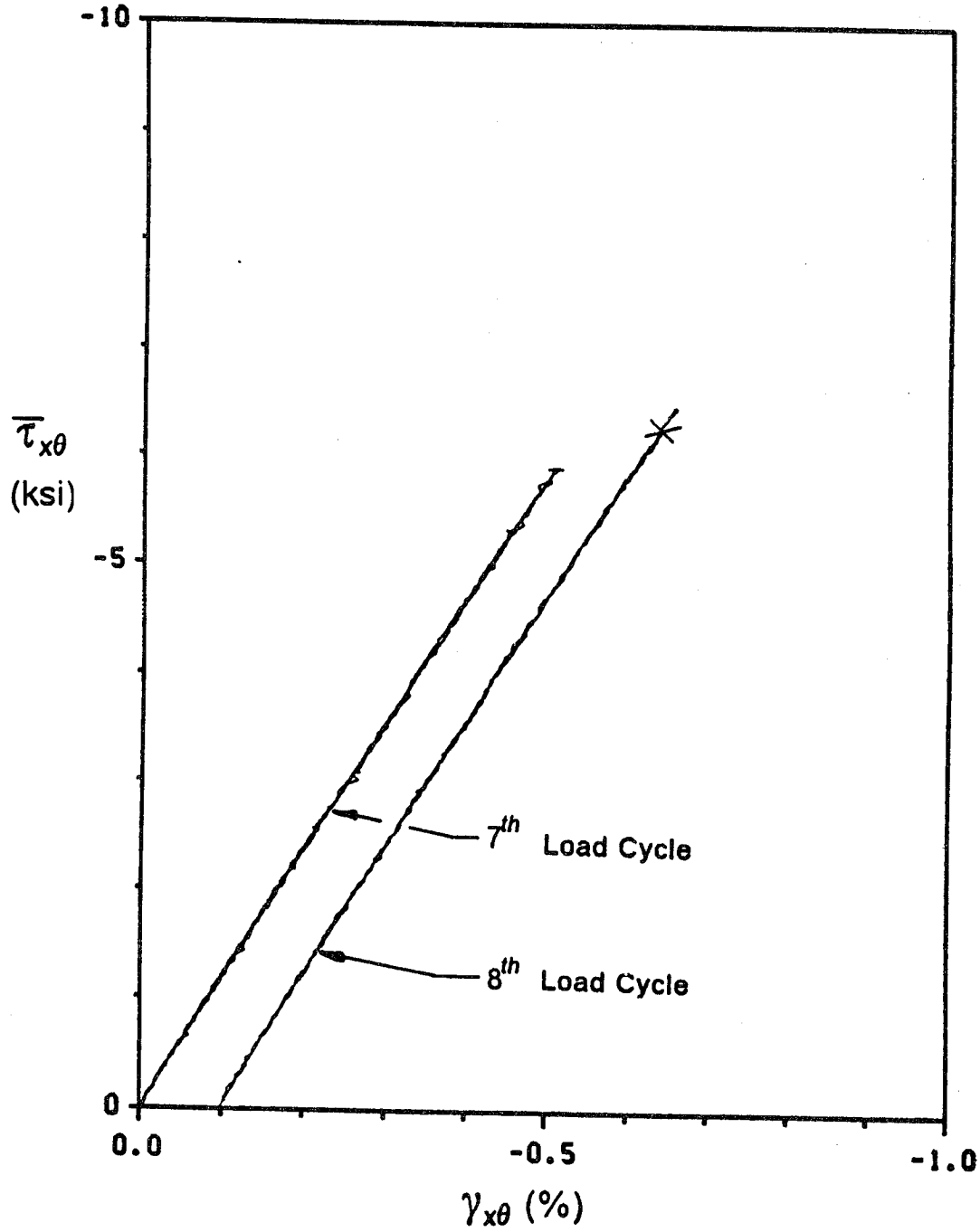

Figure 34. Shear Response of Tube LMC07 - Type IV Loading

Table 11. Summary of Laminated Tube Tests

Load Type	Tube	$G_{x\theta}$ (Msi)	Linear Limit (ksi)	$\tau_{x\theta}^{ULT}$† (ksi)	$\gamma_{x\theta}^{ULT}$† (%)	Loading at Failure‡
I	LMC08	1.32	-6.0	-8.88	-0.70	Pure Torsion(-)
II	LMB02	1.38	±4.0	-5.35	-0.36	Pure Torsion(-)
II	LMB04	1.36	±4.5	8.15	0.66	Pure Torsion(+)
II	LMC05	1.42	±4.8	-6.11	-0.42	Pure Torsion(-)
III	LMC06	1.27	3.5	9.5	0.80	Proportional (+,+)
IV	LMB01	1.37	-3.4	-5.6	-0.41	Pure Torsion(-)
IV	LMC07	1.30	-4.2	-6.47	-0.56	Pure Torsion(-)

† Corresponds to failure load rather than maximum load

‡ A single (+) or (-) represents the sign of the pure torsion applied. The double (+,+) represents the sign of the torque and axial force in the case of proportional loading.

differences between positive and negative torsion. This variance will therefore be attributed to experimental scatter.

Two loading types, II and IV, were performed in which the test was duplicated for both baseline and thermally cycled tubes. For the Type II loading, two baseline tubes, LMB02 and LMB04, and one thermally cycled tube, LMC05, were tested. Comparing the test of the thermally cycled tube, LMC05, with the test on LMB04, it is evident that the thermally cycled tube progressed further in the loading cycle than the baseline tube. The second baseline tube, LMB02, successfully completed the load cycle in which both LMB02 and LMC05 failed, and failed on the subsequent load cycle. For the Type IV loading, the thermally cycled tube, LMC07, reached a higher applied shear stress at failure than the comparable baseline tube, LMB01. The results of these tests indicate that the effect of the thermal cycling on the tubes is not significant.

The failure stress and the linear limit were dependent upon the type of loading. Under Type I loading, monotonic negative torsion to failure, the tube had a linear limit of -6.0 ksi and failed at an applied shear stress of -8.88 ksi. Four tubes of Types II and IV loading also failed in negative torsion, but they each had a loading history prior to failure. Under Type II loading, tubes LMB02 and LMC05 had linear limits of ± 5.0 and ± 4.8 ksi, respectively, and failure stresses of -5.35 and -6.11 ksi. In both cases of Type II loading, stresses of higher magnitude had been applied in positive torsion prior to failure. The effect of the loading history on these tubes was to reduce both the linear limits and the ultimate strength in negative torsion.

Tubes tested in Type IV loading, LMB01 and LMC07, which was combined negative torsion/compression, also exhibited a reduction in the linear limits and the failure stress. Both tubes tested under this loading type failed under pure negative torsion after loading in combined proportional loading where the applied torsion had reached a higher magnitude. Prior to the load cycle in which the failure occurred, tube LMB01 had experienced six loading cycles while tube LMC07 experienced seven complete load cycles. The reduction in the failure stress appears to be a result of this loading history.

The linear limits experienced by tubes LMB01 and LMC07 under Type IV loading were over 30% less than the linear limit observed in tube LMC08 under Type I loading. Because the linear limits under Type IV loading were the same for each load cycle, the reduction from the linear limit under Type I loading appears to be the result of the addition of the compressive load rather than the loading history.

Type III and IV loading were carried out using the same ratios of torsion to axial load, and the magnitudes of the load increments were the same for each type. The only difference between the two load types was the sign of the loading. Failure in the Type III loading occurred at 9.5 ksi which is approximately a 50% increase in magnitude of the failure in Type IV loading. In addition to the magnitude of the stress at failure, the loading at failure differed between the two types; Type III failed under combined proportional positive torsion/tension loading while the Type IV tubes failed under pure negative torsion.

For the load levels tested, only the Type III loading exhibited a slight path dependent response. The path dependent phenomena did not become apparent in Type III until the magnitudes of the loads applied had surpassed those that had been attained under Type IV loading.

When failure occurred in the tubes under any of the four loading types, a crack along the length of the tube would propagate along the length. At the free edge, the tube would experience an offset of the free edge in the axial direction. This offset is a result of residual stresses present in the tube due to the fabrication process.

5.0 Analytical / Experimental Correlation

5.1 Introduction

In this chapter, results from the laminated tube tests presented in Section 4.3 will be compared with predictions of the analytical model developed in Chapter 2. The material properties determined for P75/934 graphite/epoxy in Chapter 4 will be corrected for differences in fiber volume fraction between the flat panels and the laminated tubes. These corrected properties will then be used as input for the analytical model predictions. The effect of residual stress on the initial response will be examined as well as the importance of the consideration of nonlinear material behavior at the ply level on the predictions of the tube response and failure.

5.2 *Parameters Affecting Initial Response*

5.2.1 Material Property Correction

As discussed in the Chapter 3, there is a discrepancy between the fiber volume fraction of the laminated tubes and the flat panels. The difference in the fiber volume fraction will result in a difference in material properties. In order to accurately predict the response of the tube with the analytical model, an accurate set of material properties is required for the tubes.

The causes for the discrepancy between the fiber volume fractions of the panel and the laminated tube are the lower density of fibers within the layers and the existence of resin-rich regions separating these layers. For accurate predictions from the analytical model, consideration for both causes will be made. The properties of the layers in the tube will be determined with the help of a micromechanical model using the known material properties determined from the flat panel, and the resin-rich regions between the layer will be characterized for use in the analytical model.

5.2.1.1 Micromechanical Model

The micromechanical model chosen for the purpose of correcting for the lower fiber volume fraction is the model developed by Aboudi[36]. The fibers are assumed to be square and arranged in a uniform, square array. A representative cell is chosen that consists of four subcells; one subcell contains the fiber while the other three contain the matrix, see Figure 35. By requiring that the continuity of tractions and displacements at the interfaces of the subcells be satisfied, the average properties of the lamina can be determined from known fiber and matrix properties at a given fiber volume fraction.

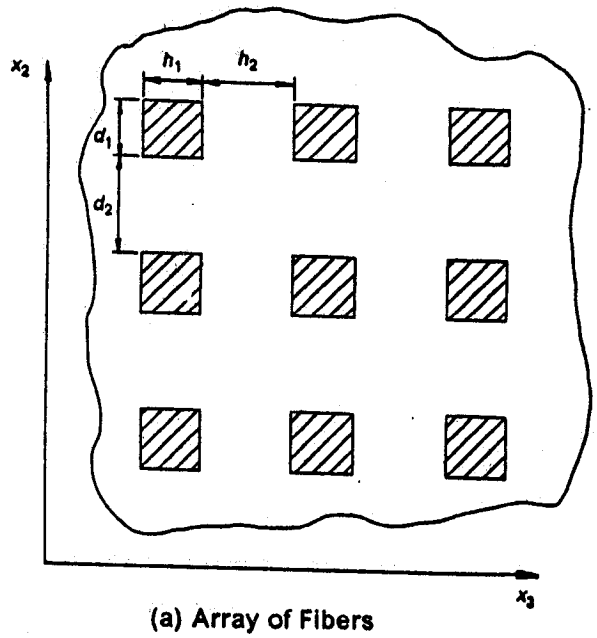

(a) Array of Fibers

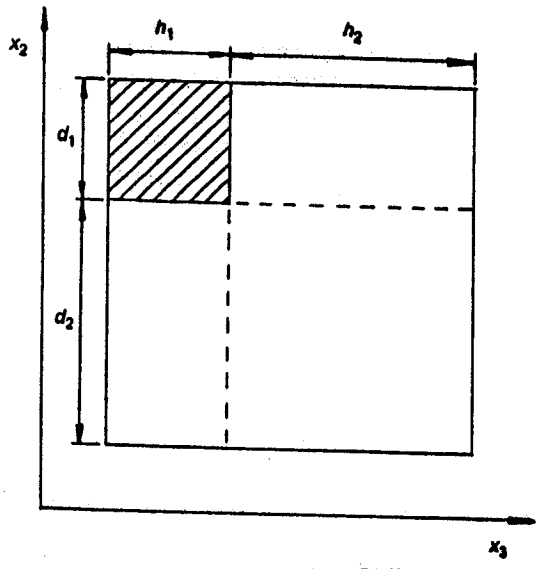

(b) Representative Cell

Figure 35. Micromechanical Model

Rather than determining the properties of the composite from known constituent properties, the properties of the fiber will be determined from known matrix and composite properties. The lamina properties are already known as determined in the previous chapter. The properties of the 934 epoxy matrix have been determined by Fox et al[37]. For the fiber volume fraction of the panels (65%), the fiber properties can be determined. The results of this procedure are:

$$E_A = 53.90 \text{ Msi}$$
$$E_T = 1.24 \text{ Msi}$$
$$\nu_A = 0.343$$
$$\nu_T = 0.440$$
$$G_A = 1.120 \text{ Msi}$$

where the subscript A represents the axial direction and T the transverse direction. The results given above have been independently verified by Professor Aboudi[38].

From the known fiber and matrix properties, the lamina properties can now be calculated for a fiber volume fraction of the layers in the tube (57%) from the Aboudi Model. The reduced lamina properties of the P75/934 graphite/epoxy in the tubes are:

$$E_{11} = 30.99 \text{ Msi} \quad (-12.1\%)$$
$$E_{22} = 1.003 \text{ Msi} \quad (-16.4\%)$$
$$\nu_{12} = 0.352 \quad (+6.3\%)$$
$$\nu_{23} = 0.499 \quad (+1.8\%)$$
$$G_{12} = 0.515 \text{ Msi} \quad (-9.6\%)$$

where the percentage changes from the properties determined from the material characterization tests are also given. The nonlinear behavior of the material will be assumed to be unaffected by the change in fiber volume fraction.

5.2.1.2 *Modeling the Tube Cross Section*

In Section 3.4, the configuration of the laminated tubes was discussed. It was determined that the resin-rich regions at the ply interfaces and inner and outer surfaces, if considered as separate plies, accounted for approximately 7% of the overall thickness of the tube.

So that the thickness of each resin layer and graphite/epoxy layer does not have to be measured from the micrographs for each tube for incorporation into the analytical model, several assumptions will be made. Since all seven tubes that were tested were cut from a single ten foot long tube, the fiber volume fraction of the graphite/epoxy layers and the percentage of resin layers will be assumed to be the same for each tube. For simplicity, we will assume that all of the graphite/epoxy layers are the same thickness. The same assumption will be made for the resin layers.

Using these assumption, the procedure for determining the thickness of each of the plies is as follows. The overall thickness of the tube is measured in four locations around the circumference of the tube and averaged. The total thickness of the graphite/epoxy layers is determined by multiplying the average overall thickness by 0.93; this is in turn divided by the number of layers (12) to obtain the individual ply thickness. Similarly, the individual ply thickness for the resin layers is obtained by multiplying the average overall tube thickness by 0.07 and dividing by the number of resin layers (13).

Figure 36 shows a comparison between the pure cyclic torsion experiment (Type II) on tube LMB02 and the predictions of the analytical model using uncorrected material properties (as determined in Chapter 4) and corrected properties and cross section in the absence of residual stress. The initial shear modulus for the experimental curve is 1.38 Msi, and the shear modulus for the analytical model using corrected and uncorrected material properties are 1.50 Msi and 1.32 Msi. The correction of the material properties and consideration for the actual cross section does more accurately predict the initial shear response of the experiment.

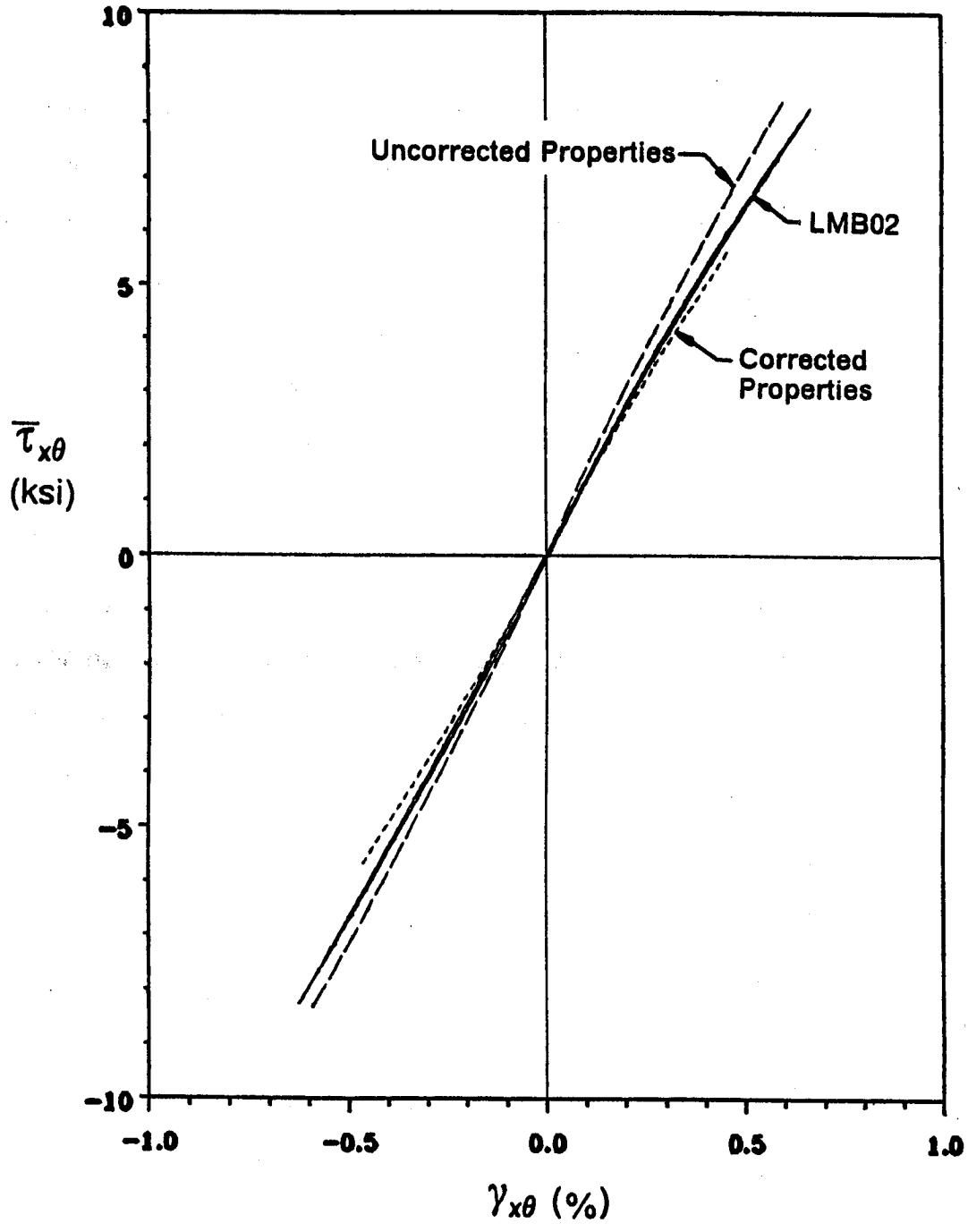

Figure 36. Comparison of Corrected to Uncorrected Properties

5.2.2 Residual Stress

As pointed out in the previous chapter, there is evidence of residual thermal stresses being present in the laminated tubes that were tested. For the purpose of predicting the magnitudes of the residual stresses on the basis of the outlined analytical model, a stress-free temperature of 350°F will be used. This temperature is the cure temperature for P75/934 graphite/epoxy, and, although it may be a conservative (high) estimate for the stress-free temperature, a more accurate estimate is presently not available. All of the experiments performed on the laminated tubes were carried out at room temperature so the temperature difference used to calculate the residual stress is -275°F.

According to linear analysis, the inclusion of residual stresses does not affect the initial response due to a mechanically applied load. Nonlinear analysis, on the other hand, does predict a difference between the initial modulus with residual stress and without residual stress. Figure 37 shows a comparison between pure cyclic torsion on tube LMB02 and non-linear analysis with and without residual stresses. The incorporation of the residual stresses decreases the initial modulus of the shear response predicted by the analytical model from 1.32 Msi to 1.20 Msi.

The reason for the difference in the initial response predicted by linear and nonlinear analyses is the state of stress in the tube due to the temperature change. Figure 38 and Figure 39 show the distribution of the σ_1 and σ_6 stress components through the thickness of the tube. The solid lines represent the residual state of stress for $\Delta T = -275°F$, and the dashed lines represent the state of stress resulting from the subsequent application of the first load increment in torsion. It is evident that the external $+15°$ layers are the most highly stressed layers with axial stress of -12.5 ksi and shear stresses of -1.7 ksi following the application of torsion. The result of the presence of residual stresses in these layers is that the nonlinear region of the material is reached as soon as the torsion is applied.

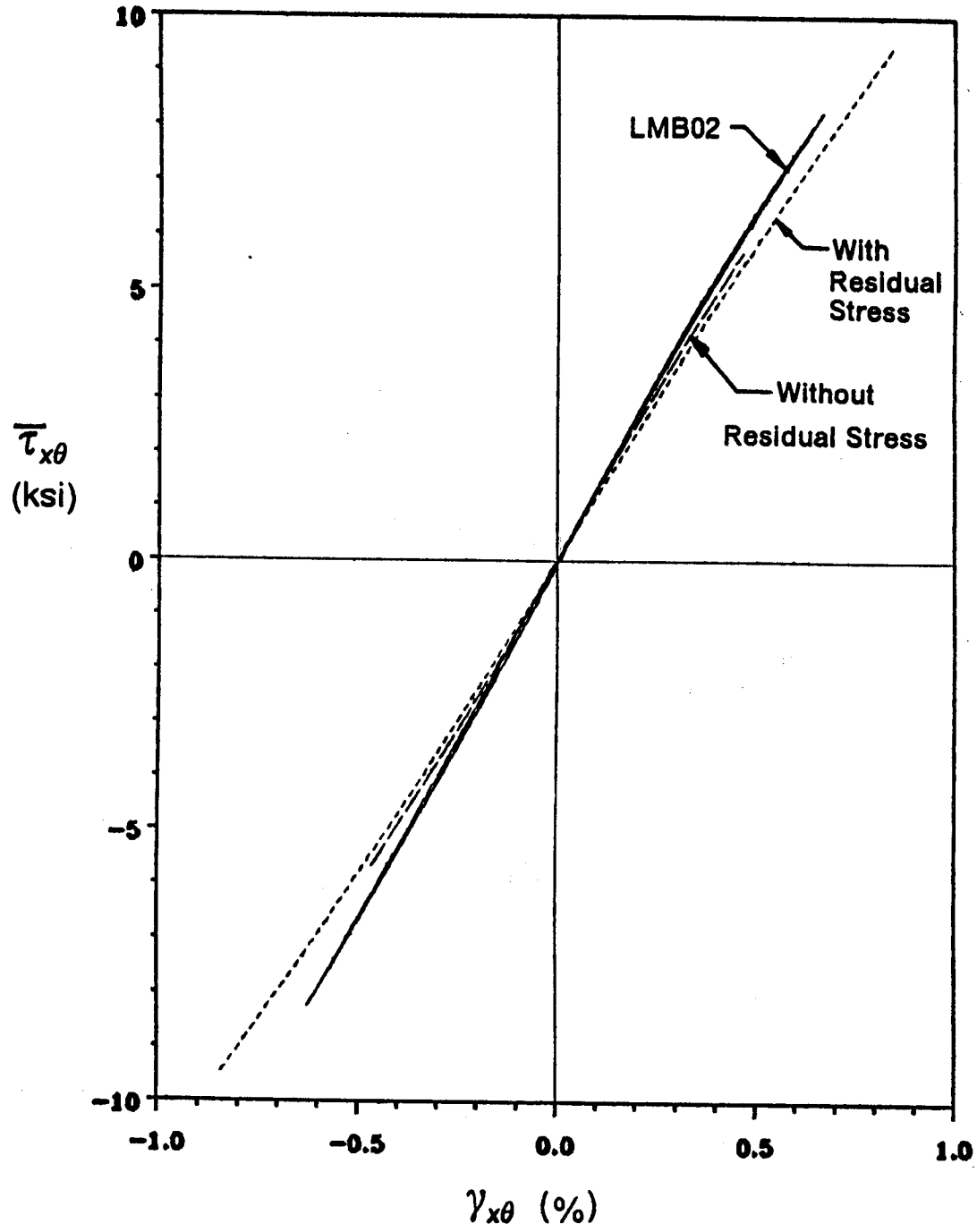

Figure 37. Comparison of Residual Stresses to No Residual Stresses

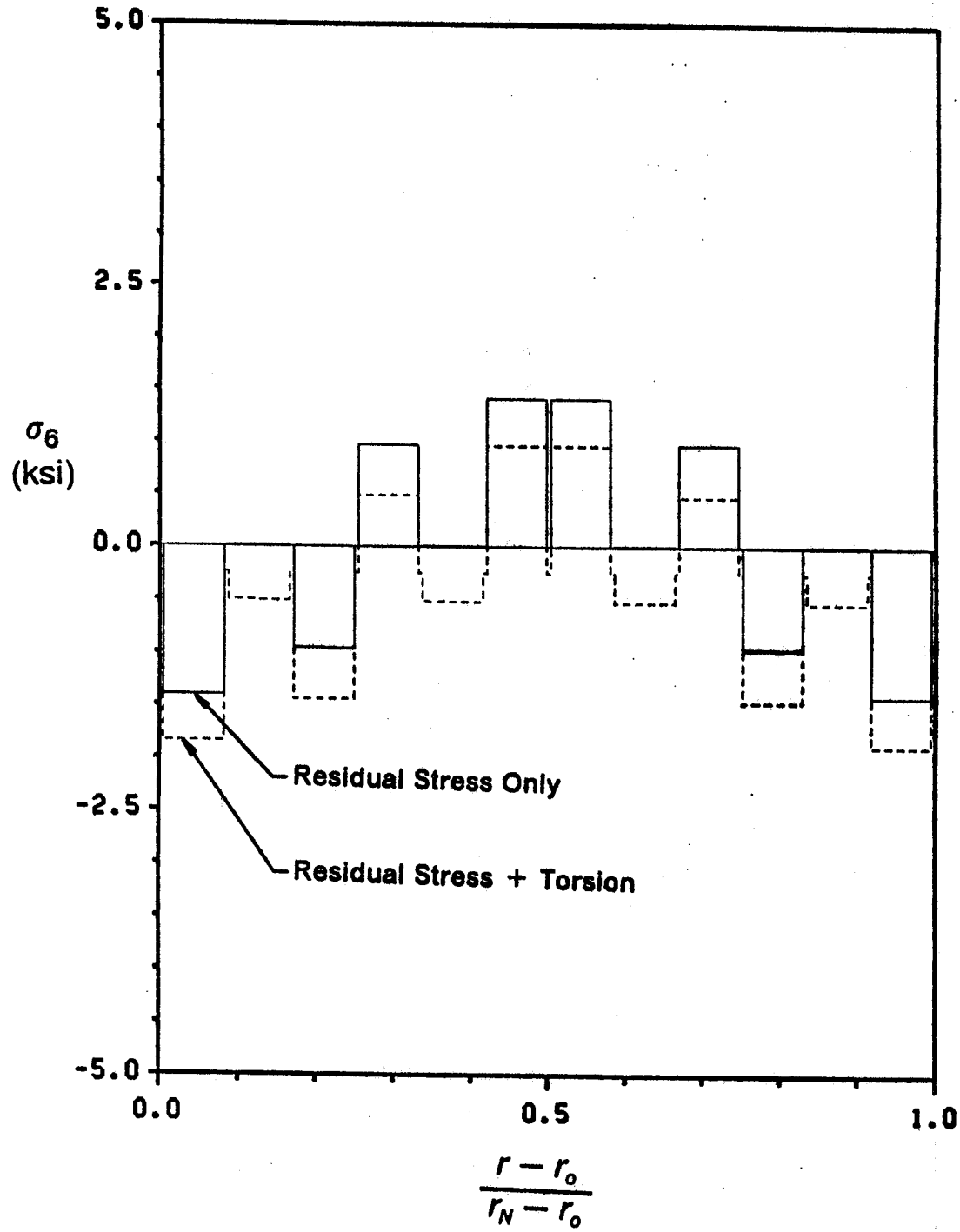

Figure 38. Distribution of Axial Residual Stresses

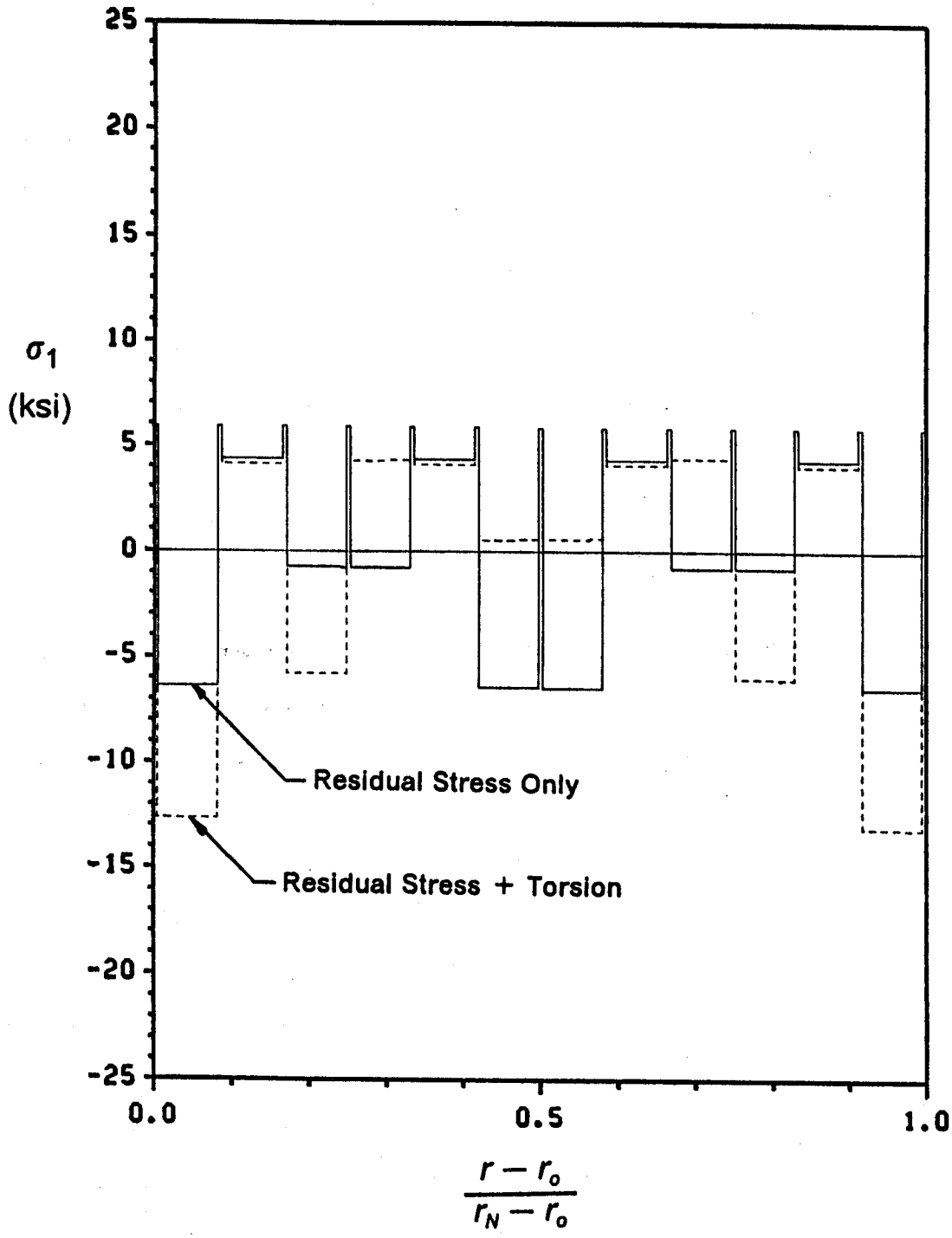

Figure 39. Distribution of Shear Residual Stresses

5.3 *Predictions of the Analytical Model*

Nonlinearity in the response of the laminated tubes is evident from the results of the experiments presented in Chapter 4. The prediction of the nonlinear behavior is an important objective for the development of the analytical model.

5.3.1 Stress-Strain Response

5.3.1.1 Contributions to Global Nonlinearity

The nonlinear stress-strain response of the tube, prior to the occurrence of localized failure in the individual layers, is a result of the uncoupled nonlinear response in the axial direction - stiffening in tension and softening in compression - and to shear stress. Because the nonlinear stress components are uncoupled, the contribution of each nonlinear component to the global nonlinear shear response can be investigated. Figure 41 and Figure 40 show the global response of the tube under pure cyclic torsion loading (Type II loading) plotted with the separated effects of the axial and shear nonlinearities. Figure 40 shows the response without residual stress and Figure 41 shows the response with residual stress. Without residual stresses, the initial moduli of the three curves are identical as demonstrated in the previous section. In this case, the response in which the only nonlinearity considered is σ_1 follows nearly the same path as the case for which both σ_1 and σ_6 nonlinearities are considered. The response due to the consideration of nonlinearities in σ_6 only is nearly linear. The same trends are evident for the case of residual stresses. This indicates that the global nonlinear response to torsion is due primarily to the nonlinear behavior in the axial direction,

and, since the response is softening, the nonlinearities are dominated by the nonlinear response in compression.

5.3.1.2 Combined Loading Response

Figure 42 shows a comparison of the predicted global stress-strain response to Type III loading using linear and nonlinear analysis. The linear curve predicts the same shear response for combined proportional loading and pure torsion. In other words, the linear model does not predict coupling between axial loading and shear strain.

The nonlinear analysis predicts the same initial shear modulus for the combined proportional loading and for pure torsional loading which is softer than that predicted using linear analysis as demonstrated in Section 5.2.2. The predicted response due to combined proportional loading exhibits a higher degree of softening than for pure torsion. In addition, coupling between axial tension and shear strain is present.

Figure 43 shows the linear and nonlinear analytical predictions of the global stress-strain response for Type IV loading. As with the predictions for Type III loading, the linear model is incapable of predicting differences in response due to the different loading paths. For this type of loading, the nonlinear analysis predicts the response to pure torsional loading to be more nonlinear than the response due to combined proportional loading. This is in contrast to the predictions for Type III loading. Coupling between axial loading and shear strain is also predicted for this type of loading.

5.3.2 Failure

The nonlinearity observed in the global response of the tubes tested can be the result of material nonlinearities as well as damage evolution in the form of individual ply failures.

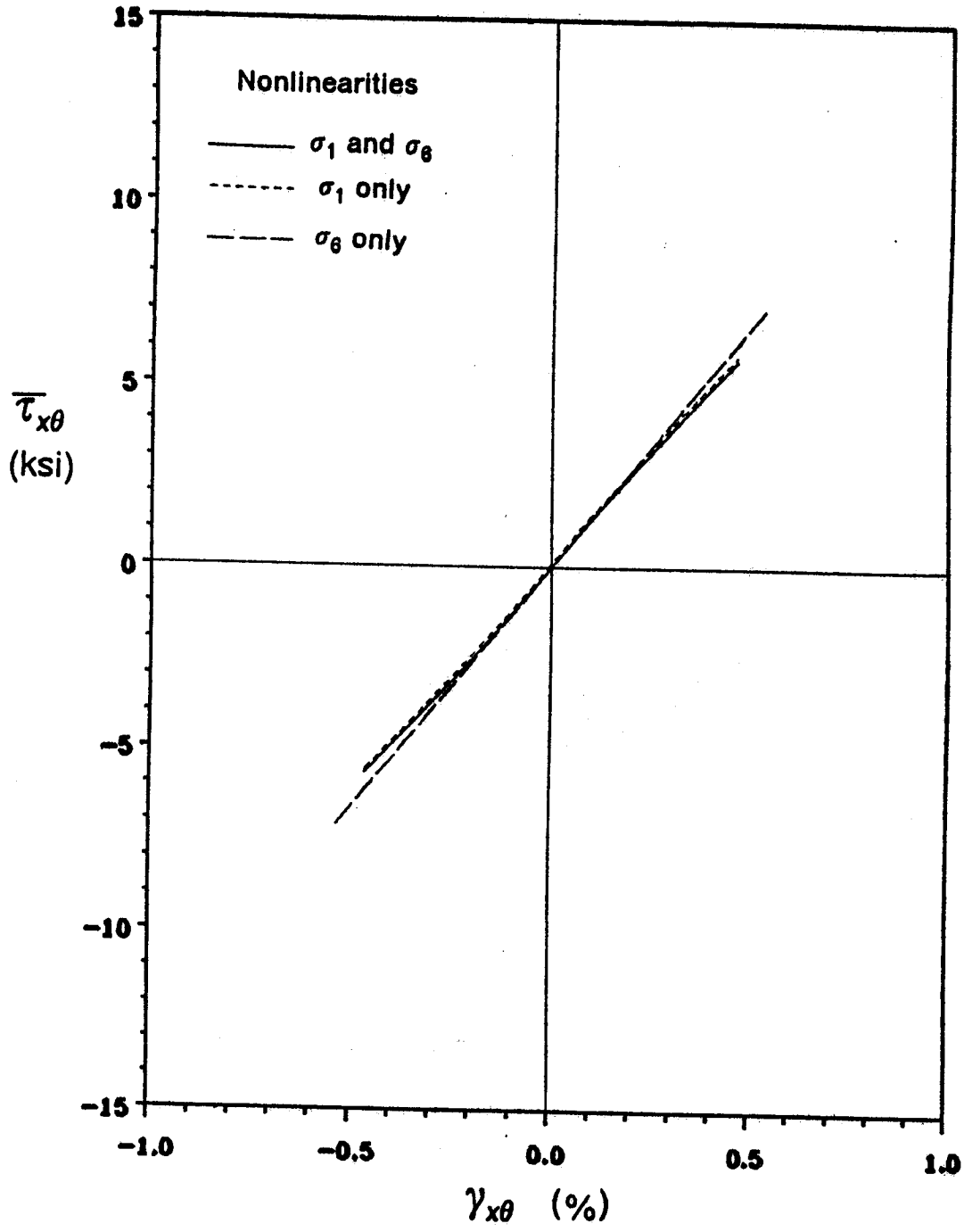

Figure 40. Contributions to Global Nonlinearity - Without Residual Stress

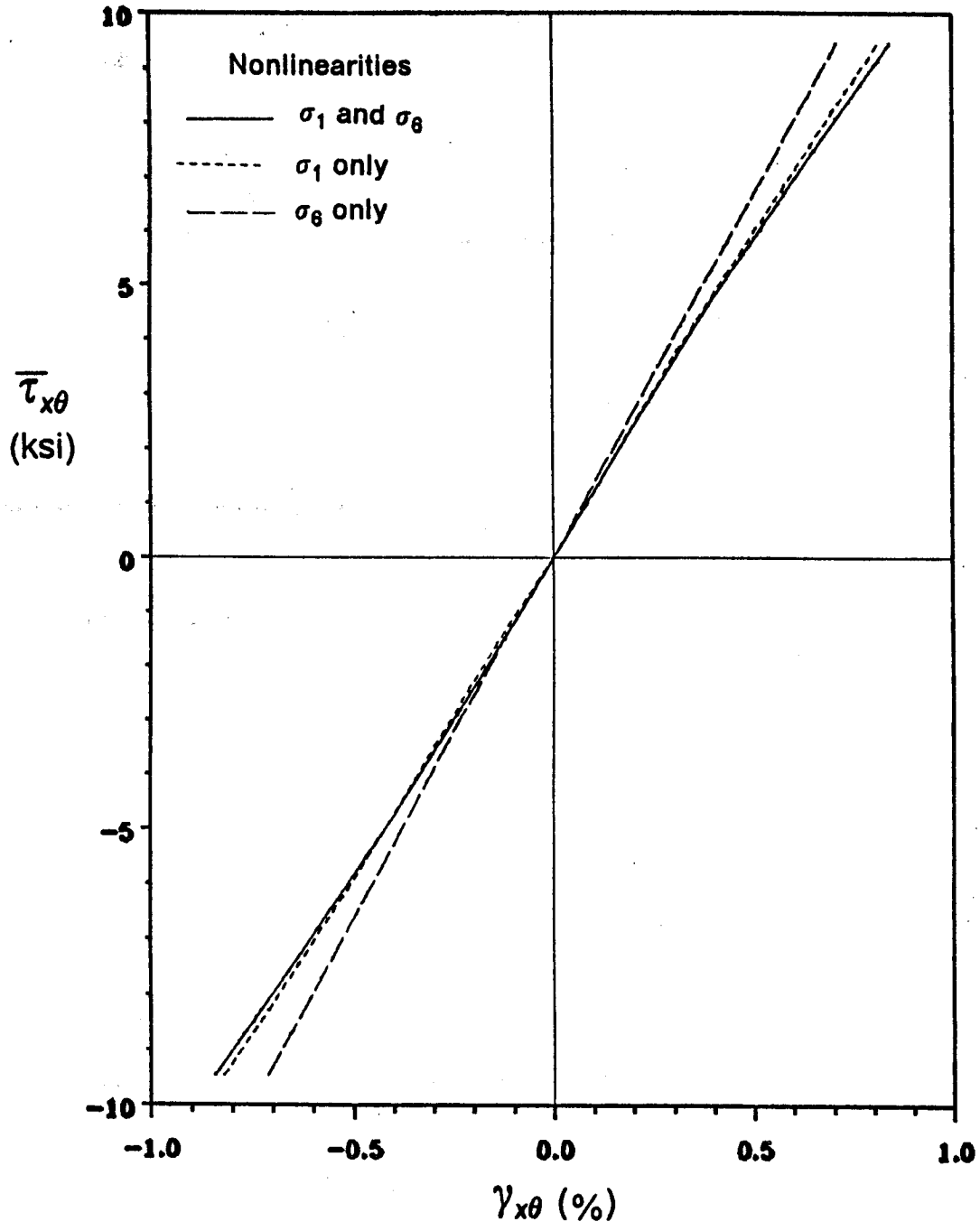

Figure 41. Contributions to Global Nonlinearity - With Residual Stress

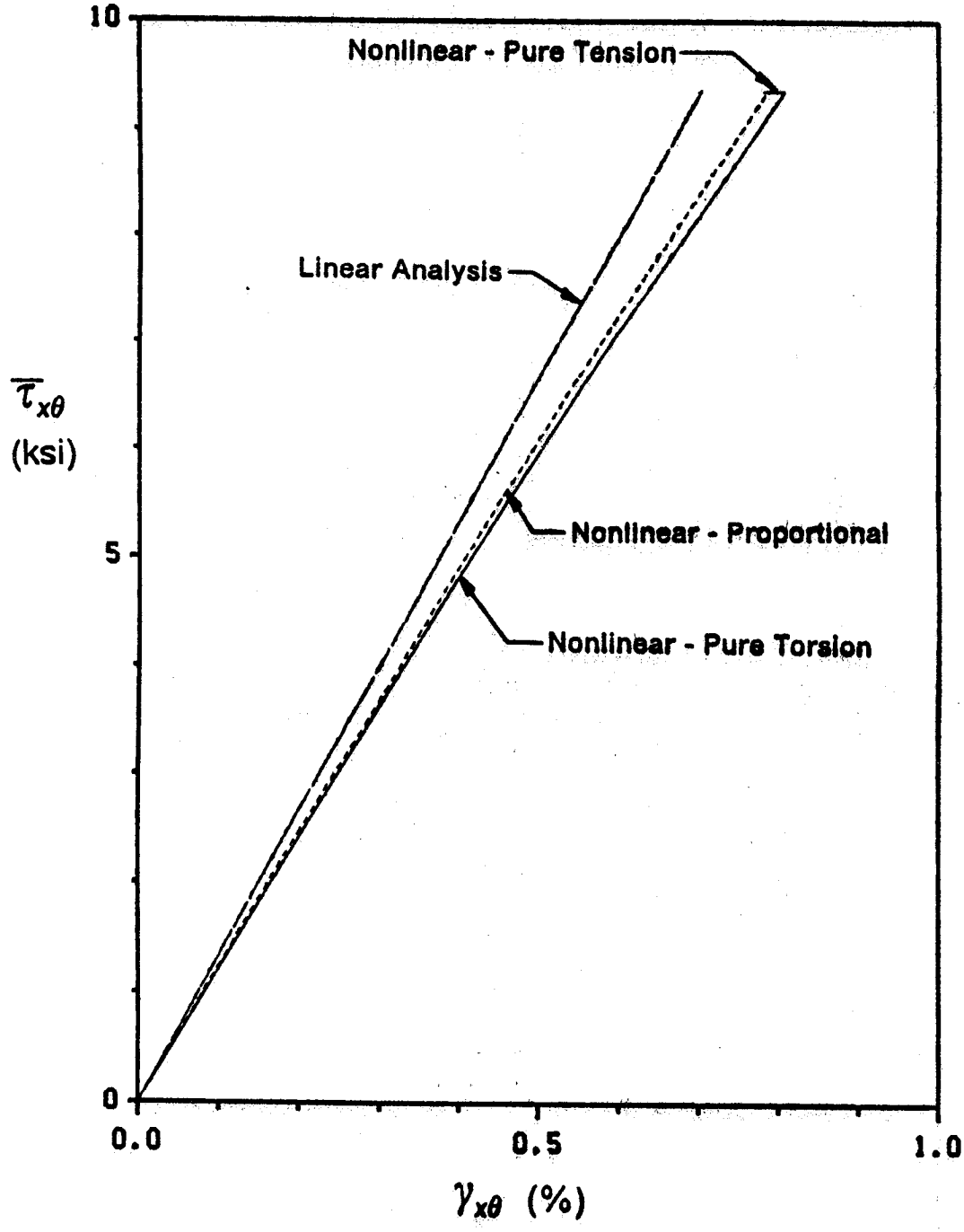

Figure 42. Comparison of Linear and Nonlinear Analysis - Type III Loading

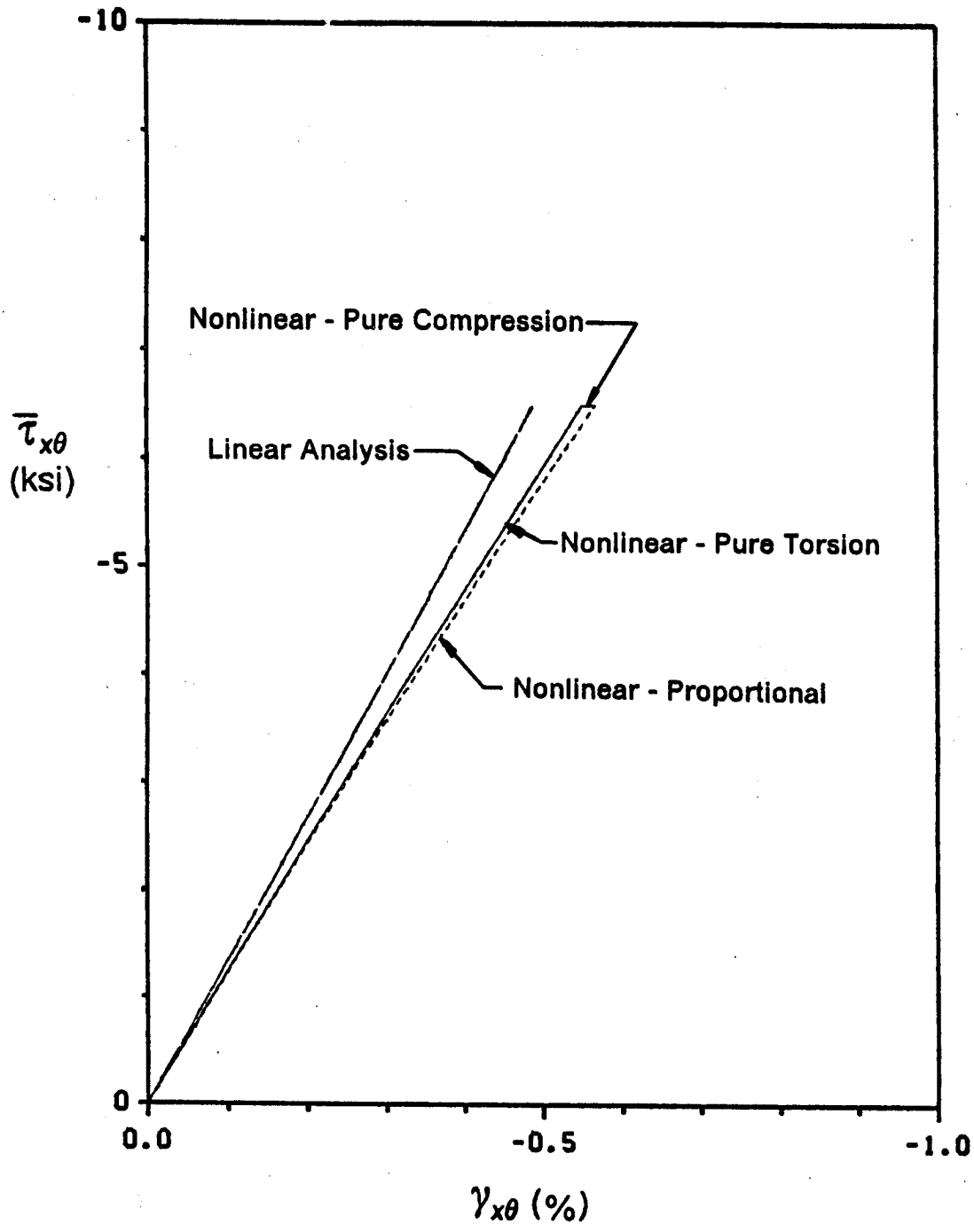

Figure 43. Comparison of Linear and Nonlinear Analysis - Type IV Loading

In order to properly evaluate the underlying causes of the observed nonlinear response, it is necessary to predict the magnitude of the applied loads at which first ply failure occurs. Using the Tsai-Wu failure criterion described in Chapter 2, a failure envelope for the laminated tubes has been determined. The failure envelope will describe the state of applied average shear stress, $\tau_{x\theta}$, and average axial stress, σ_x , at which first ply failure in the laminated tube will occur.

Figure 44 shows the failure envelopes for the linear and nonlinear cases where residual stresses have not been included. These surfaces were determined using three points in each quadrant. Each surface in this figure is symmetric about $\tau_{x\theta} = 0$, but, due to the large difference between the tensile and compressive ultimate strengths in the fiber direction, the failure surface predicts failure for larger magnitudes of combined loading for which the axial component is positive than for which the axial component is negative. The linear and nonlinear failure surfaces predict similar loading state at failure for combined loading states in which σ_x is compressive, but significant differences exist between the linear and nonlinear failure surfaces for combined loading states with positive σ_x. In addition to predicting lower failure loads for positive σ_x, the curvature of the nonlinear failure surface is concave. Palmer, Maier, and Drucker[39] discussed the issue of concavity in reference to yield surfaces. They found that for a composite for which one of the constituents is elastic-perfectly plastic and the other is nonlinearly elastic of the stiffening type, the yield surface in concave. They concluded that the concavity was a result of the stiffening behavior of the one constituent. Mathematically, the descriptions of both the yield surfaces and failure surfaces involve quadratic functions of the stress components whose constant values represent convex surfaces in the appropriate stress space. Depending upon the definitions of yield and failure that are employed, the yield and failure surfaces can be coincident. The concavity of the failure surface shown in Figure 44, then, is due to the stiffening behavior in the fiber direction.

Figure 45 shows the results of adding the effect of residual stresses for the linear and nonlinear cases. The residual stresses have the effect of reducing the failure loads for all

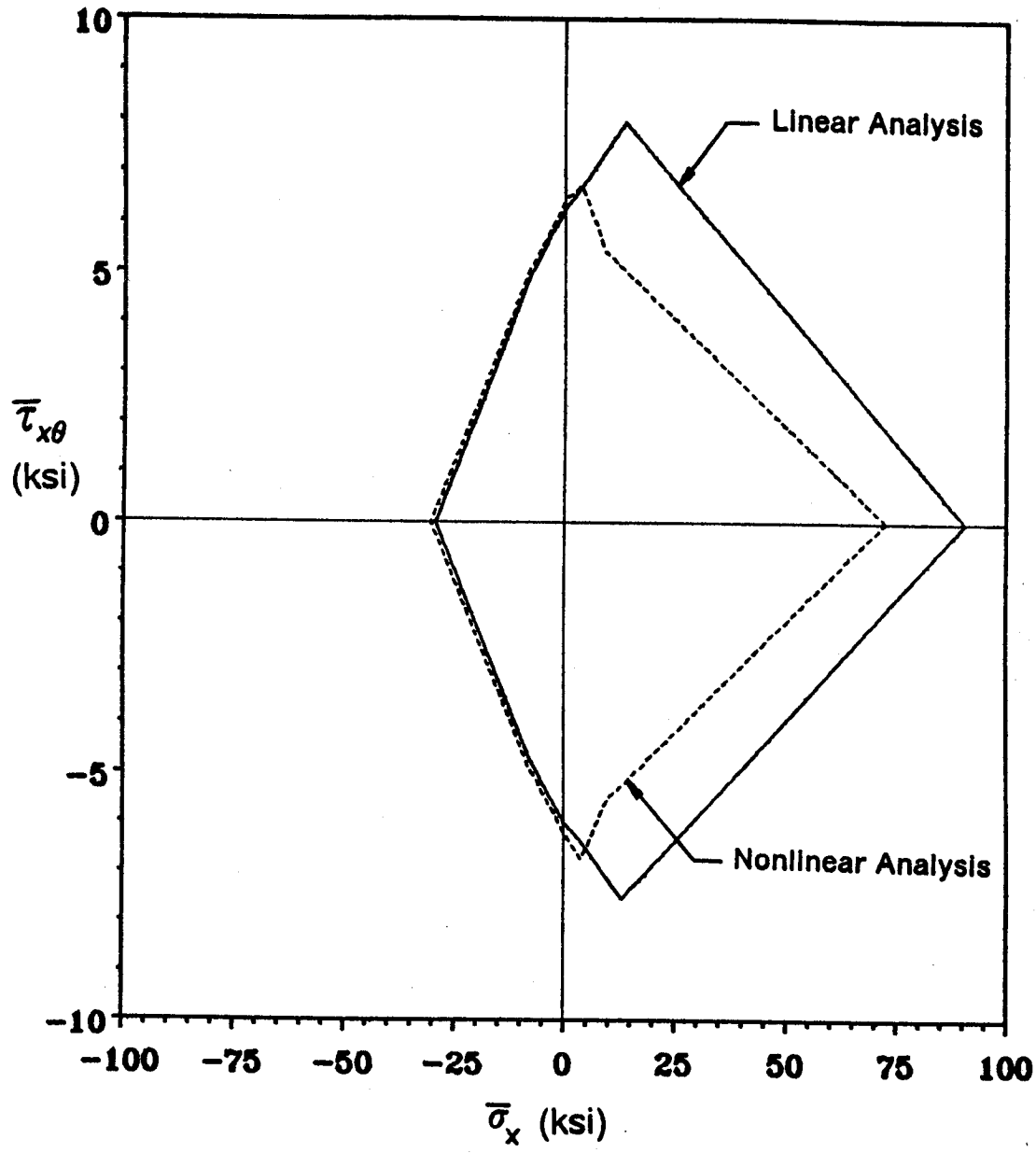

Figure 44. Failure Envelopes Based on Linear and Nonlinear Analyses - Without Residual Stress

proportions of loads, and, interestingly, the concave characteristics disappear in the presence of residual stresses.

5.4 Correlation of Results

In this section the predictions of the analytical model for Types II, III, and IV loading will be compared with the experimental results. Corrected material properties as determined in Section 5.2.1 will be used, and the effects of residual stresses will be included.

5.4.1 Type II Loading

A comparison between analysis and experimental results for the test on tube LMB02 has been shown earlier in this chapter in Figure 37 where the stress-strain response of the third of four load cycles is shown. As noted previously, the prediction of the initial modulus (including residual stress) is 1.20 Msi, and the shear modulus determined from the experiment is 1.38 Msi. In terms of nonlinearity, the experimental results exhibit a slightly larger amount of softening than is predicted by analysis. The linear limit from the experiment, as shown in Table 11 is 4.0 ksi; the analytical prediction for the linear limit is 4.6 ksi.

The nonlinear analysis predicts first ply failure in the -15° layers at $\tau_{x\theta}$ = 4.17 ksi in positive torsion. In negative torsion, first ply failure is predicted in the +15° layers at $\tau_{x\theta}$ = -4.23 ksi. The onset of the experimentally observed nonlinearity appears to correlate well with the analytical prediction for first ply failure. Tube LMB02 failed in negative torsion at $\tau_{x\theta}$ = -5.35 ksi subsequent to loading in positive torsion to higher magnitudes of applied shear stress. This failure stress is also well below that achieved in monotonic negative torsion, -8.88 ksi. Tube LMC05 exhibited similar characteristics of failure. The reason for failure at an appar-

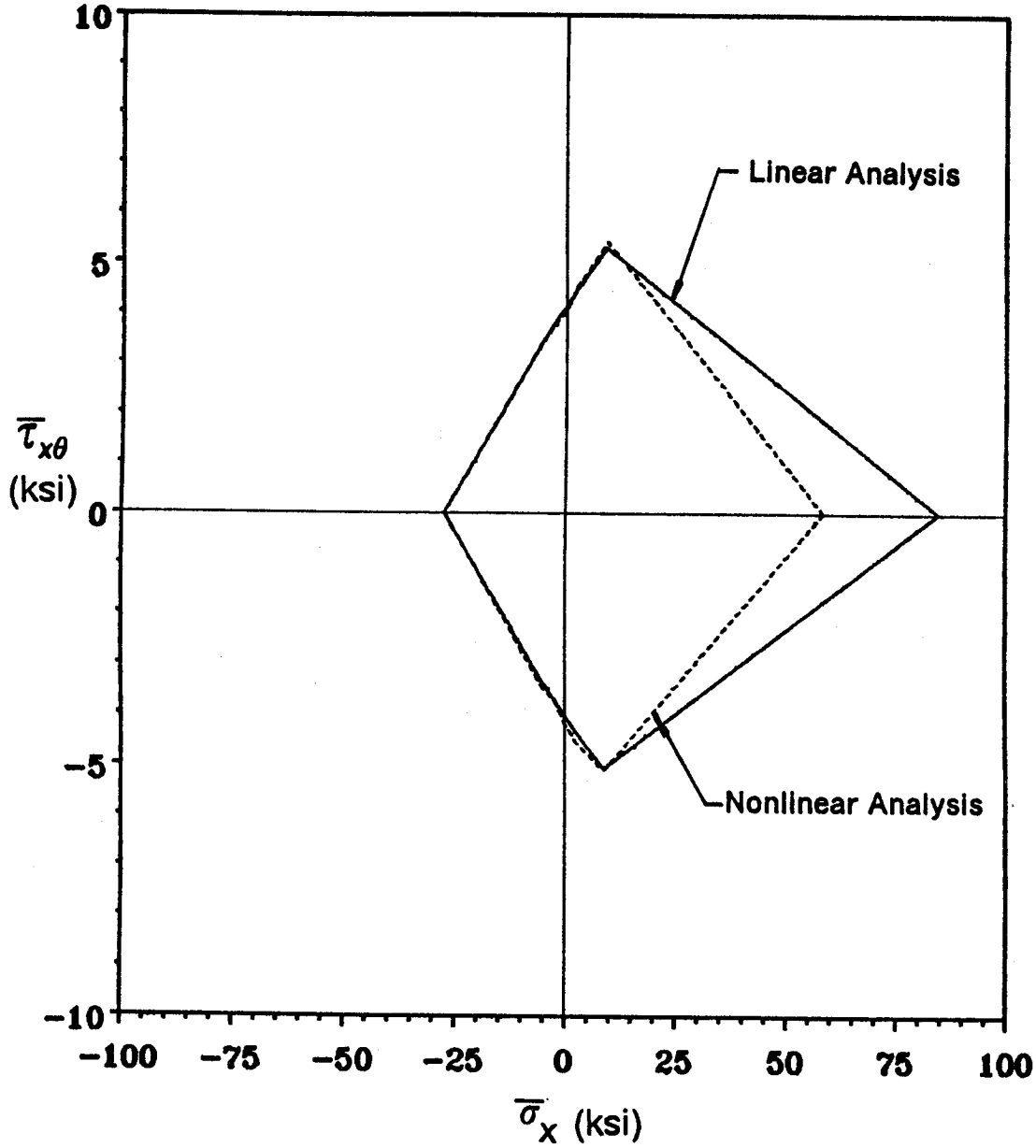

Figure 45. Failure Envelope Based on Linear and Nonlinear Analyses - With Residual Stress

ently low applied stress is that in previous load cycles, stress at first ply failure had been exceeded for both positive and negative torsion. Therefore both the +15° layers on the surface of the tube and the -15° layers on the interior of the laminate have been failed, reducing the load bearing capability under cyclic loading in, say, negative torsion only.

5.4.2 Type III Loading

Figure 46 shows the comparison between analysis (shown previously in Figure 42) and the experimental results (shown previously in Figure 32) from the test performed on tube LMC06 under combined tension/positive torsion. The curves shown represent the results from the thirteenth of fourteen cycles. The prediction of the initial shear modulus matches the experimentally determined shear modulus of 1.27 Msi. The linear limit determined from experiment is 3.5 ksi and 5.5 ksi determined from the analysis. The trends predicted by the analytical model correlate well with the experiment; the pure torsion response exhibits a higher degree of nonlinearity than the combined loading and coupling between the axial tension and shear strain does exist. At peak loading of the experiment, a difference in shear strain of 0.01% was observed between the two loading paths. This path dependence is not predicted by the analytical model.

Under proportional loading, nonlinear analysis predicts first ply failure at $\tau_{x\theta}$ = 4.46 ksi. The prediction for the first ply failure under pure torsion is $\tau_{x\theta}$ =4.17 ksi. These are indicated in Figure 46. For both paths the failures are predicted to initiate in the -15° layers in the center of the laminate. Because the experimentally observed linear limit, as well as the predictions for first ply failure, fall below the prediction for the linear limit, the onset of nonlinearity may be the result of first ply failure. Experimentally, the tube failed under combined proportional loading although the first ply failure is predicted at a lower stress under pure torsion. For stress levels less than the predicted first ply failure, the agreement between analysis and

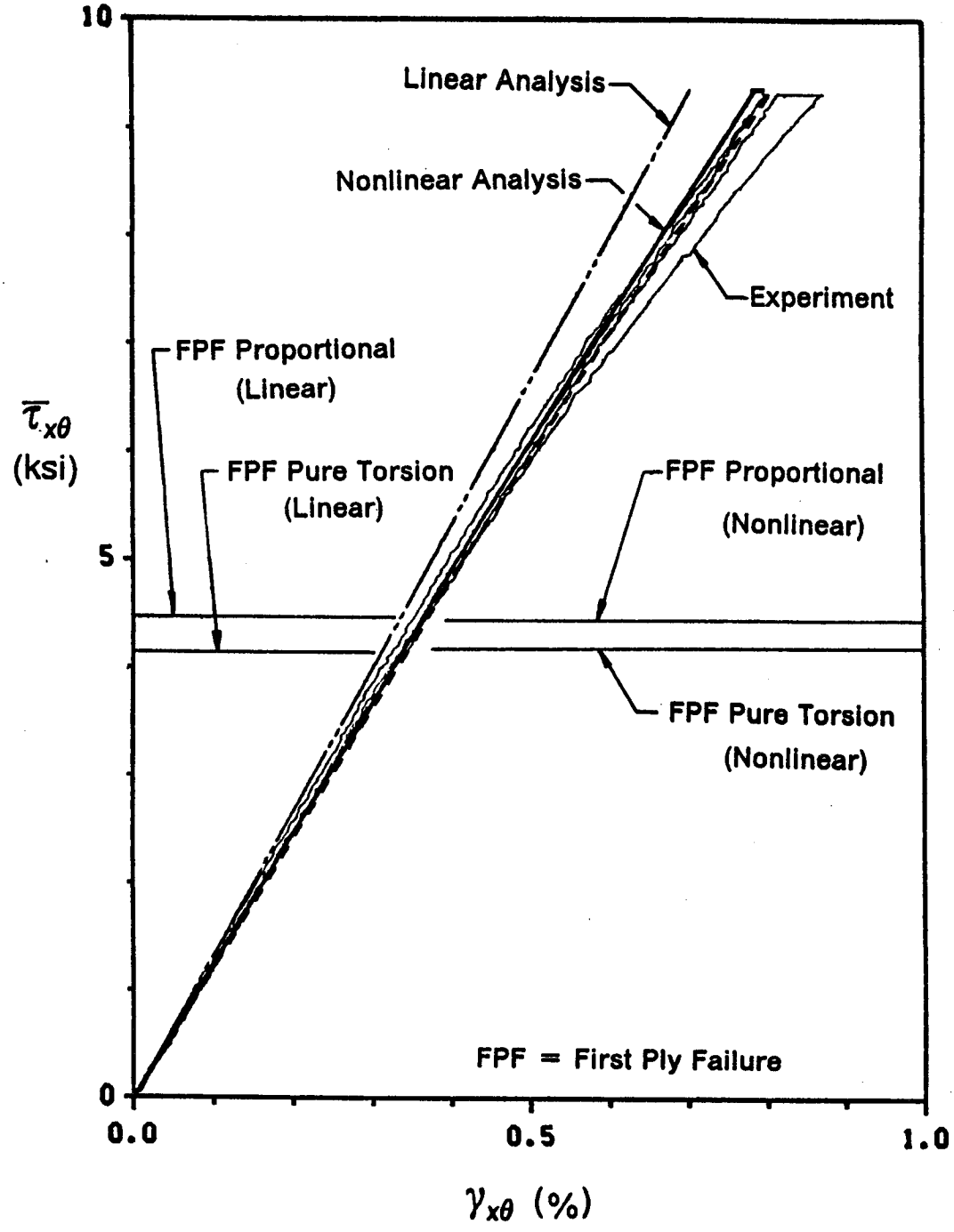

Figure 46. Analytical/Experimental Correlation - Type III Loading

experiment is good. At stresses higher than the predicted first ply failure, the experiment becomes more nonlinear than is predicted by the analysis.

5.4.3 Type IV Loading

Figure 47 shows a comparison between analysis and the results from the experiment performed on tube LMB01 under combined compression/negative torsion. The experimental results are from the sixth of seven load cycles. The initial shear modulus for this test, as shown in Table 11, is 1.37 Msi while the analysis predicts 1.22 Msi. For this test, the initial shear modulus is more closely predicted using the linear analysis. This indicates that the prediction of the initial modulus using nonlinear analysis in the absence of residual stress would more closely match the experimentally observed shear modulus. The curvature of the prediction, however, matches that from the experiment. The trends exhibited in the experiment, stiffer response in pure negative torsion which is softened with the application of pure compression, is predicted by the analytical model. The experimentally observed linear limit is -3.4 ksi. Using nonlinear analysis, -4.0 ksi is predicted for the linear limit.

First ply failure is predicted at $\tau_{x\theta}$ = -3.77 ksi under proportional loading and $\tau_{x\theta}$ = -4.28 ksi under pure torsion. These are indicated in Figure 47. For both the pure torsion and combined loading, the failure is predicted in the +15° layers which are on the outside and inside surfaces of the tube. The dominant stress in the failure prediction is the σ_1 which is compressive under these loading conditions. For both tubes tested under Type IV loading, failure of the tube occurred when loading in pure torsion, although the lowest prediction for first ply failure is for proportional loading.

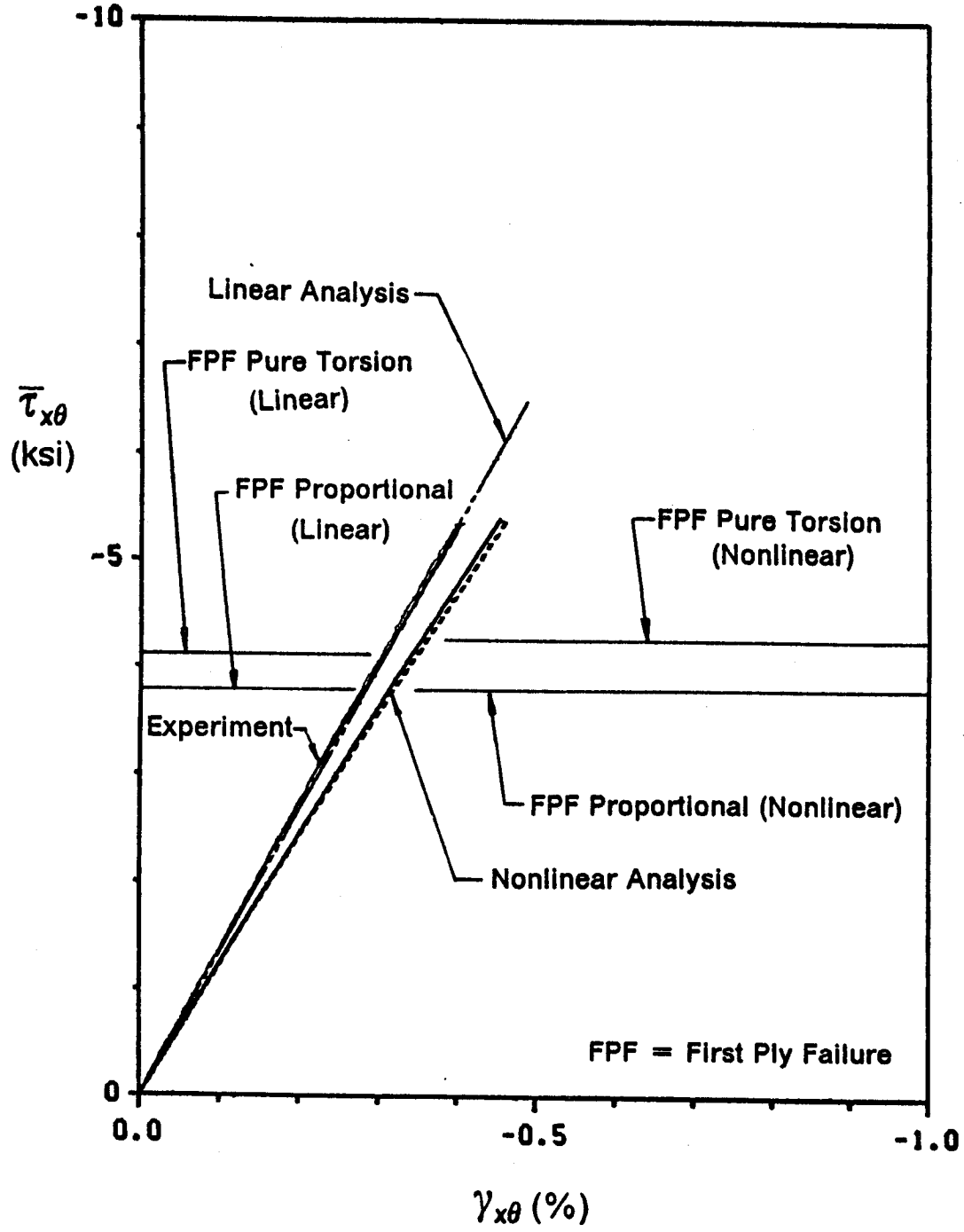

Figure 47. Analytical/Experimental Correlation - Type IV Loading

5.5 *Discussion*

In two of the tubes tested under Type II loading, failure occurred in negative torsion at magnitudes of stress lower that had been reached previously. This apparent premature failure can be attributed to the ply failures occurring in both the -15° layers and the +15° layers due to the reversal of the torsion.

Under Type III loading, there are differences in the nonlinearity of the analytical prediction and the experimental results. In addition, a difference of 0.01% strain was observed experimentally between the two loading paths, but the analysis did not predict it. These differences can be explained by an accumulation of damage in the tube. The presence of damage may enhance the nonlinearity of the material and induce a path dependence on the material response. If damage is occurring in the tube, the nonlinear response is no longer a pure material response but a combination of material and structural response.

The above hypothesis is supported by the correlation between the predictions of first ply failure and the experimentally observed initiation of nonlinearity in the global shear response. Table 12 summarizes the results presented in Section 5.4. Because the initiation of damage can both the reduce the linear limit and enhance the nonlinearity, the consideration of damage is necessary for accurate prediction of nonlinear response.

As stated previously, the difference between Type III and Type IV loading was only in the sign of the loads applied; the proportions of torsion and axial loading were identical. The applied shear stress at the failure of the tube was significantly less for Type IV than for Type III. The first ply failure predictions for the different loading types were within 15% of one another, and the mode of failure for both types was compression in the fiber direction. The difference between the two loading types is in the location of the first ply failure prediction. For Type III loading, first ply failure is predicted in the -15° layers in the center of the laminate, and the first ply failure is predicted in the external +15° layers for Type IV loading. This result

Table 12. Comparison Between Linear Limits and First Ply Failure

Load Type	Tube	Linear Limit (Experiment) (ksi)	Linear Limit (Analysis) (ksi)	FPF (Nonlinear) (ksi)	FPF (Linear) (ksi)
II	LMC02	±4.0	±4.6	4.17 -4.23	4.16 -4.05
III	LMC06	3.5	5.5	4.46(prop) 4.17(tor)	4.48(prop) 4.16(tor)
IV	LMB01	-3.4	-4.0	-3.77(prop) -4.23(tor)	-3.78(prop) -4.05(tor)

indicates that a ply failure on the external surface of the type may be more critical to the integrity of the tube than a failure in an internal layer.

In Section 5.3, it was pointed out that the dominant component of stress in the global nonlinear response of the tube was the σ_1 component. The σ_1 component of stress also is the dominant component in the predicted failure of the tubes. Both the softening nonlinearity and failure in the fiber direction are a result of the compressive properties of the material. The cyclic pure torsion tests of the Type II experiments presented in Chapter 4 exhibited a nonlinear reversible unloading response up until the load cycle in which failure occurred. The experiments performed using Type III and Type IV loading also exhibited a reversible behavior with the successive loading and unloading cycles. These reversible characteristics of the experiments support the assumption that the response in the fiber direction, whether stiffening in tension or softening in compression, is elastic. Prior to the failure observed in Type II loading, the stress-strain response exhibited dissipative behavior. In view of the fact that the first ply failure had been exceeded for both positive and negative torsion, it appears that this dissipation is the result of damage that had accumulated in the tube.

6.0 Conclusions and Recommendations

The results of this study indicate that the consideration of material nonlinearities has a significant effect on the predicted response and failure of tubes made from P75/934 graphite/epoxy with a stacking sequence of $[15/0/\pm 10/0/-15]_s$. The softening response of the individual plies in the fiber direction under compressive stress was found to be the dominant factor in the observed global nonlinear response of the tubes tested under the loading conditions employed in this investigation. The softening in shear was found to make very little contribution to the global nonlinear response. The stiffening response in the fiber direction due to tension results in the curvature of the failure surface becoming concave in the absence of residual stress. Nonlinear analysis was found to be capable of qualitatively predicting the experimentally observed differences in the shear response under pure torsion and combined proportional loading. The observed coupling between axial loading and shear strain was also predicted using the nonlinear analysis. However, the correlation between the initiation of global nonlinear response and the first ply failure predicted by the analytical model indicates that the observed nonlinear response is due to both material nonlinearity at the ply level and damage evolution due to successive ply cracking.

The inclusion of residual stresses in the determination of the response and failure was found to be important. In the case of nonlinear analysis, residual stresses reduce the initial

shear modulus of the tube. The magnitudes of failure loads were also reduced by the residual stresses, and the concavity of the failure surface mentioned above was eliminated by the residual stresses.

In addition to residual stresses, another factor found to important in accurately predicting the initial modulus was proper modeling of the tube cross section. The tubes used in this investigation were found to contain resin-rich regions at the ply interfaces. These regions accounted for seven percent of the overall wall thickness of the tube. The predictions of the shear modulus was reduced by ten percent when incorporating the resin "layers" into the analysis as well as correcting the material properties for the difference in the fiber volume fraction found between the laminated tubes and the panel.

In order to more accurately predict the shear response, it was found that the tube must be modeled using the resin "layers". The inclusion of residual stresses was found to give more accurate predictions of tube response in some cases while, in other cases, it did not. An offset of the free edge at a longitudinal crack indicated that residual stresses were present in the tubes tested. An improvement can be made to the analytical prediction if an accurate determination of the stress free temperature can be made for use in calculating the residual stresses.

The magnitude of the applied stress at failure was found to be path dependent. This dependence was seen in the tests performed using pure torsion cyclic loading where the tubes were subjected to increasingly higher magnitudes of loads in positive and negative torsion. Under this sequence of loading, failure occurred at loads lower than had been applied during the preceding cycle once a certain stress level was reached. The applied stress at failure, then, is a function of the previous loading history. It appears that a critical damage envelope (CDE) may exist beyond which failure becomes a path dependent phenomenon.

Some recommendations for future work in nonlinear analysis of composite tubes are:

- Incorporate a damage model into the analytical model to predict accumulation of damage and its effect on the response of tubes.

- Expand the experimental program to investigate different ratios of torsion and axial loads.

- Characterize the unloading response of P75/934 graphite/epoxy to verify the assumptions made concerning the unloading behavior.

- Develop model for predicting the magnitudes of the residual stress from the offset of the free edge at a longitudinal crack.

- Perform an experimental investigation similar to that carried out in this research using a more nonlinear composite system.

References

1 D.E. Bowles, and D.R. Tenney, "Composite Tubes for the Space Station Truss Structure", Proceedings of the 18th International SAMPE Technical Conference, Seattle, WA, Oct. 1986.

2 E.Reissner, "On Axially Uniform Stress and Strain in Axially Homogeneous Cylindrical Shells ", *International Journal of Solids and Structures*, Vol 6, 1970, pp 133-138.

3 E. Reissner, and W.T. Tsai, "Pure Bending, Stretching and Twisting of Anisotropic Cylindrical Shells", *Journal of Applied Mechanics*, Vol 39, March 1972, pp. 148-154.

4 E. Reissner, and W.T. Tsai, "On Pure Bending and Stretching of Orthotropic Laminated Cylindrical Shells", *Journal of Applied Mechanics*, Vol 41, March 1974, pp. 168-172.

5 S.T. Gulati, and F. Essenburg, "Effects of Anisotropy in Axisymmetric Cylindrical Shells", *Journal of Applied Mechanics*, Vol 34, September 1967, pp. 659-666.

6 J.M. Whitney, and J.C. Halpin, "Analysis of Laminated Anisotropic Tubes Under Combined Loading", *Journal of Composite Materials*, Vol 2, July 1968, pp.360-367.

7 R.E. Sherrer, "Filament-Wound Cylinders with Axial-Symmetric Loads", *Journal of Composite Materials*, Vol 1, 1967, pp. 344-355.

8 J.M. Whitney, "On the Use of Shell Theory for Determining Stresses in Composite Cylinders", *Journal of Composite Materials*, Vol 5, July 1971, pp.340-353.

9 R.R. Rizzo, and A.A. Vicario, "A Finite Element Analysis of Laminated Anisotropic Tubes (Part I - A Characterization of the Off-Axis Tensile Specimens)", *Journal of Composite Materials*, Vol 4, July 1970, pp. 344-359.

10 D. Cohen, and M.W. Hyer, "Residual Stresses in Cross-Ply Composite Tubes", Center for Composite Materials and Structures Report # CCMS-84-04, Virginia Polytechnic Institute and State University, Blacksburg, Virginia 24061, June 1984.

11 M.W. Hyer, D.E. Cooper, and D. Cohen, "Stresses and Deformations in Cross-Ply Composite Tubes Subjected to a Uniform Temperature Change: Elasticity and Approximate Solutions", Center for Composite Materials and Structures Report # CCMS-85-06, Virginia Polytechnic Institute and State University, Blacksburg, Virginia 24061, June 1985.

[12] M.W. Hyer, and D.E. Cooper, "Stresses and Deformations in Composite Tubes Due to a Circumferential Temperature Gradient", *Journal of Applied Mechanics*, Vol 53, December 1986, pp. 757-764.

[13] C.Q. Rousseau, M.W. Hyer, and S.S. Tompkins, "Stresses and Deformations in Angle Ply Composite Tubes", Center for Composite Materials and Structures Report # CCMS-87-04, Virginia Polytechnic Institute and State University, Blacksburg, Virginia 24061, February 1987.

[14] G. Orgill, and J.F. Wilson, "Finite Deformations of Nonlinear Orthotropic Cylindrical Shells", *Journal of Applied Mechanics*, Vol 53, June 1986, pp. 257-266.

[15] V.K.S. Choo, "Effect of Loading Path on the Failure of Fibre Reinforced Composite Tubes", *Journal of Composite Materials*, Vol 19, November 1985, pp.525-532.

[16] M.-J. Pindera, Theory of Elasticity (ESM 6120 Class notes), Spring 1987, Virginia Polytechnic Institute and State University.

[17] K.C. Valanis "A Theory of Viscoplasticity Without a Yield Surface," Part I. General Theory, *Archives of Mechanics*, Vol. 23, No. 4, 1971, pp. 517-533.

[18] K.C. Valanis "A Theory of Viscoplasticity Without a Yield Surface," Part II. Application to Mechanical Behavior of Metals, *Archives of Mechanics*, Vol. 23, No. 4, 1971, pp. 517-533.

[19] M.-J. Pindera and C.T. Herakovich, "An Endochronic Theory for Transversely Isotropic Fibrous Composites,"Report VPI-E-81-27, Virginia Polytechnic Institute and State University, Blacksburg, Virginia 24061, August 1981.

[20] S.R. Mathison, C.T. Herakovich, M.-J. Pindera, and M. Shuart, "Nonlinear Analysis for the Response and Failure of Compression-Loaded Angle-Ply Laminates with a Hole," Center for Composite Materials and Structures Report # CCMS-87-12, Virginia Polytechnic Institute and State University, Blacksburg, Virginia 24061, July 1987.

[21] S.W. Tsai and E.M. Wu, "A General Theory of Strength for Anisotropic Materials", *Journal of Composite Materials*, January 1971, pp 58-80.

[22] J.T. King, *Introduction to Numerical Computing,* McGraw-Hill, 1984, pp. 111-118.

[23] T. Knott, Personal Communication.

[24] D.E. Bowles, Personal Communication.

[25] J.S. Hidde, J.L. Beuth, Jr., and C.T. Herakovich, "MATPAC v.2.0 - A PC-Based Software Package for Materials Testing", January 1988.

[26] M.-J. Pindera, and C.T. Herakovich, "Shear Characterization of Unidirectional Composites with the Off-Axis Tension Test", *Experimental Mechanics*, Vol 26, No 1, pp 103-112, March 1986.

[27] Z. Gürdal and J.M. Starbuck, "Compressive Characterization of Unidirectional Composite Materials", Proceedings of Analytical and Testing Methodologies for Design with Advanced Materials (ATMAM), August 1987, Montreal, Quebec, Canada.

[28] M.-J. Pindera, Z. Gürdal, J. Hidde, and C.T. Herakovich, "Mechanical and Thermal Characterization of Unidirectional Aramid/Epoxy", Center for Composite Materials and Structures Report #CCMS-86-08, Virginia Polytechnic Institute and State University, Blacksburg, Virginia 24061, February 1987.

[29] D.E. Walrath and D.F. Adams, "Analysis of the Stress State in an Iosipescu Shear Test Specimen", Report UWME-DR-301-102-1, Dept of Mechanical Engineering, University of Wyoming, Laramie, WY (June 1983).

[30] J. Highton, and P.D.W. Soden, "End Reinforcement and Grips for Anisotropic Tubes" *Journal of Strain Analysis* , Vol 17, No 1, (1982), pp. 31-43.

[31] G.R. Toombes, S.R. Swanson, and D.S. Cairns, "Biaxial Testing of Composite Tubes", *Experimental Mechanics* , June 1985, pp. 186-192.

[32] T.R. Guess, and C.B. Haizlip, Jr., "End-Grip Configurations for Axial Loading of Composite Tubes", *Experimental Mechanics* , January 1980, pp. 31-36.

[33] S.K. Datta, H.M. Ledbetter, and R.D. Kriz, "Predicted Elastic Constants of Transversely Isotropic Composites Containing Anisotropic Fibers", *Progress in Science and Engineering of Composites*, Proceeding of the Fourth International Conference on Composite Materials (1984), eds. T. Hayashi, K. Kawata, S. Umekawa, Vol 1, p. 349.

[34] M.-J. Pindera, G. Choksi, J.S. Hidde, and C.T. Herakovich, "A Methodology for Accurate Shear Characterization of Unidirectional Composites", *Journal of Composite Materials*, Vol 21, December 1987, pp. 1164-1184.

[35] M.-J. Pindera, and C.T. Herakovich, "An Elastic Potential for the Nonlinear Response of Unidirectional Graphite Composites", *Journal of Applied Mechanics*, Vol 51, September 1984, pp. 546-550.

[36] J. Aboudi,"A Continuum Theory for Fiber Reinforced Elasto-Viscoplastic Composites", *International Journal of Engineering Science*, Vol 20, No 5, 1982, pp. 605-621.

[37] D.J. Fox, G.F. Sykes, Jr., and C.T. Herakovich, "Space Environmental Effects on Graphite/Epoxy Compressive Properties and Epoxy Tensile Properties", Center for Composite Materials and Structures Report # CCMS-87-11, Virginia Polytechnic Institute and State University, Blacksburg, Virginia 24061, July 1987.

[38] J. Aboudi, Personal Communication.

[39] A.C. Palmer, G. Maier, and D.C. Drucker, "Normality Relations and Convexity of Yield Surfaces for Unstable Materials or Structural Elements", *Journal of Applied Mechanics*, Vol 34, June 1967, p. 464.

Appendix A. Elements of Local Stiffness Matrices

The radial displacements in the tube were determined by solving a system of equations that were generated by assembling a set of local stiffness matrices and force vectors that are determined for each layer by writing an expression for the radial component of the radial stress at the inside and outside surface of each layer. These expressions are, in matrix form,

$$\begin{bmatrix} -\sigma_r^{k-} \\ \sigma_r^{k+} \end{bmatrix} = \begin{bmatrix} K_{11}^k & K_{12}^k & K_{13}^k & K_{14}^k \\ K_{21}^k & K_{22}^k & K_{23}^k & K_{24}^k \end{bmatrix} \begin{bmatrix} w_k^- \\ w_k^+ \\ \varepsilon_o \\ \gamma_o \end{bmatrix} - \begin{bmatrix} F_{NL}^{k-} + F_T^{k-} \\ F_{NL}^{k+} + F_T^{k+} \end{bmatrix}$$

where a quantity with a k superscript or subscript represents that quantity for the k^{th} layer, a "-" superscript represents a quantity at the inside radius of the layer while a "+" superscript represents the quantity at the outside radius of the layer. The expressions for the individual terms for a transversely isotropic layer are as follows:

$$K_{11}^k = \frac{\bar{C}_{22}^k (r_k^2 + r_{k-1}^2)}{r_{k-1}(r_k^2 - r_{k-1}^2)} - \frac{\bar{C}_{23}^k}{r_{k-1}}$$

$$K_{12}^k = -\frac{2\bar{C}_{22}^k r_k}{r_k^2 - r_{k-1}^2}$$

$$K_{21}^{k} = -\frac{2\overline{C}_{22}^{k} r_{k-1}}{r_k^2 - r_{k-1}^2}$$

$$K_{22}^{k} = \frac{\overline{C}_{22}^{k}(r_k^2 + r_{k-1}^2)}{r_k(r_k^2 - r_{k-1}^2)} + \frac{\overline{C}_{23}^{k}}{r_k}$$

$$K_{13}^{k} = -\overline{C}_{12}^{k}$$

$$K_{23}^{k} = \overline{C}_{12}^{k}$$

$$K_{14}^{k} = -\overline{C}_{36}^{k} r_{k-1} - \frac{\overline{C}_{26}^{k} - 2\overline{C}_{36}^{k}}{3\overline{C}_{22}^{k}} \left[\left(\overline{C}_{23}^{k} + 2\overline{C}_{22}^{k}\right) r_{k-1} - \left(\overline{C}_{23}^{k} + \overline{C}_{22}^{k}\right) \frac{(r_k^3 - r_{k-1}^3)}{r_k^2 - r_{k-1}^2} + \frac{(\overline{C}_{23}^{k} - \overline{C}_{22}^{k})}{r_k + r_{k-1}} r_k^2 \right]$$

$$K_{24}^{k} = \overline{C}_{36}^{k} r_k + \frac{\overline{C}_{26}^{k} - 2\overline{C}_{36}^{k}}{3\overline{C}_{22}^{k}} \left[\left(\overline{C}_{23}^{k} + 2\overline{C}_{22}^{k}\right) r_k - \left(\overline{C}_{23}^{k} + \overline{C}_{22}^{k}\right) \frac{(r_k^3 - r_{k-1}^3)}{r_k^2 - r_{k-1}^2} + \frac{(\overline{C}_{23}^{k} - \overline{C}_{22}^{k})}{r_k + r_{k-1}} r_{k-1}^2 \right]$$

$$\begin{aligned}
F_{NL}^{k-} = {} & \overline{P}_1^{k} \left[\left(\overline{C}_{23}^{k} + \overline{C}_{22}^{k}\right) \ln r_{k-1} + \overline{C}_{22}^{k} - \frac{(\overline{C}_{23}^{k} + \overline{C}_{22}^{k})}{r_k^2 - r_{k-1}^2} \left(r_k^2 \ln r_k - r_{k-1}^2 \ln r_{k-1}\right) - \right. \\
& \left. \frac{(\overline{C}_{23}^{k} - \overline{C}_{22}^{k})}{r_k^2 - r_{k-1}^2} r_k^2 \ln\left(\frac{r_{k-1}}{r_k}\right) \right] + \\
& \overline{P}_2^{k} \left[(\overline{C}_{23}^{k} + 2\overline{C}_{22}^{k}) r_{k-1} - (\overline{C}_{23}^{k} + \overline{C}_{22}^{k}) \frac{(r_k^3 - r_{k-1}^3)}{r_k^2 - r_{k-1}^2} + \frac{(\overline{C}_{23}^{k} - \overline{C}_{22}^{k})}{r_k + r_{k-1}} r_k^2 \right] + \\
& P_3^{k} \left[(\overline{C}_{23}^{k} + 3\overline{C}_{22}^{k}) r_{k-1}^2 - (\overline{C}_{23}^{k} + \overline{C}_{22}^{k})(r_k^2 + r_{k-1}^2) + (\overline{C}_{23}^{k} - \overline{C}_{22}^{k}) r_k^2 \right] + \\
& P_4^{k} \left[(\overline{C}_{23}^{k} + 4\overline{C}_{22}^{k}) r_{k-1}^3 - \frac{(\overline{C}_{23}^{k} + \overline{C}_{22}^{k})}{r_k^2 - r_{k-1}^2} (r_k^5 - r_{k-1}^5) + \frac{(\overline{C}_{23}^{k} - \overline{C}_{22}^{k})}{r_k^2 - r_{k-1}^2} r_k^2 (r_k^3 - r_{k-1}^3) \right] + \\
& P_5^{k} \left[(\overline{C}_{23}^{k} + 5\overline{C}_{22}^{k}) r_{k-1}^4 - \frac{(\overline{C}_{23}^{k} + \overline{C}_{22}^{k})}{r_k^2 - r_{k-1}^2} (r_k^6 - r_{k-1}^6) + \frac{(\overline{C}_{23}^{k} - \overline{C}_{22}^{k})}{r_k^2 - r_{k-1}^2} r_k^2 (r_k^4 - r_{k-1}^4) \right] + \\
& P_6^{k} \left[(\overline{C}_{23}^{k} + 6\overline{C}_{22}^{k}) r_{k-1}^5 - \frac{(\overline{C}_{23}^{k} + \overline{C}_{22}^{k})}{r_k^2 - r_{k-1}^2} (r_k^7 - r_{k-1}^7) + \frac{(\overline{C}_{23}^{k} - \overline{C}_{22}^{k})}{r_k^2 - r_{k-1}^2} r_k^2 (r_k^5 - r_{k-1}^5) \right] - \\
& \left[H_{13}^{k} \varepsilon_1^{NL}(r_{k-1}) + H_{23}^{k} \varepsilon_2^{NL}(r_{k-1}) + H_{63}^{k} \varepsilon_6^{NL}(r_{k-1}) + \overline{C}_{33}^{k} \varepsilon_3^{NL}(r_{k-1}) \right]
\end{aligned}$$

$$F_{NL}^{k+} = -\bar{P}_1^k\left[\left(\bar{C}_{23}^k + \bar{C}_{22}^k\right)\ln r_k + \bar{C}_{22}^k - \frac{(\bar{C}_{23}^k + \bar{C}_{22}^k)}{r_k^2 - r_{k-1}^2}\left(r_k^2 \ln r_k - r_{k-1}^2 \ln r_{k-1}\right) - \right.$$

$$\left.\frac{(\bar{C}_{23}^k - \bar{C}_{22}^k)}{r_k^2 - r_{k-1}^2} r_{k-1}^2 \ln\left(\frac{r_{k-1}}{r_k}\right)\right] -$$

$$\bar{P}_2^k\left[(\bar{C}_{23}^k + 2\bar{C}_{22}^k)r_k - (\bar{C}_{23}^k + \bar{C}_{22}^k)\frac{(r_k^3 - r_{k-1}^3)}{(r_k^2 - r_{k-1}^2)} + \frac{(\bar{C}_{23}^k - \bar{C}_{22}^k)}{r_k + r_{k-1}} r_{k-1}^2\right] -$$

$$P_3^k[(\bar{C}_{23}^k + 3\bar{C}_{22}^k)r_k^2 - (\bar{C}_{23}^k + \bar{C}_{22}^k)(r_k^2 + r_{k-1}^2) + (\bar{C}_{23}^k - \bar{C}_{22}^k)r_{k-1}^2] -$$

$$P_4^k\left[(\bar{C}_{23}^k + 4\bar{C}_{22}^k)r_k^3 - \frac{(\bar{C}_{23}^k + \bar{C}_{22}^k)}{r_k^2 - r_{k-1}^2}(r_k^5 - r_{k-1}^5) + \frac{(\bar{C}_{23}^k - \bar{C}_{22}^k)}{r_k^2 - r_{k-1}^2} r_{k-1}^2(r_k^3 - r_{k-1}^3)\right] -$$

$$P_5^k\left[(\bar{C}_{23}^k + 5\bar{C}_{22}^k)r_k^4 - \frac{(\bar{C}_{23}^k + \bar{C}_{22}^k)}{r_k^2 - r_{k-1}^2}(r_k^6 - r_{k-1}^6) + \frac{(\bar{C}_{23}^k - \bar{C}_{22}^k)}{r_k^2 - r_{k-1}^2} r_{k-1}^2(r_k^4 - r_{k-1}^4)\right] -$$

$$P_6^k\left[(\bar{C}_{23}^k + 6\bar{C}_{22}^k)r_k^5 - \frac{(\bar{C}_{23}^k + \bar{C}_{22}^k)}{r_k^2 - r_{k-1}^2}(r_k^7 - r_{k-1}^7) + \frac{(\bar{C}_{23}^k - \bar{C}_{22}^k)}{r_k^2 - r_{k-1}^2} r_{k-1}^2(r_k^5 - r_{k-1}^5)\right] +$$

$$\left[H_{13}^k \varepsilon_1^{NL}(r_k) + H_{23}^k \varepsilon_2^{NL}(r_k) + H_{63}^k \varepsilon_6^{NL}(r_k) + \bar{C}_{33}^k \varepsilon_3^{NL}(r_k)\right]$$

$$F_T^{k-} = \frac{F_i^k \varepsilon_i^T}{2\bar{C}_{22}^k}\left[(\bar{C}_{23}^k + \bar{C}_{22}^k)\ln r_{k-1} + \bar{C}_{22}^k - \frac{(\bar{C}_{23}^k + \bar{C}_{22}^k)}{r_k^2 - r_{k-1}^2}(r_k^2 \ln r_k - r_{k-1}^2 \ln r_{k-1}) - \right.$$

$$\left.\frac{(\bar{C}_{23}^k - \bar{C}_{22}^k)}{r_k^2 - r_{k-1}^2} r_k^2 \ln\left(\frac{r_{k-1}}{r_k}\right)\right] - \left(\bar{C}_{13}^k \alpha_x^k + \bar{C}_{23}^k \alpha_\theta^k + \bar{C}_{33}^k \alpha_r^k + \bar{C}_{36}^k \alpha_{x\theta}^k\right)\Delta T$$

$$F_T^{k+} = -\frac{F_i^k \varepsilon_i^T}{2\bar{C}_{22}^k}\left[(\bar{C}_{23}^k + \bar{C}_{22}^k)\ln r_k + \bar{C}_{22}^k - \frac{(\bar{C}_{23}^k + \bar{C}_{22}^k)}{r_k^2 - r_{k-1}^2}(r_k^2 \ln r_k - r_{k-1}^2 \ln r_{k-1}) - \right.$$

$$\left.\frac{(\bar{C}_{23}^k - \bar{C}_{22}^k)}{r_k^2 - r_{k-1}^2} r_{k-1}^2 \ln\left(\frac{r_{k-1}}{r_k}\right)\right] + \left(\bar{C}_{13}^k \alpha_x^k + \bar{C}_{23}^k \alpha_\theta^k + \bar{C}_{33}^k \alpha_r^k + \bar{C}_{36}^k \alpha_{x\theta}^k\right)\Delta T$$

where

$$\bar{P}_1^k = \left(\frac{F_i^k}{2\bar{C}_{22}^k} a_i^k - m^k n^k \frac{C_{66}^k}{\bar{C}_{22}^k} a_6^k\right)$$

$$\bar{P}_2^k = \frac{1}{3}\left[\left(\frac{C_{i3}^k}{\bar{C}_{22}^k} + \frac{F_i^k}{\bar{C}_{22}^k}\right)b_i^k - 2m^k n^k \frac{C_{66}^k}{\bar{C}_{22}^k} b_6^k\right]$$

$$m^k = \cos\phi^k$$

$$n^k = \sin\phi^k$$

$$\varepsilon_i^T = \alpha_i \Delta T, \qquad i = 1,2,3$$

For layers that are monoclinic or orthotropic, the expressions for the individual terms of the local stiffness matrix and force vectors become

$$K_{11}^k = \frac{(\bar{C}_{23}^k + \lambda_k \bar{C}_{33}^k) r_{k-1}^{2\lambda_k - 1}}{r_k^{2\lambda_k} - r_{k-1}^{2\lambda_k}} - \frac{(\bar{C}_{23}^k - \lambda_k \bar{C}_{33}^k) r_k^{2\lambda_k}}{r_{k-1}(r_k^{2\lambda_k} - r_{k-1}^{2\lambda_k})}$$

$$K_{21}^k = -\frac{2\lambda_k \bar{C}_{33}^k r_k^{\lambda_k - 1} r_{k-1}^{\lambda_k}}{r_k^{2\lambda_k} - r_{k-1}^{2\lambda_k}}$$

$$K_{12}^k = -\frac{2\lambda_k \bar{C}_{33}^k r_k^{\lambda_k} r_{k-1}^{\lambda_k - 1}}{r_k^{2\lambda_k} - r_{k-1}^{2\lambda_k}}$$

$$K_{22}^k = \frac{(\bar{C}_{23}^k + \lambda_k \bar{C}_{33}^k) r_k^{2\lambda_k - 1}}{r_k^{2\lambda_k} - r_{k-1}^{2\lambda_k}} - \frac{(\bar{C}_{23}^k - \lambda_k \bar{C}_{33}^k) r_{k-1}^{2\lambda_k}}{r_k(r_k^{2\lambda_k} - r_{k-1}^{2\lambda_k})}$$

$$K_{13}^k = -B_1^k\left[\bar{C}_{23}^k + \bar{C}_{33}^k - \frac{(\bar{C}_{23}^k + \lambda_k \bar{C}_{33}^k)}{r_k^{2\lambda_k} - r_{k-1}^{2\lambda_k}}\left(r_k^{\lambda_k + 1} r_{k-1}^{\lambda_k - 1} - r_{k-1}^{2\lambda_k}\right) - \frac{(\bar{C}_{23}^k - \lambda_k \bar{C}_{33}^k)}{r_k^{2\lambda_k} - r_{k-1}^{2\lambda_k}}\left(r_k^{2\lambda_k} - r_k^{\lambda_k + 1} r_{k-1}^{\lambda_k - 1}\right)\right] - \bar{C}_{13}^k$$

$$K_{23}^k = B_1^k\left[\bar{C}_{23}^k + \bar{C}_{33}^k - \frac{(\bar{C}_{23}^k + \lambda_k\bar{C}_{33}^k)}{r_k^{2\lambda_k} - r_{k-1}^{2\lambda_k}}\left(r_k^{2\lambda_k} - r_k^{\lambda_k-1}r_{k-1}^{\lambda_k+1}\right) - \right.$$
$$\left.\frac{(\bar{C}_{23}^k - \lambda_k\bar{C}_{33}^k)}{r_k^{2\lambda_k} - r_{k-1}^{2\lambda_k}}\left(r_k^{\lambda_k-1}r_{k-1}^{\lambda_k+1} - r_{k-1}^{2\lambda_k}\right)\right] + \bar{C}_{13}^k$$

$$K_{14}^k = -B_2^k\left[(\bar{C}_{23}^k + 2\bar{C}_{33}^k)r_{k-1} - \frac{(\bar{C}_{23}^k + \lambda_k\bar{C}_{33}^k)}{r_k^{2\lambda_k} - r_{k-1}^{2\lambda_k}}(r_k^{\lambda_k+2}r_{k-1}^{\lambda_k-1} - r_{k-1}^{2\lambda_k+1}) - \right.$$
$$\left.\frac{(\bar{C}_{23}^k - \lambda_k\bar{C}_{33}^k)}{r_k^{2\lambda_k} - r_{k-1}^{2\lambda_k}}(r_k^{2\lambda_k}r_{k-1} - r_k^{\lambda_k+2}r_{k-1}^{\lambda_k-1})\right] - \bar{C}_{36}^k r_{k-1}$$

$$K_{24}^k = -B_2^k\left[(\bar{C}_{23}^k + 2\bar{C}_{33}^k)r_k - \frac{(\bar{C}_{23}^k + \lambda_k\bar{C}_{33}^k)}{r_k^{2\lambda_k} - r_{k-1}^{2\lambda_k}}(r_k^{2\lambda_k+1} - r_k^{\lambda_k-1}r_{k-1}^{\lambda_k+2}) - \right.$$
$$\left.\frac{(\bar{C}_{23}^k - \lambda_k - \bar{C}_{33}^k)}{r_k^{2\lambda_k} - r_{k-1}^{2\lambda_k}}(r_k^{\lambda_k-1}r_{k-1}^{\lambda_k+2} - r_k r_{k-1}^{2\lambda_k})\right] + \bar{C}_{36}^k r_k$$

$$
\begin{aligned}
\bar{F}_{NL} = \bar{G}_1^k \Bigg[& \bar{C}_{23}^k + \bar{C}_{33}^k - \frac{(\bar{C}_{23}^k + \lambda_k \bar{C}_{33}^k)}{r_k^{2\lambda_k} - r_{k-1}^{2\lambda_k}} (r_k^{\lambda_k+1} r_{k-1}^{\lambda_k-1} - r_{k-1}^{2\lambda_k}) - \frac{(\bar{C}_{23}^k - \lambda_k \bar{C}_{33}^k)}{r_k^{2\lambda_k} - r_{k-1}^{2\lambda_k}} (r_k^{2\lambda_k} - r_k^{\lambda_k+1} r_{k-1}^{\lambda_k-1}) \Bigg] + \\
& \bar{G}_2^k \Bigg[(\bar{C}_{23}^k + 2\bar{C}_{33}^k) r_{k-1} - \frac{(\bar{C}_{23}^k + \lambda_k \bar{C}_{33}^k)}{r_k^{2\lambda_k} - r_{k-1}^{2\lambda_k}} (r_k^{\lambda_k+2} r_{k-1}^{\lambda_k-1} - r_{k-1}^{2\lambda_k+1}) - \\
& \frac{(\bar{C}_{23}^k - \lambda_k \bar{C}_{33}^k)}{r_k^{2\lambda_k} - r_{k-1}^{2\lambda_k}} (r_k^{2\lambda_k} r_{k-1} - r_k^{\lambda_k+2} r_{k-1}^{\lambda_k-1}) \Bigg] + \\
& G_3^k \Bigg[(\bar{C}_{23}^k + 3\bar{C}_{33}^k) r_{k-1}^2 - \frac{(\bar{C}_{23}^k + \lambda_k \bar{C}_{33}^k)}{r_k^{2\lambda_k} - r_{k-1}^{2\lambda_k}} (r_k^{\lambda_k+3} r_{k-1}^{\lambda_k-1} - r_{k-1}^{2\lambda_k+2}) - \\
& \frac{(\bar{C}_{23}^k - \lambda_k \bar{C}_{33}^k)}{r_k^{2\lambda_k} - r_{k-1}^{2\lambda_k}} (r_k^{2\lambda_k} r_{k-1}^2 - r_k^{\lambda_k+3} r_{k-1}^{\lambda_k-1}) \Bigg] + \\
& G_4^k \Bigg[(\bar{C}_{23}^k + 4\bar{C}_{33}^k) r_{k-1}^3 - \frac{(\bar{C}_{23}^k + \lambda_k \bar{C}_{33}^k)}{r_k^{2\lambda_k} - r_{k-1}^{2\lambda_k}} (r_k^{\lambda_k+4} r_{k-1}^{\lambda_k-1} - r_{k-1}^{2\lambda_k+3}) - \\
& \frac{(\bar{C}_{23}^k - \lambda_k \bar{C}_{33}^k)}{r_k^{2\lambda_k} - r_{k-1}^{2\lambda_k}} (r_k^{2\lambda_k} r_{k-1}^3 - r_k^{\lambda_k+4} r_{k-1}^{\lambda_k-1}) \Bigg] + \\
& G_5^k \Bigg[(\bar{C}_{23}^k + 5\bar{C}_{33}^k) r_{k-1}^4 - \frac{(\bar{C}_{23}^k + \lambda_k \bar{C}_{33}^k)}{r_k^{2\lambda_k} - r_{k-1}^{2\lambda_k}} (r_k^{\lambda_k+5} r_{k-1}^{\lambda_k-1} - r_{k-1}^{2\lambda_k+4}) - \\
& \frac{(\bar{C}_{23}^k - \lambda_k \bar{C}_{33}^k)}{r_k^{2\lambda_k} - r_{k-1}^{2\lambda_k}} (r_k^{2\lambda_k} r_{k-1}^4 - r_k^{\lambda_k+5} r_{k-1}^{\lambda_k-1}) \Bigg] + \\
& G_6^k \Bigg[(\bar{C}_{23}^k + 6\bar{C}_{33}^k) r_{k-1}^5 - \frac{(\bar{C}_{23}^k + \lambda_k \bar{C}_{33}^k)}{r_k^{2\lambda_k} - r_{k-1}^{2\lambda_k}} (r_k^{\lambda_k+6} r_{k-1}^{\lambda_k-1} - r_{k-1}^{2\lambda_k+5}) - \\
& \frac{(\bar{C}_{23}^k - \lambda_k \bar{C}_{33}^k)}{r_k^{2\lambda_k} - r_{k-1}^{2\lambda_k}} (r_k^{2\lambda_k} r_{k-1}^5 - r_k^{\lambda_k+6} r_{k-1}^{\lambda_k-1}) \Bigg] - \\
& \left[H_{13}^k \varepsilon_1^{NL}(r_k) + H_{23}^k \varepsilon_2^{NL}(r_k) + H_{63}^k \varepsilon_6^{NL}(r_k) + \bar{C}_{33}^k \varepsilon_3^{NL}(r_k) \right]
\end{aligned}
$$

$$F_{NL}^{+} = -\overline{G}_1^k\left[\overline{C}_{23}^k + \overline{C}_{33}^k - \frac{(\overline{C}_{23}^k + \lambda_k\overline{C}_{33}^k)}{r_k^{2\lambda_k} - r_{k-1}^{2\lambda_k}}(r_k^{2\lambda_k} - r_k^{\lambda_k-1}r_{k-1}^{\lambda_k+1}) - \frac{(\overline{C}_{23}^k - \lambda_k\overline{C}_{33}^k)}{r_k^{2\lambda_k} - r_{k-1}^{2\lambda_k}}(r_k^{\lambda_k-1}r_{k-1}^{\lambda_k+1} - r_{k-1}^{2\lambda_k})\right] -$$

$$\overline{G}_2^k\left[(\overline{C}_{23}^k + 2\overline{C}_{33}^k)r_k - \frac{(\overline{C}_{23}^k + \lambda_k\overline{C}_{33}^k)}{r_k^{2\lambda_k} - r_{k-1}^{2\lambda_k}}(r_k^{2\lambda_k+1} - r_k^{\lambda_k-1}r_{k-1}^{\lambda_k+2}) -\right.$$

$$\left.\frac{(\overline{C}_{23}^k - \lambda_k\overline{C}_{33}^k)}{r_k^{2\lambda_k} - r_{k-1}^{2\lambda_k}}(r_k^{\lambda_k-1}r_{k-1}^{\lambda_k+2} - r_k r_{k-1}^{2\lambda_k})\right] -$$

$$G_3^k\left[(\overline{C}_{23}^k + 3\overline{C}_{33}^k)r_{k-1}^2 - \frac{(\overline{C}_{23}^k + \lambda_k\overline{C}_{33}^k)}{r_k^{2\lambda_k} - r_{k-1}^{2\lambda_k}}(r_k^{2\lambda_k+2} - r_k^{\lambda_k-1}r_{k-1}^{\lambda_k+3}) -\right.$$

$$\left.\frac{(\overline{C}_{23}^k - \lambda_k\overline{C}_{33}^k)}{r_k^{2\lambda_k} - r_{k-1}^{2\lambda_k}}(r_k^{\lambda_k-1}r_{k-1}^{\lambda_k+3} - r_k^2 r_{k-1}^{2\lambda_k})\right] -$$

$$G_4^k\left[(\overline{C}_{23}^k + 4\overline{C}_{33}^k)r_{k-1}^3 - \frac{(\overline{C}_{23}^k + \lambda_k\overline{C}_{33}^k)}{r_k^{2\lambda_k} - r_{k-1}^{2\lambda_k}}(r_k^{2\lambda_k+3} - r_k^{\lambda_k-1}r_{k-1}^{\lambda_k+4}) -\right.$$

$$\left.\frac{(\overline{C}_{23}^k - \lambda_k\overline{C}_{33}^k)}{r_k^{2\lambda_k} - r_{k-1}^{2\lambda_k}}(r_k^{\lambda_k-1}r_{k-1}^{\lambda_k+4} - r_k^3 r_{k-1}^{2\lambda_k})\right] -$$

$$G_5^k\left[(\overline{C}_{23}^k + 5\overline{C}_{33}^k)r_{k-1}^4 - \frac{(\overline{C}_{23}^k + \lambda_k\overline{C}_{33}^k)}{r_k^{2\lambda_k} - r_{k-1}^{2\lambda_k}}(r_k^{2\lambda_k+4} - r_k^{\lambda_k-1}r_{k-1}^{\lambda_k+5}) -\right.$$

$$\left.\frac{(\overline{C}_{23}^k - \lambda_k\overline{C}_{33}^k)}{r_k^{2\lambda_k} - r_{k-1}^{2\lambda_k}}(r_k^{\lambda_k-1}r_{k-1}^{\lambda_k+5} - r_k^4 r_{k-1}^{2\lambda_k})\right] -$$

$$G_6^k\left[(\overline{C}_{23}^k + 6\overline{C}_{33}^k)r_{k-1}^5 - \frac{(\overline{C}_{23}^k + \lambda_k\overline{C}_{33}^k)}{r_k^{2\lambda_k} - r_{k-1}^{2\lambda_k}}(r_k^{2\lambda_k+5} - r_k^{\lambda_k-1}r_{k-1}^{\lambda_k+6}) -\right.$$

$$\left.\frac{(\overline{C}_{23}^k - \lambda_k\overline{C}_{33}^k)}{r_k^{2\lambda_k} - r_{k-1}^{2\lambda_k}}(r_k^{\lambda_k-1}r_{k-1}^{\lambda_k+6} - r_k^5 r_{k-1}^{2\lambda_k})\right] +$$

$$\left[H_{13}^k\varepsilon_1^{NL}(r_{k-1}) + H_{23}^k\varepsilon_2^{NL}(r_{k-1}) + H_{63}^k\varepsilon_6^{NL}(r_{k-1}) + \overline{C}_{33}^k\varepsilon_3^{NL}(r_{k-1})\right]$$

$$F_T^{k-} = \frac{F_I^k\varepsilon_i^T}{\overline{C}_{33}^k - \overline{C}_{22}^k}\left[\overline{C}_{23}^k + \overline{C}_{33}^k - \frac{(\overline{C}_{23}^k + \lambda_k\overline{C}_{33}^k)}{r_k^{2\lambda_k} - r_{k-1}^{2\lambda_k}}(r_k^{\lambda_k+1}r_{k-1}^{\lambda_k-1} - r_{k-1}^{2\lambda_k}) -\right.$$

$$\left.\frac{(\overline{C}_{23}^k - \lambda_k\overline{C}_{33}^k)}{r_k^{2\lambda_k} - r_{k-1}^{2\lambda_k}}(r_k^{2\lambda_k} - r_k^{\lambda_k+1}r_{k-1}^{\lambda_k-1})\right] - \left(\overline{C}_{13}^k\alpha_x^k + \overline{C}_{23}^k\alpha_\theta^k + \overline{C}_{33}^k\alpha_r^k + \overline{C}_{36}^k\alpha_{x\theta}^k\right)\Delta T$$

$$F_T^{k+} = -\frac{F_i^{k\,T}\varepsilon_i}{\bar{C}_{33}^k - \bar{C}_{22}^k}\left[\bar{C}_{23}^k + \bar{C}_{33}^k - \frac{(\bar{C}_{23}^k + \lambda_k \bar{C}_{33}^k)}{r_k^{2\lambda_k} - r_{k-1}^{2\lambda_k}}(r_k^{2\lambda_k} - r_k^{\lambda_k - 1} r_{k-1}^{\lambda_k - 1}) - \right.$$

$$\left.\frac{(\bar{C}_{23}^k - \lambda_k \bar{C}_{33}^k)}{r_k^{2\lambda_k} - r_{k-1}^{2\lambda_k}}(r_k^{\lambda_k - 1} r_{k-1}^{\lambda_k + 1} - r_{k-1}^{2\lambda_k})\right] + (\bar{C}_{13}^k \alpha_x^k + \bar{C}_{23}^k \alpha_\theta^k + \bar{C}_{33}^k \alpha_r^k + \bar{C}_{36}^k \alpha_{x\theta}^k)\Delta T$$

where

$$B_1^k = \frac{(\bar{C}_{12}^k - \bar{C}_{13}^k)}{(\bar{C}_{33}^k - \bar{C}_{22}^k)}$$

$$B_2^k = \frac{(\bar{C}_{26}^k - 2\bar{C}_{36}^k)}{(4\bar{C}_{33}^k - \bar{C}_{22}^k)}$$

$$\bar{G}_1^k = \frac{F_i^k a_i^k - 2m^k n^k C_{66}^k a_6^k}{\bar{C}_{33}^k - \bar{C}_{22}^k}$$

$$\bar{G}^{2k} = \frac{(C_{i3}^k + F_i^k) b_i^k - 2m^k n^k C_{66}^k b_6^k}{4\bar{C}_{33}^k - \bar{C}_{22}^k}$$

The integral force equation is of the form

$$\sum_{k=0}^{N} \Phi_k w_k + \Phi_{N+1}\varepsilon_o + \Phi_{N+2}\gamma_o = F_x + F_{NL}^F + F_T^F$$

where, for transversely isotropic layers,

$$\Phi_o = -2\pi \bar{C}_{12}^1 r_o$$

$$\Phi_k = 2\pi(\bar{C}_{12}^k - \bar{C}_{12}^{k+1}) r_k, \qquad k = 1,2,\ldots,N-1$$

$$\Phi_N = 2\pi \bar{C}_{12}^N r_N$$

$$\Phi_{N+1} = \pi \sum_{k=1}^{N} \overline{C}_{11}^{k}(r_k^2 - r_{k-1}^2)$$

$$\Phi_{N+2} = \frac{2\pi}{3} \sum_{k=1}^{N} \overline{C}_{16}^{k}(r_k^3 - r_{k-1}^3)$$

$$F_{NL}^{F} = 2\pi \sum_{k=1}^{N} \Bigg[(H_{11}^{k} a_1^{k} + H_{21}^{k} a_2^{k} + H_{61}^{k} a_6^{k} + \overline{C}_{12}^{k} a_3^{k}) \left(\frac{r_k^2 - r_{k-1}^2}{2} \right)$$
$$(H_{11}^{k} b_1^{k} + H_{21}^{k} b_2^{k} + H_{61}^{k} b_6^{k} + \overline{C}_{12}^{k} b_3^{k}) \left(\frac{r_k^3 - r_{k-1}^3}{3} \right)$$
$$(H_{11}^{k} c_1^{k} + H_{21}^{k} c_2^{k} + H_{61}^{k} c_6^{k} + \overline{C}_{12}^{k} c_3^{k}) \left(\frac{r_k^4 - r_{k-1}^4}{4} \right)$$
$$(H_{11}^{k} d_1^{k} + H_{21}^{k} d_2^{k} + H_{61}^{k} d_6^{k} + \overline{C}_{12}^{k} d_3^{k}) \left(\frac{r_k^5 - r_{k-1}^5}{5} \right)$$
$$(H_{11}^{k} e_1^{k} + H_{21}^{k} e_2^{k} + H_{61}^{k} e_6^{k} + \overline{C}_{12}^{k} e_3^{k}) \left(\frac{r_k^6 - r_{k-1}^6}{6} \right)$$
$$(H_{11}^{k} f_1^{k} + H_{21}^{k} f_2^{k} + H_{61}^{k} f_6^{k} + \overline{C}_{12}^{k} f_3^{k}) \left(\frac{r_k^7 - r_{k-1}^7}{7} \right) \Bigg]$$

$$F_T^F = 2\pi \sum_{k=1}^{N} \left[\overline{C}_{11}^{k} \alpha_x^{k} + \overline{C}_{12}^{k} (\alpha_\theta^{k} + \alpha_r^{k}) + \overline{C}_{16}^{k} \alpha_{x\theta}^{k} \right] \left(\frac{r_k^2 - r_{k-1}^2}{2} \right) \Delta T$$

and for monoclinic layers,

$$\Phi_o = \frac{(\bar{C}_{12}^1 - \lambda_1 \bar{C}_{13}^1)(r_1^{1-\lambda_1} - r_0^{1-\lambda_1}) r_1^{2\lambda_1} r_o^{\lambda_1}}{(1-\lambda_1)(r_1^{2\lambda_1} - r_o^{2\lambda_1})}$$

$$\Phi_k = \frac{(\bar{C}_{12}^k + \lambda_k \bar{C}_{13}^k)(r_k^{1+\lambda_k} - r_{k-1}^{1+\lambda_k}) r_k^{\lambda_k}}{(1+\lambda_k)(r_k^{2\lambda_k} - r_{k-1}^{2\lambda_k})} + \frac{(\bar{C}_{12}^{k+1} - \lambda_{k+1} \bar{C}_{13}^{k+1})(r_{k+1}^{1-\lambda_{k+1}} - r_k^{1-\lambda_{k+1}}) r_{k+1}^{2\lambda_{k+1}} r_k^{\lambda_{k+1}}}{(1-\lambda_{k+1})(r_{k+1}^{2\lambda_{k+1}} - r_k^{2\lambda_{k+1}})},$$

where k=1,2,...,N-1

$$\Phi_N = \frac{(\bar{C}_{12}^N + \lambda_N \bar{C}_{12}^N)(r_N^{1-\lambda_N} - r_{N-1}^{1-\lambda_N}) r_N^{\lambda_N}}{(1-\lambda_N)(r_N^{2\lambda_N} - r_{N-1}^{2\lambda_N})}$$

$$\Phi_{N+1} = 2\pi \sum_{k=1}^{N} \left\{ \bar{C}_{11}^k \left(\frac{r_k^2 - r_{k-1}^2}{2} \right) + \frac{\bar{C}_{12}^k - \bar{C}_{13}^k}{\bar{C}_{33}^k - \bar{C}_{22}^k} \left[(\bar{C}_{12}^k + \bar{C}_{13}^k) \left(\frac{r_k^2 - r_{k-1}^2}{2} \right) - \right. \right.$$
$$\frac{(\bar{C}_{12}^k + \lambda_k \bar{C}_{13}^k)(r_k^{1+\lambda_k} - r_{k-1}^{1+\lambda_k})^2}{(1+\lambda_k)(r_k^{2\lambda_k} - r_{k-1}^{2\lambda_k})} -$$
$$\left. \left. \frac{(\bar{C}_{12}^k - \lambda_k \bar{C}_{13}^k)(r_k^{2\lambda_k} r_{k-1}^{1+\lambda_k} - r_k^{1+\lambda_k} r_{k-1}^{2\lambda_k})(r_k^{1-\lambda_k} - r_{k-1}^{1-\lambda_k})}{(1-\lambda_k)(r_k^{2\lambda_k} - r_{k-1}^{2\lambda_k})} \right] \right\}$$

$$\Phi_{N+2} = 2\pi \sum_{k=1}^{N} \left\{ \bar{C}_{16}^k \left(\frac{r_k^3 - r_{k-1}^3}{3} \right) + \frac{\bar{C}_{26}^k - 2\bar{C}_{36}^k}{4\bar{C}_{33}^k - \bar{C}_{22}^k} \left[(\bar{C}_{12}^k + \bar{C}_{13}^k) \left(\frac{r_k^3 - r_{k-1}^3}{3} \right) - \right. \right.$$
$$\frac{(\bar{C}_{12}^k + \lambda_k \bar{C}_{13}^k)(r_k^{2+\lambda_k} - r_{k-1}^{2+\lambda_k})(r_k^{1+\lambda_k} - r_{k-1}^{1+\lambda_k})}{(1+\lambda_k)(r_k^{2\lambda_k} - r_{k-1}^{2\lambda_k})} -$$
$$\left. \left. \frac{(\bar{C}_{12}^k - \lambda_k \bar{C}_{13}^k)(r_k^{2\lambda_k} r_{k-1}^{2+\lambda_k} - r_k^{2+\lambda_k} r_{k-1}^{2\lambda_k})(r_k^{1-\lambda_k} - r_{k-1}^{1-\lambda_k})}{(1-\lambda_k)(r_k^{2\lambda_k} - r_{k-1}^{2\lambda_k})} \right] \right\}$$

$$F_{NL}^{F} = -2\pi \sum_{k=1}^{N} \left\{ \overline{G}_1^k \left[(\overline{C}_{12}^k + \overline{C}_{13}^k)\left(\frac{r_k^2 - r_{k-1}^2}{2} \right) - \frac{(\overline{C}_{12}^k + \lambda_k \overline{C}_{13}^k)(r_k^{1+\lambda_k} - r_{k-1}^{1+\lambda_k})^2}{(1+\lambda_k)(r_k^{2\lambda_k} - r_{k-1}^{2\lambda_k})} - \right.\right.$$

$$\left. \frac{(\overline{C}_{12}^k - \lambda_k \overline{C}_{13}^k)(r_k^{2\lambda_k} r_{k-1}^{1+\lambda_k} - r_k^{1+\lambda_k} r_{k-1}^{2\lambda_k})(r_k^{1-\lambda_k} - r_{k-1}^{1-\lambda_k})}{(1-\lambda_k)(r_k^{2\lambda_k} - r_{k-1}^{2\lambda_k})} \right] + \overline{G}_2^k \left[(\overline{C}_{12}^k + 2\overline{C}_{13}^k)\left(\frac{r_k^3 - r_{k-1}^3}{3} \right) - \right.$$

$$\frac{(\overline{C}_{12}^k + \lambda_k \overline{C}_{13}^k)(r_k^{2+\lambda_k} - r_{k-1}^{2+\lambda_k})(r_k^{1+\lambda_k} - r_{k-1}^{1+\lambda_k})}{(1+\lambda_k)(r_k^{2\lambda_k} - r_{k-1}^{2\lambda_k})} -$$

$$\left. \frac{(\overline{C}_{12}^k - \lambda_k \overline{C}_{13}^k)(r_k^{2\lambda_k} r_{k-1}^{2+\lambda_k} - r_k^{2+\lambda_k} r_{k-1}^{2\lambda_k})(r_k^{1-\lambda_k} - r_{k-1}^{1-\lambda_k})}{(1-\lambda_k)(r_k^{2\lambda_k} - r_{k-1}^{2\lambda_k})} \right] +$$

$$G_3^k \left[(\overline{C}_{12}^k + 3\overline{C}_{13}^k)\left(\frac{r_k^4 - r_{k-1}^4}{4} \right) - \frac{(\overline{C}_{12}^k + \lambda_k \overline{C}_{13}^k)(r_k^{3+\lambda_k} - r_{k-1}^{3+\lambda_k})(r_k^{1+\lambda_k} - r_{k-1}^{1+\lambda_k})}{(1+\lambda_k)(r_k^{2\lambda_k} - r_{k-1}^{2\lambda_k})} - \right.$$

$$\left. \frac{(\overline{C}_{12}^k - \lambda_k \overline{C}_{13}^k)(r_k^{2\lambda_k} r_{k-1}^{3+\lambda_k} - r_k^{3+\lambda_k} r_{k-1}^{2\lambda_k})(r_k^{1-\lambda_k} - r_{k-1}^{1-\lambda_k})}{(1-\lambda_k)(r_k^{2\lambda_k} - r_{k-1}^{2\lambda_k})} \right] + G_4^k \left[(\overline{C}_{12}^k + 4\overline{C}_{13}^k)\left(\frac{r_k^5 - r_{k-1}^5}{5} \right) - \right.$$

$$\frac{(\overline{C}_{12}^k + \lambda_k \overline{C}_{13}^k)(r_k^{4+\lambda_k} - r_{k-1}^{4+\lambda_k})(r_k^{1+\lambda_k} - r_{k-1}^{1+\lambda_k})}{(1+\lambda_k)(r_k^{2\lambda_k} - r_{k-1}^{2\lambda_k})} -$$

$$\left. \frac{(\overline{C}_{12}^k - \lambda_k \overline{C}_{13}^k)(r_k^{2\lambda_k} r_{k-1}^{4+\lambda_k} - r_k^{4+\lambda_k} r_{k-1}^{2\lambda_k})(r_k^{1-\lambda_k} - r_{k-1}^{1-\lambda_k})}{(1-\lambda_k)(r_k^{2\lambda_k} - r_{k-1}^{2\lambda_k})} \right] +$$

$$G_5^k \left[(\overline{C}_{12}^k + 5\overline{C}_{13}^k)\left(\frac{r_k^6 - r_{k-1}^6}{6} \right) - \frac{(\overline{C}_{12}^k + \lambda_k \overline{C}_{13}^k)(r_k^{5+\lambda_k} - r_{k-1}^{5+\lambda_k})(r_k^{1+\lambda_k} - r_{k-1}^{1+\lambda_k})}{(1+\lambda_k)(r_k^{2\lambda_k} - r_{k-1}^{2\lambda_k})} - \right.$$

$$\left. \frac{(\overline{C}_{12}^k - \lambda_k \overline{C}_{13}^k)(r_k^{2\lambda_k} r_{k-1}^{5+\lambda_k} - r_k^{5+\lambda_k} r_{k-1}^{2\lambda_k})(r_k^{1-\lambda_k} - r_{k-1}^{1-\lambda_k})}{(1-\lambda_k)(r_k^{2\lambda_k} - r_{k-1}^{2\lambda_k})} \right] + G_6^k \left[(\overline{C}_{12}^k + 6\overline{C}_{13}^k)\left(\frac{r_k^7 - r_{k-1}^7}{7} \right) - \right.$$

$$\frac{(\overline{C}_{12}^k + \lambda_k \overline{C}_{13}^k)(r_k^{6+\lambda_k} - r_{k-1}^{6+\lambda_k})(r_k^{1+\lambda_k} - r_{k-1}^{1+\lambda_k})}{(1+\lambda_k)(r_k^{2\lambda_k} - r_{k-1}^{2\lambda_k})} -$$

$$\left. \frac{(\overline{C}_{12}^k - \lambda_k \overline{C}_{13}^k)(r_k^{2\lambda_k} r_{k-1}^{6+\lambda_k} - r_k^{6+\lambda_k} r_{k-1}^{2\lambda_k})(r_k^{1-\lambda_k} - r_{k-1}^{1-\lambda_k})}{(1-\lambda_k)(r_k^{2\lambda_k} - r_{k-1}^{2\lambda_k})} \right] -$$

$$(H_{11}^k a_1^k + H_{21}^k a_2^k + H_{61}^k a_6^k + \overline{C}_{13}^k a_3^k)\left(\frac{r_k^2 - r_{k-1}^2}{2} \right) - (H_{11}^k b_1^k + H_{21}^k b_2^k + H_{61}^k b_6^k + \overline{C}_{13}^k b_3^k)\left(\frac{r_k^3 - r_{k-1}^3}{3} \right) -$$

$$(H_{11}^k c_1^k + H_{21}^k c_2^k + H_{61}^k c_6^k + \overline{C}_{13}^k c_3^k)\left(\frac{r_k^4 - r_{k-1}^4}{4} \right) - (H_{11}^k d_1^k + H_{21}^k d_2^k + H_{61}^k d_6^k + \overline{C}_{13}^k d_3^k)\left(\frac{r_k^5 - r_{k-1}^5}{5} \right) -$$

$$\left. (H_{11}^k e_1^k + H_{21}^k e_2^k + H_{61}^k e_6^k + \overline{C}_{13}^k e_3^k)\left(\frac{r_k^6 - r_{k-1}^6}{6} \right) - (H_{11}^k f_1^k + H_{21}^k f_2^k + H_{61}^k f_6^k + \overline{C}_{13}^k f_3^k)\left(\frac{r_k^7 - r_{k-1}^7}{7} \right) \right\}$$

$$F_T^F = 2\pi \sum_{k=1}^{N} \left\{ (\bar{C}_{11}^k \alpha_x^k + \bar{C}_{12}^k \alpha_\theta^k + \bar{C}_{13}^k \alpha_r^k + \bar{C}_{16}^k \alpha_{x\theta}^k) \left(\frac{r_k^2 - r_{k-1}^2}{2} \right) \Delta T - \right.$$
$$\frac{F_i^k \varepsilon_i^t}{\bar{C}_{33}^k + \bar{C}_{22}^k} \left[(\bar{C}_{12}^k + \bar{C}_{13}^k) \left(\frac{r_k^2 - r_{k-1}^2}{2} \right) - \frac{(\bar{C}_{12}^k + \lambda_k \bar{C}_{13}^k)(r_k^{1+\lambda_k} - r_{k-1}^{1+\lambda_k})^2}{(1+\lambda_k)(r_k^{2\lambda_k} - r_{k-1}^{2\lambda_k})} - \right.$$
$$\left. \left. - \frac{(\bar{C}_{12}^k - \lambda_k \bar{C}_{13}^k)(r_k^{2\lambda_k} r_{k-1}^{1+\lambda_k} - r_k^{1+\lambda_k} r_{k-1}^{2\lambda_k})(r_k^{1-\lambda_k} - r_{k-1}^{1-\lambda_k})}{(1-\lambda_k)(r_k^{2\lambda_k} - r_{k-1}^{2\lambda_k})} \right] \right\}$$

The integral torque equation is of the form

$$\sum_{k=0}^{N} \Psi_k W_k + \Psi_{N+1} \varepsilon_o + \Psi_{N+2} \gamma_o = T_x + F_{NL}^T + F_T^T$$

where, for transversely isotropic layers, the coefficients are

$$\Psi_0 = \frac{(\bar{C}_{26}^1 - \bar{C}_{36}^1) r_1^2 r_0}{r_1 + r_0} - \frac{(\bar{C}_{26}^1 + \bar{C}_{36}^1)(r_1^3 - r_0^3) r_0}{3(r_1^2 - r_0^2)}$$

$$\Psi_k = \frac{(\bar{C}_{26}^k + \bar{C}_{36}^k)(r_k^3 - r_{k-1}^3) r_k}{3(r_k^2 - r_{k-1}^2)} - \frac{(\bar{C}_{26}^k - \bar{C}_{36}^k) r_k r_{k-1}^2}{(r_k + r_{k-1})} +$$
$$\frac{(\bar{C}_{26}^{k+1} - \bar{C}_{36}^{k+1}) r_{k+1}^2 r_k}{r_{k+1} + r_k} - \frac{(\bar{C}_{26}^{k+1} + \bar{C}_{36}^{k+1})(r_{k+1}^3 - r_k^3) r_k}{3(r_{k+1}^2 - r_k^2)}$$

where k = 1,2.,...,N-1

$$\Psi_N = \frac{(\bar{C}_{26}^N + \bar{C}_{36}^N)(r_N^3 - r_{N-1}^3) r_N}{3(r_N^2 - r_{N-1}^2)} - \frac{(\bar{C}_{26}^N - \bar{C}_{36}^N) r_N r_{N-1}^2}{r_N + r_{N-1}}$$

$$\Psi_{N+1} = 2\pi \sum_{k=1}^{N} \bar{C}_{16}^{k} \left(\frac{r_k^3 - r_{k-1}^3}{3} \right)$$

$$\Psi_{N+2} = 2\pi \sum_{k=1}^{N} \left\{ \bar{C}_{66}^{k} \left(\frac{r_k^4 - r_{k-1}^4}{4} \right) + \frac{\bar{C}_{26}^{k} - 2\bar{C}_{36}^{k}}{3\bar{C}_{22}^{k}} \left[(\bar{C}_{26}^{k} + 2\bar{C}_{36}^{k}) \left(\frac{r_k^4 - r_{k-1}^4}{4} \right) - \frac{(\bar{C}_{26}^{k} + \bar{C}_{36}^{k})(r_k^3 - r_{k-1}^3)}{3(r_k^2 - r_{k-1}^2)} - \frac{(\bar{C}_{26}^{k} - \bar{C}_{36}^{k})}{r_k + r_{k-1}} (r_k^2 r_{k-1}^3 - r_k^3 r_{k-1}^2) \right] \right\}$$

$$F_{NL}^{T} = -2\pi \sum_{k=1}^{N} \Bigg\{ \bar{P}_1^k \Bigg[\bar{C}_{36}^k \left(\frac{r_k^3 - r_{k-1}^3}{3} \right) + \frac{1}{3} (\bar{C}_{26}^k + \bar{C}_{36}^k) \left[r_k^3 \left(\ln r_k - \frac{1}{3} \right) - r_{k-1}^3 \left(\ln r_{k-1} - \frac{1}{3} \right) \right] -$$

$$\frac{(\bar{C}_{26}^k + \bar{C}_{36}^k)(r_k^3 - r_{k-1}^3)}{3(r_k^2 - r_{k-1}^2)} \left(r_k^2 \ln r_k - r_{k-1}^2 \ln r_{k-1} \right) - \frac{(\bar{C}_{26}^k - \bar{C}_{36}^k) r_k^2 r_{k-1}^2}{r_k + r_{k-1}} \ln \left(\frac{r_{k-1}}{r_k} \right) \Bigg] +$$

$$\bar{P}_2^k \Bigg[(\bar{C}_{26}^k + 2\bar{C}_{36}^k) \left(\frac{r_k^4 - r_{k-1}^4}{4} \right) - \frac{(\bar{C}_{26}^k + \bar{C}_{36}^k)(r_k^3 - r_{k-1}^3)^2}{3(r_k^2 - r_{k-1}^2)} - \frac{(\bar{C}_{26}^k - \bar{C}_{36}^k)}{r_k + r_{k-1}} (r_k^2 r_{k-1}^3 - r_k^3 r_{k-1}^2) \Bigg] +$$

$$P_3^k \Bigg[(\bar{C}_{26}^k + 3\bar{C}_{36}^k) \left(\frac{r_k^5 - r_{k-1}^5}{5} \right) - \frac{(\bar{C}_{26}^k + \bar{C}_{36}^k)(r_k^3 - r_{k-1}^3)(r_k^4 - r_{k-1}^4)}{3(r_k^2 - r_{k-1}^2)} -$$

$$\frac{(\bar{C}_{26}^k - \bar{C}_{36}^k)}{r_k + r_{k-1}} (r_k^2 r_{k-1}^4 - r_k^4 r_{k-1}^2) \Bigg] + P_4^k \Bigg[(\bar{C}_{26}^k + 4\bar{C}_{36}^k) \left(\frac{r_k^6 - r_{k-1}^6}{6} \right) -$$

$$\frac{(\bar{C}_{26}^k + \bar{C}_{36}^k)(r_k^3 - r_{k-1}^3)(r_k^5 - r_{k-1}^5)}{3(r_k^2 - r_{k-1}^2)} - \frac{(\bar{C}_{26}^k - \bar{C}_{36}^k)}{r_k + r_{k-1}} (r_k^2 r_{k-1}^5 - r_k^5 r_{k-1}^2) \Bigg] +$$

$$P_5^k \Bigg[(\bar{C}_{26}^k + 5\bar{C}_{36}^k) \left(\frac{r_k^7 - r_{k-1}^7}{7} \right) - \frac{(\bar{C}_{26}^k + \bar{C}_{36}^k)(r_k^3 - r_{k-1}^3)(r_k^6 - r_{k-1}^6)}{3(r_k^2 - r_{k-1}^2)} -$$

$$\frac{(\bar{C}_{26}^k - \bar{C}_{36}^k)}{r_k + r_{k-1}} (r_k^2 r_{k-1}^6 - r_k^6 r_{k-1}^2) \Bigg] + P_6^k \Bigg[(\bar{C}_{26}^k + 6\bar{C}_{36}^k) \left(\frac{r_k^8 - r_{k-1}^8}{8} \right) -$$

$$\frac{(\bar{C}_{26}^k + \bar{C}_{36}^k)(r_k^3 - r_{k-1}^3)(r_k^7 - r_{k-1}^7)}{3(r_k^2 - r_{k-1}^2)} - \frac{(\bar{C}_{26}^k - \bar{C}_{36}^k)}{r_k + r_{k-1}} (r_k^2 r_{k-1}^7 - r_k^7 r_{k-1}^2) \Bigg] -$$

$$(H_{16}^k a_1^k + H_{26}^k a_2^k + H_{66}^k a_6^k + \bar{C}_{36}^k a_3^k) \left(\frac{r_k^3 - r_{k-1}^3}{3} \right) - (H_{16}^k b_1^k + H_{26}^k b_2^k + H_{66}^k b_6^k + \bar{C}_{36}^k b_3^k) \left(\frac{r_k^4 - r_{k-1}^4}{4} \right) -$$

$$(H_{16}^k c_1^k + H_{26}^k c_2^k + H_{66}^k c_6^k + \bar{C}_{36}^k c_3^k) \left(\frac{r_k^5 - r_{k-1}^5}{5} \right) - (H_{16}^k d_1^k + H_{26}^k d_2^k + H_{66}^k d_6^k + \bar{C}_{36}^k d_3^k) \left(\frac{r_k^6 - r_{k-1}^6}{6} \right) -$$

$$(H_{16}^k e_1^k + H_{26}^k e_2^k + H_{66}^k e_6^k + \bar{C}_{36}^k e_3^k) \left(\frac{r_k^7 - r_{k-1}^7}{7} \right) - (H_{16}^k f_1^k + H_{26}^k f_2^k + H_{66}^k f_6^k + \bar{C}_{36}^k f_3^k) \left(\frac{r_k^8 - r_{k-1}^8}{8} \right) \Bigg\}$$

$$F_T^T = 2\pi \sum_{k=1}^{N} \left\{ (\bar{C}_{16}^k \alpha_x^k + \bar{C}_{26}^k \alpha_\theta^k + \bar{C}_{36}^k \alpha_r^k + \bar{C}_{66}^k \alpha_{x\theta}^k) \left(\frac{r_k^3 - r_{k-1}^3}{3} \right) \Delta T - \right.$$

$$\frac{F_I^k \varepsilon_I^T}{2\bar{C}_{22}^k} \left[\bar{C}_{36}^k \left(\frac{r_k^3 - r_{k-1}^3}{3} \right) + \frac{(\bar{C}_{26}^k + \bar{C}_{36}^k)}{3} \left[r_k^3 \left(\ln r_k - \frac{1}{3} \right) - r_{k-1}^3 \left(\ln r_{k-1} - \frac{1}{3} \right) \right] - \right.$$

$$\left. \left. \frac{(\bar{C}_{26}^k + \bar{C}_{36}^k)(r_k^3 - r_{k-1}^3)}{3(r_k^2 - r_{k-1}^2)} \left(r_k^2 \ln r_k - r_{k-1}^2 \ln r_{k-1} \right) - \frac{(\bar{C}_{26}^k - \bar{C}_{36}^k) r_k^2 r_{k-1}^2}{r_k + r_{k-1}} \ln \left(\frac{r_{k-1}}{r_k} \right) \right] \right\}$$

For monoclinic layers, the terms of the integral torque equation become

$$\Psi_0 = \frac{(\bar{C}_{26}^1 - \lambda_1 \bar{C}_{36}^1)(r_1^{2-\lambda_1} - r_0^{2-\lambda_1}) r_1^{2\lambda_1} r_0^{\lambda_1}}{(2-\lambda_1)(r_1^{2\lambda_1} - r_0^{2\lambda_1})} - \frac{(\bar{C}_{26}^1 + \lambda_1 \bar{C}_{36}^1)(r_1^{2+\lambda_1} - r_0^{2+\lambda_1}) r_0^{\lambda_1}}{(2+\lambda_1)(r_1^{2\lambda_1} - r_0^{2\lambda_1})}$$

$$\Psi_k = \frac{(\bar{C}_{26}^k + \lambda_k \bar{C}_{36}^k)(r_k^{2+\lambda_k} - r_{k-1}^{2+\lambda_k}) r_k^{\lambda_k}}{(2+\lambda_k)(r_k^{2\lambda_k} - r_{k-1}^{2\lambda_k})} - \frac{(\bar{C}_{26}^k - \lambda_k \bar{C}_{36}^k)(r_k^{2-\lambda_k} - r_{k-1}^{2-\lambda_k}) r_k^{\lambda_k} r_{k-1}^{2\lambda_k}}{(2-\lambda_k)(r_k^{2\lambda_k} - r_{k-1}^{2\lambda_k})} +$$

$$\frac{(\bar{C}_{26}^{k+1} - \lambda_{k+1} \bar{C}_{36}^{k+1})(r_{k+1}^{2-\lambda_{k+1}} - r_k^{2-\lambda_{k+1}}) r_{k+1}^{2\lambda_{k+1}} r_k^{\lambda_{k+1}}}{(2-\lambda_{k+1})(r_{k+1}^{2\lambda_{k+1}} - r_k^{2\lambda_{k+1}})} - \frac{(\bar{C}_{26}^{k+1} + \lambda_{k+1} \bar{C}_{36}^{k+1})(r_{k+1}^{2+\lambda_{k+1}} - r_k^{2+\lambda_{k+1}}) r_k^{\lambda_{k+1}}}{(2+\lambda_{k+1})(r_{k+1}^{2\lambda_{k+1}} - r_k^{2\lambda_{k+1}})}$$

where k=1,2,...,N-1

$$\Psi_N = \frac{(\bar{C}_{26}^N + \lambda_N \bar{C}_{36}^N)(r_N^{2+\lambda_N} - r_{N-1}^{2+\lambda_N}) r_N^{\lambda_N}}{(2+\lambda_N)(r_N^{2\lambda_N} - r_{N-1}^{2\lambda_N})} - \frac{(\bar{C}_{26}^N - \lambda_N \bar{C}_{36}^N)(r_N^{2-\lambda_N} - r_{N-1}^{2-\lambda_N}) r_N^{\lambda_N} r_{N-1}^{2\lambda_N}}{(2-\lambda_N)(r_N^{2\lambda_N} - r_{N-1}^{2\lambda_N})}$$

$$\Psi_{N+1} = 2\pi \sum_{k=1}^{N} \left\{ \overline{C}_{16}^{k} \left(\frac{r_k^3 - r_{k-1}^3}{3} \right) + \frac{\overline{C}_{12}^{k} - \overline{C}_{13}^{k}}{\overline{C}_{33}^{k} - \overline{C}_{22}^{k}} \left[(\overline{C}_{26}^{k} + \overline{C}_{36}^{k}) \left(\frac{r_k^3 - r_{k-1}^3}{3} \right) - \right.\right.$$

$$\frac{(\overline{C}_{26}^{k} + \lambda_k \overline{C}_{36}^{k})(r_k^{1+\lambda_k} - r_{k-1}^{1+\lambda_k})(r_k^{2+\lambda_k} - r_{k-1}^{2+\lambda_k})}{(2+\lambda_k)(r_k^{2\lambda_k} - r_{k-1}^{2\lambda_k})} -$$

$$\left.\left. \frac{(\overline{C}_{26}^{k} - \lambda_k \overline{C}_{36}^{k})(r_k^{2\lambda_k} r_{k-1}^{1+\lambda_k} - r_k^{1+\lambda_k} r_{k-1}^{2\lambda_k})(r_k^{2-\lambda_k} - r_{k-1}^{2-\lambda_k})}{(2-\lambda_k)(r_k^{2\lambda_k} - r_{k-1}^{2\lambda_k})} \right] \right\}$$

$$\Psi_{N+2} = 2\pi \sum_{k=1}^{N} \left\{ \overline{C}_{66}^{k} \left(\frac{r_k^4 - r_{k-1}^4}{4} \right) + \frac{\overline{C}_{26}^{k} - 2\overline{C}_{36}^{k}}{4\overline{C}_{33}^{k} - \overline{C}_{22}^{k}} \left[(\overline{C}_{26}^{k} + 2\overline{C}_{36}^{k}) \left(\frac{r_k^4 - r_{k-1}^4}{4} \right) - \right.\right.$$

$$\left.\left. \frac{(\overline{C}_{26}^{k} + \lambda_k \overline{C}_{36}^{k})(r_k^{2+\lambda_k} - r_{k-1}^{2+\lambda_k})^2}{(2+\lambda_k)(r_k^{2\lambda_k} - r_{k-1}^{2\lambda_k})} - \frac{(\overline{C}_{26}^{k} - \lambda_k \overline{C}_{36}^{k})(r_k^{2\lambda_k} r_{k-1}^{2+\lambda_k} - r_k^{2+\lambda_k} r_{k-1}^{2\lambda_k})(r_k^{2-\lambda_k} - r_{k-1}^{2-\lambda_k})}{(2-\lambda_k)(r_k^{2\lambda_k} - r_{k-1}^{2\lambda_k})} \right] \right\}$$

$$F_{NL}^{T} = -2\pi \sum_{k=1}^{N} \left\{ \overline{G}_{11}^{k} \left[(\overline{C}_{26}^{k} + \overline{C}_{36}^{k}) \left(\frac{r_k^3 - r_{k-1}^3}{3} \right) - \frac{(\overline{C}_{26}^{k} + \lambda_k \overline{C}_{36}^{k})(r_k^{2+\lambda_k} - r_{k-1}^{2+\lambda_k})(r_k^{1+\lambda_k} - r_{k-1}^{1+\lambda_k})}{(2+\lambda_k)(r_k^{2\lambda_k} - r_{k-1}^{2\lambda_k})} - \right.\right.$$

$$\left.\left. \frac{(\overline{C}_{26}^{k} - \lambda_k \overline{C}_{36}^{k})(r_k^{2\lambda_k} r_{k-1}^{1+\lambda_k} - r_k^{1+\lambda_k} r_{k-1}^{2\lambda_k})(r_k^{2-\lambda_k} - r_{k-1}^{2-\lambda_k})}{(2-\lambda_k)(r_k^{2\lambda_k} - r_{k-1}^{2\lambda_k})} \right] + \overline{G}_{2}^{k} \left[(\overline{C}_{26}^{k} + 2\overline{C}_{36}^{k}) \left(\frac{r_k^4 - r_{k-1}^4}{4} \right) - \right.$$

$$\left. \frac{(\overline{C}_{26}^{k} + \lambda_k \overline{C}_{36}^{k})(r_k^{2+\lambda_k} - r_{k-1}^{2+\lambda_k})^2}{(2+\lambda_k)(r_k^{2\lambda_k} - r_{k-1}^{2\lambda_k})} - \frac{(\overline{C}_{26}^{k} - \lambda_k \overline{C}_{36}^{k})(r_k^{2\lambda_k} r_{k-1}^{2+\lambda_k} - r_k^{2+\lambda_k} r_{k-1}^{2\lambda_k})(r_k^{2-\lambda_k} - r_{k-1}^{2-\lambda_k})}{(2-\lambda_k)(r_k^{2\lambda_k} - r_{k-1}^{2\lambda_k})} \right] -$$

$$G_{3}^{k} \left[(\overline{C}_{26}^{k} + 3\overline{C}_{36}^{k}) \left(\frac{r_k^5 - r_{k-1}^5}{5} \right) - \frac{(\overline{C}_{26}^{k} + \lambda_k \overline{C}_{36}^{k})(r_k^{2+\lambda_k} - r_{k-1}^{2+\lambda_k})(r_k^{3+\lambda_k} - r_{k-1}^{3+\lambda_k})}{(2+\lambda_k)(r_k^{2\lambda_k} - r_{k-1}^{2\lambda_k})} - \right.$$

$$\left. \frac{(\overline{C}_{26}^{k} - \lambda_k \overline{C}_{36}^{k})(r_k^{2\lambda_k} r_{k-1}^{3+\lambda_k} - r_k^{3+\lambda_k} r_{k-1}^{2\lambda_k})(r_k^{2-\lambda_k} - r_{k-1}^{2-\lambda_k})}{(2-\lambda_k)(r_k^{2\lambda_k} - r_{k-1}^{2\lambda_k})} \right] -$$

$$G_{4}^{k} \left[(\overline{C}_{26}^{k} + 4\overline{C}_{36}^{k}) \left(\frac{r_k^6 - r_{k-1}^6}{6} \right) - \frac{(\overline{C}_{26}^{k} + \lambda_k \overline{C}_{36}^{k})(r_k^{2+\lambda_k} - r_{k-1}^{2+\lambda_k})(r_k^{4+\lambda_k} - r_{k-1}^{4+\lambda_k})}{(2+\lambda_k)(r_k^{2\lambda_k} - r_{k-1}^{2\lambda_k})} - \right.$$

$$\left. \frac{(\overline{C}_{26}^{k} - \lambda_k \overline{C}_{36}^{k})(r_k^{2\lambda_k} r_{k-1}^{4+\lambda_k} - r_k^{4+\lambda_k} r_{k-1}^{2\lambda_k})(r_k^{2-\lambda_k} - r_{k-1}^{2-\lambda_k})}{(2-\lambda_k)(r_k^{2\lambda_k} - r_{k-1}^{2\lambda_k})} \right] -$$

$$G_{5}^{k} \left[(\overline{C}_{26}^{k} + 5\overline{C}_{36}^{k}) \left(\frac{r_k^7 - r_{k-1}^7}{7} \right) - \frac{(\overline{C}_{26}^{k} + \lambda_k \overline{C}_{36}^{k})(r_k^{2+\lambda_k} - r_{k-1}^{2+\lambda_k})(r_k^{5+\lambda_k} - r_{k-1}^{5+\lambda_k})}{(2+\lambda_k)(r_k^{2\lambda_k} - r_{k-1}^{2\lambda_k})} - \right.$$

$$\left. \frac{(\overline{C}_{26}^{k} - \lambda_k \overline{C}_{36}^{k})(r_k^{2\lambda_k} r_{k-1}^{5+\lambda_k} - r_k^{5+\lambda_k} r_{k-1}^{2\lambda_k})(r_k^{2-\lambda_k} - r_{k-1}^{2-\lambda_k})}{(2-\lambda_k)(r_k^{2\lambda_k} - r_{k-1}^{2\lambda_k})} \right] -$$

$$G_{6}^{k} \left[(\overline{C}_{26}^{k} + 6\overline{C}_{36}^{k}) \left(\frac{r_k^8 - r_{k-1}^8}{8} \right) - \frac{(\overline{C}_{26}^{k} + \lambda_k \overline{C}_{36}^{k})(r_k^{2+\lambda_k} - r_{k-1}^{2+\lambda_k})(r_k^{6+\lambda_k} - r_{k-1}^{6+\lambda_k})}{(2+\lambda_k)(r_k^{2\lambda_k} - r_{k-1}^{2\lambda_k})} - \right.$$

$$\left. \frac{(\overline{C}_{26}^{k} - \lambda_k \overline{C}_{36}^{k})(r_k^{2\lambda_k} r_{k-1}^{6+\lambda_k} - r_k^{6+\lambda_k} r_{k-1}^{2\lambda_k})(r_k^{2-\lambda_k} - r_{k-1}^{2-\lambda_k})}{(2-\lambda_k)(r_k^{2\lambda_k} - r_{k-1}^{2\lambda_k})} \right] -$$

$$(H_{16}^{k} a_1^{k} + H_{26}^{k} a_2^{k} + H_{66}^{k} a_6^{k} + \overline{C}_{36}^{k} a_3^{k}) \left(\frac{r_k^3 - r_{k-1}^3}{3} \right) - (H_{16}^{k} b_1^{k} + H_{26}^{k} b_2^{k} + H_{66}^{k} b_6^{k} + \overline{C}_{36}^{k} b_3^{k}) \left(\frac{r_k^4 - r_{k-1}^4}{4} \right) -$$

$$(H_{16}^{k} c_1^{k} + H_{26}^{k} c_2^{k} + H_{66}^{k} c_6^{k} + \overline{C}_{36}^{k} c_3^{k}) \left(\frac{r_k^5 - r_{k-1}^5}{5} \right) - (H_{16}^{k} d_1^{k} + H_{26}^{k} d_2^{k} + H_{66}^{k} d_6^{k} + \overline{C}_{36}^{k} d_3^{k}) \left(\frac{r_k^6 - r_{k-1}^6}{6} \right) -$$

$$\left. (H_{16}^{k} e_1^{k} + H_{26}^{k} e_2^{k} + H_{66}^{k} e_6^{k} + \overline{C}_{36}^{k} e_3^{k}) \left(\frac{r_k^7 - r_{k-1}^7}{7} \right) - (H_{16}^{k} f_1^{k} + H_{26}^{k} f_2^{k} + H_{66}^{k} f_6^{k} + \overline{C}_{36}^{k} f_3^{k}) \left(\frac{r_k^8 - r_{k-1}^8}{8} \right) \right\}$$

$$F_T^T = 2\pi \sum_{k=1}^{N} \left\{ (\bar{C}_{16}^k \alpha_x^k + \bar{C}_{26}^k \alpha_\theta^k + \bar{C}_{36}^k \alpha_r^k + \bar{C}_{66}^k \alpha_{x\theta}^k) \left(\frac{r_k^3 - r_{k-1}^3}{3} \right) \Delta T - \right.$$

$$\frac{F_i^k \varepsilon_i^T}{\bar{C}_{33}^k - \bar{C}_{22}^k} \left[(\bar{C}_{26}^k + \bar{C}_{36}^k) \left(\frac{r_k^3 - r_{k-1}^3}{3} \right) - \frac{(\bar{C}_{26}^k + \lambda_k \bar{C}_{36}^k)(r_k^{1+\lambda_k} - r_{k-1}^{1+\lambda_k})(r_k^{2+\lambda_k} - r_{k-1}^{2+\lambda_k})}{(2+\lambda_k)(r_k^{2\lambda_k} - r_{k-1}^{2\lambda_k})} - \right.$$

$$\left. \left. \frac{(\bar{C}_{26}^k - \lambda_k \bar{C}_{36}^k)(r_k^{2\lambda_k} r_{k-1}^{1+\lambda_k} - r_k^{1+\lambda_k} r_{k-1}^{2\lambda_k})(r_k^{2-\lambda_k} - r_{k-1}^{2-\lambda_k})}{(2-\lambda_k)(r_k^{2\lambda_k} - r_{k-1}^{2\lambda_k})} \right] \right\}$$

Appendix B. Least Squares Polynomial Approximation

For a given layer, the nonlinear strains, $\varepsilon_i^{NL}(r)$ were approximated by a fifth order polynomial to allow for a solution to the governing differential equation for w(r). For a given layer and component of strain, the nonlinear strain is approximated by

$$\varepsilon^{NL}(r) \simeq a + br + cr^2 + dr^3 + er^4 + fr^5$$

The difference,D, between the true value and the approximation is

$$D = a + br + cr^2 + dr^3 + er^4 + fr^5 - \varepsilon^{NL}(r)$$

For the least squares method, the squares of this difference is summed over all of the data points within the layer.

$$g = \sum_{j=1}^{m} D_j^2$$

where m is the total number of data points. To minimize the function g, the derivative of g with respect to each coefficient is set to zero.

$$\frac{\partial g}{\partial a} = \frac{\partial g}{\partial b} = \frac{\partial g}{\partial c} = \frac{\partial g}{\partial d} = \frac{\partial g}{\partial e} = \frac{\partial g}{\partial f} = 0$$

The results of these operations is

$$\frac{\partial g}{\partial a} = 2\sum_{j=1}^{m}(a + br_j + cr_j^2 + dr_j^3 + er_j^4 + fr_j^5 - \varepsilon_j^{NL}) = 0$$

$$\frac{\partial g}{\partial b} = 2\sum_{j=1}^{m}(a + br_j + cr_j^2 + dr_j^3 + er_j^4 + fr_j^5 - \varepsilon_j^{NL})r_j = 0$$

$$\frac{\partial g}{\partial c} = 2\sum_{j=1}^{m}(a + br_j + cr_j^2 + dr_j^3 + er_j^4 + fr_j^5 - \varepsilon_j^{NL})r_j^2 = 0$$

$$\frac{\partial g}{\partial d} = 2\sum_{j=1}^{m}(a + br_j + cr_j^2 + dr_j^3 + er_j^4 + fr_j^5 - \varepsilon_j^{NL})r_j^3 = 0$$

$$\frac{\partial g}{\partial e} = 2\sum_{j=1}^{m}(a + br_j + cr_j^2 + dr_j^3 + er_j^4 + fr_j^5 - \varepsilon_j^{NL})r_j^4 = 0$$

$$\frac{\partial g}{\partial f} = 2\sum_{j=1}^{m}(a + br_j + cr_j^2 + dr_j^3 + er_j^4 + fr_j^5 - \varepsilon_j^{NL})r_j^5 = 0$$

This system of equations can be solved for the coefficients a, b, c, d, e, and f. In matrix form, the system of equations is

$$\begin{bmatrix} m & \sum r_j & \sum r_j^2 & \sum r_j^3 & \sum r_j^4 & \sum r_j^5 \\ \sum r_j & \sum r_j^2 & \sum r_j^3 & \sum r_j^4 & \sum r_j^5 & \sum r_j^6 \\ \sum r_j^2 & \sum r_j^3 & \sum r_j^4 & \sum r_j^5 & \sum r_j^6 & \sum r_j^7 \\ \sum r_j^3 & \sum r_j^4 & \sum r_j^5 & \sum r_j^6 & \sum r_j^7 & \sum r_j^8 \\ \sum r_j^4 & \sum r_j^5 & \sum r_j^6 & \sum r_j^7 & \sum r_j^8 & \sum r_j^9 \\ \sum r_j^5 & \sum r_j^6 & \sum r_j^7 & \sum r_j^8 & \sum r_j^9 & \sum r_j^{10} \end{bmatrix} \begin{bmatrix} a \\ b \\ c \\ d \\ e \\ f \end{bmatrix} = \begin{bmatrix} \sum \varepsilon_j^{NL} \\ \sum \varepsilon_j^{NL} r_j \\ \sum \varepsilon_j^{NL} r_j^2 \\ \sum \varepsilon_j^{NL} r_j^3 \\ \sum \varepsilon_j^{NL} r_j^4 \\ \sum \varepsilon_j^{NL} r_j^5 \end{bmatrix}$$

where each of the summations is from 1 to m.

Appendix C. Individual Test Results

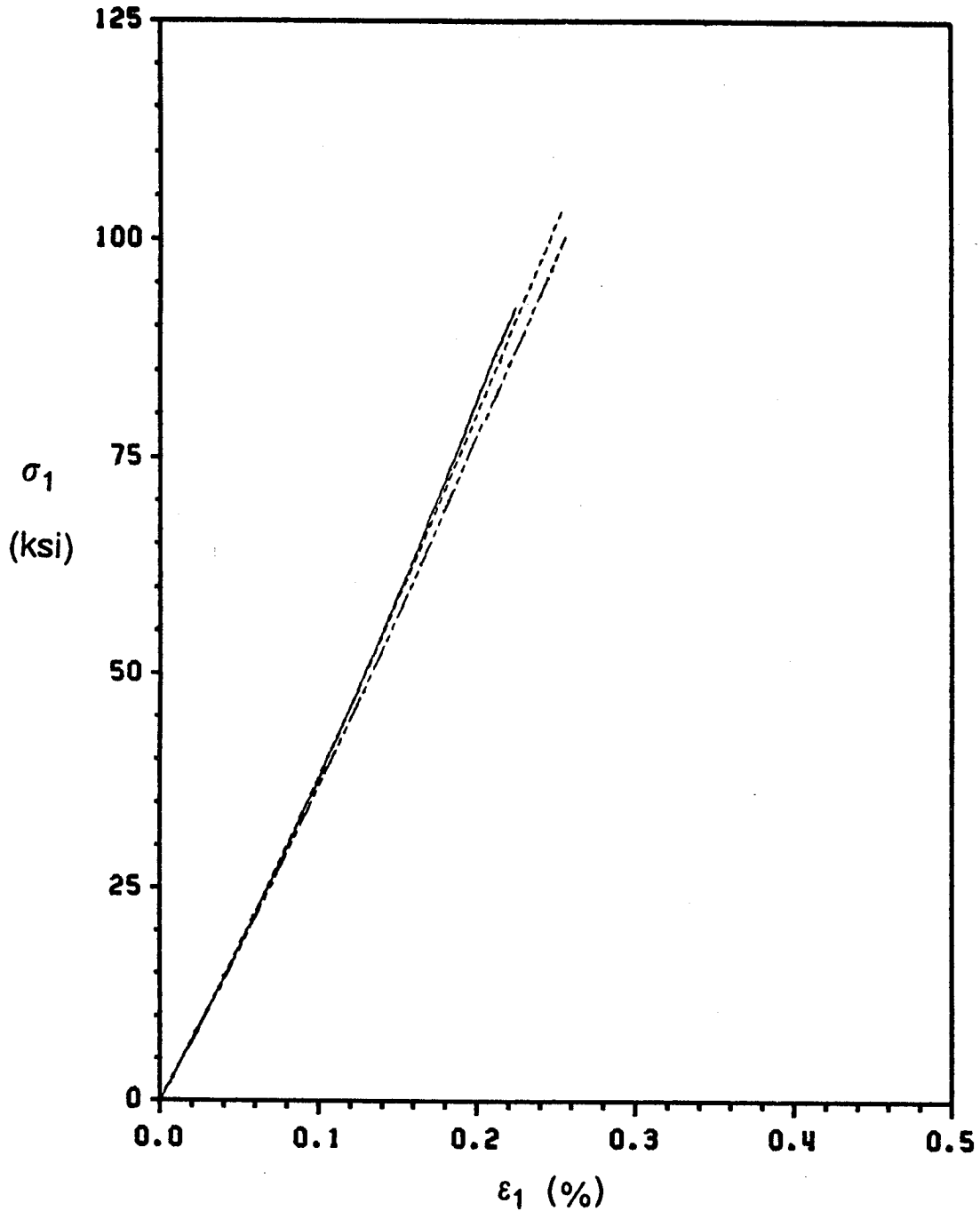

Figure 48. 0° Tension Response

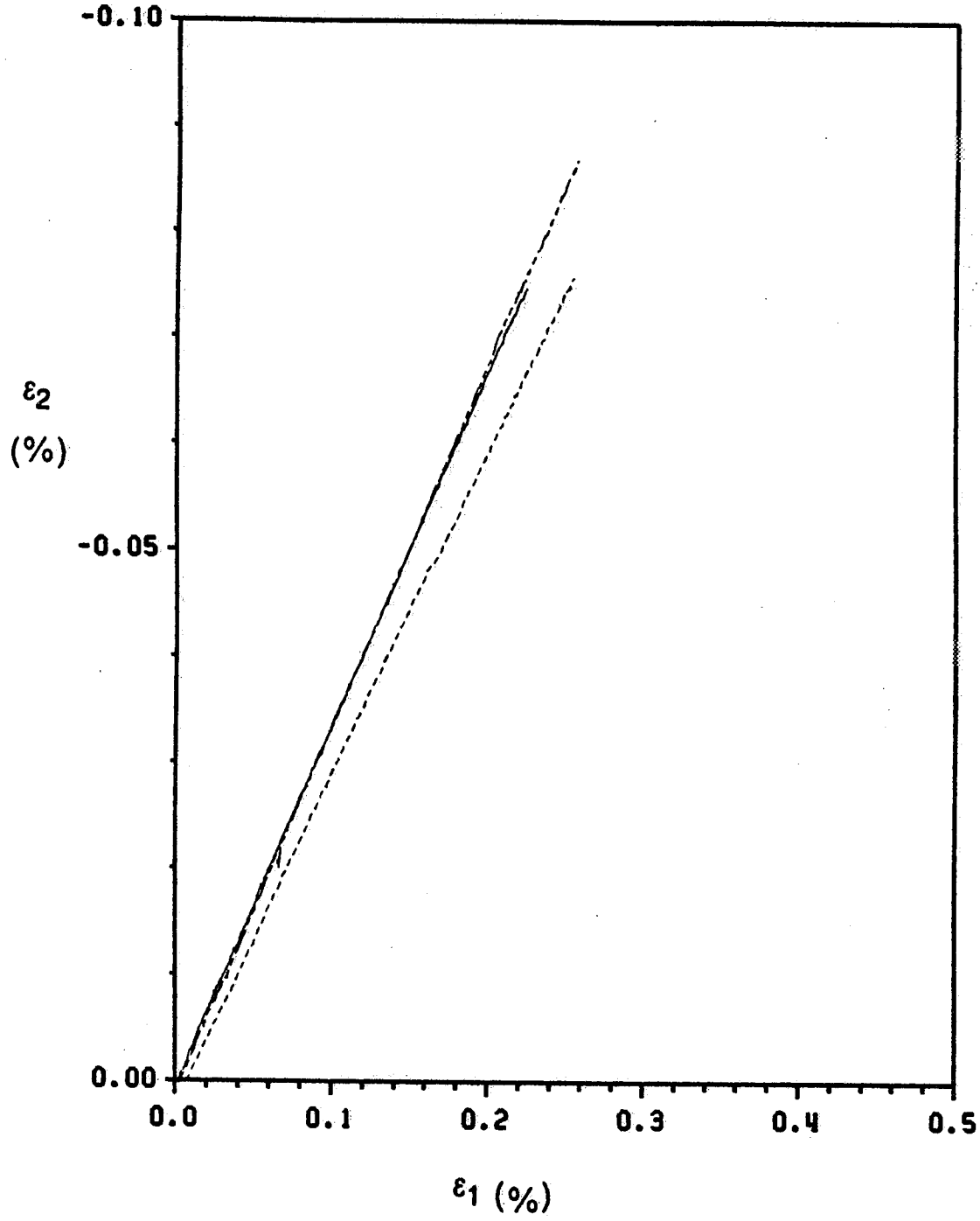

Figure 49. 0° Poisson's Response in Tension

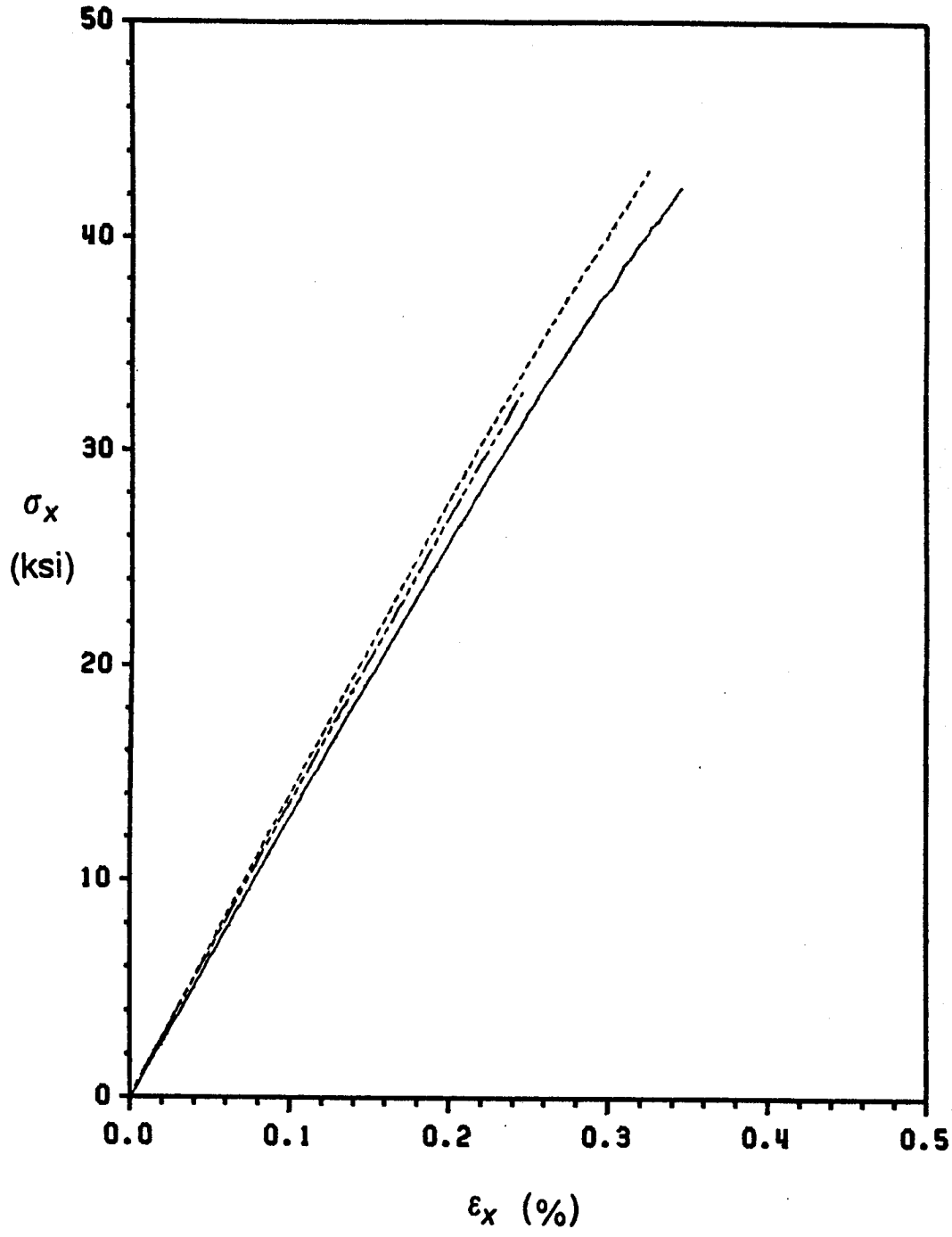

Figure 50. 10° Tension Response

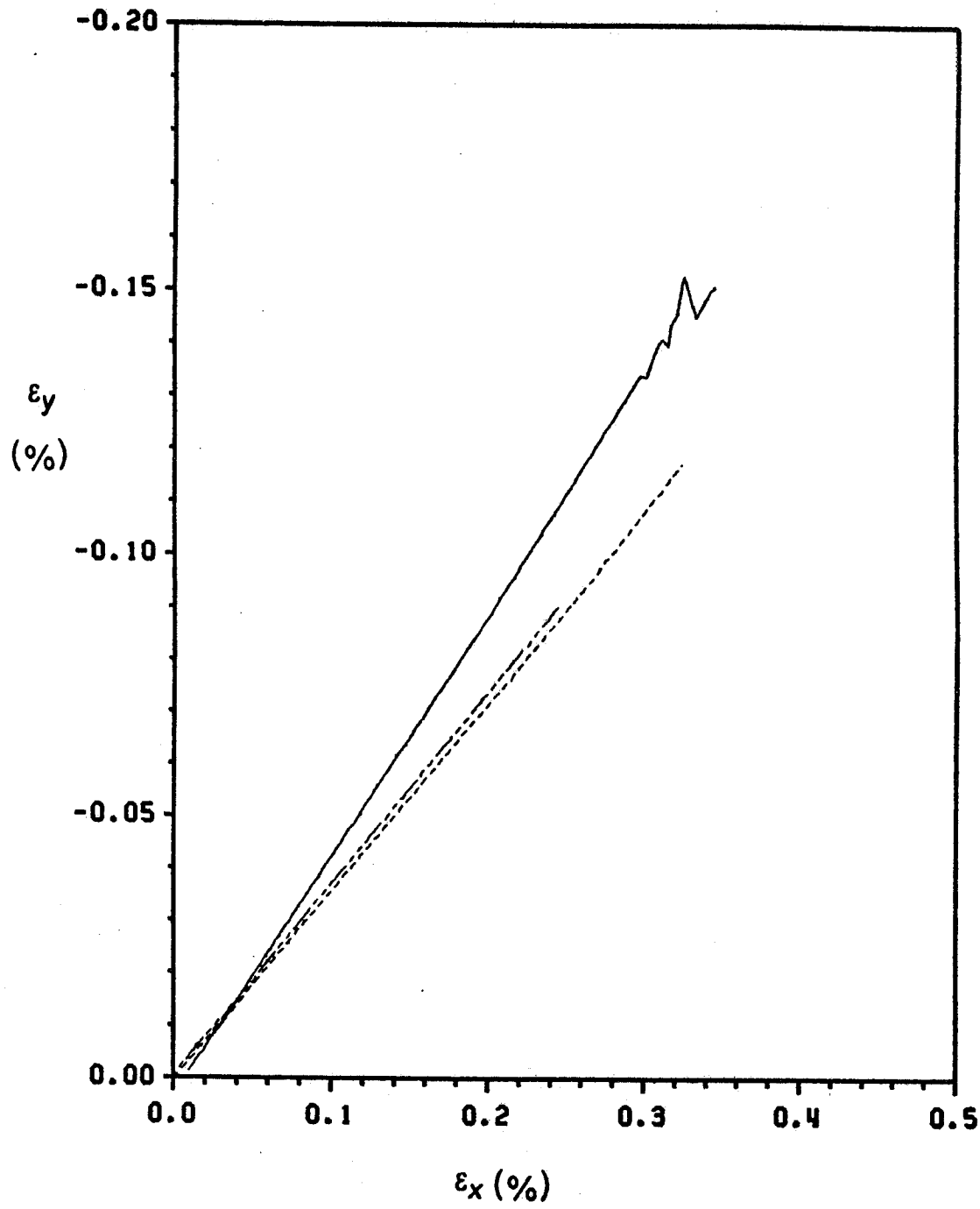

Figure 51. 10° Poisson's Response in Tension

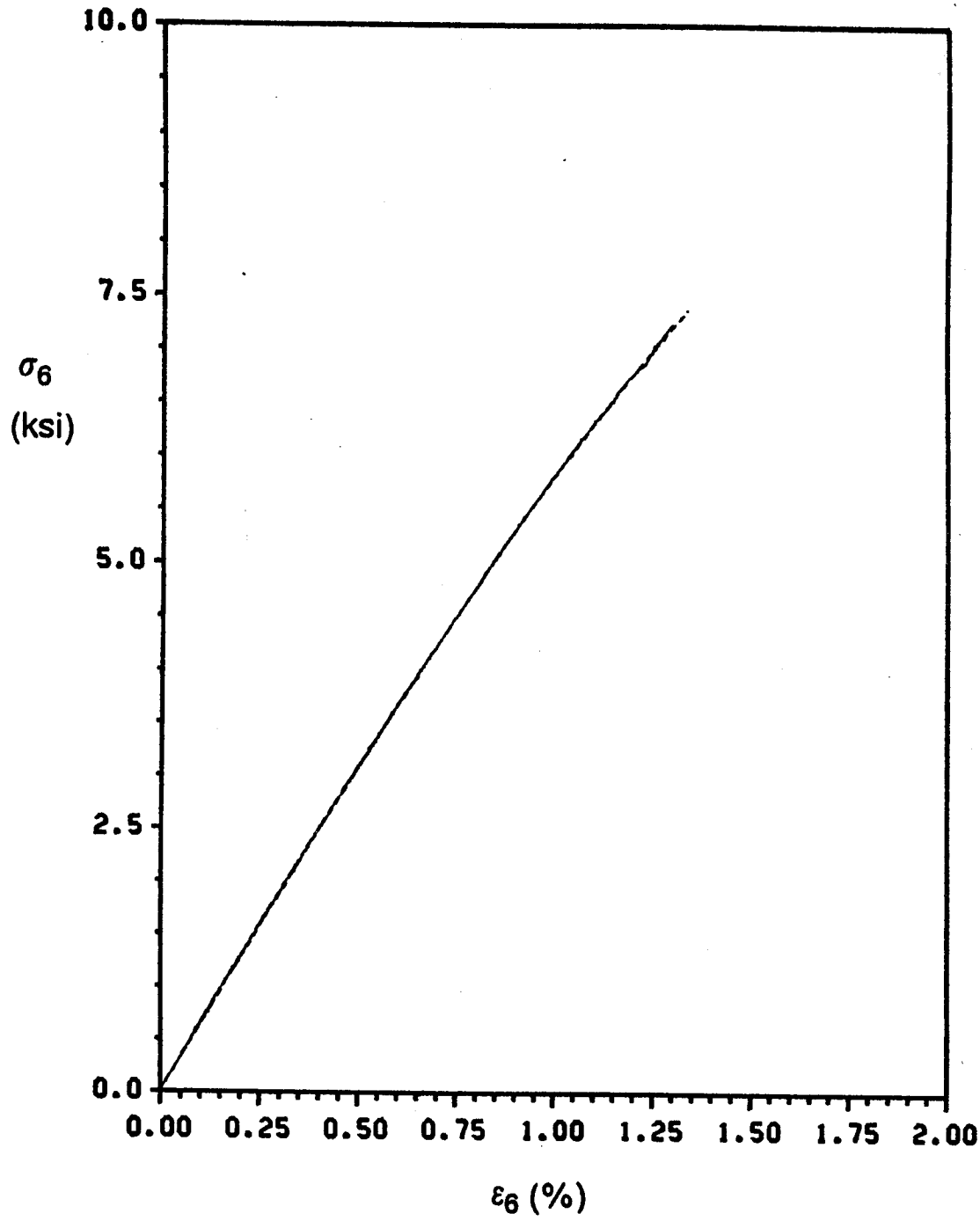

Figure 52. 10° Shear Response in Tension

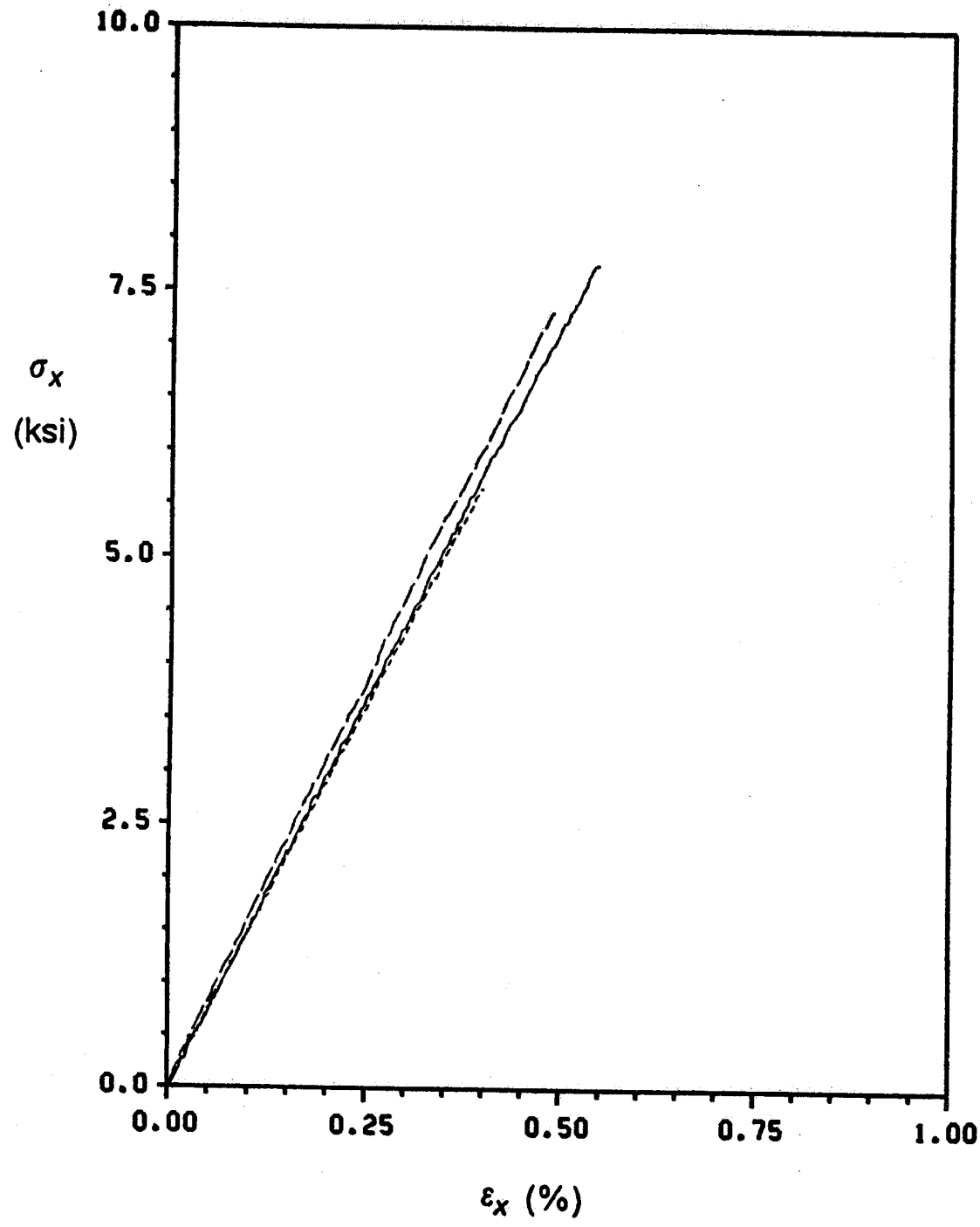

Figure 53. 45° Tension Response

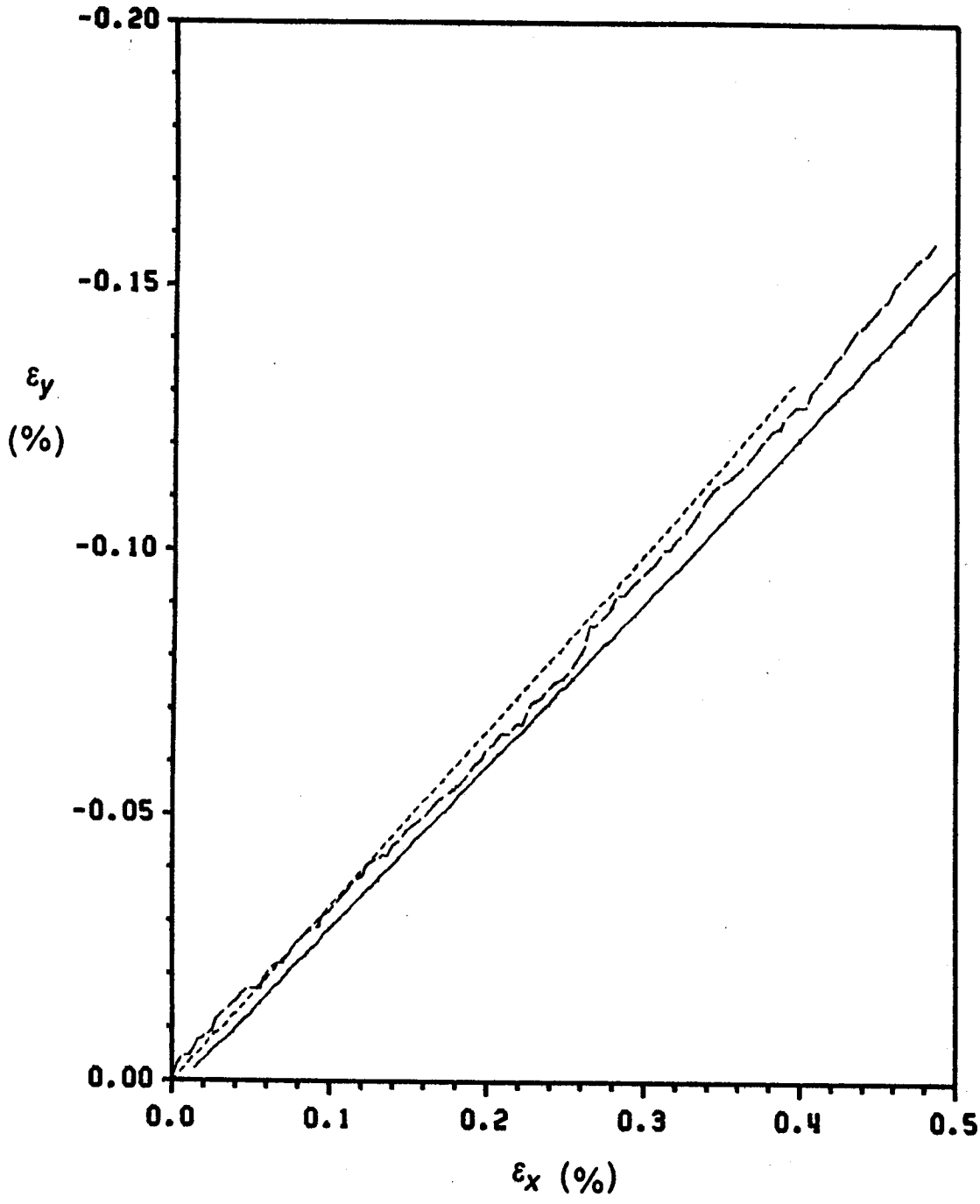

Figure 54. 45° Poisson's Response in Tension

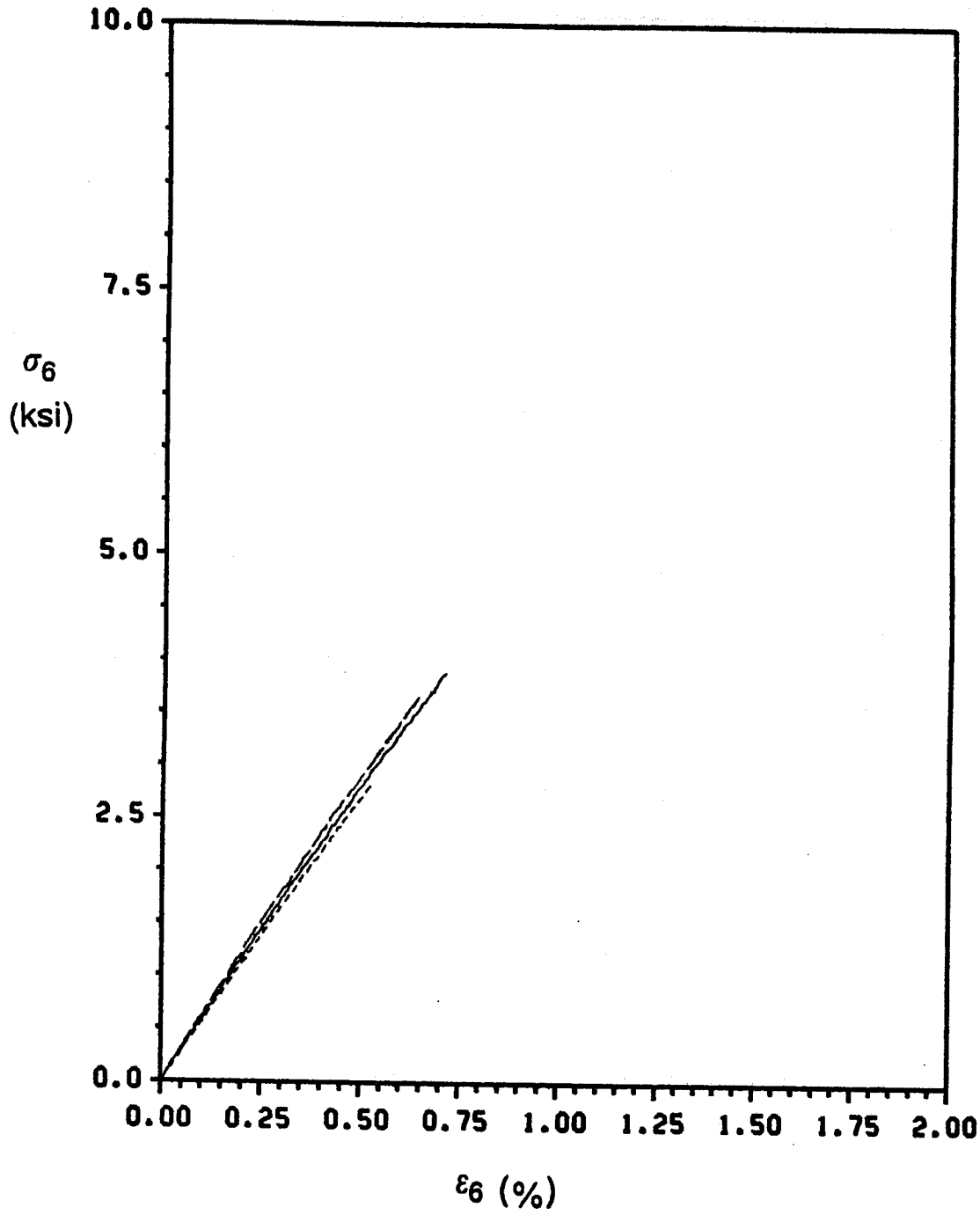

Figure 55. 45° Shear Response in Tension

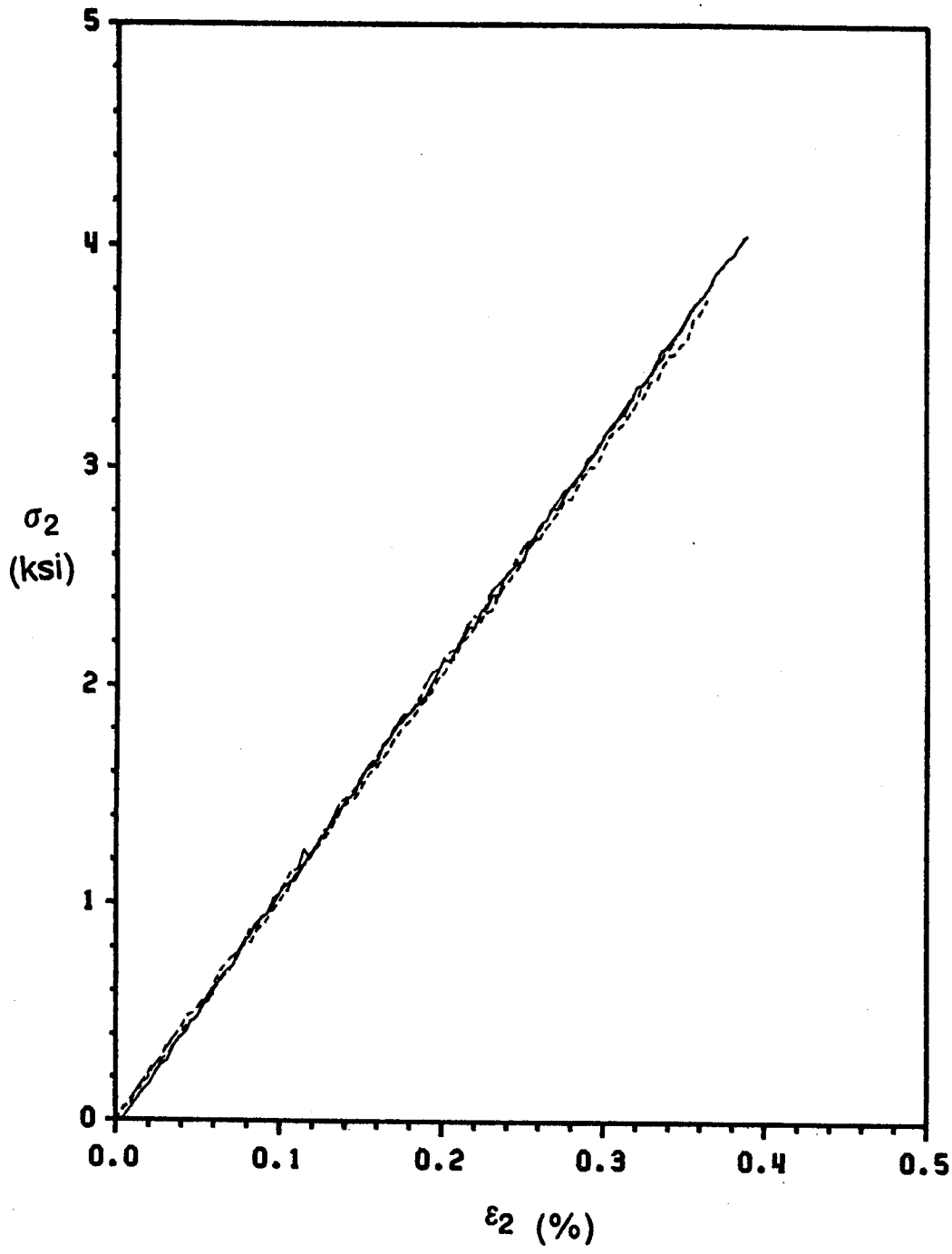

Figure 56. 90° Tension Response

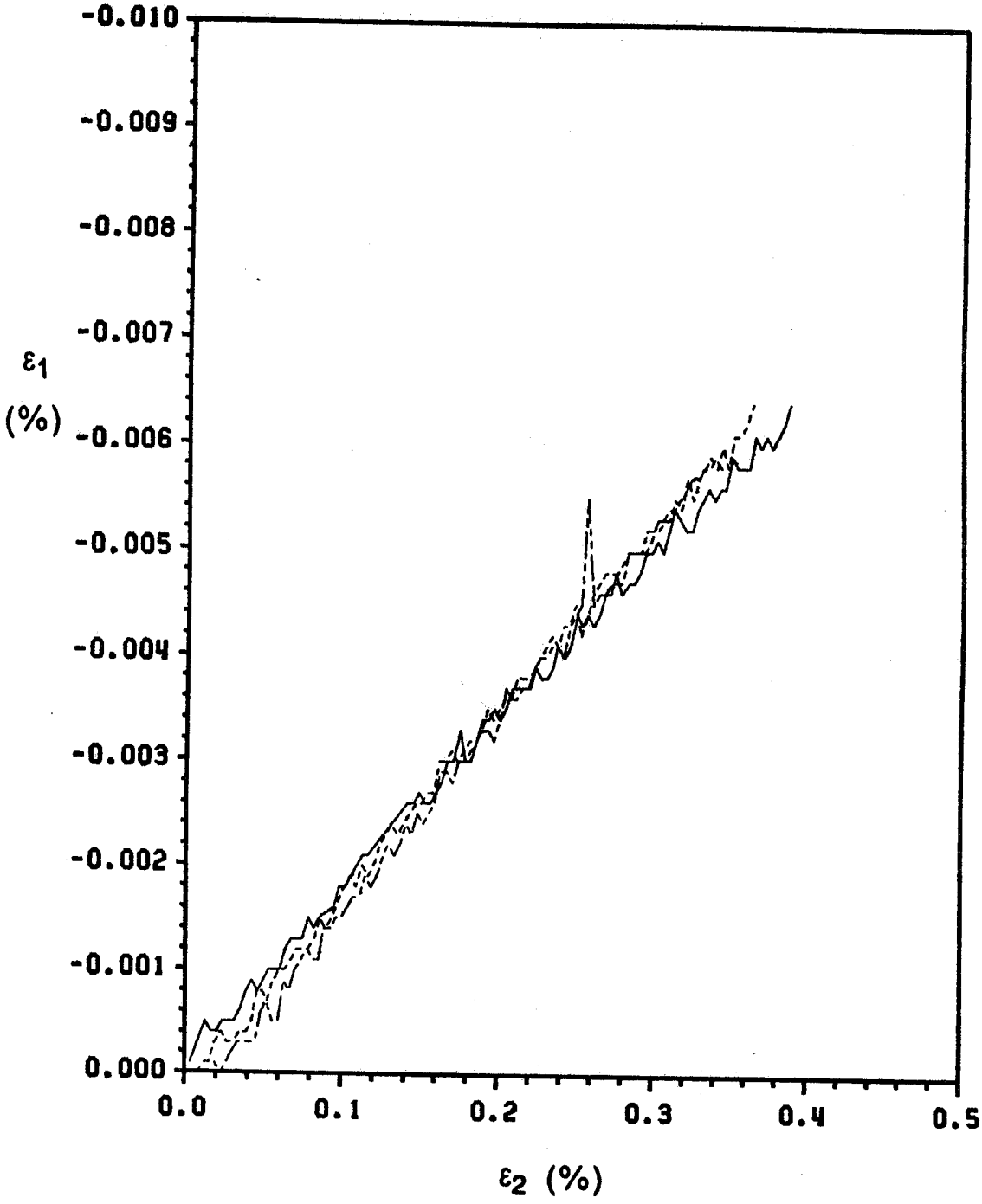

Figure 57. 90° Poisson's Response in Tension

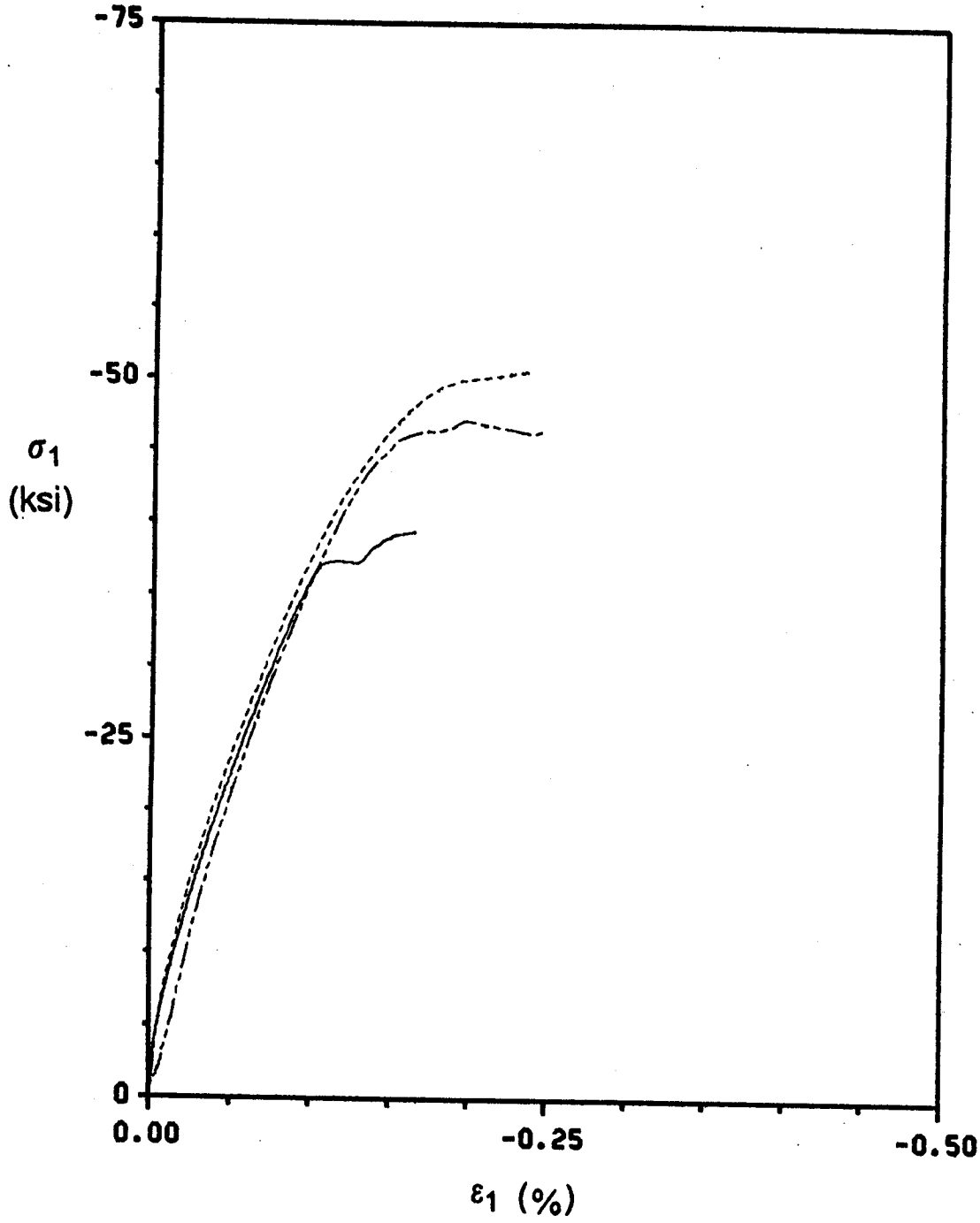

Figure 58. 0° Compression Response

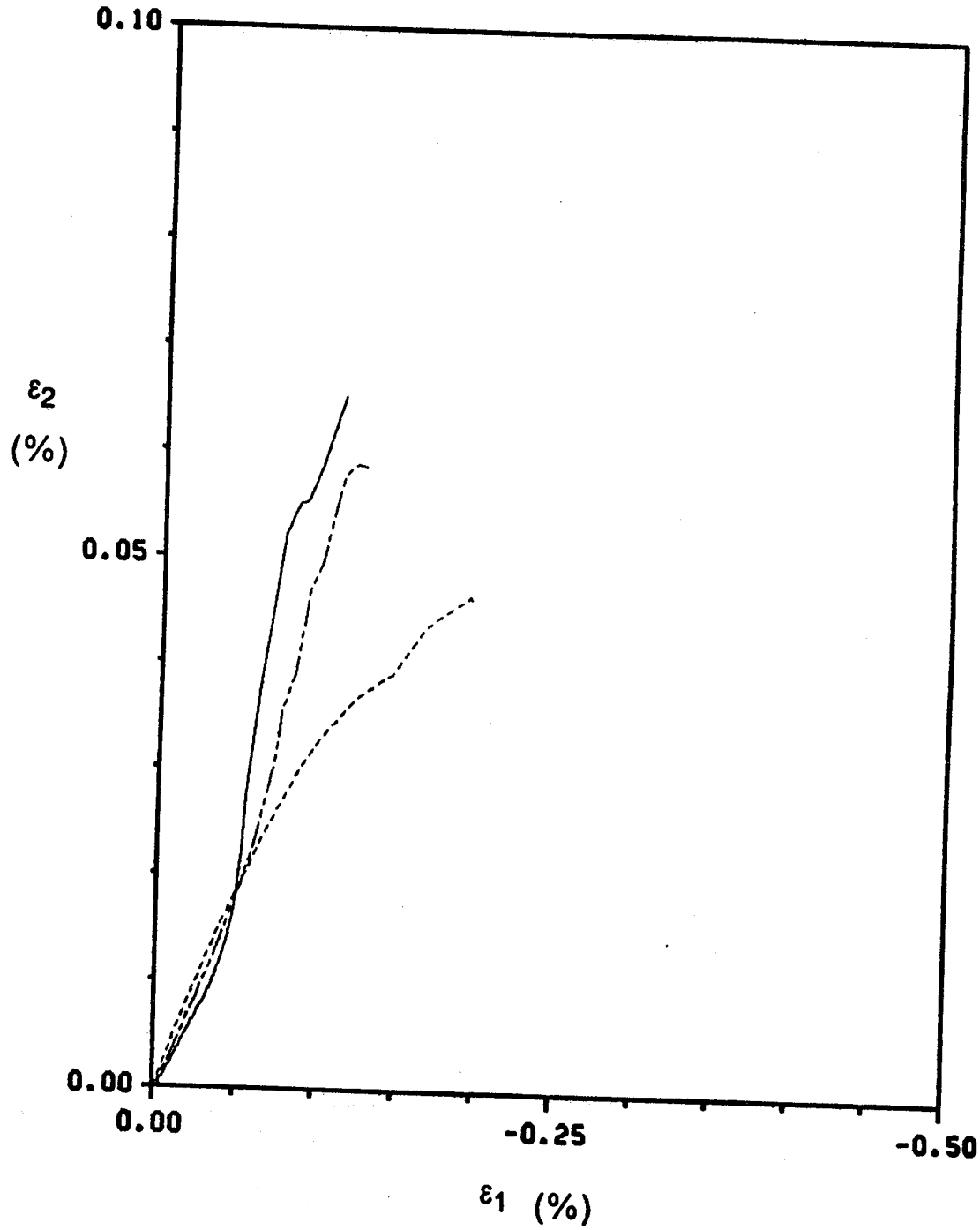

Figure 59. 0° Poisson's Response in Compression

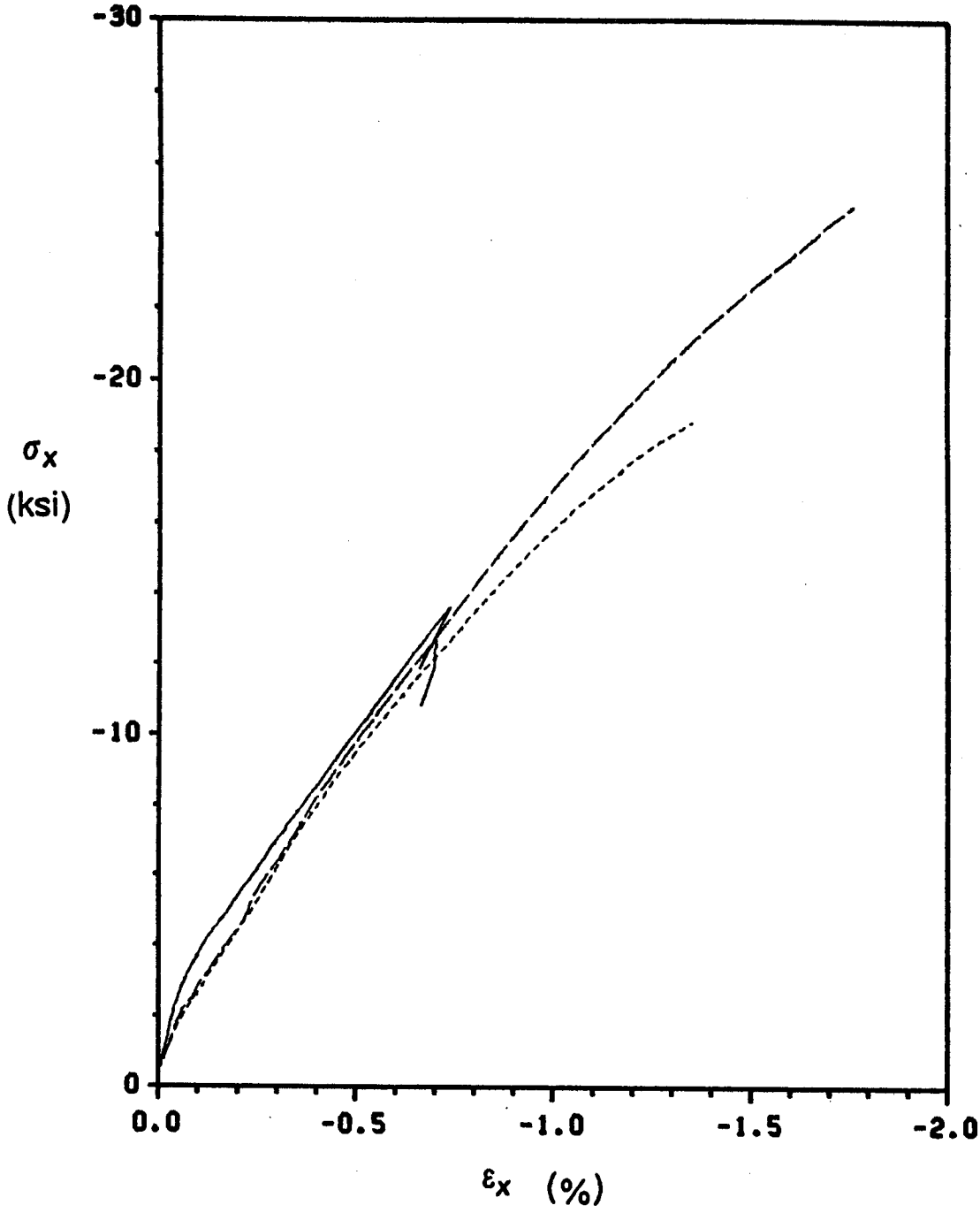

Figure 60. 45° Compression Response

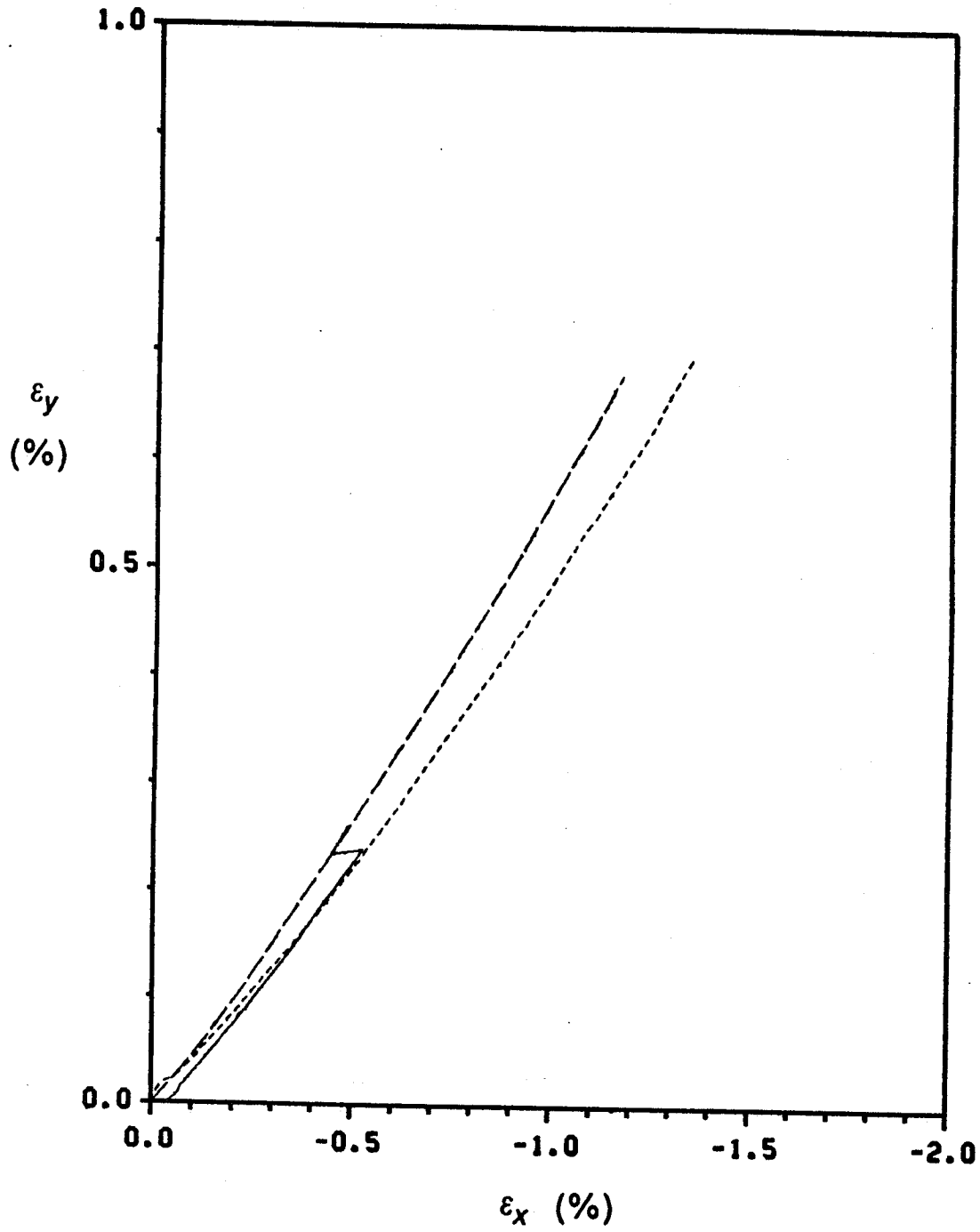

Figure 61. 45° Poisson's Response in Compression

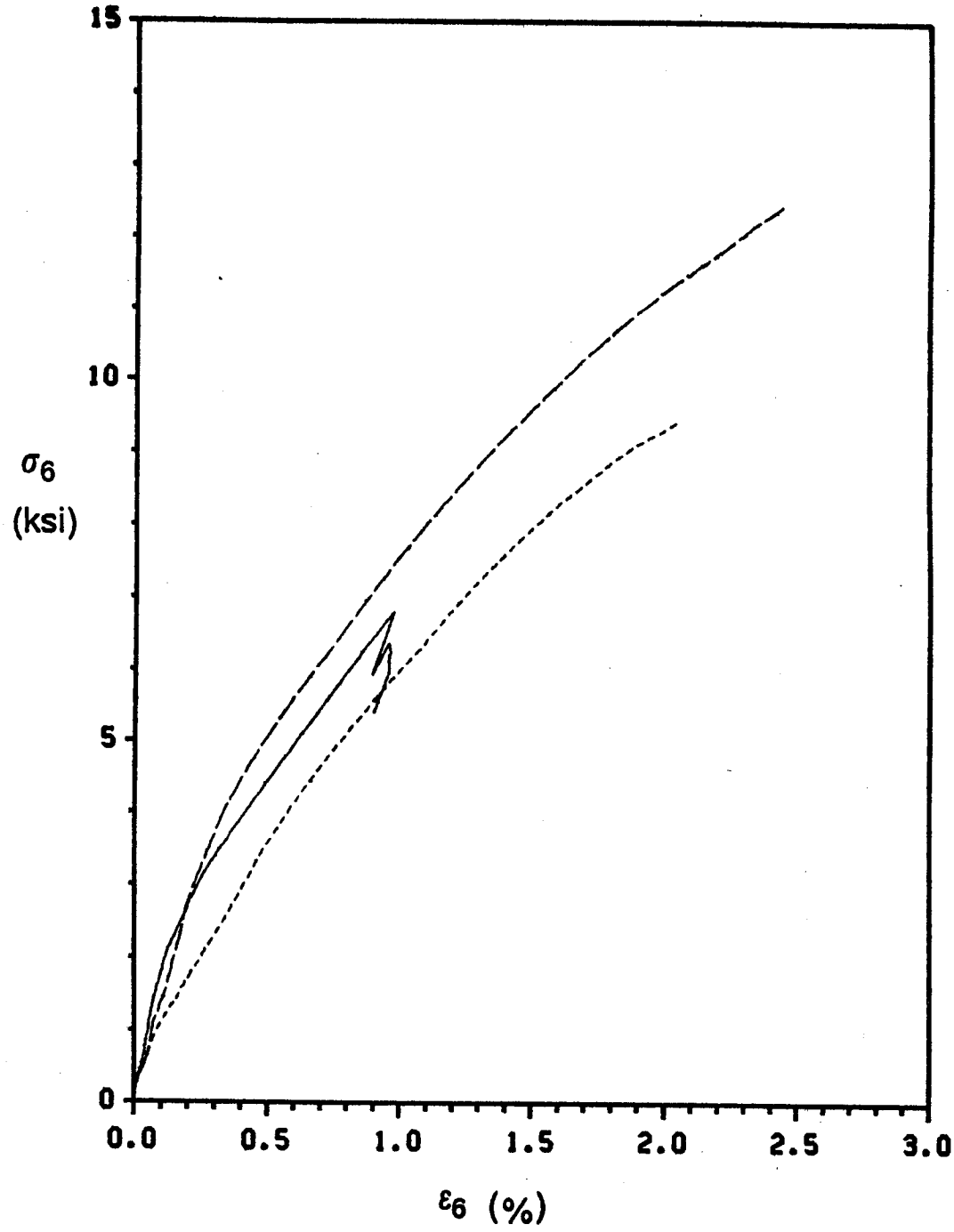

Figure 62. 45° Shear Response in Compression

C-3

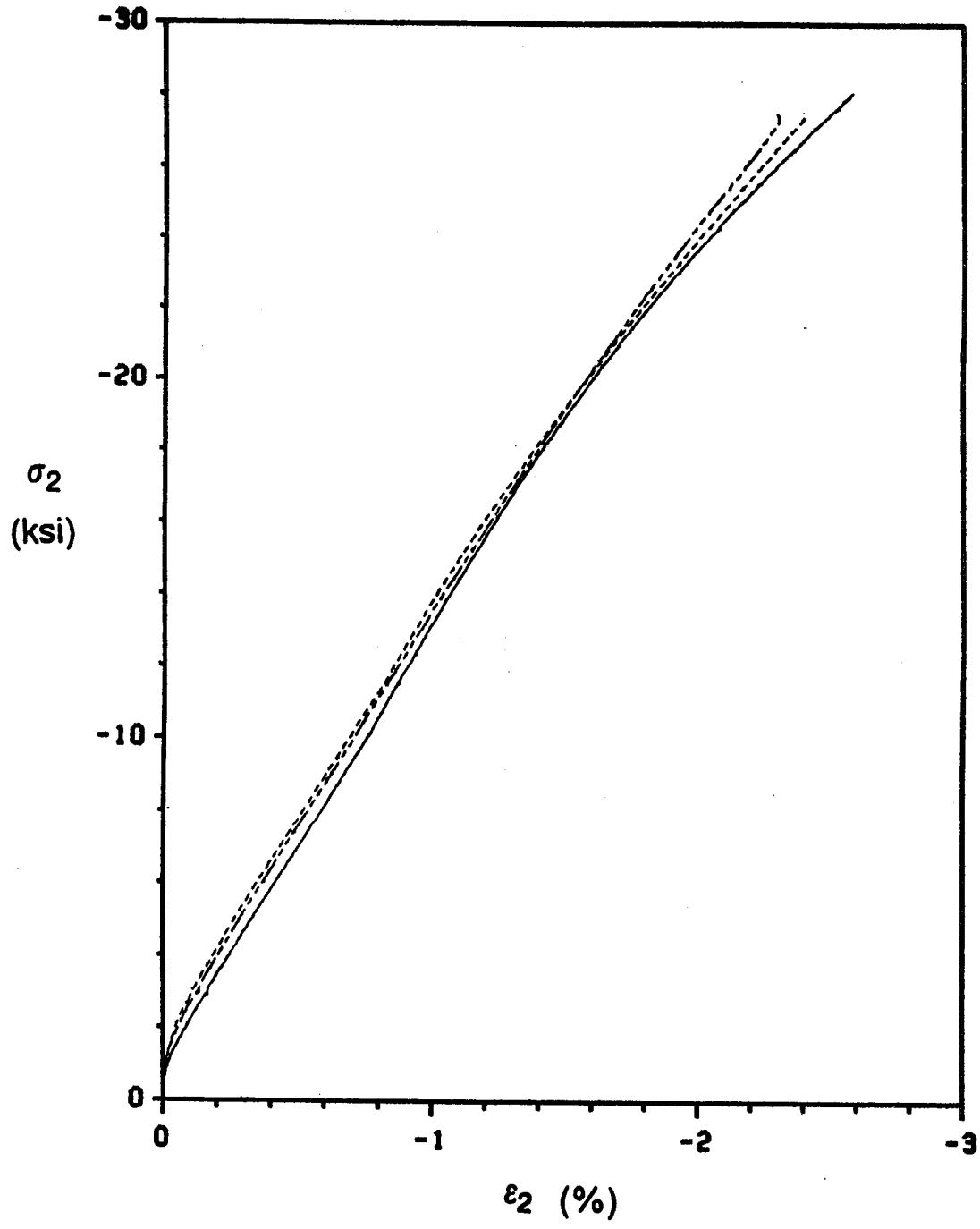

Figure 63. 90° Compression Response

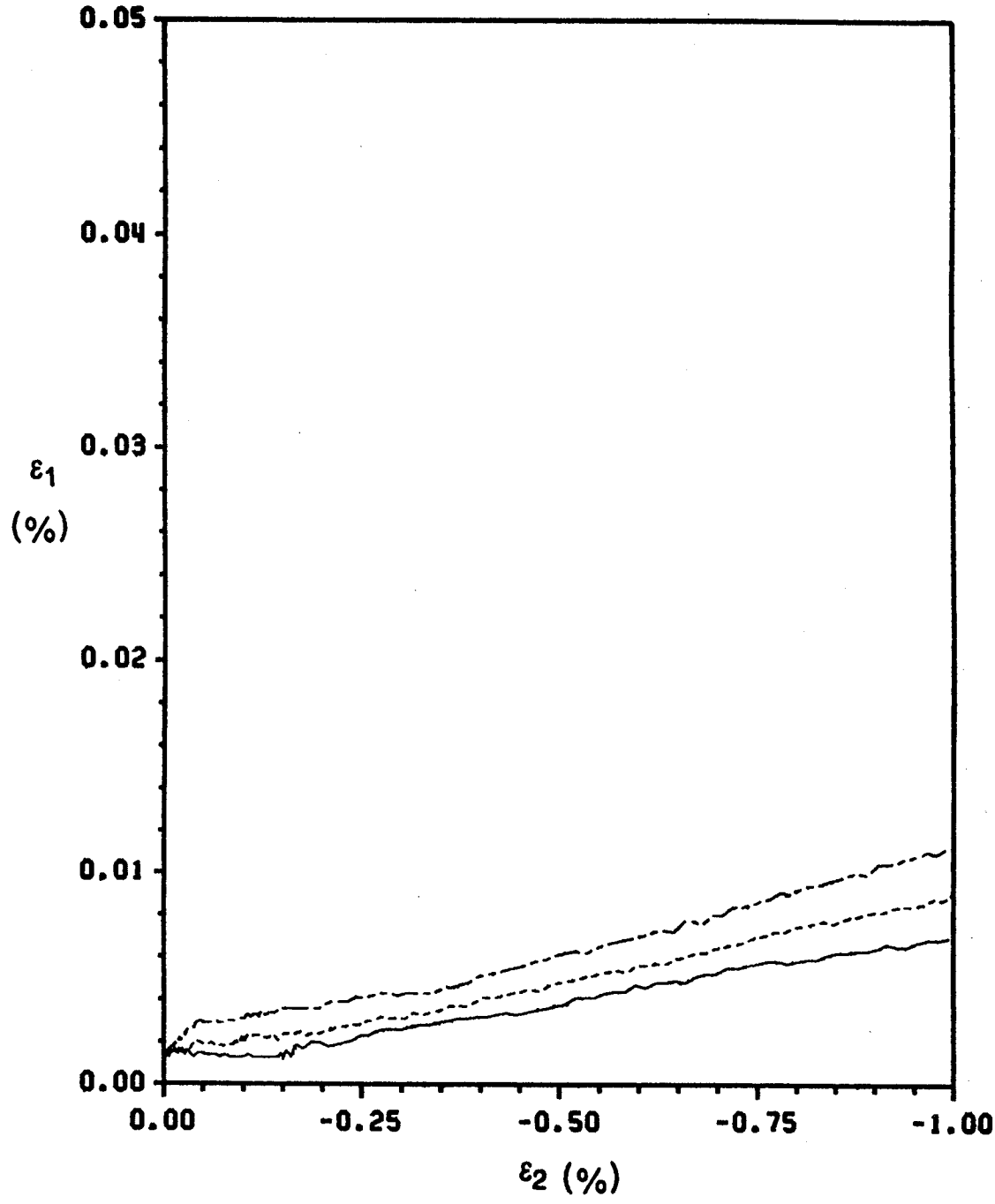

Figure 64. 90° Poisson's Response in Compression

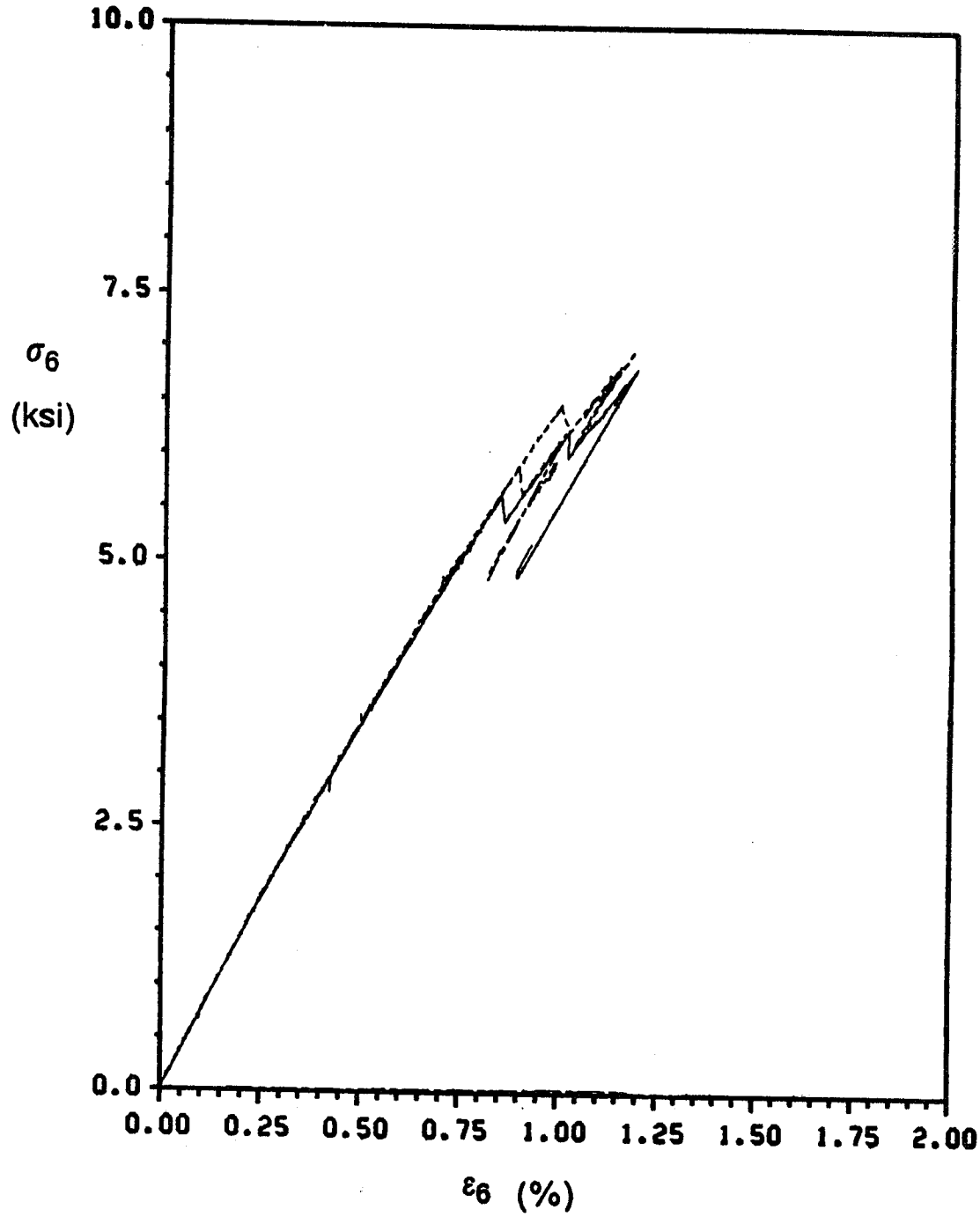

Figure 65. 0° Iosipescu Shear Response

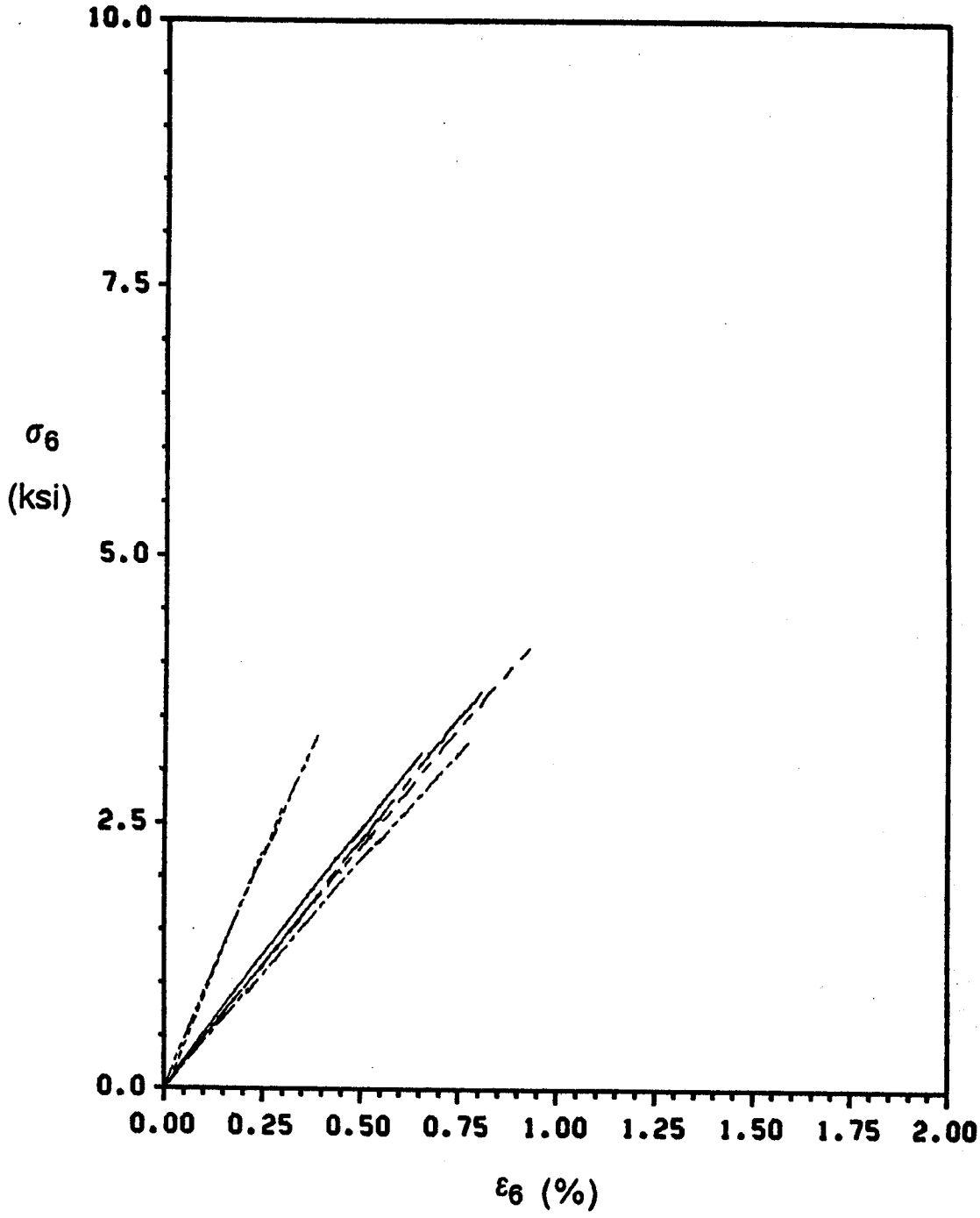

Figure 66. 90° Iosipescu Shear Response